TECHNOLOGIA I JAKOŚĆ WYROBÓW

Przedmowa

Szanowni Czytelnicy,

zachęcam do lektury artykułów naukowych ujętych w najnowszym wydaniu rocznika.

Czasopismo wydawane jest w trybie open access, bez opłat publikacyjnych, a językiem publikacji jest angielski. Rocznik stosuje zasady etyki publikacyjnej COPE, jest także indeksowany w bazach: ERIH Plus, Chemical Abstracts, BAZ – TECH. Artykuły posiadają identyfikację elektronicznych wersji publikacji naukowych DOI.

Systematycznie zwiększamy zakres tematyczny prac ujętych w naszym czasopiśmie. Aktualnie Redakcja realizuje szereg wielopłaszczyznowych działań mających na celu usprawnienie procesu wydawniczego, podniesienie doskonałości naukowej publikowanych prac oraz ich umiędzynarodowienie, przy jednoczesnym wzroście rozpoznawalności rocznika Technologia i Jakość Wyrobów (TJW), zwłaszcza w zagranicznych środowiskach naukowych.

Nasz rocznik został ujęty w komunikacie Ministra Edukacji i Nauki z dn. 3 listopada 2023 r. o zmianie i sprostowaniu komunikatu w sprawie wykazu czasopism naukowych i recenzowanych materiałów z konferencji międzynarodowych i posiada przypisanych 100 pkt.

Serdecznie zapraszam do dalszej współpracy i życzę kolejnych sukcesów wraz z naszą Redakcją.

Redaktor Naczelna,

dr hab. inż. Katarzyna Ławińska

Signed by /
Podpisano przez:

Katarzyna
Ławińska

Date / Data:
2023-12-29 20:06

Spis treści

Influence of weft density on selected parameters of fabric surface

Wpływ liczności wątku na wybrane parametry powierzchni tkanin

Gabriela Kosiuk[1,2*], Małgorzata Matusiak[1]

[1] Lodz University of Technology, Faculty of Material Technologies and Textile Design, Institute of Architecture of Textiles, Poland

[2] Institute of Security Technologies 'MORATEX', Lodz, Poland

Abstrakt

Struktura geometryczna powierzchni materiałów tekstylnych ma duże znaczenie funkcjonalne, eksploatacyjne i estetyczne. Podstawowymi parametrami struktury tkanin są: gęstość splotu, osnowy i wątku oraz gęstość liniowa osnowy i wątku. Chropowatość jest jedną z cech jakości powierzchni najczęściej ocenianych za pomocą wskaźników ilościowych, zwanych parametrami chropowatości powierzchni. Celem prezentowanych badań była analiza parametrów charakteryzujących strukturę geometryczną powierzchni tkanin bawełnianych o splocie skośnym. Pomiary topografii powierzchni przeprowadzono przy użyciu profilometru MicroSpy® Profile firmy FRT the art of metrology™. Badania potwierdziły, że na podstawie wyników uzyskanych za pomocą profilometru można kompleksowo analizować topografię powierzchni tkaniny.

Abstract

The geometric structure of surface of textile materials have significant functional, operational and aesthetic importance. The basic parameters of the woven fabrics' structure are the following: weave, warp and weft density as well as warp and weft linear density. Roughness is one of the surface quality features most often assessed by quantitative indicators called surface roughness parameters. The aim of the presented research was to analyze the parameters characterizing the geometric structure of the surface of cotton woven fabrics with twill weave. Surface topography measurements were performed using the MicroSpy® Profile profilometer by FRT the art of metrology™. The research confirmed that, on the basis of the results obtained with the profilometer, it is possible to analyze comprehensively the topography of the fabric surface.

Słowa kluczowe: chropowatość, profilometr, splot, tkanina, powierzchnia

Keywords: roughness, profilometer, weave, fabric, surface

1. Introduction

There are many features that characterize the quality of fabrics. Żyliński [1] divided them into 3 main groups:

• features significant from the point of view of the possibility of formatting the desired product,

• features affecting the performance of the manufactured product,

• features determining the durability of products.

The shaping of particular properties of fabrics depends on their structure. The basic structural parameters of the woven fabrics are:

• weave,

• the density of warp and weft,

• linear density of warp and weft.

The weaving pattern determines the way the warp and weft are interlaced. The twill weave is one of the basic weaves of the woven fabrics. In twill weave, the weft thread runs successively under three and then over one warp thread (Fig. 1).
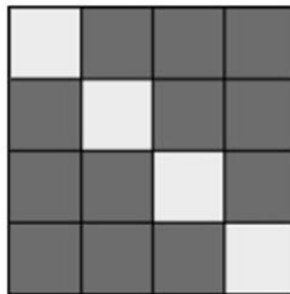
twill 3/1 S

Fig. 1. The interweaving of warp and weft threads in a twill weave fabric.
Source: [own source].

The density of threads determines the number of threads per unit of length. It reflects the density (compactness) of the fabric structure. A distinction is made

between the density of warp and density of weft. The linear density of yarn is a parameter characterizing the thickness of the yarn and it is most often expressed in the tex unit. 1 tex corresponds to the weight of a 1 km (1000 m) length of yarn. Numerous studies have shown that the above-mentioned parameters of the fabric structure affect their properties: mechanical, technological, aesthetic and functional [2 – 7]. One of the important quality features of fabrics is the quality of their surface. It affects both the appearance of fabrics and their performance properties. This applies especially to fabrics used in direct contact with human skin [7]. In contact with human skin, as well as in the mutual contact of fabrics, an important role is played by the surface topography characterizing the shape of the surface as well as the presence and mutual position of characteristic objects and points. There are many methods of studying the surface topography of objects. Generally, these methods can be divided into contact and non-contact methods [8]. In the textile industry, the most popular and most frequently used method is the measurement of the surface parameters of textiles using the KES (Kawabata Evaluation System) system module - KES - FB 4 [8]. It is a contact method in which the surface roughness is determined. The disadvantage of contact methods is the possibility of deformation of the surface of the textiles due to the movement of the sensor of measuring instrument on the measured surface. This can lead to measurement errors. The aim of presented work to characterize the surface topography of the woven fabrics of twill weave by using the contactless method of measurement. The influence of linear density of weft yarn on selected roughness parameters of the investigated fabrics was also analyzed and discussed.

2. Materials and methods

2.1. Materials

In order to analyze the influence of weave on the surface properties of woven fabrics, 5 variants of cotton woven twill weaves fabrics have been manufactured.

OE cotton yarns with different linear density were used for manufacturing the fabrics: 50 tex as the warp as well as 100, 60, 50, 40, 30 tex as the weft. The fabrics were made of the same warp yarn and of the same density of warp and weft. The basic parameters of the investigated fabrics are presented in table 1.

Tab. 1. The basic parameters of the investigated fabrics.

Sample	Weft linear density [tex]	Mass per square meter [g/m2]	Warp density *Threads* [/dm]	Weft density *Threads* [/dm]	Thickness [mm]
1	100	292	317	116	0.78
2	60	238	317	117	0.70
3	50	225	317	116	0.68
4	40	215	320	118	0.65
5	30	198	318	118	0.61

2.2. Methods

The fabric surface topography tests were performed using the MicroSpy® Profile profilometer by FRT the art of metrology™ (Figure 2). For each fabric variant, a sample scanning was performed on the right side of the fabrics. The scanning area was 49 mm x 49 mm. The obtained fabric scans were processed in a specialized Mark III software. First, the obtained images were modified in order to remove defective and missing data. Based on the scan results obtained, the surface topography of the tested fabrics was analyzed. The parameters characterizing the

geometric structure of the fabric surface were determined according to the PN EN ISO 4287: 1993 standard [9].

Fig. 2. MicroSpy® Profile profilometer by the FRT the art of metrology™.

Source: [own source].

3. Results and Discussion

In order to assess an influence of linear density of weft yarn on the parameters characterizing the geometric structure of the fabric surface the statistical analysis has been performed using the ANOVA. Figure 3 shows the example of the obtained images of the tested fabrics.
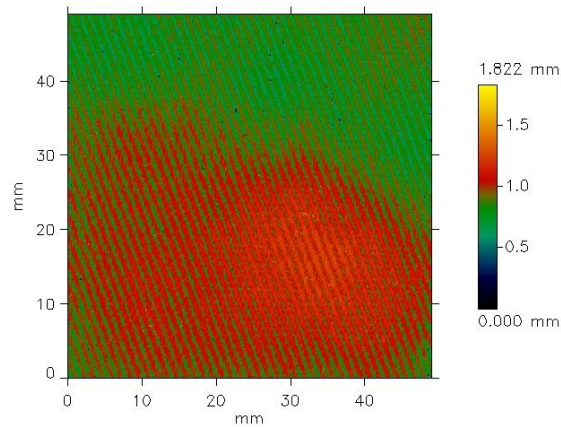
Fig. 3. Image of the fabric before applying the filter.

Source: [own source].

Next to the images on the right side there is a scale for the z (height) value. Fabrics are flexible materials. They show a certain shape memory. Therefore, it is impossible to arrange the fabric samples in such a way that they perfectly adhere to the measuring table of the profilometer. Due to this fact the phenomenon of waviness has been observed. It does not result from the waviness of the fabric surface, but from the inaccurate adherence of the samples to the table, and thus the position of the samples slightly deviating from the horizontal plane. To eliminate this, when determining the roughness parameters, an appropriate filter (cut-off filter) was used to eliminate the waviness phenomenon. The surface image of the tested fabric after eliminating the waviness is shown in Figure 3. It is clearly visible that the height distribution (z value) is more even, and the range of z-value is significantly smaller than that recorded for the images of fabrics before the filter was applied (Figure 4).
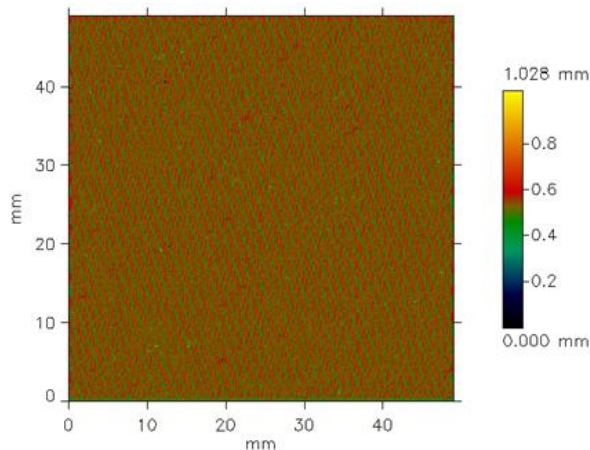
Fig. 4. Image of the fabric after applying the cut-off filter.
Source: [own source].

The fabrics images after removing the waviness component have been analyzed using the Mark III software. Selected parameters for the whole area of the investigated samples are presented in the table 2.

Tab. 2. Results from the MicroSpy® Profile profilometer for the sample area.

Sample	Weft linear density [tex]	Ra [mm]	Rq [mm]	Rz [mm]	Rk [mm]
1	100	0.034	0.047	1.060	0.079
2	60	0.034	0.046	0.931	0.076
3	50	0.032	0.045	1.036	0.075
4	40	0.032	0.045	1.069	0.073
5	30	0.029	0.040	1.034	0.069

In the table 2 there are presented the values of the following parameters: Ra, Rq, Rz and Rk. The Ra, Rq and Rz are the height parameters. The Ra is an arithmetic mean of the absolute of the ordinate values within a defined area. It is an arithmetical mean height of a line. It expresses, as an absolute value, the difference in height of each point compared to the arithmetical mean height of the surface, The Rq is a root mean square value of the ordinate values within a defined area. It is equivalent to the standard deviation of heights. Rz expresses the maximum height. It is equivalent to the sum of the maximum peak height Rp and maximum valley depth Rv. Last parameter 0 – Rk is a core height. It is functional parameter derived from the Material Ratio curve. Rk expresses the difference between the upper and lower levels of the core of the material being investigated. It is clear that the values the are different for each fabric variant. In the case of the Ra, Rq and Rk, the values of the parameters decrease with the decrease of the linear density of weft yarn. For the Rz parameter any clear tendency was observed. Due to the fact that the structure of the fabrics was changed by changing only one system of threads – weft, the

influence of the structure changes on the surface parameters was analyzed separately for both directions warp and weft. In order to do it, for each fabric variant the profiles have been created in warp and weft directions. Exemplary profile and place of the profile of the fabric surface are presented in the Figure 5.

a)

b)
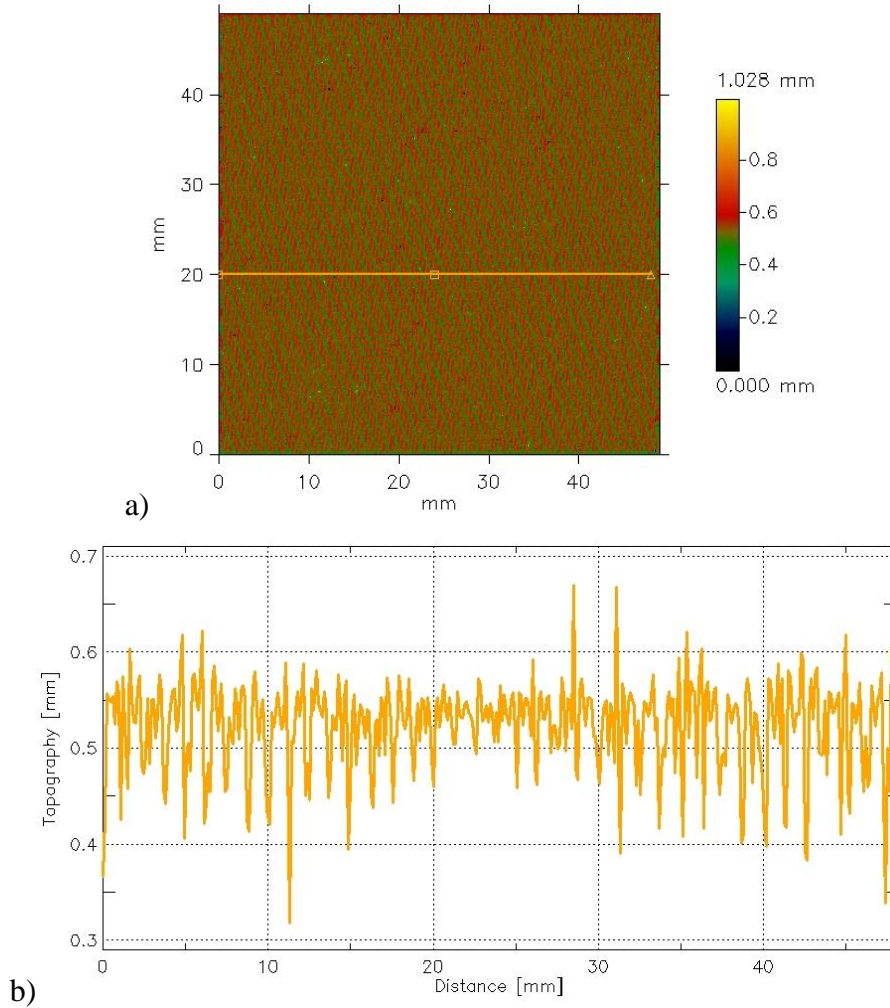
Fig. 5. Exemplary profile created in the weft direction: a) place of the profile on the sample surface, b) created horizontal profile; Source: [own source].

For each created profile the Mark III software provides the values of the roughness parameters. The values of the selected parameters for the profiles created in weft direction of the investigated fabrics are presented in the Table 3.

Tab. 3. Results from the MicroSpy® Profile profilometer for the horizontal profiles.

Sample	Weft linear density [tex]	Ra [mm]	Rq [mm]	Rz [mm]	Rk [mm]
1	100	0.035	0.048	0.261	0.085
2	60	0.033	0.044	0.215	0.072
3	50	0.036	0.048	0.240	0.077
4	40	0.030	0.041	0.215	0.086
5	30	0.027	0.035	0.161	0.068

Next, in the same way the vertical profiles – in warp direction have been created and assessed. The results for the vertical profiles are presented in the Table 4.

Tab. 4. Results from the MicroSpy® Profile profilometer for the vertical profiles.

Sample	Weft linear density [tex]	Ra [mm]	Rq [mm]	Rz [mm]	Rk [mm]
1	100	0.032	0.045	0.260	0.084
2	60	0.030	0.040	0.194	0.068
3	50	0.029	0.040	0.211	0.061
4	40	0.033	0.047	0.245	0.071
5	30	0.028	0.042	0.237	0.057

Figure 6 presents the comparison of the Ra parameter determined for the investigated fabrics for whole area of the sample (A symbol) as well as for the created profiles: horizontal (H symbol) and vertical (V symbol).
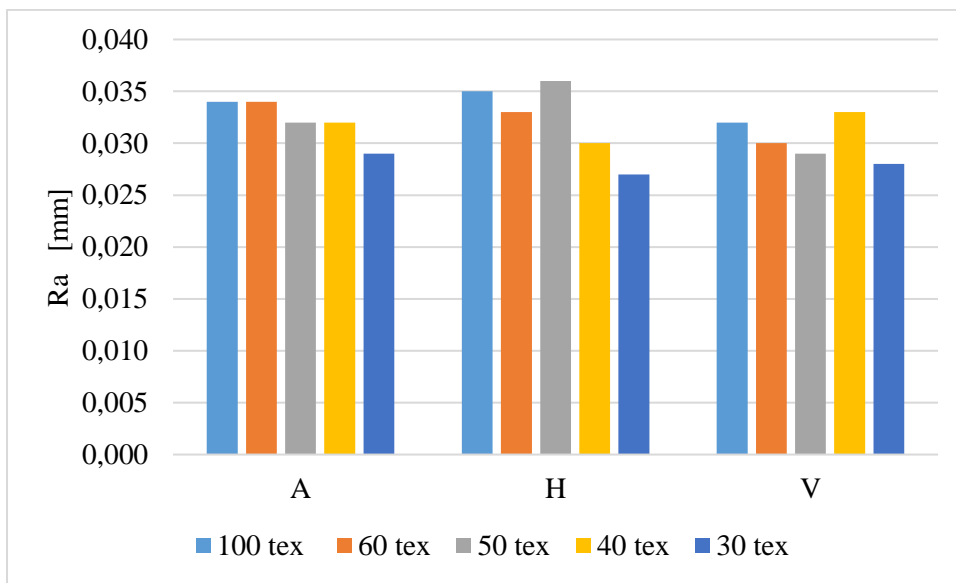
Fig. 6. The comparison of the Ra parameter determined for the investigated fabrics for whole area of the sample (A symbol) as well as for the created profiles: horizontal (H symbol) and vertical (V symbol). Source: [own source].

For the Rq parameter the tendencies are the same as for the Ra parameter (Figure 7) but the values of Rq are higher that the values of the Ra. Interesting situation is observed in the case of the Rz parameter. The values of the Rz parameter for the whole area of the sample are ca. 5 times higher that that for the profiles. The Rz parameter is the sum of the maximum peak height Rp and maximum valley depth Rv in the analyzed area. It is obvious that in the whole area it is much more points being investigated that in the case of the profiles. On the whole area are all picks and valleys present on the sample surface. It is probable that the highest pick and the deepest valley determining the Rz parameter for the whole area of the sample are located in a different place than the created profiles (Figure 8).
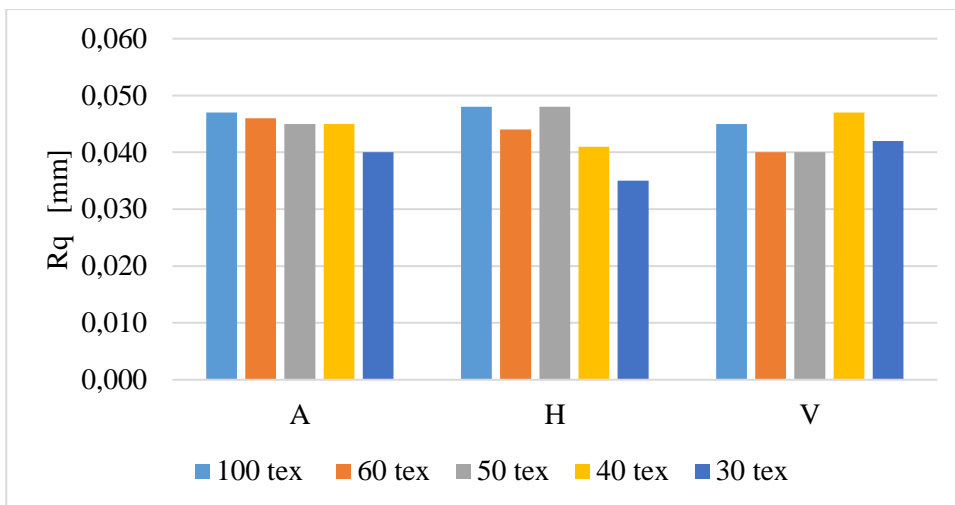
Fig. 7. The comparison of the Rq parameter determined for the investigated fabrics for whole area of the sample (A symbol) as well as for the created profiles: horizontal (H symbol) and vertical (V symbol); Source: [own source].
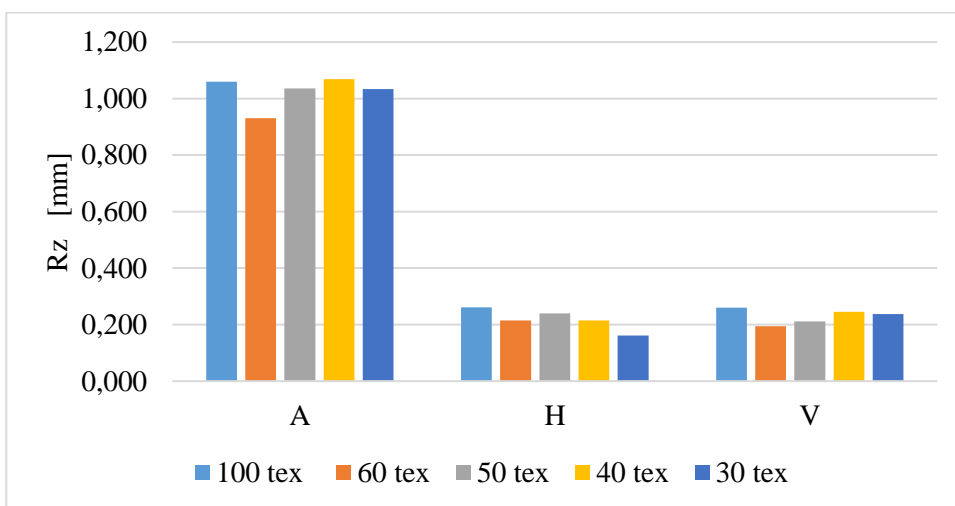
Fig.8. The comparison of the Rz parameter determined for the investigated fabrics for whole area of the sample (A symbol) as well as for the created profiles: horizontal (H symbol) and vertical (V symbol); Source: [own source].

It is clearly seen that the linear density of the weft yarn influences the value of the Ra parameter. In the case of the whole sample area the lower the linear density of the weft yarn is the lower value of the Ra parameter. Similar situation is observed

for the profiles. However, in both cases the horizontal and vertical directions the trend is disrupted. In the weft direction(horizontal) the fabric variant with the 50 tex weft yarn is characterized by the highest value of the Ra parameter whereas, in the warp direction (vertical) the highest value of the Ra parameter occurs fir the fabric with the 40 tex weft yarn. Using the MicroSpy® Profile Profilometer supported by the Mar II software it is possible to determine a range of parameters and functions. All of them can be applied to complex characterization of the surface topography of textile materials. For instance it is possible to create the histograms of height presenting the distribution of height of all points on measured surface. Figure 9 presents exemplary histogram for the fabric with the 100 tex weft yarn.
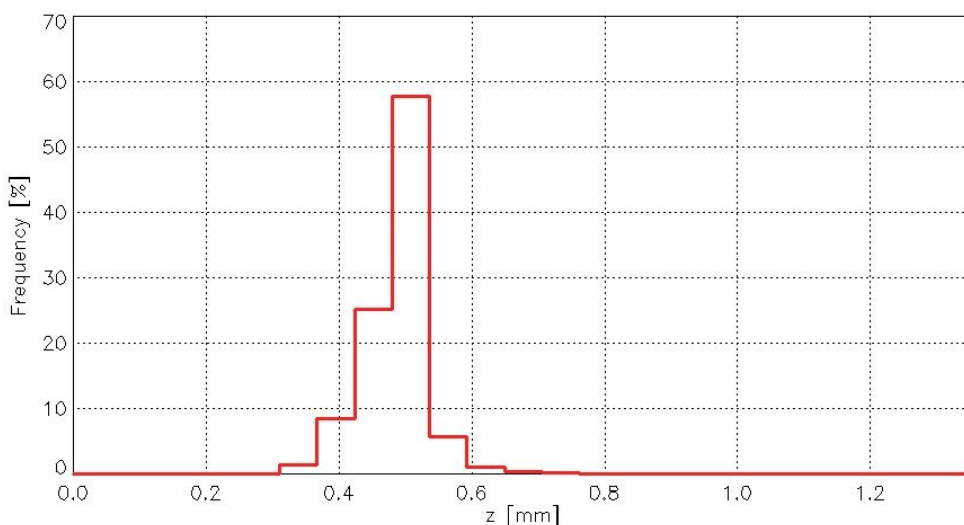
Fig. 9. An example of histogram illustration the height (z value) distribution on the surface of fabric with the100 tex weft yarn. Source: [own source].

There are two parameters characterizing the shape of histogram: the most frequent height and histogram maximum. The values of the parameters are presented in the Table 5. The table presents also the fractal dimension determined at the initial cell height 2.5 mm. A fractal dimension is a ratio expressing a complexity of a surface.

Tab. 5. Results from the MicroSpy® Profile profilometer for the whole area.

Sample	Weft linear density [tex]	The most frequent height [mm]	Histogram maximum [%]	Fractal dimension
1	100	0.508	57.716	2.399
2	60	0.514	49.035	2.399
3	50	0.574	58.445	2.399
4	40	0.493	47.449	2.411
5	30	0.410	44.650	2.482

The linear density of the weft yarn influence both the histogram parameters and fractal dimension. However, it is difficult to stat and clear trend. It needs further investigations. So far, no similar studies have been conducted that could be the subject of reference to the results obtained. Surface measurement of textile materials using non-contact methods is very rare. The works published so far concern other textile materials. For example, Matusiak [10] conducted research on seersucker woven fabrics. The topography of seersucker woven fabrics has a completely different character than that of standard fabrics. Therefore, at present it is not possible to compare the obtained results with literature reports.

4. Conclusions

Based on the performed investigations and obtained results it can be concluded that:

- the MicroSpy® Proflie profilometer by FRT and the Mark III software enable comprehensive studies of the geometrical structure of the textile surface,

- investigated cotton fabrics of twill weave with different weft yarns differ between each other in the range of all presented surface topography parameters,

- a change in the linear density of the weft yarn while maintaining the same other parameters of the fabric structure affects the surface topography; the values of the Ra, Rq and Rk parameters decrease with the decrease of the linear density of the weft yarn while other structural parameters are unchanged.

- The influence of the structural parameters of the fabrics on their surface topography needs further investigations.

Acknowledgements

References

[1]   Żyliński T. *Textile metrology III* (in Polish), WNT, Warsaw 1969.

[2]   Matusiak, M. *Influence of the Structural Parameters of Woven Fabrics on their Drapeability*, Fibres & Textiles in Eastern Europe **25**, 1(121), 2017, pp. 56-64.

[3]   Backer S. *The relationship between the Structural Geometry of a Textile Fabric and Its Physical Properties, Part IV.:* Interstice Geometry and Air Permeability. Textile Research Journal **21**, 10, 1951, pp. 703–714.

[4]   Nofitoska M.; Demboski G.; Carvalho M.A.F. *Effect of Fabric Structure Variation on Garment Aesthetic Properties*, Tekstie ve Konfeksiyon **24(2)**, 2014, pp. 132-136.

[5]   Kumpikaitė E. *Analysis of Dependencies of Woven Fabric's Breaking Force and Elongation at Break on its Structure Parameters*, Fibres & Textiles in Eastern Europe **1(60)**, 2007, pp. 35-38.

[6]   Milašius V.; Milašius R.; Kumpikaité E.; Olšauskiené A. *Influence of Fabric Structure on Some Technological and End-use Properties*, Fibres and Textiles in Eastern Europe **11**, No 2 (41), 2003, pp. 48-51.

[7]   Matusiak M.; Sikorski K. *Influence of the structure of woven fabrics on their thermal insulation properties,* Fibres and Textiles in Eastern Europe **88**, 5, 2011, pp. 46-53.

[8]   Krucińska I.; Konecki W.; Michalak M. Measuring systems in textiles (in Polish). ISBN 83-7283-148-3. Lodz 2006, pp. 252-329.

[9]   Polish Standard PN-EN ISO 4287: 1993 Specifications of product geometry - Geometric structure of the surface: profile method - Terms, definitions and parameters of the geometric structure of the surface.

[10]   Matusiak M., Wpływ efektu gofrowania na wybrane właściwości tkanin gofrowanych, Technologia i Jakość Wyrobów **66**, 2021, pp. 46-64.

The lightfastness and structure of semi-permanent hair dyes, derivatives of *o*-nitro-*N*- β-hydroxyethylaniline.

Odporność na działanie światła i budowa barwników typu "semi-permanent", pochodnych *o*-nitro-*N*-*β*-hydroksyetyloaniliny stosowanych do bawienia włosów.

Lucjan Szuster[1*], Krzysztof Wojciechowski[2], Joanna Rutowicz[1]

[1] Łukasiewicz – Łódź Institute of Technology, 73 Zgierska Str., 91-463 Łódź, Poland

[2] Institute of Environmental Engineering and Building Installations, Lodz University of Technology, Al. Politechniki 6, 90-924 Łódź, Poland

Abstrakt

Celem pracy było zbadanie wpływu podstawników na działanie światła i właściwości spektralne pochodnych o-nitro-N-β-hydroksyetyloaniliny, stosowanych w półtrwałych farbach (semi-permanent) do barwienia włosów. Stwierdzono, że szybkość zaniku barwy włosów zależy od charakteru podstawników ED i EA w o-nitro-N-β-hydroksyetyloanilinie. Pochodne o-nitro-N-β-hydroksyetyloaniliny ulegają odbarwieniu zgodnie z kinetyką reakcji 1-go rzędu. Ujemna wartość współczynnika nachylenia wskazuje na mechanizm utleniający reakcji. Z zależności lmax=f(σ) obliczono stałe σp─Hammetta. Stosując półempiryczną metodę kwantowo-chemiczną AM1, obliczyliśmy budowę barwników pochodnych N-β-hydroksyetyloamino-nitrobenzenu. Struktury barwników optymalizowano przy użyciu MM +, DM oraz AM1.

Abstract

The aim of this study was to examine the substituent effects on lightfastness and spectral properties of o-nitro-N-β-hydroxyethylaniline derivatives, used in semi-permanent hair dyes of HC (Hair Color-Dyes) type. It has been found that the fading rate of the color of hair dyed depends on the nature of the ED and EA substituents in the o-nitro-N-β-hydroxyethylaniline. The o-nitro-N-β-hydroxyethyl aniline derivatives undergo discoloration according to kinetics of the first order reaction. A negative value of the slope coefficient indicates the oxidative mechanism of the reaction. From the relationship lmax=f(σ) σp─Hammett's constant were calculated. Using the semi-empirical AM1 quantum chemical method, we calculated the structures of hair dyes The dye structures were optimized using MM +, DM, and AM1

Słowa kluczowe: półtrwałe farby do włosów, degradacja fotochemiczna, równanie Hammetta, geometria cząsteczek, metoda kwantowo-chemiczna AM1

Keywords: semi-permanent hair dyes, photochemical degradation, Hammett equation, molecules geometry, AM1 quantum-chemical method

1. Introduction

Hair dyes consist of properly selected single dyes or, in general, their mixtures and also contain standardizing additives: conditioners, antioxidants, dispersants, inorganic salts, dextrins or lubricants to facilitate combing. The quantitative composition of these mixtures is not known, as it is usually covered by the manufacturer's trade secret [1-8]. There are three basic groups of dyes for dyeing hair. The division into groups is a consequence of the method of their application, the type of dye and the different resistance of dyes to dyed hair.

a) "Permanent" - permanent dyeing

b) "Semi-permanent" - semi-permanent dyeing

c) "Temporary" - impermanent or temporary

Hair dyed with "Permanent" dyes shows good resistance to washout and light. The reason for this is their polymeric structure formed as a result of chemical reactions during application. The other two groups of dyes do not have very high resistance to external factors, especially to light. "Temporary" dyes, the purpose of which is to give a permanent color for a period of several hours, may even have very low light fastness. "Semi-permanent" dyes, which are intended for temporary coloring of hair for a period of several days, should show such resistances that will ensure their permanent color for this time. Semi-permanent dyes are becoming more and more popular due to their durability, enough for 6-8 shampooing. Basically, they serve more to darken the hair than to change its color dramatically [8]. Semi-permanent dyes are poorly soluble in water, low molecular weight non-ionic dyes, usually used in mixtures with other dyes. The group of these products includes low molecular weight compounds, such as phenylenediamines, nitroanilines, nitrophenyldiamines and nitroaminophenols, they are often used with selected azo or anthraquinone dyes [1,9-13]. They do not require the use of H_2O_2 [1,10]. It was found in practice that the shampoos and coloring toners used, the ingredients of which were Semi-permanent dyes, changed their colors in the

summer under the influence of sunlight. The problem of light fastness of "Semi-permanent" dyes is important because that many of these dyes are allergenic or even toxic. As a consequence, some of the dyes used, after clinical tests of their toxicity, were withdrawn from the market. It seemed advisable to study the course of degradation of semi-permanent dyes under the influence of light. In the first stage, it was necessary to study the rate of degradation processes on the fibre, determine the kinetics of these processes and determine the effect of substituents on the rate of reaction. Research on commercial hair dyes is hampered by the fact that the same or very similar shades can be obtained in coloring products with different compositions from different manufacturers. The selection of mixes depends on aesthetic requirements. Semi-permanent dyes are also added to oxidative dyes to enhance the shade and broaden the color palette. Another problem is the selection of research material for hair dyeing due to the variable properties of different types of human hair. The natural color of hair depends on the amount of melanin in the hair cortex, and more specifically on the ratio of eumelanin to pheomelanin. Hair dyed with semi-permanent dyes gives different shades depending on the initial color of the hair. As a result of sunlight, the hair becomes lighter and mechanically weakened by breaking the sulfur bonds of keratin, protein degradation and the formation of —COOH and —NH2 groups. Sunlight can lead to dry hair, reduced strength, roughness, loss of color and shine, stiffness and fragility; the disintegration of the surface layer of the epidermis (cuticuli) precedes the degeneration of the cortical layer of the hair [12, 14-16]. Using human hair after bleaching does not ensure reproducible results. Shades of hair color will depend on the pH of the bleaching agents, their concentration and alkalizing additives. Repeatedly bleached hair becomes more porous, brittle and dry for longer. An increase in porosity reduces their resistance to subsequent discoloration. Damaged hair absorbs more dyes and auxiliaries. One-time bleaching weakens the mechanical strength of the hair by up to 15% and can even lead to the removal of the proteins of the cortical layer. Repeated dyeing means that subsequent hair

dyeing will give unique results [17, 18]. A suitable material for the dyeing process would be white, melanin-free llama hair [19], but this material is difficult to obtain. Instead, the test used white wool, which is normally used to assess dye fastness according to EN ISO 105 F01. The dyeing procedure was analogous to the hair dyeing procedure proposed by the manufacturers of commercial products.

The light fastness of dyes is affected by their molecular structure, i.e. the nature of the substituents and their substitution location, as well as the ability to form intramolecular hydrogen bonds [20-23]. For safety reasons, the EU Cosmetics Directive defines the permissible maximum concentration of hair dyes in approved commercial products [24-27]. For example, the maximum allowable concentrations for the semi-permanent dyes HC Blue 2, HC Red 3 and HC Yellow 2 are 2.8%, 3% and 1%, respectively [27,29]. The resistance of the dye molecule to light, washing and mechanical processing is also determined by the highly polar structure of the fiber (or hair), in which ionic interactions play an important role. These interactions are involved in the transfer of excitation energy from the molecule to the fiber and often cause an increase in resistance. In addition, the properties of the fibers affect the spectral properties of the dye, influencing its distribution of electron density and the maximum absorption value λmax [21,28]. In real conditions, all these factors may occur, which is manifested by changes in the rate and sequence of photochemical redevelopment reactions. The limits of safe concentrations in hair dyes vary depending on the chemical nature of the dyes.

The aim of our research was to investigate the spectral and photochemical properties of semi-permanent hair dyes containing N-β- hydroxyethylamine. Depending on the nature of the substituents and their position in the aromatic ring, wool was colored yellow to violet-blue. For dyeing, as stated earlier, a woolen fabric was used, in accordance with the EN ISO 105 F01 standard. First, the rate of photochemical decomposition of semi-permanent dyes exposed to light was examined, and the influence of the nature of the substituents and their position in the ring on the kinetics of the reaction was also investigated.

2. Experimental

The group of six dyes were used in this study, *N*-β-hydroxyethyl and *N,N*-(di-β-hydroxyethyl)-2-nitro-4-phenylenediamine derivatives (B1-B5) and derivative of 3-nitro-4-aminophenol (B6) of the general formula 1 (Tab.1). Their physicochemical properties are shown in Table 1. Tested semi-permanent dyes have been purchased from the trading company Hangzou Haichem Co., Ltd. and used without further purification. All dyes were of 99% purity (checked by HPLC), with moisture content max. 0.5%, ash <0.5% and iron 40-100ppm. Melting points were consistent with the manufacturer's specifications and further confirmed by DSC (Perkin Elmer DSC 400). Chemical reagents and solvents were purchased from the POCh Poland and were of analytical grade.

Tab. 1. Physico-chemical properties of dyes B1 – B6

	B1[*1)]	B2	B3	B4	B5[*2)]	B6
Commercial Name	HC Yellow 2	HC Red 3	HC Blue 2	HC Violet BS	---	HC Red B54
X	H	NH_2	$N(C_2H_4OH)_2$	NHC_2H_4OH	NO_2	OH
M.w.	182.18	197.19	285.30	241.25	227.18	198.18
CAS	4926-55-0	2871-01-4	33229-34-4	84041-77-0	1945-92-2	65235-31-6
EINECS	225-555-8	220-701-7	251-410-3	281-856-4[*3)]	-------	265-648-0
m.p. [°C]	70	124	106-9	103-4	86-88	140-3
m.p. [DSC] [°C][*4)]	74.7	126.8	109.6	105.4	87.5	146.0
Purity (%)	> 99	> 99	> 99	≥ 99	---	≥ 99.5
Ash [%]	< 0.5	< 0.5	< 0.5	< 0.1	---	< 0.5
Fe [ppm]	40	40	100	< 50	---	40
Moisture [%]	< 0.5	0.5	< 0.5	< 0.5	---	---
TLC[*5)]	0.85	0.76	0.79 (0.16[*6)])	0.78	0.81 (0.44[*6)])	0.86
IR						
$\nu_{CN}[cm^{-1}]$	1197.1228	1203.1215	1196.1248	1203	1231.1300.	1218
$\nu_{NH}[cm^{-1}]$	3335	3297	3299	3321	3330	3326
$\nu_{asNO}[cm^{-1}]$	1417.1567	1409.1568	1421.1563	1395.1533	1401.1582	1422.1580
$\nu_{asCO}[cm^{-1}]$	1043	1062	1034.1057	1047.1065	1039.1086	1053.1210
$\nu_{C=C\ ar.}[cm^{-1}]$	1507	1521	1519	1513	1497	1519

[*1)] No 17501 (SDBS No.31996) [30], [*2)] 2,4-dinitro-N-(2-hydroxyethyl)aniline [GC MS m/z=227(mother backbone), 196(highest peak)],
[*3)] sulphate, [*4)] heating rate 10°C/min[-1] [DSC Perkin Elmer DSC 400], [*5)]TLC analysis: Kieselgel 254 Merc (uv-254), eluent: Bz: AcOH=6:2 (v/v), [*6)] Ethyl Acetate:PrOH:H_2O=1:6:3 (v/v).
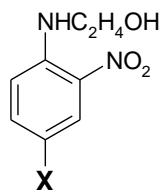
2.1. Synthesis of 2,4- dinitro-N-(2-hydroxyethyl)aniline (B5) [7,31,32]

20mL of 50% ethanol was heated to 55°C and 5.05g (0.025M) of 2,4-dinitrochlorobenzen was added. The whole was heated to 75°C and then, within 1,5 hours, 3.36g monoethanolamine (0.055M) was added dropwise. The mixture was stirred to complete the reaction. The TLC chromatography control (Kisielgel 254 Merck UV 254, Eluent - Ethyl Acetate:PrOH:H_2O=1:6:3 (v/v) was carried out (R_f = 0.44). After cooling the reaction mixture was filtered and washed with ethanol. 5.39g of dye B5 was obtained (yield 95.0%, melting point 87.51°C by DSC; Perkin Elmer DSC 400). IR: ν_{C-OH} 1039cm^{-1}, ν_{O-H} 1086cm^{-1}, ν_{C-N} 1231, 1300cm^{-1}, ν_{NO2} 1333, 1401, 1582cm^{-1}, ν_{N-H} 33306cm^{-1}; GC MS m/z=227 (mother backbone), 196 (highest peak) [33].

2.2. Dyeing procedure

Wool 5g sample, previously washed 20min in surfactant (Pretepon G), has been dying for 45min. in 40±0.1°C with 250mg of B1-B6 dye (5% dyeing, pH≈9-9.5 from NH_3/H_2O). The sample was washed 3 times with 200cm^3 of water at 40°C, until a colorless effluent. Then the fabric samples were dried (Fig 1).
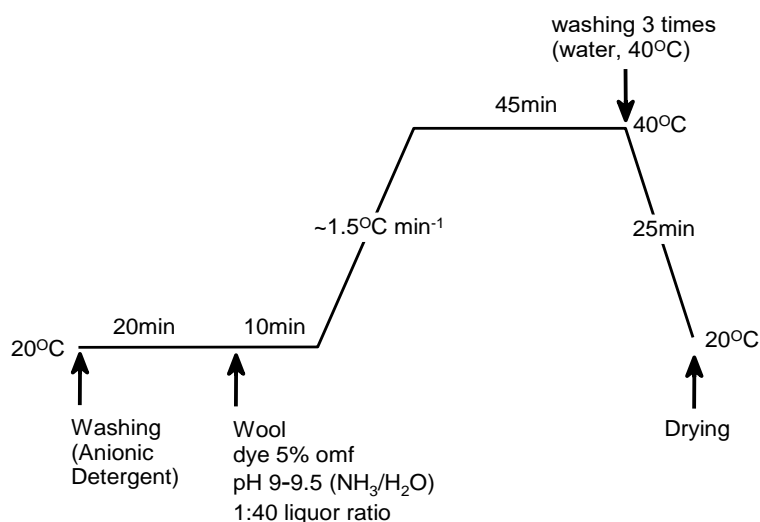
Fig.1. Dyeing method

2.3. Photofading analysis

Dyed wool fabric was irradiated with xenon lamp in the Suntest device for 35 hours. Changes in the K/S value of the dye on the fiber were analyzed every 1h. The reflection spectra of the dyed wool fabric were obtained on the Mackbeth ColorEye 2020, in the wavelength range of

400-700nm recording changes in the dyes concentrations according to the Kubelka-Munk equation [34,35] and formula (1):

$$\frac{K}{S} = \frac{(1-R)^2}{2R} \qquad (1)$$

The K/S values are proportional to the concentration of the dye on the fiber according to the relation (2):

$$\frac{K}{S} = \gamma\, c_w \qquad (2)$$

where K - absorption coefficient, S - scattering coefficient, R - reflectance coefficient γ - proportionality coefficient, c_w – the concentration of the dye on the wool fiber.

2.4. Spectral analysis

Spectral analysis were performed in 50% acetone/water solution (pH≈9.5) for dyes in concentration of $10^{-4} \div 10^{-5}$ mole/dm^3 using spectrophotometer Specord Uv-Vis (Zeiss Jena) in the wavelength range of 320 – 700nm. Ir spectra were measured with Nicolat iS10 (Thermo Scientic) infrared spectrometer using KBr pellets.

2.5. AM1 calculation method [36,37]

A structure all derivatives of N-β-hydroxyethylamine-o-nitrophenyl molecules have been fully optimised using semi-empirical quantum chemical calculation AM1 methods with full optimization of all bonds length, angles and torsion angles (HyperChem v.8.0.6, Hypercube Inc.). Once the ground state optimized structures had been obtains by molecular mechanics method (MM+, atomic charge option), the geometry of the molecule were completely optimized without any geometrical restriction using the eigenvector following routine (RMS gradient 0,01kcal/A mol), the molecular dynamic (MD; run time 1ps, step size 0.001ps, simulation temperature 300K) and by AM1 or PM3 methods. Finally, unrestricted Hartree-Fock (UMF) Hamiltonian was used to calculate the single point CI, energy in gaseous phase at 25°C. Calculation MD and AM1 were performed 3 to 5 times until constant lowest standard enthalpy of formation H_f (kcal mol^{-1}) (convergence limit 0.01, accelerate convergence) was obtained. In calculating the properties of dyes, the molecules were assumed to be in vacuum. Changes in the total energy of a molecule associated with its spatial structure were analyzed as a function of E = f(α) for $\Delta\alpha^o = 2^o$.

3. Results and Discussion

3.1. Analysis of photochemical decomposition of B1 – B6 dyes

Reaction order of photochemical decomposition of dye on the fiber is not always the constant value. In the beginning it could be I-order reaction but finally it may become zero-order reaction. For the examined B1 – B6 dyes plots lgK/S = f(t) were drawn and used to determine the final concentration of each dye after 35 hours of radiation and the rate of its degradation on the wool fabric (Fig.2,3).
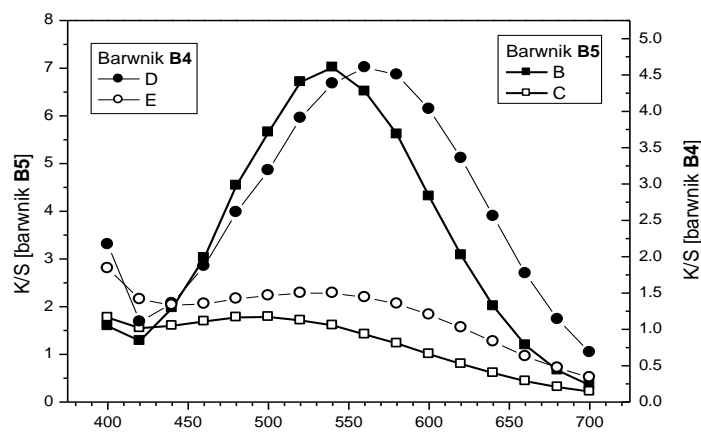
Fig.2. Reflectance spectra of B4 and B5 dyes at 0 and after 35 hours of exposure
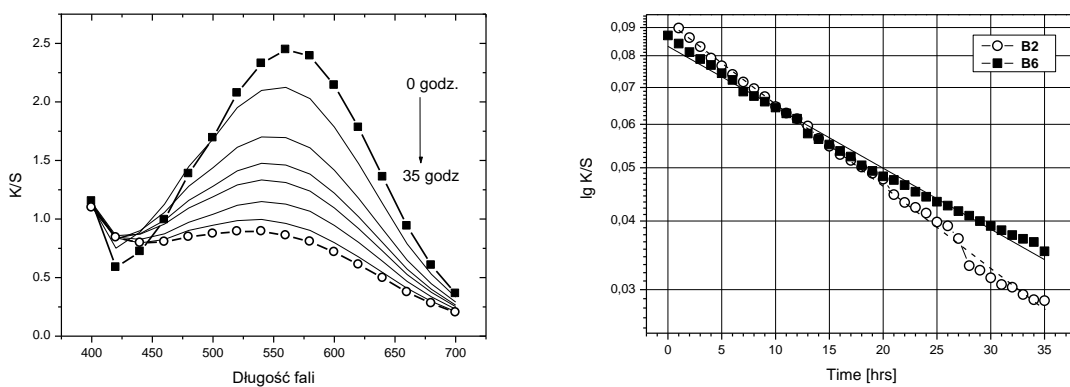
Fig.3. Example of changes in the relationship K/S = f(λ,T) for dyes: a)B4 and lg K/S =f (t) b) B2, B6.

Table 2 shows a straight lines equations and correlation coefficients R for the dyes B1-B6. In all cases the high values of correlation coefficients R for lgK/S=f (t) function were obtained which indicates that the discoloration of dyes follows the kinetics of the first order reaction.

Spectra of decomposition of dyes B2 and B6 after $0 \div 35$ hours are compared and illustrated in Figure 2.

Tab 2. The rate constants k of dyes decay, correlation coefficients R of $lg(K/S) = f(t)$ function and half-life $T_{1/2}$ [hrs] of $B1 \div B6$ dyes.

Dye	Substituent	$k \times 10^3$	R	$T_{1/2}$ [hrs]	σ_p [38]
B1	H	8.38	0.999	36.42	0.0
B2	NH_2	14.64	0.999	20.53	-0.620
B3	$N(C_2H_4OH)_2$	13.60	0.999	20.55	-0.810[*]
B4	NHC_2H_4OH	17.04	0.994	17.47	-0.680[*]
B5	NO_2	11.13	0.987	26.92	0.778
B6	OH	10.69	0.999	28.03	-0.370

[*] calculated values (Fig.4., Tab.3.)

The tested dyes are characterized by the presence of the strong group E_A – NO_2 in the *orto-* position to E_D - NHC_2H_4OH substituent. The presence of donor and acceptor substituents in *para-* position may affect the electron density of N-β-hydroxyethylamine group and the spatial structure of adjacent substituents. The group of B1 – B6 dyes have been selected to possess the greatest differences in σ-Hammett constants of substituents in *para*-position. Among them B5 has the strongest E_A substituent (*p*-NO_2), while B2 dye has the strongest E_D substituent (*p*-NH_2) [39]. The knowledge of the rate constants of decomposition reactions allows to determine the values of σ-Hammett constants for *N*-β-hydroxyethyl- and *N,N'*-(di-β-hydroxyethyl)amine substituents.

3.2. Spectrophotometric analysis of B1-B6 dyes in solution and on the dyed wool fabric

The unknown σ_p values for *N*-β-hydoxyethylamine and di(*N*-β-hydroxyethyl-amine) substituents were calculated based on $\lambda_{max} = f(\sigma_p)$ relationship for dyes in solution.

Tab. 3. The λ_{max} values of **B1** – **B6** in 50% Ac/H_2O solution and on the dyed wool fabric, and calculated σ_p-constants[*1]; 1 [50% Ac/H_2O], 2 [wool], 3 [EtOH, lit.40].

Dye	λ_{max} [nm]	λ_{max} [nm]	λ_{max} [nm]	σ_p[*1] [38]
B1	438	440	429	0.0
B2	504	520	499	-0.620
B3	556	560	508	-0.81[*1]
B4	526	540	519	-0.68[*1]
B5	356		---	+0.778
B5ion	---	[400][*2]	---	[+0.778]
B6		[500]	476	-0.370
B6ion	556[*2]		---	-0.81[*2]

[*1] calculated values σ_p (fig.4), [*2] absorption of ionic forms **B5ion**, **B6ion**.
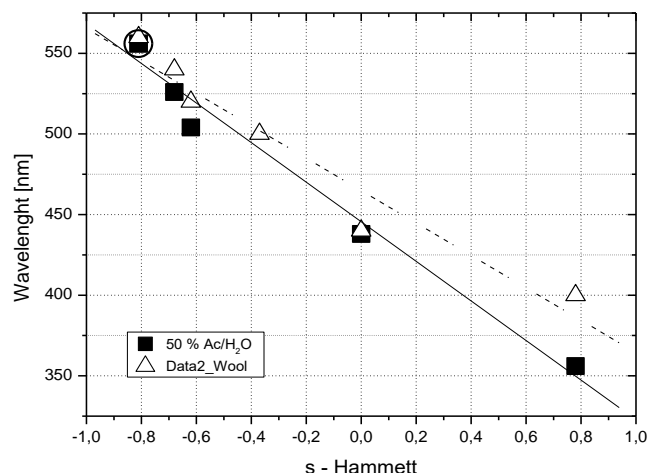
Fig. 4. A plot of $\lambda_{max} = f(\sigma)$ of B1-B6 (■ spectra in 50% Acetone/H$_2$O solution, △ reflectance spectra on wool). Relative error 5%.

Only the σ_p value for -NHC$_2$H$_4$OH (-0.87) is given in the literature [39].

The correlation coefficients of function $\lambda_{max} = f(\sigma)$ are:

50% Acetone/H$_2$O solution: $\lambda_{max} = (445.5 \pm 6.2) - (122.7 \pm 9.0) \times \sigma$:   R = -0.989

Wool: $\lambda_{max} = (464.8 \pm 7.6) - (100.5 \pm 12.4) \times \sigma$:   R = -0.970

   The tested dyes in 50% Acetone/H$_2$O solution show a slight hypsochromic effect (2-16nm) compared to dyes on wool (Tab. 3). A determination of correlations mentioned above allowed to calculate the unknown σ-Hammett values of *p*-NHC$_2$H$_4$OH and *p*-N(C$_2$H$_4$OH)$_2$ substituents, which are -0.68 (B4) and -0.81 (B3) respectively (in 50% Ac/H$_2$O solution, Tab. 3). Among the tested dyes, B5 and B6 show significant changes in $\Delta\lambda_{max}$ location in solution and on the fabric. Strong E$_A$ character of *o-* and *p*-nitro groups ($\Delta\lambda_{max} = 44$nm, bathochromic effect) and possible ionization of *p*-OH group ($\Delta\lambda_{max} = 56$nm, hypsochromic effect, pH = 9.5) can cause significant changes in the electron density in the molecules of analyzed dyes. The values of σ-Hammett constants, obtained from spectrophotometric study, help to illustrate dependence of the degradation rate of dyes as a function of σ_p-Hammett constants. An image of this relationship is shown in Fig. 4.
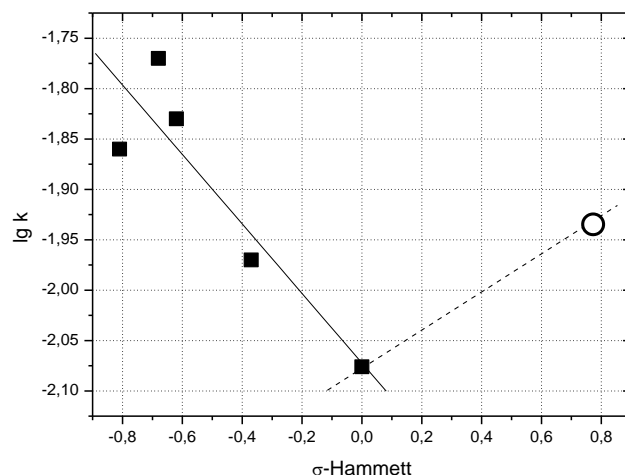
Fig. 5. The plot of the function lgk = f(σ) for **B1** – **B6** dyes (for 5% dyeing of wool).

As it can be seen in Figure 5, negative value of the slope of the straight line in the area of the value of influence parameter λ_{max}=f(σ) points to photooxidizing mechanism of decomposition reaction [41,42].

3.3. Structure analysis dyes B1 – B6 by AM1 method [36]

According to the literature [36], the spatial structure of dyes may be one of the reasons determining their resistance to light, washing...etc. This is determined by the ability to form intramolecular hydrogen bonds or intermolecular bonds with the polymer matrix (wool, collagen) or with the other dye molecule. These factors affect the ease of diffusion of molecules into the interior of the polymer, which in such a situation plays a protective role against the oxidizing and destructive effect, active in the photo-oxidation reaction of the singlet oxygen atom $^1O_2$. Analysis of the spatial structure of dyes B1 ÷ B7 and. analysis of changes in the total energy of the molecule as a function of changes in the rotation angle of the o-NO$_2$ group around the C─N bond and its position relative to the phenolic ring plane by the AM1 method was performed. First of all, attention was paid to the spatial structure of the N-β-hydroxyethylamine residue and the o-NO$_2$ group. The position of these groups will have a decisive influence on the possibility of hydrogen bond formation and the effects of coupling to the E_A or E_D substituent in the *para*-position. Analysis of the changes in the rotation energy of the o-NO$_2$ group as a function of the rotation angle relative to the phenyl ring E_R = f(α) is shown in Fig.6a and 6b.
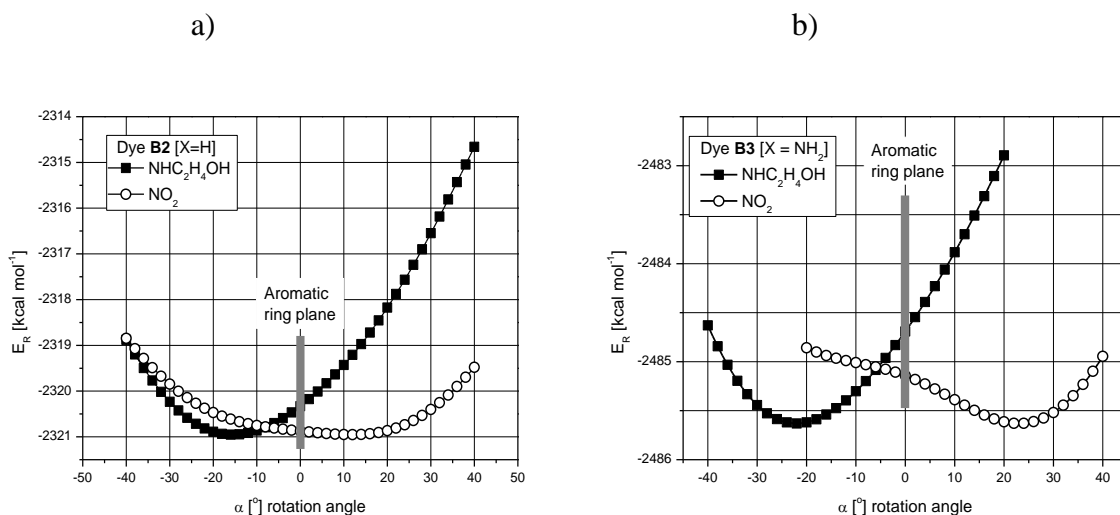
Fig. 6. Example analysis of changes in angle α and energy of E_R molecule due to rotation of group (a) -NO$_2$ (-○-) and (b) N-β-hydroxyethylamine (-■-) relative to the phenyl ring plane for dyes B2 and B3 calculated by AM1 method (table 6) in range -50° ÷ +50° (Fig.6a) and -45° ÷ +45° (Fig. 6b).

Analysis of the obtained quantities indicates that the position of the nitro group relative to the phenolic ring plane changes, as does the value of the energy that can accompany this change. For example, for dye B2, the optimal angle between the -NO$_2$ group and the phenyl ring at which the molecule has the lowest energy is 11.39°, while the energy barrier of rotation around the C─N bond is only 0.08kcal/mol. These values for dye B3 are respectively: 23.02° and ΔE_R = 0.49 kcal/mol. An analogous analysis of the change in rotation energy ΔE_R resulting from the rotation of the -NHC$_2$H$_4$OH group is respectively: 15.29° and 0.56 kcal/mol [B2] and 21.96° and 0.94 kcal/mol for [B3].
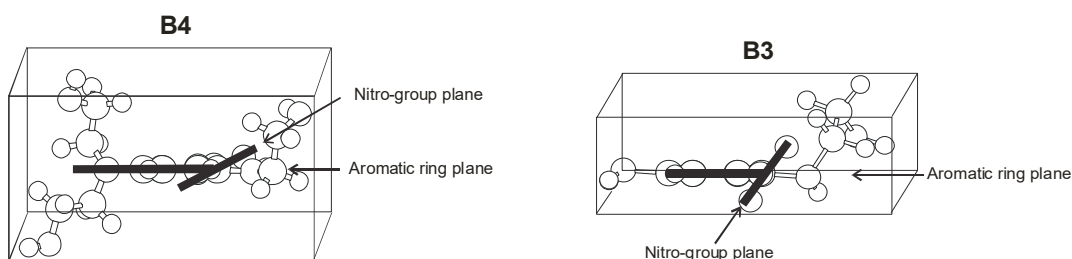
Rys.7. Spatial structure of dyes B4 and B3 and the position of the nitro group with respect to the aromatic ring for E_{min} of the molecule (Table 3).

A similar analysis was performed for the other dyes. The results of the analyses are quoted in Table 4.

Tab.4. Energy of calculated rotation barrier E_{min} dyes **B1** ÷ **B6** and *o*-nitroaniline (**oNA**), *m*-nitroaniline (**mNA**), *p*-nitroaniline (**pNA**), N,N-di(β-hydroxyethyl)amine (**NA**), 2,4-dinitro-N,N-di(β-hydroxyethyl)amine (**NDA**), angle values for α_{min}[NO2], α_{min}[NHR] (R = C_2H_4OH), α_{min} [X] and aromatic ring and corresponding energies for $\Delta E = E_\alpha - E_o$. α_{min}[NO2] and α_{min}[NH] - minimum torsion angle of *o*-NO_2 and -NHC_2H_4OH group to aromatic ring for E_{min}; (Fig.6); ΔE_{NO2}, ΔE_{NH} - energy difference corresponding to coplanar position of NO_2 or NHC_2H_4OH group relative to phenyl ring (Fig.5), $\Sigma\Delta E$ - total energy change, [1] ionized N-β-hydroxyethylamine group [$N^-C_2H_4OH$], l [Å] - bond length NH O (l_{min} (calc.) = 1. 530Å), α_{min} [X] torsion angle ─X relative to the phenyl ring, [2] 2-, 3- or 4-nitroaniline, [3] - sign - or + indicates torsion in front of or out of the plane of the phenyl ring (calculated by AM1 method), [4] N,N-di(β-hydroxyethyl)amine, [5] 2,4-dinitro-N,N-di(β-hydroxyethylamine)

Dye	*p*-X	E_{min} [kcal/mol][3]	α_{min} [NO$_2$] [°][3]	ΔE_{NO2} [kcal/mol]	$\Delta\alpha_{min}$ [NHR] [°][3]	ΔE_{NHR} [kcal/mol]	$\Sigma\Delta E$ [kcal mol^{-1}/ kJ mol^{-1}]	α_{min} [X] [°][3]	l [NH··O] [Å]
B1	H	-28.135	+11.35	0.072	+6.63	0.164	0.236/0.988	-----	2.0580
B2	NH$_2$	-27.803	+22.26	0.482	+18.06	0.939	1.421/5.949	[NH$_2$] +23.62	2.1043
B3	N(C$_2$H$_4$OH)$_2$	-121.355	+21.05	0.932	+50.38	2.554	3.486/14.595	[NR$_2$] -28.62	2.1409
B4	NHC$_2$H$_4$OH	-77.156	+21.29	0.415	+13.66	0.565	0.980/4.103	[NR] -27.85	2.0862
B5	NO$_2$	-22.607	+14.90	0.177	-0.09	0.003	0.180/0.753	[NO$_2$] -0.34	2.0536
B5ion	NO$_2$[1]	-69.941	+18.06	1.258	+2.32	0.139	1.397/---	[NO$_2$] +3.24	-----
B6	OH	-69.798	+20.06	0.387	+11.27	0.631	1.018/4.262	[OH] +1.88	2.0780
B6ion	O$^-$	-108.438	+26.10	1.017	+71.68	8.473	9.496/---	-----	2.1940
o-NA	[2-NO$_2$][2]	20.541	+4.27	0.010	-4.44	0.067	0.077/0.322	-----	2.0967
m-NA	[3-NO$_2$][2]	23.808	-1.20	0.0	-24.35	1.000	1.000/4.186	-----	-----
p-NA	[4-NO$_2$][2]	21.363	-1.60	0.0	-16.46	0.690	0.690/2.888	-----	-----
NA[4]	-----	-67.911	-----	-----	-39.82	42.71	-----	-----	-----
DNA[5]	NO$_2$	-60.052	+55.15	18.339	+59.03	107.807	126.146/---	[NO$_2$] +0.28	-----

In the dye B5 and its ionized form B5ion, there are very significant energy differences due to electrostatic interactions of the $-N^-C_2H_4OH$ group with the highly polar nitro group. The maximum E_R rotation energy differences for the NO_2 group are about 6.17 kcal/mol and 11.44 kcal/mol for B5ion, respectively. For B6 dyes and its ionic form B6ion, the values are close to each other, at 5.52 and 4.68 kcal/mol, respectively. In the latter case, the spatial structure of the N-β-hydroxyethyl-amine substituent is not changed only its E_D character due to ionization of the -OH group at the 4-position. These calculations further underscore the significant role played by substituents in position 4-. They affect not only the electronic and functional properties of the dyes (Table 2), but additionally their spatial structure (Table 4), which determines the interaction of the dye with the dyed wool fiber or hair keratin. Dyes B1 ÷ B6 and oNA form intramolecular hydrogen bonds (WWW) between the $-NO_2$ and $-$HNR groups (R=C_2H_4OH). Their strength depends on the magnitude of the twist angle relative to the phenyl ring plane. Ideally, these groups should be in its plane, because then the hydrogen bond is strongest and its length should be 1.530Å (AM1). In reality, as shown by the calculations performed, these distances are larger and amount to 2.058 ÷ 2.141Å. It also turned out that these values are affected by the type of substituent in position 4-. If it is a substituent of E_D nature (NH_2, NHR, NR_2), it is strongly tilted out of the plane of the ring by an angle of approx. 23 ÷ 29°, while if it is an E_A substituent (NO_2) it is only about 0.3 ÷ 3.2° and this is a typical value even for compounds in which hydrogen bonding does not occur i.e. in DNA, for example. The exception is the $-$OH (E_D) group, where this angle is 1.88°. The spatial structure of the dyes studied can significantly affect their crystal structure, in which a measure of the ordering of molecules is the change in the enthalpy of the phase transition during the melting process of the compound crystal. The strongly branched $-NR_2$ substituents are tilted out of the phenyl ring plane by 33 ÷ 60°, so they must affect the ability of the molecules to pack tightly in the crystal. They probably also affect the possibility of forming weak WWs or van der Waals. The lowest transformation enthalpies have compounds in which intermolecular hydrogen bonds (MWW) cannot form B1, oNA. A comparison of ΔH values of oNA and B1 also highlights the possibility that B1 can form an additional weak MWW bond through the $-$OH group with $-C_2H_4OH$, whose energy is 1.526kJ/mol. In dye B2, MWW can also be additionally formed by the $-NH_2$ group at the 4-position. The total energy change in this case is 10.798 kJ/mol, of which the $-NH_2$ group accounts for 10.185 kJ/mol. The extended $-$NHR substituent lowers the value to 9.864 kJ/mol (B4) while the additional $-C_2H_4OH$ group raises it to 21.330 kJ/mol (B3).

As the analysis of ΔH changes for B5 and B6 shows, the ability to form MWW is mainly determined by the E_D nature of the substituents, E_A substituents have less influence. Thus, for example, B5 has this energy of 3.380 kJ/mol (NO₂) while B6 is close to that of B2 at 9.966 kJ/mol. Calculations also indicate that in NA the ─NR₂ group does not lie in the plane of the ring and is tilted by 39.82°. The compound, moreover, under normal conditions, is in a semi-liquid state, so it should be assumed that it does not form intermolecular H-bonds.

4. Conclusions

Study on lightfastness of semi-pemanent dyes have been published. In this work research on lightfastness of *o*-nitro-*N*- β-hydroxyethylaniline derivatives used in commercially semi-permanent hair dyes was performed. Their photochemical decomposition rate, spectral properties in 50% Ac/H₂0 and on wool as well their electron structure were examined. As a result of irradiation, selected dyes B1-B6 are subject to photo degradation with the kinetics of the I-order reaction (Table 2). These changes are described by the relationship lg(K/S) = f(t), with correlation coefficient R = 0.987 - 0.999. Analysis of changes in function $\lambda_{max}^{sol} = f(\sigma)$ allowed to determine values of σ_p -Hammett constant for *N*-β-hydroxyetylamine (B4) and *N,N*-β-dihydroxydietylamine substituents (B3) (Table 3). Negative value of the slope coefficient of the function lgk = f(σ) indicates the oxidizing mechanism of the photodegradation of tested dyes. It was found that the values of energy ΔE_R necessary for the molecule to adopt a flat structure and be able to form intramolecular hydrogen bonds are 0.64 ÷ 1.43 kcal mol⁻¹. Electrostatic forces act on the dye molecule in the polymer matrix, affecting the rate of diffusion into the interior of the polymer matrix, the ability to form hydrogen bonds with the polymer or aggregation with other dye molecules. The cage of the polymer matrix is hindered by reactive singlet oxygen ¹O₂, so the rate of photochemical decomposition of dyes should also decrease. Factors related to the electron structure and spatial conformation of dyes, play no lesser role, however not fully explained. Such include the spatial structure of the substituents, i.e. their size and intermolecular aggregation, affecting the diffusion of the dye and the ability of the dye to form intramolecular hydrogen bonds (WWW), which has an impact on increasing the dyes' resistance to light. Literature data show that o-NO2aniline derivatives form WWW, but they are very weak, much weaker than, for example, in o-NO2phenol derivatives. However, there are no data on the possibility of such bonds being formed by o-NO2-N-β-hydroxyethylamine derivatives. The effect of o-substitution on intra- and intermolecular hydrogen bonds in nitroaniline derivatives was investigated using NMR, IR and AM1 calculation. Nitro and NHR

functionalities were approximately coplanar with the phenyl ring. The 2-nitroaniline derivatives formed an intramolecular hydrogen bond creating a six-membered chelate ring. The AM1 method was used to calculate the barrier energy of group rotation: NO_2 and NHR. The nitro group tilt angle from the phenyl ring plane was $+11.35 \div +26.10°$. The torsion of the NHR group against the C-C bond of the aromatic ring varies between $-0.09 \div +50.38°$. The dyes studied show the dependence of functional, spectrophotometric and performance properties on the geometric structure of the molecules. It affects the ability of molecules to form inter- and intramolecular hydrogen bonds, their aggregation, and the rate and possibility of diffusion of the dye into the interior of the polymer matrix. The easier this process is, the slower the rate of photochemical reaction, as the "availability" and rate of diffusion into the dye molecule in the "cage" of the polymer of excited oxygen in the singlet $^1O_2$ state decreases. The individual dyes forming a mixture of color decompose with diverse speed after the process of their application which results in a color change of dyed hair. This is the result of different lightfastness of *o*-nitro-N-β-hydroxyethylaniline derivatives used in cosmetic formulations for dyeing hair.

References

[1] Ballarin B., Galli, S., Morigi M.: *Study of dyeing properties of semipermanant dyestuffs for hair*, Int.J.Cosm.Sci. **29**, 2007, pp. 49-57.

[2] Pohl S., Hnatchenko M. (Clariol Inc.), US4776855 A; 1988.

[3] Schrader D., Neuhaus W. (Henkel), US4927627 A; 1990.

[4] Brown K.C., Pohl S., Kezer A.E., Cohen D.: *Oxidative dyeing of keratin fibers*, J. Soc. Cosmet. Chem. **36**, 1985, p. 31.

[5] Zviak C.: *Oxidation Coloring" in "The Science of Hair Care"*, ed.C Zviak, E Marcel Dekker, NYork 1986;

[6] Tucker H H.: *Coloring of human hair with semipermanent dyes*, J. Soc. Cosmet. Chem., **22**, 1971, p. 379.

[7] Venkataraman K.: „*The Chemistry of Synthetic Dyes.Vol.VI*", Academic Press, NYork 1972

[8] Draelos Z.K.: *Hair cosmetics*, Dermatol Clin. **9**, 1991, pp. 19-27.

[9] Corbett J.F.: *The chemistry of hair-care products*, J.S.D.C. **92,** 1976, pp. 285-303.

[10] Madnari N., Khan K.: *Hair cosmetics*, Indian J.Dermatol.Venereol Lepro. **79**(5), 2013,pp.654-67.

[11] Corbett J.F.: *Hair dyes – their chemistry and toxicology*, Cosmet.Toilet **91,** 1976, pp. 21-28.

[12] Guthrie J.T., Kazlauciunas A., Rongong L., Rush S.: *The Characterization Of Treated And Dyed Hair*, Dyes Pigm., **29,** 1995, pp. 3-44.

[13] Fishman H.M., Harvey M.: *Nonpermanent hair dyes,* Household Pers.Prod.Ind, **25,** 1988, pp.62-99.

[14] Dario M.F., Baby A.R., Velasco M.V.R., *Effects of solar radiation on hair and photoprotection*, J.Photochem.Photobiol.,B:Biology, **153**, 2015, pp. 240-6.

[15] Dawber R.: *Hair: Its Structure and Response to Cosmetic Preparations*, Clinics in Dermatology, **14,** 1996, pp. 105-112.

[16] O'Donoghue M.N.: *Hair care products*. In: Olsen EA, editor. Disorders of hair growth. New York: McGraw-HilI, 1994, pp. 386-7.

[17] Halal J.: *Hair Structure and Chemistry Simplified. IV Ed.*, Milady Thompson Learning, Canada (2002).

[18] Bouillon C., Wilkinson J.: *The Science of Hair Care. II Ed.*, Taylor and Francis, London (2004).

[19] Yoshio T., Yoshikaru Y., Kuniaki S.: US4961925; 1995.

[20] Szadowski J., Przybylski C.: *Relationship Between the Structure of Nitrodiphenylamine Derived Monoazo Acid and their Spectroscopic and Fastness Properties*", Dyes Pigments **5**, 1984, 49.

[21] Asquith R., Peters A., Wallach F.: *Fading of Nitrodiphenylamine Disperse Dyes in Relation to their Structure and Ultraviolet Absorption Spectra*, J.Soc.Dyers Colour., **84**, 1968, 507.

[22] Kuramoto N., Kitao T.: *The Photofading Of 1-Arylazo-2-Naphthols In Solution .2. Contribution Of Photo-Reduction To The Anomalous Photofading Of 1-(Para And Ortho-Nitrophenylazo)-2-Naphthols In Alcoholic Solvents*, J. Soc. Dyers Colour., **96** , 1980, 529.

[23] Skulski L. (*doctor thesis*), Ed.Technical University of Warsaw, 1966.

[24] Lewis D., Mama J., Hawkes J.: *A Review of Aspects of Oxidation Hair Dye Chemistry with Special Reference to N-Nitrosoamine Formation*, Materials **6,** 2013, pp. 517-534.

[25] Mirvish S.S.: *Formation of N-nitroso compounds-chemistry, kinetics, and in vivo occurrence*, Toxicol.Appl.Pharmacol. **31**, 1975, pp. 325-351.

[26] European Commission Scientific Committee on Consumer Safety (SCCS), „Opinion on Nitrosamines and Secondary Amines in Cosmetics Products". Online: http://ec.europa.eu/health/scintific_committees/consumer_safety/docs/sccs_o_090.pdf

[27] Commission Regulation (EU) No. 658/2013, Official Journal of the EU, L 190, vol.56, 11 july 2013 amending Annexes II and III to Regulation (EC) No 1223/2009 of the European Parliament and of the Council of 30 November 2009 on cosmetic products.

[28] Pudov W.S., Buchachenko A.L.: *Radical Degradation and Stabilisation Reactions of Solid Polymers*, Russ. Chem. Rev., **39**, 1970, 70.

[29] Heikkinen S., Pitkaniemi J., Sarkeala T., Halila N., Koskenvuo M.: *Does Hair Dye Use increase the Risk of Breast Cancer? A Populatio-Based Core-Control Study of Finnish Women*, PLoS ONE 8/11/2015, **vol.8** (10), pp.1-14.

[30] National Institute of Advances Industrial Science and Technology NIAST (date of access 05.2014, http://sdbs.db.aist.go.jpn)

[31] Pat.GB 812211, (Loreal),

[32] Pat.GB707618,1080154 (Unilever),

[33] [CAS No 1945-92-2]; info@chemsigma.com and www.chemlab613.com/cas/1945-92-2.html.

[34] Kubelka P., Munk F., *Ein Beitag zur Optic der Farbenstriche*, Z.Techn.Physik. **12,** 1931, 593.

[35] Perkampus H.H.: *UV-VIS Spectroscopy and Its Application*, Springer-Verlag, Berlin 1992, p.95

[36] Dewar M.J.D., Zoebisch E.G., Healy E.F., Stewart J.J.P.: *The Development and Use of Quantum-Mechanical Molecular-Models. 76. AM1-A New General-Purpose Quantum-Mechanical Molecular-Model*, J.Am.Chem.Soc. **107**, 1985, 3902.

[37] Dewar M.J.S., Dieter K.M.: *Evaluation of AM1 calculated proton affinities and deprotonation enthalpies*, *J.Am.Chem.Soc.*, **108,** 1986, 8075.

[38] Majerz I., Dziembowska T.:„*Geometric Aspects of Aromaticity: Interrelation between Intramolecular Hydrogen Bonds, Steric Effects and π-Electron Delocalisation in Nitroanilines*”, *Eur.J.Org.Chem.*, 2011, 280.

[39] D H McDaniel, H C Brown, „*An Extended Table of Hammett Substituent Constants Based on the Ionisation of Sustited Benzoic Acids*”, J.Org.Chem., **23**, 1958, 420

[40] K Y Chu, J Griffiths, " *Colour and Constitution of the Nitro- and Dinitro-p-phenylenediamines and their N-Methyl Derivatives*”, J.S.C.Perkin I 1978, 1194.

[41] H.Zollinger, "*Colour Chemistry*”, VCH Weinheim 1991.

[42] H.Meier, "*Photochemistry of Dyes" in "The Chemistry of Synthetic Dyes*”, vol.IV ed. K.Venkataraman, 1971, 389.

Analysis of rheological properties of potato starch pastes as a potential binding liquid in the granulation process

Analiza właściwości reologicznych kleików skrobi ziemniaczanej jako potencjalnej cieczy wiążącej w procesie granulacji

Magdalena Orczykowska*

Lodz University of Technology, Faculty of Process and Environmental Engineering

ul. Wólczańska 213, 90-924 Łódź

Abstrakt

W pracy przedstawiono ocenę właściwości reologicznych kleików komercyjnej skrobi ziemniaczanej, jako źródła stanowiącego ciecz wiążącą w procesie granulacji jedno i wieloskładnikowych materiałów sypkich poprzez zastosowanie modelu Carreau-Yasudy. Na podstawie uzyskanych wyników stwierdzono, że wysokie wartości lepkości kleików skrobiowych i znacząca sztywność ich struktury wewnętrznej nie są gwarancją odporności tej struktury na działanie sił zewnętrznych, mogą ponadto obniżać efektywność samego procesu granulacji.

Abstract

The paper presents an assessment of rheological properties of commercial potato starch pastes as a binding liquid source in the process of granulation of single and multi-component loose materials using by Carreau-Yasuda model Based on the obtained results, it was found that high viscosity values of starch pastes and significant stiffness of their internal structure are not a guarantee of resistance of this structure to external forces, and may also reduce the efficiency of the granulation process itself.

Słowa kluczowe: skrobia ziemniaczana, lepkość, granulacja, materiały sypkie

Keywords: potato starch, viscosity, granulation, loose materials

1. Introduction

Starch is one of the most important plant polysaccharides. It is a biodegradable, non-toxic and fully biocompatible natural polymer. It is a reserve material of plants and is deposited in their tissues in the form of grains, the so-called granules, the shape and size of which depend on the botanical origin of the starch. Starch is a white solid substance, tasteless and odorless, which has found its application in many industries. In the food industry, starch has been used as a starting material for the production of hydrolysates (glucose, maltodextrin, starch syrups) and as a raw material for the production of modified starches. In baking, it is used as a bread ingredient that improves water retention and delays staleness of bread, and as an addition to pastry products. In the production of food concentrates, it is used as a thickener in powdered food (sauces, soups, puddings, jellies) and ketchups. In the textile industry, it is used for gluing yarn and starching. In the paper industry, it is needed for dyeing, satining, printing and finishing, as well as for gluing paper pulp. In the chemical industry, it has found application in the production of glues, dextrins, and even in the production of explosives. In the pharmaceutical industry, it is used for the production of baby powders, talcum powders and pills for medicines, as well as a functional additive to cosmetics. So many specialty applications of starch and its derivatives enable manufacturers to develop a range of products related to technical applications. Thanks to all these possible applications, starch as a functional material turned out to be irreplaceable in many industries. This also results in the search for new sources of its acquisition, so it should not be surprising that research on starch obtained from kiwifruit *(Actinidia deliciosa)* [1], banana *(Musa paradisiaca)* [2], common pea *(Pisum sativum)* [3], acorns *(Quercus ilex L.)* [4], or chestnuts *(Castanea sativa Mill.)* [5]. However, it is also unique because it is a hydrocolloid showing a large physicochemical diversity with an unchanged chemical structure. The starch molecule has a heterogeneous structure, composed of amorphous linear structures - amylose and

branched crystalline structures - amylopectin - Fig. 1. It is the content of amylose and amylopectin in starch granules that determines its technological usefulness and physicochemical properties.
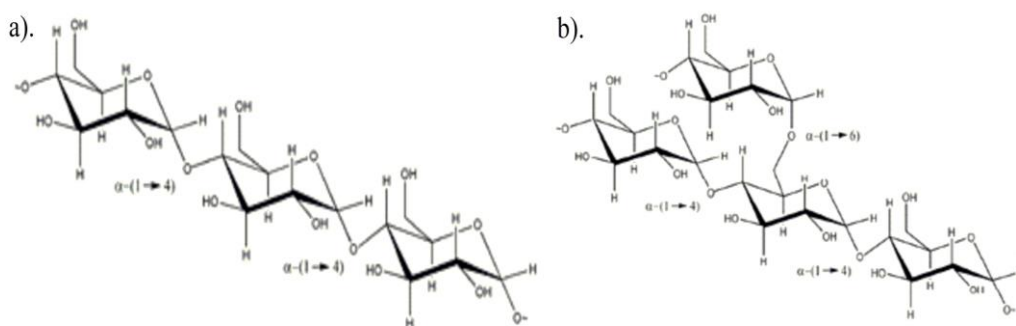
Fig. 1. Structure of molecules: a). amylose, b). amylopectin [6].

Starch, or rather a suspension of starch granules subjected to the heating process, creates the so-called paste, in which dissolved starch granules (amylose) form a continuous phase, and swollen remains of granules (amylopectin) act as fillers. It should be noted, however, that in the process of heating starch granules obtained from edible tubers (e.g. potato and tapioca starch), the primary structure of the granules is completely destroyed and a homogeneous suspension of macromolecules or their aggregates is obtained. Hence the pastes of these starches resemble opalescent solutions. It is the possibility of obtaining a homogeneous paste from potato starch that may predispose it to be used as a binding liquid in the granulation process. The granulation of powdered materials and the accompanying processes, such as mixing or grinding, depend to a large extent on the physical and rheological properties of the materials involved. Previous studies [7-10] have shown that the properties of the wetting liquid affect the nucleation and, consequently, the granulation effect, especially when it comes to the formation of agglomerates from materials that are difficult to combine, such as mixtures of

biomass and mineral materials. It is the binding liquid that is responsible for producing a granular product with the desired properties. Despite the wide spectrum of research, there are no models that would take into account the impact of rheological parameters on granulation, describing both the properties related to the viscosity and elasticity of binding liquids.

Therefore, the aim of the presented work is to evaluate the rheological properties of pastes obtained from domestic, commercial potato starches in terms of their usefulness as binding liquids for the granulation process of loose materials..

2. Materials and Methods

The research material was commercial potato starch from various companies of the potato industry, operating on the domestic market and available in every grocery store. These starches were: starch Superior Standard from Trzemeszno and Grula brand starch also from Trzemeszno, Jermapol starch from Konopnica, Niechlów starch from Niechlów, and Melvit starch from Kruki.

In the tested commercial samples of potato starches, the content of amylose was determined using the spectrophotometric method with iodine according to Morrison and Laingelet [11]. Absorbance measurements were performed at a wavelength of λ=640nm using a Specord M42 spectrophotometer (Carl Zeiss, Germany).

Potato starch samples in the form of 5% aqueous suspensions were gelatinized at 95^0C for 90 minutes. After the gelatinization process was completed, the samples were cooled for 60 minutes. The gelatinized starch samples were then left at rest for a further 60 minutes at an ambient temperature of 25^0C to remove any air bubbles. After this time, the paste sample was placed in the measurement system of the rotational rheometer and left to rest for 30 minutes at a constant temperature of 25^0C to reach thermal and mechanical equilibrium. The rheological properties of the tested potato starches were determined using a Physica MCR 301 rotational rheometer by Anton Paar in a cone-plate measuring system with a cone diameter of

50 mm, an angle of inclination of 10 and a distance between the measuring elements, i.e. a cone and a plate of 0.048 mm. Rheological tests were carried out to measure the viscous properties of the tested samples of commercial potato starch in the range of shear rate from 0.001 to 100s-1, i.e. in the range of five logarithmic decades, taking 6 measurement points for each decade of shear rate.

The Carreau-Yasuda model [12-14] was used to describe the viscosity curves obtained as a result of rheometric measurements:

$$\eta(\dot{\gamma}) = [1 + (\lambda \cdot \dot{\gamma})^a]^{\frac{(n-1)}{a}} \cdot \left(\eta_0 - \eta_\infty \right) + \eta_\infty \qquad (1)$$

where the rheological parameters of this model are:

η_0 i η_∞ - the zero-shear viscosity and the infinity-shear viscosity, [Pa·s], λ - time constant, [s], n - time constant, [-], a - width of the transition region between Newtonian and power-law behavior, [-].

Determination of the rheological parameters of the Carreau-Yasuda model (especially the time constant λ) made it possible to determine the critical value of the shear rate γ_{cr} at which the transition from the behavior typical of Newtonian fluids to the behavior characteristic of non-Newtonian fluids occurs. The numerical value of this shear rate is given by the equation:

$$\gamma_{cr} = \frac{1}{\lambda} \qquad (2)$$

γ_{cr} – the critical shear rate denoting the one of shear-thinning behavior [s^{-1}]

At the same time, the knowledge of the viscosity η_0 (obtained as an independent variable, directly from rheometric measurements) and the time constant λ determined from the Carreau-Yasuda model allowed to determine the value of the shear stress τ_{cr} at which the Newtonian behavior of the fluid changes to the behavior typical for a non-Newtonian fluid:

$$\tau_{cr} = \frac{\eta_0}{\lambda} \qquad (3)$$

τ_{cr} – the critical shear stress at the transition between Newtonian and power-law regions [Pa].

Thus, thanks to the determined parameters of the Carreau-Yasuda model, two additional parameters were obtained to characterize the viscous properties of the starch pastes tested.

Mathematical analysis concerning the determination of rheological parameters of the Carreau-Yasuda model was carried out using non-linear regression methods from the Excel program. One of the tools of this program was used, namely the Solver add-on, used to solve the mathematical modeling task, i.e. to find such parameters of the mathematical model that the tested lubricants could be described in the best possible way. Using the numerical minimization procedures that the Solver tool uses, local minimization procedures were used. Therefore, for a multimodal objective function having many local minima, a solution was found that depended on the initial value of the objective function's independent variables. One of the initial values of the independent variables of the objective function was the experimentally determined value of zero viscosity η_0.

In order to assess the correctness of the description of the experimental data with the Carreau-Yasuda model equation, a statistical evaluation of the fit of the model curves to the experimental curves was carried out in relation to the value obtained directly from the rheometric measurements of the apparent viscosity η. This assessment was made by estimating the effectiveness of modeling R^2.

3. Results and Discussion

Table 1 presents the results of determining the amylose content, and thus amylopectin, in the tested samples of commercial potato starch. The data presented in Table 1 shows that commercial potato starches differ in terms of amylose and amylopectin content, and these differences can be significant - the difference between potato starch with the highest amylose content (Trzemeszno Superior Standard starch) and potato starch with the lowest amylose content (Melvit starch). This is probably due to from the starchiness of potato varieties used for the

production of commercial potato starches.

Tab. 1. Content of amylose and amylopectin in the tested potato starches

Potato Starch	Amylose content [%]	Amylopectin content [%]
Trzemeszno Superior Standard	39.38	60.62
Niechlów	37.30	62.70
Jermapol	37.17	62.83
Trzemeszno brand Grula	35.95	64.05
Melvit	14.99	85.01

The graph in Fig. 2 shows the viscosity curves for all tested samples of commercial potato starch and Table 2 presents the values of rheological parameters obtained as a result of describing the viscosity curves with the Carreau-Yasuda model.

The analysis of the obtained experimental data presented in Fig. 2 allowed to conclude that for all the tested samples of potato starch, the apparent viscosity decreases with the increase of the shear rate. This indicates that the tested pastes of commercial potato starch should be treated as non-Newtonian media, shear thinned media. The shape of viscosity curves obtained from rheometric measurements, which shows zero viscosity η_0 at low shear rate values, justifies the choice of the Carreau-Yasuda model to evaluate the rheological properties of the starch pastes tested. The analysis of the data presented in Table 2 shows that:

- the highest value of viscosity η_0 at the zero shear rate is characteristic for Superior Standard potato starch from Trzemeszno, while the lowest value of zero viscosity is shown by Melvit potato starch,

- the width of the transition area between Newtonian and non-Newtonian behavior is the largest for potato starch from Trzemeszno, brand Grula, and the smallest for potato starch from Niechlów,

- the time constant λ, reflecting the susceptibility of the internal structure to

destruction by shearing, has the highest value for Superior Standard potato starch from Trzemeszno, and the lowest for Melvit potato starch from Kruki,

- Jermapol potato starch has the highest value of the characteristic flow index, whereas potato starch from Niechlów has the lowest value,

- the critical value of the shear rate at which the behavior of the pastes changes from Newtonian to non-Newtonian, i.e. when the apparent viscosity of the starch paste begins to decrease, is the highest for Melvit potato starch, and the lowest for Superior Standard potato starch from Trzemeszno,

- the values of the critical shear stress at which the starch gruel begins to show the characteristics of a non-Newtonian fluid are the highest for Superior Standard potato starch from Trzemeszno, the lowest for Melvit potato starch.
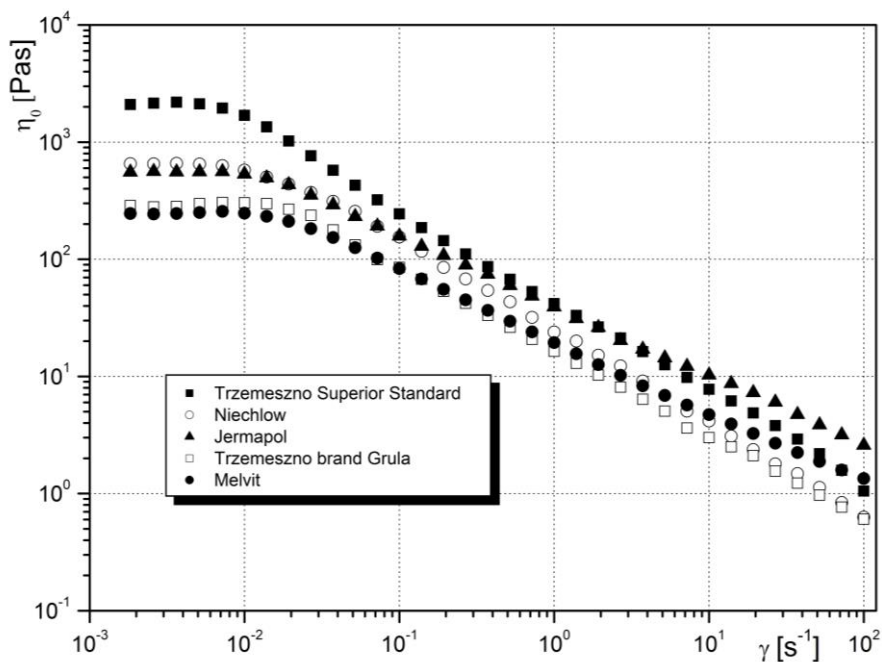
Fig. 2. Viscosity curves of the pastes of the tested potato starches.

Tab. 2. Rheological parameters of the Carreau-Yasuda model

Potato Starch	η_0 [Pa·s]	a [-]	λ [s]	n [-]	γ_{cr} [s^{-1}]	τ_{cr} [Pa]	R^2 [-]
Trzemeszno Superior Standard	2300.0	1.897	123.457	0.187	0.0081	18.630	0.999
Niechlów	675.0	1.249	99.010	0.178	0.0101	6.817	0.998
Jermapol	600.0	2.044	79.365	0.387	0.0126	7.560	0.998
Trzemeszno brand Grula	298.0	4.269	61.728	0.292	0.0162	4.828	0.998
Melvit	256.0	2.673	57.803	0.376	0.0173	4.429	0.997

For all the starch pastes tested, a very high matching efficiency was obtained, at the level of 0.997÷0.999. In order to better illustrate the nature of changes in the obtained rheological parameters of the Carreau-Yasuda model, some of them, i.e. zero viscosity η_0 and time constant λ as a function of amylose content in starch, are presented graphically in Figure 3. This graph clearly shows that with increasing amylose in potato starch, the value of zero viscosity increases η_0. At the same time, it is also accompanied by an increase in the time constant λ and the critical shear stress τ_{cr}.

The high value of the time constant for the potato starch paste Superior Standard from Trzemeszno means that this paste has a structure most susceptible to destruction by shearing. This may indicate the low mechanical stability of its structure, which is also not guaranteed by high values of the critical shear stress τ_{cr}, which here reflects the rigidity of this structure. Of all the tested potato starch pastes, it is Melvit starch, i.e. the starch with the lowest amylose content, as 14.99%, seems to be the one whose internal structure is resistant to damage caused by external force (low values of constant λ and structure stiffness in stress value τ_{cr}). The internal structure with very similar rheological properties has a paste made of starch from Trzemeszno, but of the Grula brand - its viscosity η_0 is higher by 42Pas, the time constant λ by less than 4s, and the stiffness of the internal structure by 0.4Pa.
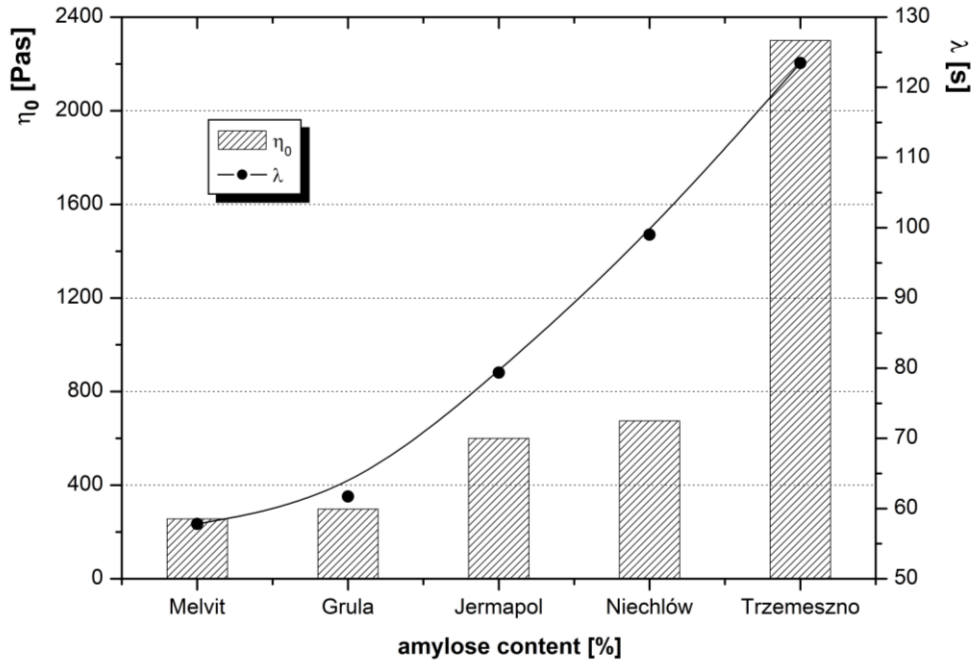
Fig. 3. Changes in some rheological parameters of the Carreau-Yasuda model.

What distinguishes Grula starch from Melvit starch is the width of the transition area between Newtonian and non-Newtonian behavior, the value of which is 1.596. This area, defined in the Carreau-Yasuda model by the parameter a, can be identified with the polydispersity of the PDI medium, which in turn may indicate that the polydispersity of potato starch Grula from Trzemeszno is greater than that of Melvit starch. Potato starches Jermapol and Niechlów have over 2 times higher zero viscosity η_0 and almost 2 times higher time constant λ with 1.5 times higher structure stiffness in the form of τ_{cr}. In addition to the susceptibility of the internal structure of the potato starch pastes to damage caused by shear forces present in the granulation process, it may also result in difficulties in uniform distribution of these pastes as binding liquids over the granulated material.

4. Conclusions

The assessment of rheological properties of pastes obtained from commercial potato starch as a material for the binding liquid in the granulation process allowed to conclude that:

- starch pastes are non-Newtonian fluids, shear thinning, the apparent viscosity of which decreases with increasing shear rate,
- high content of amylose in starch, which translates into high viscosity of the paste, does not guarantee the resistance of the structure of this paste to external forces,
- high stiffness values of the internal structure are not a guarantee of its mechanical stability,
- high values of both viscosity and stiffness of the paste may be an obstacle to the even distribution of the binding liquid over the granulated bulk material, which may consequently contribute to the low efficiency of this process.

However, commercial potato starch can be a valuable and relatively cheap source for granulating loose materials, and the characteristics of its pastes will be responsible for producing a granulated product with the desired properties.

References

[1] Stevenson D.G., Johnson S.R., Jane J.L., Inglett G.E.: *Chemical and Physical Properties of Kiwifruit (Actinidia deliciosa) starch.* Starch/Stärke **58**, 2006, pp. 323-329.

[2] Zhang P., Whistler R.L., BeMiller J.N., Hamaker B.R.: *Banana starch: production, physicochemical properties, and digestibility - a review.* Carbohydrate Polymers **59**, 2005, pp. 443–458.

[3] Ratnayake W.S., Hoover R., Warkentin T.: *Pea starch: Composition, structure and properties - a review.* Starch/Stärke **54**, 2002, pp. 217–234.

[4] Stevenson D.G., Jane J.L., Inglett G.E.: *Physicochemical properties of Pin Oak*

(Quercus palustris Muenchh.) acorn starch. Starch ∕ Stärke **58**, 2006, pp. 553–560.

[5] Correia P., Cruz-Lopes L., Beirao-da-Costa M.L.: *Morphology and structure of chestnut starch isolated by alkali and enzymatic methods.* Food Hydrocolloids **28**, 2012, pp. 313–319.

[6] Gunther T.: *Skrobia i jej pochodne.* Polskie towarzystwo Technologii Żywności, Kraków (2010).

[7] Xue B.C., Liu T., Huang H., Liu E.B.: *The effect of the intimate structure of the solid binder on material viscosity during drum granulation.* Powder Technol. **253**, 2014, pp. 584–589.

[8] Gluba T., Obraniak A.: *Nucleation and granule formation during disc granulation process,* Physicochem. Prob. Mineral Process. **48**, 2012, pp. 113–120.

[9] Obraniak A.: *Analysis of the phenomenon of nuclei mass transfer during the disc granulation.* Przem. Chem. **96**, 2017, pp. 241–244.

[10] Obraniak A., Orczykowska M., Olejnik T.P.: *The effects of viscoelastic properties of the wetting liquid on the kinetics of the disc granulation process.* Powder Technol. **342**, 2019, pp. 38-334.

[11] Morrison W.R., Laignelet B.: *An improved colorimetric procedure for determining apparent and total amylose in cereal and other starches.* J. Cereal Sci. **1**, 1983, pp. 9-20.

[12] Zare, Y., Park, S.P., Rhee, K.Y.: *Analysis of complex viscosity and shear thinning behavior in poly (lactic acid)/poly (ethylene oxide)/carbon nanotubes biosensor based on Carreau–Yasuda model.* Results in Physics **13**, 2019, pp. 1-8.

[13] Wu, Y., Guo, R., Gao, N., Sun, X., Sui, Z., Guo, Q. *A systematical rheological study of polysaccharide from Sophora alopecuroides L. seeds.* Carbohydrate Polymers **180**, 2018, pp. 63-71.

[14] Dziubiński M., Kiljański T., Sęk J.: *Podstawy reologii i reometrii płynów.* Wydawnictwo Politechniki Łódzkiej, Łódź (2009).

Assessment of rheological properties of selected viscosupplements used in knee osteoarthritis

Ocena właściwości reologicznych wybranych wiskosuplementów stosowanych w chorobie zwyrodnieniowej stawów kolanowych

Magdalena Orczykowska*

Lodz University of Technology, Faculty of Process and Environmental Engineering

ul. Wólczańska 213, 90-924 Łódź

Abstrakt

W pracy przedstawiono ocenę właściwości reologicznych wiskosuplementów opartych na bazie kwasu hialuronowego, a powszechnie stosowanych w chorobie zwyrodnieniowej stawów kolanowych. W oparciu o pomiary reometryczne wyznaczono moc i gęstość usieciowania oraz charakterystyczne wymiary liniowe sieci tych wiskosuplementów. Wykazano, że przebadane wiskosuplementy cechują się siecią luźno splątanych łańcuchów, które mogą tworzyć podobny, bądź zróżnicowany typ struktury.

Abstract

The paper presents an evaluation of the rheological properties of viscosupplements based on hyaluronic acid, commonly used in knee osteoarthritis. On the basis of rheometric measurements, cross-linking power and density of network as well as characteristic linear dimensions of the networks of these viscosupplements were determined. It has been shown that the tested viscosupplements are characterized by a network of loosely entanglement chains that can form a similar or different type of structure.

Słowa kluczowe: wiskosuplementy, kwas hialuronowy, właściwości reologiczne, moc usieciowania

Keywords: viscosupplements, hyaluronic acid, rheological properties, cross-linking power of network

1. Introduction

Hyaluronic acid, also called hyaluronan, was discovered in 1934 by Meyer and Palmer in the vitreous fluid of the bovine eye [1,2]. Today it is known that it occurs in all vertebrates - it is part of the basic substance of connective tissues such as cartilage, dermis or umbilical cord, and is also a component of synovial fluid and the already mentioned vitreous fluid. On an industrial scale, hyaluronic acid is most often obtained by extraction from rooster combs, as well as biotechnologically, in a process consisting of bacterial fermentation, extraction and purification [3,4]. From a chemical point of view, hyaluronic acid is a glycosaminoglycan composed of repeating disaccharide subunits connected by a β1-4 glycosidic bond. Each of them consists of D-glucuronic acid and N-acetyl-D-glucosamine, between which there is a β1−3 bond [5-7] – fig.1.
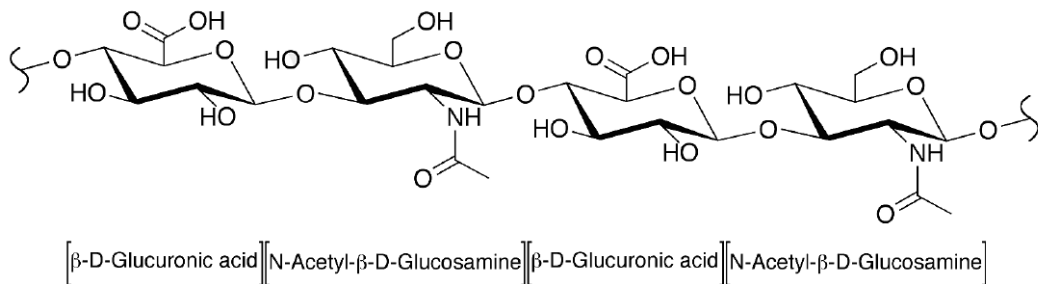
Fig. 1. Structure of hyaluronic acid [6].

Intensive research on hyaluronic acid, conducted from the moment of its discovery to the present, has shown that as a biocompatible, non-immunogenic and biodegradable compound, and at the same time having viscoelastic properties, it is perfectly suitable for use in medicine, cosmetics and pharmacy. Hyaluronic acid turned out to be particularly useful in the treatment of osteoarthritis of the synovial joints, and above all of the knee joint, improving its biomechanical conditions [2,6]. The concentration of hyaluronic acid in the synovial fluid decreases with age. This decrease is particularly pronounced when the degenerative process in the joint

progresses simultaneously with the aging process. Then, the ability of the synovial fluid to protect the cartilage and synovial membrane is reduced, which in turn leads to pain. Improvement of the patient's condition can be achieved by a series of several injections of preparations based on hyaluronic acid derivatives, i.e. viscosupplementation [8-10]. There are several preparations for viscosupplementation on the pharmaceutical market. However, they are not identical, which means that they differ in the form and origin of the hyaluronic acid contained in them and the molecular weight of the polysaccharide, but above all they differ in rheological properties.

Therefore, the aim of the presented study is to evaluate the rheological properties of selected hyaluronic acid preparations, commonly used in viscosupplementation during the treatment of knee osteoarthritis.

2. Materials and Methods

The research material consisted of three commercial preparations of hyaluronic acid - Ostenil, Hyalubrix and Orthovisc - see table 1.

Tab. 1. Properties of commercially viscosupplements

Commercially viscosupplements	Concentration [mg/ml]	Source	Molecular weight [kDa]
OSTENIL (by Trb Chemedica)	20mg/2ml	biofermentation	1000-2000 (~1200)
HYALUBRIX (by Fidia Farmaceutici)	30mg/2ml	biofermentation	>1500
ORTHOVISC (by Anika Therapeutics)	30mg/2ml	biofermentation	1100-2900

Intra-articular injection solutions, directly from the syringe, were placed in the measurement system of the rotational rheometer and left at rest for 1 h at a constant temperature of 37^0C to reach thermal and mechanical equilibrium. The rheological properties of the tested viscosupplements were determined using a Physica MCR 301 rotational rheometer by Anton Paar in a cone-plate measuring system with a

cone diameter of 50mm, an angle of inclination of 1^0 and a distance between the measuring elements, i.e. a cone and a plate of 0,048mm. The basic tests were carried out in dynamic conditions in the controlled strain mode, determining the mechanical spectra by measuring the values of the storage modulus G' and the loss modulus G" and the complex viscosity η*. The tests were carried out in the range of changes in the oscillation frequency ω from 0,01rad/s to 300rad/s, taking 6 measurement points for each decade. For all oscillation frequencies, the same relative deformation value of 5% was assumed, determined in earlier studies on the range of linear viscoelasticity of the tested viscosupplements.

A comprehensive assessment of the rheological properties of the tested viscosupplements was based on determining the characteristic linear features of the network created by the viscosupplement. In order to know the linear dimensions of the network, it was additionally necessary to know such parameters as: the value of the plateau viscoelastic modulus $G_N{}^0$, i.e. the cross-linking power, the value of the cross-linking density ω_0 and the value of the viscosity under steady-state flow conditions η_0. Taking into account the data presented in Table 1 regarding the molecular weight of the tested viscosupplements, they were treated as polydisperse materials, i.e. those in which the molecular weight distribution is statistically large. Therefore, the value of the viscoelastic modulus of the plateau $G_N{}^0$ [11-13] was determined from the following relationship:

$$G_N{}^0 = \frac{4}{\pi} \int_{-\infty}^{\omega_{max}} G''(\omega)\, d\ln \omega \qquad (1)$$

Obtaining the value of the viscoelastic modulus of the plateau $G_N{}^0$ made it possible to determine the characteristic linear dimensions of the network of the viscoelastic material tested (according to the markings presented in Fig. 2), which are:
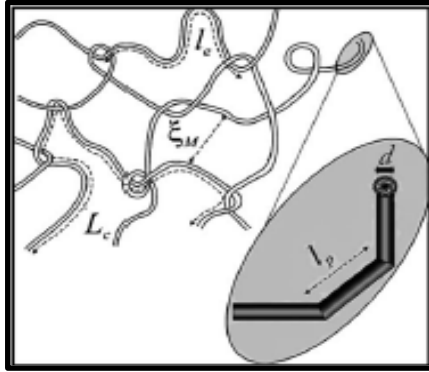
Fig. 2. Characteristic linear dimensions of the network of viscoelastic material [13].

- the mesh size of the network ξ:

$$\xi = \left(\frac{k_B \cdot T}{G_N^0}\right)^{\frac{1}{3}} \tag{2}$$

where: k_B – Boltzmann constant ($1{,}38 \cdot 10^{-23}$ J/K), T – temperature [K]

- the persistence length l_p:

$$l_p = \left(\frac{k_B \cdot T}{8 \cdot \omega_0 \cdot \eta_0}\right)^{\frac{1}{3}} \tag{3}$$

- the entanglement length l_e:

$$l_e = \frac{\xi^{\frac{5}{3}}}{l_p^{\frac{2}{3}}} \tag{4}$$

- the linear contour length L_c:

$$L_c = \frac{l_e}{\frac{G''_{min}}{G_N^0}} \tag{5}$$

where: G''_{min} – is the value of the local minimum of the loss modulus after the intersection of the curves of both modules, i.e. curve G' and G", impossible to obtain if such a point is missing,

- the network chain diameter d_e:

$$d_e = 19 \cdot l_p \tag{6}$$

The value of the viscosity at steady flow conditions η_0 was determined by extrapolating the complex viscosity to the value ω tending to 0. Thanks to the viscosity η_0 obtained in this way, the average relaxation time τ_0 was numerically

determined from the relationship:

$$\tau_0 = \frac{\eta_0}{G_N{}^0} \tag{7}$$

The reciprocal of the relaxation time τ_0 is also the cross-linking density of the structure ω_0. In addition, the knowledge of the persistence length l_p and the entanglement length l_e made it possible to estimate the semi-elasticity of the network in the form of the parameter α_e [14] from the following relationship:

$$\alpha_e = \frac{l_e}{l_p} \tag{8}$$

Moreover, thanks to the knowledge of the viscoelastic modulus of the plateau $G_N{}^0$, the packing length p was also determined [15]:

$$p = \left(\frac{13,2}{G_N{}^0}\right)^{\frac{1}{3}} \tag{9}$$

and also, based on the relationship described by equation (10):

$$G_N{}^0 = \frac{4}{5} \cdot v_s \cdot k_B \cdot T \tag{10}$$

the number of entanglements v_s in ml of solution.

3. Results and Discussion

The graphs in Figure 3 show the oscillation curves obtained during rheometric measurements for all the tested viscosupplements, while Table 2 shows the values of the G' and G" modules at ω values corresponding to walking and running, and Table 3 shows the values of the parameters describing the network of these viscosupplements. The data presented in the graphs in Figure 3 show that the higher the molecular weight of the viscosupplement, the faster - with a lower value of the oscillation frequency ω - the transition from a viscous liquid to a solid occurs, i.e. the transition from viscous properties to elastic properties. So it should come as no surprise that it is for Orthoviscu that this oscillation frequency, denoted as ω_c, has the lowest value of 1,42rad/s.
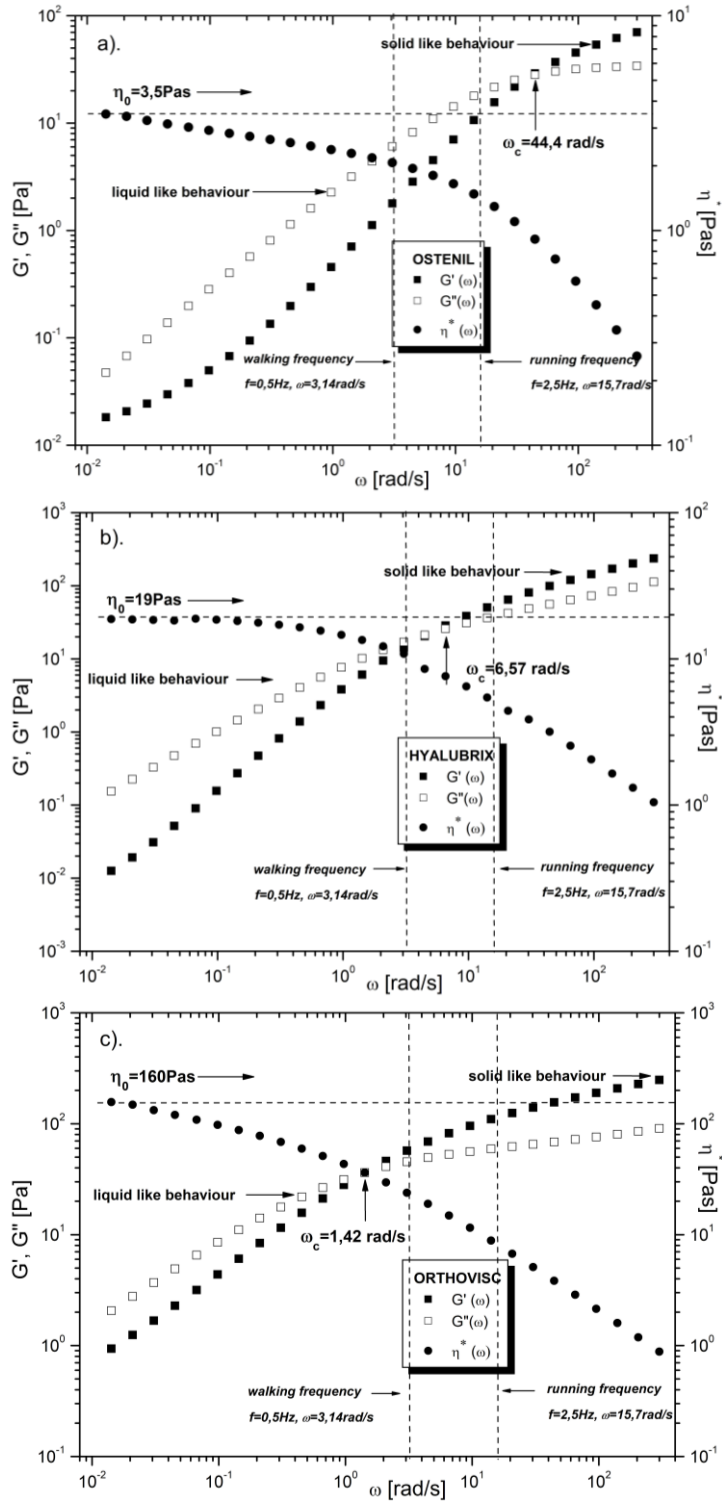
Fig. 3. Oscillation curves of tested viscosupplements at human body temperature 37^0C.

Taking into account the work of the knee joint in real conditions, it is clearly visible on the graphs in Fig. 3 that Ostenil is characterized in a wide range of oscillation frequencies ω by the predominance of viscous over elastic features, this applies especially to this particular range ω which includes the work of the knee joint when walking (3,14 rad/s or 0,5 Hz) and running (15,7 rad/s or 2,5 Hz). In Hyalubrix, the transition from viscous to elastic characteristics takes place exactly in the range of work of the knee joint. This suggests that the viscosupplement behaves like a viscous liquid while walking - when the loads on the joint are lower - and the more the speed of movement increases, it starts to behave like an elastic solid. Orthovisc, meanwhile, is a viscosupplement which in this range of oscillation frequency is characterized by a definite predominance of elastic properties over viscous ones, i.e. high elasticity - see also table 2.

Tab. 2. Value of G' and G" while walking and running

Value of G' and G"	OSTENIL	HYALUBRIX	ORTHOVISC
ω=3,14rad/s – f=0,5Hz			
G' [Pa]	1.93	13.55	57.62
G" [Pa]	6.23	16.96	44.84
ω=15.7rad/s – f=2.5Hz			
G' [Pa]	12.22	54.56	113.43
G" [Pa]	19.07	38.27	58.82

The data presented in Table 3 shows that with the increase in the molecular weight of the viscosupplement, the cross-linking power of the structure in the form of the G_N^0 parameter increases, the viscosity in the conditions of steady flow η_0, and the relaxation time τ_0. The reciprocal of the relaxation time τ_0 is the cross-linking density of the viscosupplement structure ω_0, which means that Orthovisc has the highest cross-linking density - at its lowest numerical value, it means that cross-linking occurs every $3,18s^{-1}$, so it is more frequent than in Ostenil, for which cross-linking occurs every $40,75s^{-1}$. Thus, as the molecular weight increases, the cross-linking density of the viscosupplement structure also increases.

Tab. 3. The rheological parameters of the tested viscosupplements

Rheological parameters	OSTENIL	HYALUBRIX	ORTHOVISC
G_N^0 [Pa]	142.64	340.52	509.27
η_0 [Pas]	3.5	19.0	160.0
ζ [nm]	31.07	23.25	20.33
l_p [nm]	15.54	11.63	10.17
l_e [nm]	49.33	36.91	32.27
d_e [nm]	295.2	220.9	193.1
τ_0 [s]	0.025	0.056	0.314
ω_0 [s^{-1}]	40.75	17.92	3.18
α_e [-]	3.175	3.175	3.175
p [Å]	0.452	0.338	0.296
v_s [1/ml]	$4.17 \cdot 10^{28}$	$9.94 \cdot 10^{28}$	$1.48 \cdot 10^{29}$

Moreover, the more the cross-linking density ω_0 is shifted to the left, i.e. towards smaller numerical values, the greater the mobility of the network structure elements. This property of the network translates into its ability to damp mechanical vibrations associated with movement, and thus the work of the knee joint. In practice, this means that all elements of the network structure are involved in the damping of mechanical vibrations, ensuring proper and painless functioning of the joint, if such a viscosupplement was administered by intra-articular injection. Of the three viscosupplements tested, Orthovisc is a viscosupplement that ensures such behavior of the network. At the same time, with the increase in the molecular weight of the viscosupplement, it was observed that the values of the characteristic linear dimensions of the network, such as: the mesh size ξ, the persistence length l_p and the entanglement length l_e decrease. This is additionally confirmed by the high cross-linking power of the structure, which is again in favor of Orthoviscu. In the data presented in Table 3, it is particularly significant that the semi-elasticity in the form of the αe coefficient has the same value for all three viscosupplements tested, regardless of their l_p and l_e length values. Already Zou and Larson [14] showed in their research that if the coefficient $\alpha_e > 2$, then we are dealing with a network of

loosely entanglement chains and such a network is characteristic of these three viscosupplements, which was guaranteed already at the stage of their production. However, the number of entanglements is the highest for the viscosupplement with the highest molecular weight, i.e. for Orthoviscu, for which it is $1{,}48 \cdot 10^{29}$ entanglements/ml with the lowest packing length p equal to 0,296Å.

Differences in the structure of the analyzed viscosupplements are additionally presented in the form of the so-called reduced curves in the relationship $G'/G_N^0 = f(\omega/\omega_0)$ and $G''/G_N^0 = f(\omega/\omega_0)$ - Fig. 4. This allowed to assess the superposition of the obtained experimental curves and to show that the share of shaping elements is very diverse viscous and elastic properties of the tested medium.
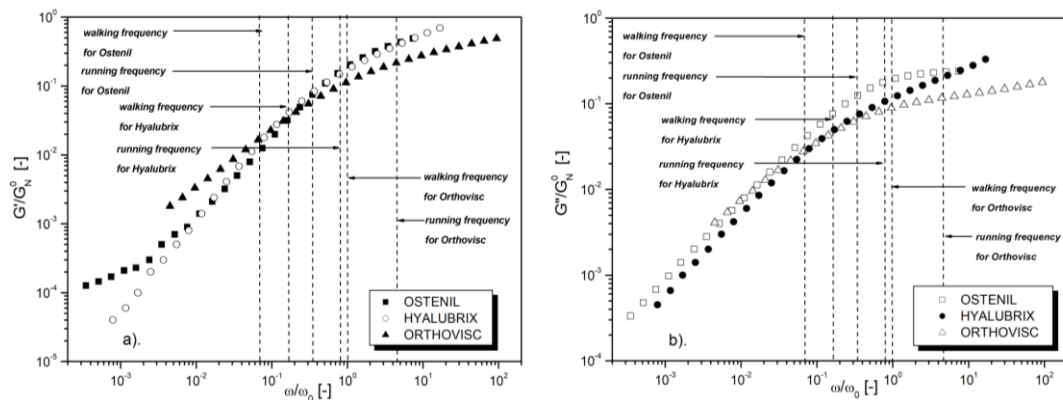
Fig. 4. Reduced curves of the tested viscosupplements.

The graph presented in Fig. 4a shows that both Ostenil and Hyalubrix form a similar type of structure in the scope of work of the knee joint, the elastic properties of these viscosupplements are not significantly differentiated - a full superposition of the reduced curves $G'/G_N^0 = f(\omega/\omega_0)$ in this range. The lack of superposition of the reduced curves $G''/G_N^0 = f(\omega/\omega_0)$ for these two viscosupplements can be seen in the graph in Fig. 4b, which proves the varied share of elements shaping the viscous properties. Orthovisc, in terms of the work of the knee joint, does not show any similarity in terms of the share of elements shaping the viscous and elastic

properties to Ostenil and Hyalubrix - because there is no superposition of the reduced curves $G'/G_N^0 = f(\omega/\omega_0)$ and $G''/G_N^0 = f(\omega/\omega_0)$ in this range. Thus, it creates a completely different type of structure than Ostenil and Hyalubrix.

4. Conclusions

The analysis of the rheological properties of three viscosupplements available on the pharmaceutical market - Ostenil, Hyalubrix and Orthoviscu - used in knee osteoarthritis showed that the molecular weight is responsible for these properties. The higher the molecular weight of the viscosupplement, the greater the power of the network, viscosity, crosslinking density of network and the number of entanglements of the viscosupplement. Although the tested viscosupplements had different characteristic linear dimensions of the network, all of them are characterized by a network of loosely entanglement chains that can form a similar or different type of structure. The obtained results may also indicate that in the case of significant advancement of knee osteoarthritis, Orthovisc turns out to be a more appropriate viscosupplement, due to the decisive advantage of elastic properties over viscous ones in the frequency range ω, covering the work of the knee joint. However, if the complaints related to the work of the knee joint are insignificant but noticeable and the patient wants to eliminate the discomfort, Hyalubrix and Ostenil seem to be good viscosupplements in the following order, which also ensure adequate lubrication of the knee joint.

References

[1] Krause W.E., Bellomo E.G., Colby R.H.: *Rheology of sodium hyaluronate under physiological conditions.* Biomacromolecules **2**, 2001, pp. 65 – 69.

[2] Necas J., Bartosikova L., Brauner P., Kolar J.: *Hyaluronic acid (hyaluronan): a review.* Veterinarni Medicina **53**, 2008, pp. 397–411.

[3] Prieto J.G., Pulido M.M., Zapico J., Molina A.J., Gimeno M., Coronel P., Alvarez A.I.: *Comparative study of hyaluronic derivatives: rheological behaviour, mechanical and chemical degradation.* Int. J. Biol. Macromol. **35**, 2005, pp. 63 – 69.

[4] Milas M., Rinaudo M., Roure I, Al-assaf S., Phillips G.O., Williams P.A.: *Comparative rheological behavior of hyaluronan from bacterial and animal sources with cross-linked hyaluronan (hylan) in aqueous solution*. Biopolymers **59**, 2001, pp. 191 – 204.

[5] Berriaud N., Milas M., Rinaudo M.: *Rheological study on mixtures of different molecular weight hyaluronates*. Int. J. Biol. Macromol. **16**, 1994, pp. 137-142.

[6] Kawasek B., Bogdał D.: *Zastosowanie kwasu hialuronowego w leczeniu choroby zwyrodnieniowej stawu kolanowego.* Technical Transaction-Chemistry **1**, 2014, pp. 58 – 68.

[7] Park HO., Hong J.S., Ahn K.H., Lee S.J., Lee S.J.: *Influence of preparation on rheological behavior and microstructure of aqueous mixtures of hyaluronic acid/poly(vinyl alcohol) Korea-Australia.* Rheology Journal **17**, 2005, pp. 79 – 85.

[8] Prekasan D., Saju K.K.: *Review of the tribological characteristics of synovial fluid.* Procedia Technology **25**, 2016, pp. 1170 – 1174.

[9] Jotanovic Z., Mihelic R., Gulan G., Sestan B., Dembic Z.: *Osteoarthritis of the hip: An overview.* Periodicum Biologorum **117**, 2015, pp. 95–108.

[10] Migliore A., Granata M.: *Intra-articular use of hyaluronic acid in the treatment of osteoarthritis.* Clinical Interventions in Aging **3**, 2008, pp. 365–369.

[11] Ferry J.: *Viscoelastic properties of polymers.* Wiley, New York (1980).

[12] Liu Ch., He J., van Ruymbeke E., Keunings R., Bailly Ch.: *Evaluation of different methods for the determination of the plateau modulus and the entanglement molecular weight.* Polymer **47**, 2006, pp. 4461-4479.

[13] Lopez-Diaz D., Castillo R.: *Microrheology of solutions embedded with thread-like supramolecular structures.* Soft Matter **7,** 2011, pp. 5926–5937.

[14] Zou W., Larson R.G.: *A mesoscopic simulation method for predicting the rheology of semi-dilute wormlike micellar solutions.* Journal of Rheology **58**, 2014, pp. 681-721.

[15] Malkin A.Y., Isayev A.I.: *Rheology - concepts, methods and applications.* ChemTec Publishing, Toronto (2006).

Moisture transport in knitted fabrics

Transport wilgoci w dzianinach

Małgorzata Matusiak[1]*, Otgonsuren Sukhbat[2]

[1] Lodz University of Technology, Faculty of Material Technologies and Textile Design, Institute of Architecture of Textiles; e-mail:malgorzata.matusiak@p.lodz.pl

[2] Lodz University of Technology, Faculty of Material Technologies and Textile Design, Institute of Architecture of Textiles

Abstrakt

Dzianiny często stosowane są w odzieży noszonej bezpośrednio przy skórze. Dlatego oczekuje się, że będą one charakteryzowały się bardzo dobrymi właściwościami wpływającymi na komfort fizjologiczny użytkowania odzieży, zwłaszcza zdolnością odprowadzania potu. W ramach pracy przeprowadzono badania 5 wariantów dzianin w zakresie zdolności do transportu potu w postaci pary oraz płynu. Badania wykonano za pomocą przyrządów Permetest i Moisture Management Tester M290. Stwierdzono, że wszystkie dzianiny charakteryzowały się bardzo dobrą przepuszczalnością pary wodnej. Transport płynnej wilgoci w dzianinach był zróżnicowany w zależności od składu surowcowego dzianin. Najlepszą zdolnością transportu płynnej wilgoci odznaczała się dzianina wykonana z mieszanki: bawełna 54%/ poliester 46%.

Abstract

Knitted fabrics are often used in clothing worn next to the skin. Therefore, they are expected to be characterized by excellent properties affecting the physiological comfort of clothing usage, especially the ability to wick away sweat. As part of the work, tests were carried out on 5 variants of knitted fabrics in terms of the ability to transport sweat in the form of vapor and liquid. The tests were performed using Permetest and Moisture Management Tester M290. It was found that all knitted fabrics were characterized by very good water-vapor permeability. The transport of liquid moisture in knitted fabrics varied depending on the raw material composition of the knitted fabrics. The best ability to transport liquid moisture was found in a knitted fabric made of a 54% cotton/46% polyester blend.

Słowa kluczowe: dzianiny, odzież, komfort, pot, pomiar, przepuszczalność pary wodnej, transport płynu

Keywords: knitted fabrics clothing, comfort, sweat, measurement, water-vapor permeability, liquid transport

1. Introduction

Knitted fabrics, especially from natural fibres, are often used in underwear and clothing worn next to skin. For this reason, they are expected to be characterized by excellent properties affecting the physiological comfort of using the clothing. Physiological comfort is one of the four basic types of clothing comfort. In addition to physiological comfort, there are: psychological, sensory and fitting comfort [1, 2]. Physiological comfort, also known as thermo-physiological comfort, is defined as the state of satisfaction with the thermal conditions of the environment [3]. The basis of physiological comfort is thermal comfort. The crucial properties of textile materials related to the thermo-physiological comfort of clothing usage are the following [4]:

- thermal resistance,
- water-vapor resistance,
- liquid moisture transport,
- air permeability.

Thermal resistance of textile materials determines their thermal insulation. It influences an ability of clothing to protect the human being against cold or overheating. The thermal resistance of textile materials can be measured using the sweating guarded hotplate test called "skin model", Permetest, Alambeta, Thermo Labo II. Two first instruments: the "skin model" and the Alambeta are the most popular all over the world [2, 5 - 7].

Water-vapor resistance (water-vapor permeability) of fabrics is usually measured be means of the "skin model" and the Permetest. In practice the Permetest is a portable "skin model" [2, 8, 9]. To assess an ability of the textile materials to transport the liquid moisture the wetting and wicking are usually determined [10]. Last decade the new instrument – the Moisture Management Tester was developed by the SDL Atlas. It makes possible to assess in a complex way an ability of textile materials to transport the liquid moisture. The instrument measures the dynamic

liquid transport properties of textiles in three aspects [11-14]:

- moisture absorbing time for inner and outer surfaces of the fabric,
- one-way transport of liquid moisture from the inner surface to outer surface of fabric,
- speed of liquid moisture spreading on the inner and outer surfaces of fabric.

The air permeability of textile materials is measured using the Air Permeability Tester [15]. One of the most important properties from the point of view of physiological comfort is an ability to wick away sweat secreted by the user's body [16]. Sweat is released in the form of vapour and should be drained from the underclothing zone to the outside. However, in certain conditions: at high ambient temperature, high humidity of the surrounding air, intense physical effort or poor water-vapor permeability of clothing, some of the sweat vapor remains in the underclothing zone and condenses on the user's skin, giving unpleasant feeling of moisture and the effect of clothing sticking to the skin. Considering the above, when selecting a knitted fabric for underwear or clothing (T-shirts, blouses, dresses) worn next to the skin, one should take into account – their ability to wick away sweat both in the form of vapour and in the form of liquid [17]. Both aspects are equivalent: sweat removal in the form of vapor and sweat removal in the form of liquid. Presented work aimed to assess the selected variants of knitted fabrics in the aspect of their ability to sweat release form the underwear zone to the environment. Five variants of thin knitted fabrics for T-shirts were measured in the range of the water-vapor resistance and moisture management ability. Measurement was performed using the Permetest by Sensora (Czech Republic) and Moisture Management Tester M290 by SDL Atlas Ltd (US).

2. Material and Methods

The knitted fabrics for underwear and next-to-ski clothing have been the objects of the investigations. There were knitted fabrics made of cotton and blends of cotton with other fibres. Generally, five variants of knitted fabrics were measured. The basic properties of the fabrics being analysed are presented in Table 1.

Tab. 1. The basic properties of the investigated knitted fabrics.

Fabric variant	Raw material	Stitch	Thickness, [mm]	Mass per square [meter, gr/m^2]
V1	CO	Single jersey	0.47	161.09
V2	CO	Rib stitch	0.61	138.59
V3	54 CO/ 46 PES	Single jersey	1.27	198.44
V4	CO (TransDry)	Single jersey	0.96	149.53
V5	51modacrylic, 26 CO/19 PA/ 2 antistatic fiber/1 elastane	Single jersey	1.32	205.47

The V1 – V3 variants are used in standard T-shirts. The V1 and V2 fabrics are made of cotton, whereas the V3 variant contains a great amount (46 %) of polyester fibres. The V4 variant is made of cotton especially treated using patented technology developed by the Cotton Incorporated (US). The TransDry® technology for cotton is a high-performance moisture management application that allows fabrics to wick and spread the perspiration. In the technology the cotton yarns are specially treated to make them water repellent. The repellent yarns are blended in the knitted fabric together with the standard untreated cotton yarns, which are sweat absorbing. Such structure (Fig. 1) makes the fabrics moisture managing [18]. The V5 variant is the knitted fabric for firefighter's T-shirt. It is

made of flame retardant / antistatic material. It is a certified flame retardant and antistatic thermo-active underwear from the PROTECT line [19].
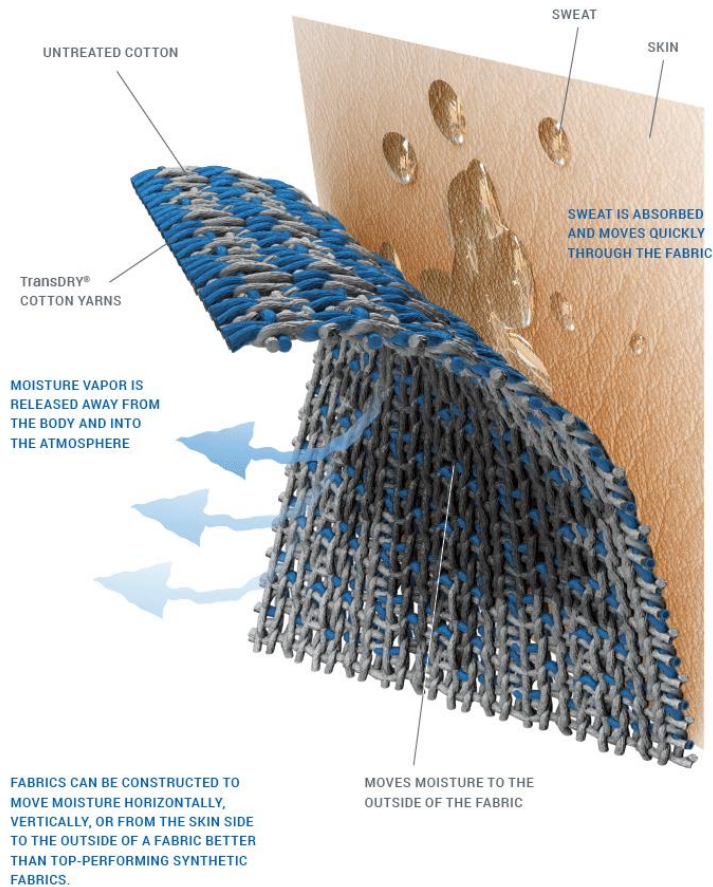
Fig. 1. T Trans Dry® technology;
https://www.cottonworks.com/en/topics/fabric-technology/performance-technologies/transdry-technology/

The knitted fabrics were measured in the range of comfort-related properties using the Permetest (Fig. 2) and Moisture Management Tester M290 (Fig. 3).

Fig. 2. The Permetest by Sensora (Czech Republic).

The Permetest is a fast response measuring instrument for the non-destructive determination of thermal resistance, water-vapor resistance and relative water-vapor permeability of textile materials [2, 8, 9]. The instrument provides all kinds of measurements very similar to the ISO Standard 11092 [20], and the results are evaluated by the identical procedure as required in the ISO 11092. In the presented work the Permetest was applied to measure the water-vapor resistance R_{et} and relative water-vapor permeability P of the knitted fabrics being analysed. During the measurement of water-vapour resistance the measuring plate of the device is wetted by the distilled water containing 0,1 % of pure non-aggressive liquid soap. The measuring head is maintained at the same temperature than the ambient temperature. Relative water-vapor permeability P determined by the Permetest is not a standardized indicator, however, it is a very practical tool for evaluating textiles from the point of view of their ability to provide physiological comfort. The value of the parameter is in the range from 0 to 100%. The value of relative water-vapor permeability P = 100% means total water-vapor permeability. The lower the value of the P index is, the lower the water vapor permeability, and thus the worse the physiological comfort of using a given product. For each fabric variant 3 repetitions of measurement were performed and next an arithmetic mean from 3 individual results was calculated as a final result. The Moisture Management Tester (MMT) is an instrument designed to measure the dynamic liquid transport properties of textiles in three aspects [11-14, 21, 22]:

- absorption of liquid moisture of inner and outer surfaces of the fabric,
- one-way transport of liquid moisture from the inner surface to outer surface of fabric,
- spreading the liquid moisture on the inner and outer surfaces of fabric.

Fig. 3. The Moisture Management Tester M290 by SDL ATLAS (US).

The device provides the values of the following parameters:
- wetting time of top (WTT) and bottom (WTB) surfaces, in s,
- absorption rate of top (TAR) and bottom (BAR) surfaces, in %/s,
- maximum wetted radius for top (MWRT) and bottom (MWRB) surfaces, in mm,
- spreading speed on top (TSS) and bottom (BSS) surfaces, in mm/s,
- accumulative one-way transport index R, in %,
- Overall Moisture Management Capacity OMMC.

The device is controlled by PC and the MMT290 SOFTWARE. Measurement is done for samples cut into 80 mm x 80 mm squares. For each fabric 5 repetitions of measurement are performed according to the ACCT standard [21] and instrument manual [22].

3. Results and Discussion

Results of measurements using the Permetest are presented in Table 2.

Tab. 2. The results from the Permetest.

Fabric variant	Ret, [m²Pa/W]		P, [%]	
	average	SD	average	SD
V1	2.90	0.10	66.20	1.00
V2	3.70	0.17	60.70	1.13
V3	3.83	0.12	60.07	0.93
V4	3.60	0.36	61.43	2.15
V5	3.43	0.15	71.57	0.55

SD – standard deviation

On the basis of the results from the Permetest it was stated that knitted fabrics being the objects of the investigation differ between each other in the range of their ability to transfer the water-vapor. The water vapor resistance R_{et} of the investigated fabrics is in the range from 2.90 to 3.83 m²Pa/W. The highest water-vapor resistance (R_{et} = 3.83 m²Pa/w) was stated for the V3 knitted fabric, whereas the lowest (R_{et} =2.90 m²Pa/W) – for the V1 fabric variant. The values od the water-vapor resistance of the V2 and V4 variants are slightly lower than that for the V3 variant (Fig. 4).
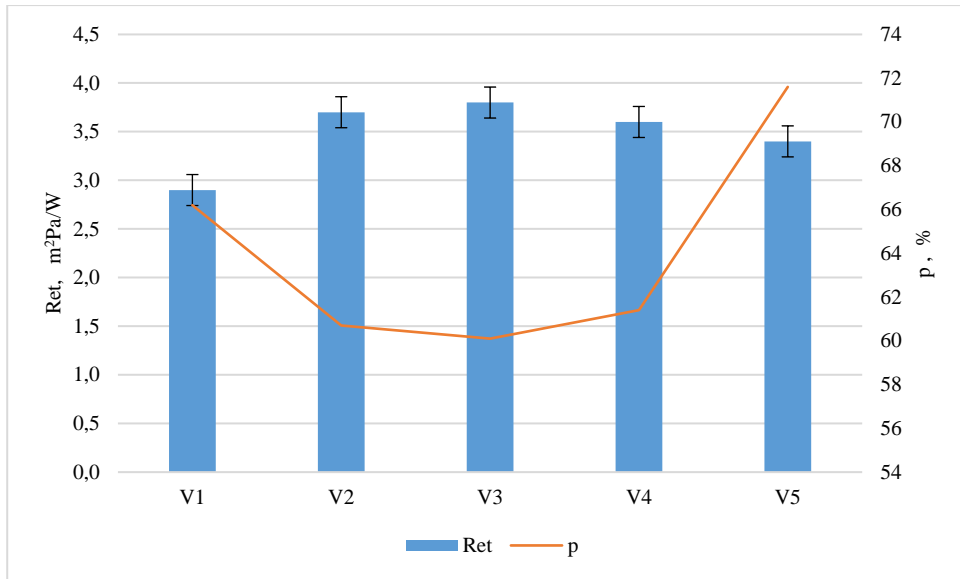
Fig. 4. Water-vapor resistance and relative water-vapor permeability of the investigated knitted fabrics.

In the aspect of the relative water-vapor permeability the highest values were stated for the V5, and next the V1 fabric variants, appropriately: 71.57 and 66.20 %. The lowest relative water-vapor permeability occurred for the V3 fabric variant. It is 60.07 %. Generally, it should be stated that the relative water-vapor permeability of all investigated variants of knitted fabrics is high, greater than 60 %. It means that all investigated fabrics transport the water-vapor well. It results from the structure of the knitted fabrics, especially their porosity. The number and size of pores between the yarns and fibres in the fabric is a crucial factor influencing bot air permeability and water-vapor permeability.

The results of liquid moisture transport measurement are presented in tables 4 and 5. The MMT provides the values of 10 parameters characterising the liquid moisture transport in the fabrics. Eight of them (WTT, WTB, TAR, BAR MWRT MWRB, SST, SSB) are connected with the sides – top (inner) and bottom (outer) of the investigated fabrics. They characterize the top and bottom surfaces. Two last parameters: R and OMMC characterize the whole fabric. They are calculated from

other parameters provided by the MMT. The R index characterizes the liquid transport from the inner to outer side of the fabric. A fabric with good accumulative one-way transport from the inner fabric side to the outer side (high value of the parameter) offers good sweat management to the wearer. It is due to the fact that with high accumulative one-way transport index the fabric keeps the skin of the wearer dry due to the transporting the perspiration towards the outer side of the fabric which is away from the skin. Positive and high values of the R parameter show that liquid sweat can be transferred from the skin to the outer surface easily and quickly.

The OMMC is calculated on the basis of absorption rate for bottom surface - BAR, spreading speed for bottom surface – BSS and accumulative one-way transport index – R. The manual of the MMT [22] suggests a classification for moisture management capability according to the OMMC value, as follows:

0 a 0.2 – very poor,

0.2 a 0.4 – poor,

0.4 a 0.6 – good,

0.6 a 0.8 – very good,

0.8 a 1.0 – excellent.

Tab. 3. The results from the Moisture Management Tester.

Fabric variant	Wetting Time, [s]		Absorption Rate, [%/s]		Max Wetted Radius, [mm]	
	Top	Bottom	Top	Bottom	Top	Bottom
V1	55.5	6.5	245.49	50.85	3	5
V2	53.7	74.5	228.55	29.65	3	2
V3	90.7	8.8	22.68	73.88	2	10
V4	5.0	5.1	36.33	50.03	26	25
V5	33.6	97.2	393.73	10.85	4	1

Tab. 4. The results from the Moisture Management Tester; continuation.

Fabric variant	Spreading Speed		R, [%]	OMMC
	average	SD		
V1	0.24	0.80	424.31	0.410
V2	0.32	0.32	-59.64	0.271
V3	0.08	2.06	1021.32	0.762
V4	3.02	3.06	-12.62	0.329
V5	0.33	0.17	-551.04	0.125

Based on the presented results it is seen that the investigated knitted fabrics differ between each other in the range of their ability to transfer the liquid moisture. Thera are also significant differences between the left (inner, top) and right (outer, bottom) sides of the fabrics.

The wetting time means the time when the surface of the measured sample start wetting after starting the test [22]. The shorter wetting time is the better ability of fabric to manage the liquid moisture. The shortest wetting time was observed for the V4 variant. It is the knitted fabric made of TransDry® technology. Both sides of the fabric wet very quickly (Fig. 5). Very short wetting time for the bottom surface was observed for the V1 and V3 fabrics. It means that the outer side of the fabrics wets fast. In is positive from the point of view of the physiological comfort. The transport of liquid to the outer (bottom) surface causes that the liquid can be quickly and ease evaporated.
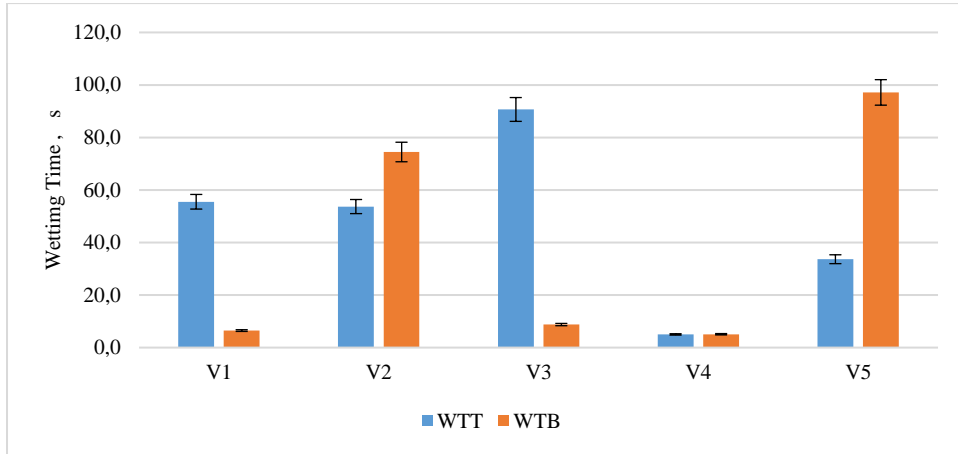
Fig. 5. Wetting time of top and bottom surfaces of the investigated knitted fabrics.
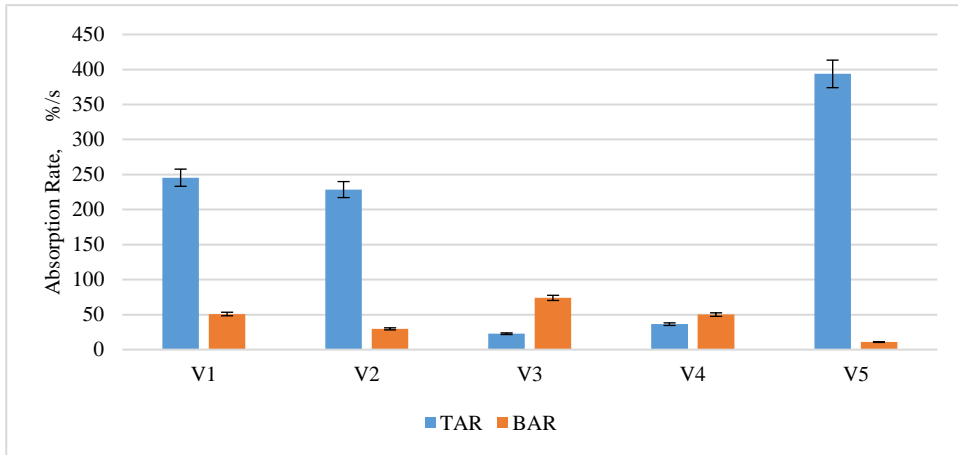
Fig. 6. Absorption Rate of top and bottom surfaces of the investigated knitted fabrics.

The absorption rate is the average speed of liquid absorption for given surface of fabric during the initial change of water content while testing [21]. The absorption of liquid by fibrous material limits the movement of liquid caused by the capillary forces. Due to this fact, the greater absorption rate is the more limited the liquid spreading on fabric surface. Additionally it should be mentioned, that great absorption rate of top surface causes that the liquid is trapped inside the fibres of the top surface. In the same time it is not effectively transferred to the outer surface

and next, to the environment. This is negative feature from the point of view of the physiological comfort. The highest absorption rate for the top surface occurred for the V5 variant next for the V1 and V2 variants (Fig. 6). It means that the mentioned variants are not good from the point of view of liquid sweat transport from the human skin to the outer surface of clothing, and next to the environment. The lowest absorption rate was stated for the V3 and V4 variants. The V3 variant is the cotton/polyester fabric. Polyester fibres are hydrophobic. They do not absorb water. The 46 % share of polyester in the V3 fabric structure is a reason of low absorption rate of the fabric. Similarly, the V4 variant contains a big amount of hydrophobic fibers (Fig. 1). There are cotton fibers specially treated using the patented technology. It casus the observed results. The maximum wetted radius expresses the maximum radius of the sensor on which the liquid has been detected. The greatest maximum wetted radius is, the better spreading the liquid on the surface, and in the same time the better condition for liquid evaporation. It concerns mostly the bottom surface of the fabric which is far from the human skin.
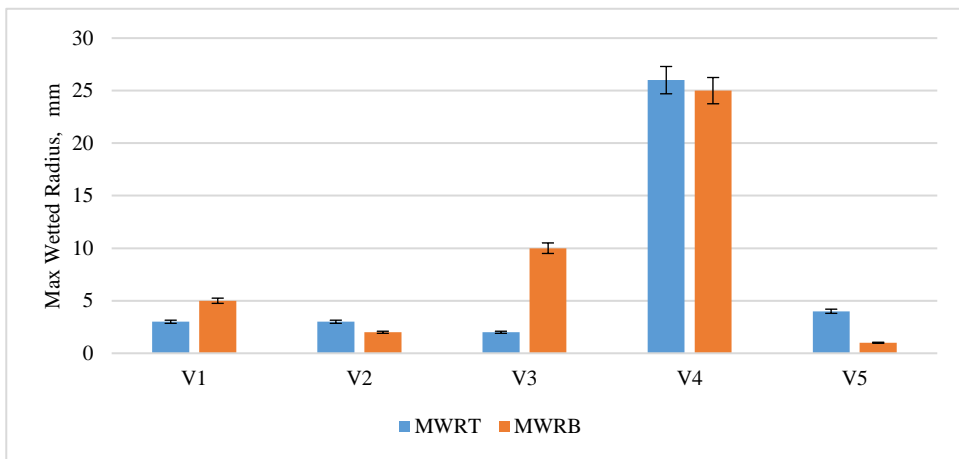
Fig. 7. Maximum wetted radius of top and bottom surfaces of the investigated knitted fabrics

In the case of the investigated knitted fabrics the greatest maximum wetted radius occurred for the V4 fabric – made in TransDry® technology (Fig. 7). Big area of liquid on the outer surface of fabric ensures quick evaporation of liquid

sweat. However, the great maximum wetted radius of the top surface is not favourable for the physiological comfort. The top (inner) surface of the fabric adheres to the user's skin. Big wet area on the inner clothing surface causes unpleasant feeling of clothing user, and additionally the liquid on the inner surface is not evaporated effectively. It remains in the underclothing zone. More favourable situation is observed in the case of the V3 variant. The maximum radius on the bottom surface is greater than that on the top surface. It causes that the sweat is not retained on the inner surface but is transferred to the outer surface of clothing and next evaporated.

Results of spreading speed (Fig. 8) are in agreement with previous results. The greatest spreading speed was stated for the V4 and next V3 fabric variants. The lowest spreading speed occurred for the V2 and V5 variants. Favourable situation occurred for the V3 and V1 variants because in both cases the spreading speed for the outer surface is significantly greater than that for the inner surface.
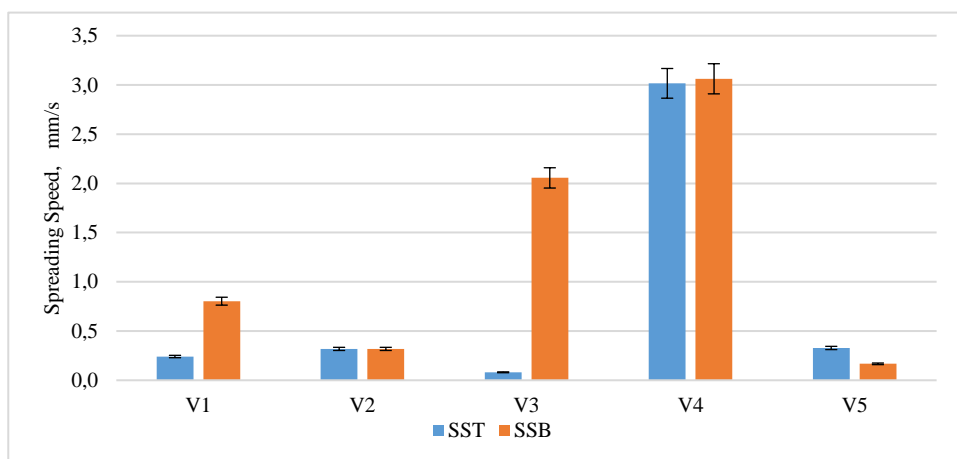
Fig. 8. Spreading Sped of top and bottom surfaces of the investigated knitted fabrics.

Based on the values of two general indicators: R and OMMC it can be stated that the best variant from the point of view of the liquid sweat transport is the knitted fabric made of cotton/polyester blend – the V3 variant. It is characterized by the highest value of the R parameter (R=1021.32%), significantly higher than the

values of the R parameter for the rest of the investigated knitted fabrics (Table 3). According to the OMMC parameter the V3 variant was classified into the Grade 4 – very good (Fig. 9).
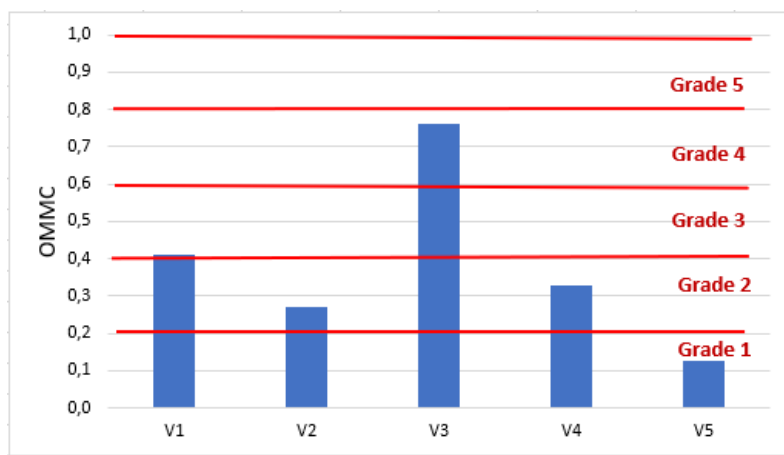
Fig. 9. Overall Moisture Management Capacity of the investigated knitted fabrics.

The lowest quality according to the OMMC value was stated for the V5 fabric variant. It is the knitted fabric for firefighter underwear. It is made of flame retardant / antistatic fibres. The share of cotton fibres is low – 26 %. Maybe it is a reason of low ability of the V5 fabric to transfer the liquid moisture.

4. Conclusions

Based on the performed investigations it was stated that the investigated knitted fabrics designed for T-shirts are characterized by very good relative water-vapor permeability – more than 60 %. It results from the structure of the fabrics, especially their porosity. The liquid moisture transport in the investigated fabrics is diversified and dependent on fibre composition of the fabrics. The best ability to transfer the liquid moisture was stated for the knitted fabric made of 54 cotton/46 polyester blend – the V3 variant. The performed investigations did not confirm the moisture management functionality of the knitted fabric made using TransDry® technology.

The fabric made of TransDry® technology was characterized by great spreading the liquid on the outer surface, what is favourable from the point of view of physiological comfort. Unfortunately, the spreading the liquid on inner surface is also great. It can cause that the fabric is wet on the inner surface adhering the user's skin. It can be a reason of unpleasant feeling causing discomfort. Additionally, the values of the wetting time and absorption rate suggest that the V4 fabric is able to ensure the liquid transport because it wets and absorb liquid moisture very fast. The results for the knitted fabric made using the Trand Dry® technology are discussable. The investigations of the Trans Dry® technology should be continued.

References

[1]   Rossi R.: *Interactions between Protection and Thermal Comfort,* w: *Textiles for Protection*, Scott R.A (red.)., England, Woodhead Publishing in Textiles, 2005, pp. 233-260.

[2]   Matusiak M.: *Tkaniny gofrowane. Właściwosci biofizyczne*. Wydawnictwo Politechniki Łódzkiej Łódź 2020.

[3]   ISO 7730:1984 Moderate thermal environments — Determination of the PMV and PPD indices and specification of the conditions for thermal comfort

[4]   Matusiak M.: *Moisture Management Properties of Seersucker Woven Fabrics of Different Structure,* Fibres & Textiles in Eastern Europe **27**, 3(135), 2019, pp. 43-50.

[5]   Matusiak M., Kowalczyk S.: *Thermal-insulation properties of multilayer textile packages*, Autex Research Journal, **14,** 4, 2014, pp. 290-307.

[6]   Özkan E.T., Kaplangiray B.M.: *Investigating thermophysiological comfort properties of polyester knitted fabrics,* Journal of Textile Engineering and Fashion Technologies; **5(1),** 2019, pp. 50-56.

[7]   Kosiuk G., Matusiak M.: *Analysis of the Heat Resistance of Multilayer Clothing Packages,* Fibres & Textiles in Eastern Europe **29**, 2(146), 2021, pp. 95-99.

[8]   Akcagun, E., Bogusławska-Bączek, M., Hes, L.: *Thermal insulation and thermal contact properties of wool and wool/PES fabrics in wet state*, Journal of Natural Fibers, **16(2),** 2019, pp. 199-208.

[9] Fung, F. T., Gao, C., Hes, L., Bajzik. V.: *Water Vapor Resistance Measured on Sweating Thermal Manikin and Permetest Skin Model in the Vertical Orientation*, Journal of Communications in Development and Assembling of Textile Products, (CDATP), September 2020. DOI: https://doi.org/10.25367/cdatp.2020.

[10] Patnaik, A., Rengasamy, R.S., Kothari, V.K., Ghosh, A*.: Wetting and Wicking in Fibrous Materials,* Textile Progress **38**, 2006, pp. 1-105.

[11] Udaya Krithika S.M., Sampath M.B., Prakash C.: Senthil Kumar, M. *Moisture management finish on woven fabrics.* Indian Journal of Fibre and Textile Research **44**, 2019, pp. 486-491.

[12] Kamińska, D., Matusiak, M.: *Does the weave matter? Analysis of moisture transport in cotton fabri*cs (in Polish). W: Modern Technologies-Strategies, Solutions and Development Prospects; Mołdoch-Mendoń, I., Skrzątek, K. (red.), Wydawnictwo TYGIEL Lublin, 2021; Volume 2, pp. 147-142.

[13] Matusiak M., Kamińska D.: *Liquid moisture transport in the cotton woven fabrics with different weft yarns*, Materials, **15**, 2022, pp. 6489. https://doi.org/10.3390/ma15186489.

[14] Sathish Kumar T., Ramesh Kumar M., Senthil Kumar B.: *Evaluation of Moisture Management Properties of Plated Interlock, Mini Flat Back Rib and Flat Back Rib Structures* Fibres & Textiles in Eastern Europe, **29**, 2021, pp. 66-74.

[15] Umair M., Hussain T., Shaker K., Nawab Y., Maqsood M., Jabbar M.: *Effect of Woven Fabric Structure on the Air Permeability and Moisture Management Properties,* Journal of Textile Institute **107**, 2016, pp. 596-605.

[16] Bartels V.T.: *Physiological comfort of sportswear*. w: *Textiles in Sports*, ed. R. Shishoo, Woodhead Publishing Limited, Cambridge 2005, pp. 177-203.

[17] Baltušnikaitė, J., Abraitienė, A., Stygienė, L., Krauledas, S., Rubežienė, V., Varnaitė-Žuravliova, S.: *Investigation of Moisture Transport Properties of Knitted Materials Intended for Warm Underwear*. Fibers &Textiles in Eastern Europe **22**, 2014, pp. 93-100.

[18] https://www.cottonworks.com/en/topics/fabric-technology/performance-technologies/transdry-technology/

[19] https://dlastrazy.pl/bielizna-podbarierowa-brubeck-trudnopalna-koszulka

[20] ISO 11092:2014 Textiles — Physiological effects — Measurement of thermal and water-vapor resistance under steady-state conditions (sweating guarded-hotplate test.

[21] AATCC Test Method 195-2011 Liquid Moisture Management Properties of Textile Fabrics.

[22] M290 MMT Moisture Management Tester. Instruction manual, Rev.1.2 (01/17), SDL Atlas Ltd., 2017.

Application of Drop Shape Analyzer to measure the wettability of cotton woven fabrics

Zastosowanie przyrządu Drop Shape Analyzer w ocenie zwilżalności powierzchni tkanin bawełnianych

Dominika Kamińska [1, 2]*, Małgorzata Matusiak[1], Ivana Čorak[3], Anita Tarbuk[3]

[1] Lodz University of Technology

[2] Institute of Security Technologies MORATEX

[3] University of Zagreb Faculty of Textile Technology

Abstrakt

Metoda pomiaru kąta zwilżania, stosowana w ocenie hydrofobowości materiałów, jest dobrze znana i nadaje się do oceny podłoży stałych o gładkiej geometrii. Dla tych podłoży ocena danych jest stosunkowo prosta. W przypadku materiałów włókienniczych interpretacja wartości kąta zwilżania jest utrudniona, głównie ze względu na dwie właściwości podłoża – chropowatość oraz zdolność podłoża do zasysania kropli cieczy. W ramach niniejszej pracy badaniom poddano 6 tkanin bawełnianych o różnych splotach (płócienny, skośny 3/1 S, skośny 2/2 S, ryps podłużny 2/2 (2), ryps poprzeczny 1/1 (0,1,0) oraz panama 2/2 (0,2,0)). Pomiary zostały przeprowadzone przy użyciu przyrządu Drop Shape Analyzer (DSA).

Abstract

The method of measuring the contact angle, applied in an assessment of material hydrophobicity, is well known and suitable for evaluating the solid substrates with smooth geometry. For these substrates data evaluation is quite straightforward. In the case of textile substrates, the interpretation of the contact angle value is difficult, mainly due to two properties of the substrate - the roughness and an ability of the substrate to absorb the liquid drops. In the presented work 6 cotton fabrics with different weaves (plain, twill 3/1 S, twill 2/2 S, rep 2/2 (2), rep 1/1 (0,1,0), hopsack 2/2 (0,2,0)) were tested. Measurements were performed using the Drop Shape Analyzer (DSA).

Słowa kluczowe: kąt zwilżania, tkanina, Drop Shape Analyzer, splot

Keywords: contact angle, woven fabric, Drop Shape Analyzer, weave

---

1. Introduction

Textile wettability refers to the ability of textile materials to absorb or repel liquids, most commonly water. This is an important feature because it affects the waterproof, breathable and stain-resistant properties of materials. With regard to humidity, moisture can affect the wearing comfort of a garment and its insulating properties [1 – 3]. Materials with good wettability properties will effectively wick away moisture from the body, which is especially important in sports and active clothing.

Textile moisture refers to the ability of a material to absorb, transfer and release moisture. It is important for both user comfort and product performance. There are two main aspects related to textile moisture [4 – 5]:

- moisture absorbency – refers to an ability of a material to absorb moisture. This is an important property that affects the comfort of wearing and using textiles. Moisture absorption is measured as the amount of water absorbed by a material relative to its weight or volume. The effect on moisture absorption depends to a large extent on the type of fiber. Natural materials such as cotton, linen and wool tend to be more absorbent than synthetic materials such as polyester and nylon. This means that these natural fibers can absorb moisture from the environment or from the wearer's body, which can be beneficial in conditions where the skin tends to perspire. Thus, the textile materials made of natural fibers have higher initial moisture content than other materials, e.g. made of the synthetic fibers. However, high moisture absorption can also have some disadvantages, such as longer drying times and the possibility of loss of insulation properties for winter clothing.

- wicking – this is an ability of material to transfer moisture from one part of the fabric to another and to surface of the material from which the liquid can be evaporated. Materials with good wicking properties allow for quick

dissipation of moisture, which helps to keep the contact layer between the body and clothing dry and comfortable.

The study of the contact angle in textiles is important because it helps to understand how liquids spread over the surface of the fabric. Contact angle measurement is commonly used to evaluate surface quality. The measurement of the contact angle is used to determine an ability of the solid substrate to repel or attract liquids. If the substrate repels the liquid, then we are dealing with the phenomenon of hydrophobicity. If the substrate absorbs the liquid, then we are dealing with the phenomenon of hydrophilicity. In the case where water is the test liquid, substrates with a contact angle higher than 90 ° (CA > 90 °) are considered as hydrophobic. If the contact angle is lower than 90 ° (CA < 90°) the substrates are considered as hydrophilic [6 – 7]. In the case of ultra-hydrophobic materials with so-called lotus effect, the contact angle approaches the theoretical limit of 180°. Contact angle on different materials is presented on Fig. 1.
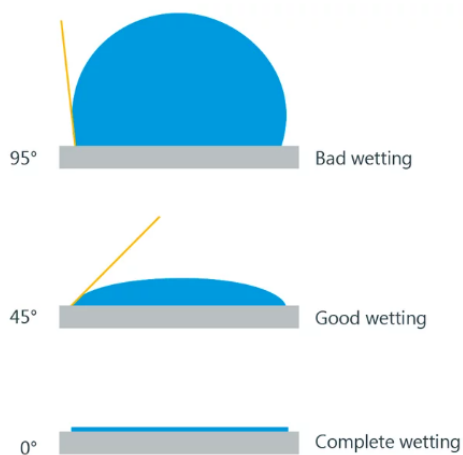
Fig. 1. Contact angle on different materials
Source: [8].

Young found that the contact angle with the surface can be thought of as the mechanical equilibrium of a drop resting on a flat solid surface under the influence

of three surface tensions [9]:

- γ_{sv} (interface of the solid and vapor phase),

- γ_{sl} (interface of the solid and liquid phases),

- γ_{lv} (interface of the liquid and vapor phases).

  Young's equation has the following form:

$$\gamma_{sv} - \gamma_{sl} = \gamma_{lv}cos\theta \tag{1}$$
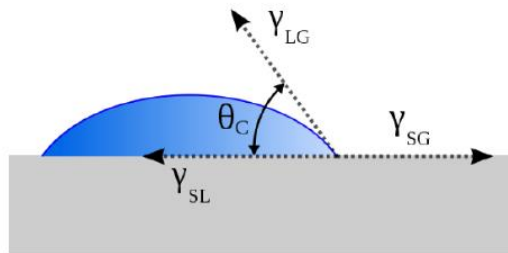
Fig. 2. Schematic diagram of contact angle

Source: [9].

Legend:

- θ_C – contact angle of the liquid on the solid (º)
- γ_{sv} (interface of the solid and vapor phase),
- γ_{sl} (interface of the solid and liquid phases),
- γ_{lv} (interface of the liquid and vapor phases).

The aim of presented work was to assess the contact angle of cotton woven fabrics of different weaves. Totally, 6 variants of cotton fabrics have been measured using the Drop Shape Analyzer by Krüss (Germany).

2. Materials and methods

2.1. Materials

As part of this study, 6 cotton woven fabrics of various weaves were tested. They were fabrics of the following weaves: plain, twill 3/1 S, twill 2/2 S, rep 2/2 (2), rep

1/1 (0,1,0), hopsack 2/2 (0,2,0). The repeats of weaves applied in the investigated fabrics are presented in Fig. 3. All fabric variants were manufactured based on the same warp – 50 tex CO OE (Open End). The 100 tex CO OE yarn was applied as a weft.
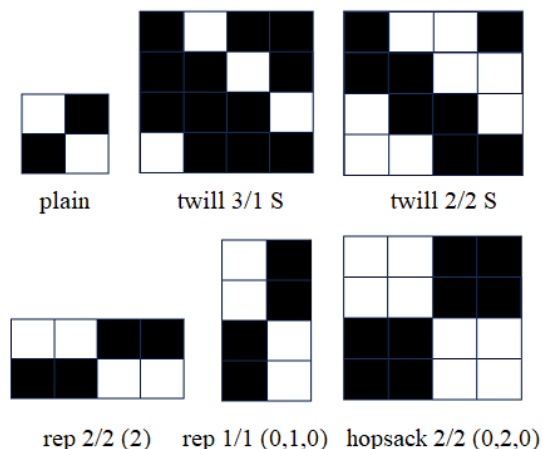
Fig. 3. Weaves applied in the fabric variants being analyzed.

All fabrics have been finished in the same way. The finishing process included: desizing, washing, rinsing and drying. The basic parameters of the tested fabrics are shown in Tab. 1.

Tab. 1. Basic structural properties of fabrics investigated.

Parameter	Unit	Value					
		1	2	3	4	5	6
Weave	-	plain	twill 3/1 S	twill 2/2 S	rep 2/2 (2)	rep 1/1 (0,1,0)	hopsack 2/2 (0,2,0)
Warp	-	50 tex					
Weft	-	100 tex					
Warp density	cm^{-1}	31.2	31.7	31.9	31.1	31.7	31.6
Weft density	cm^{-1}	11.5	11.6	11.6	11.5	11.9	11.7
Mass per square metre	g m^{-2}	292	292	287	284	293	287
Warp crimp	%	14.2	7.9	7.0	7.3	9.8	6.4
Weft crimp	%	2.9	3.3	2,7	1.2	3.9	2.3
Thickness	mm	0.67	0.78	0.79	0.83	0.65	0.79

2.2. Methods

Drop Shape Analyzer (DSA) by Krüss (Germany) for contact angle measurement is optimized for simplicity in use. It measures interfacial properties such as contact angle (CA) and surface tension (SFT). During the measurement using the DSA the sample is first placed on the sample table and its image is show on the PC screen. A droplet whose volume is controlled by analyzing the shape of the pendant drop is then created and dropped on the fabric surface. All parameters are preset for a quick start but they can by modified by the user. As the droplet is placed on the table the software automatically starts analyzing the contact angle of the droplet on both sides (left and right) to show the results immediately. Analysis can be done with multiply analyzing models like the Young – Laplace and other automatic or manual baseline. The results are automatically saved and can be compared and presented with ease [8].

Fig. 4. The Drop Shape Analyzer by Krüss.
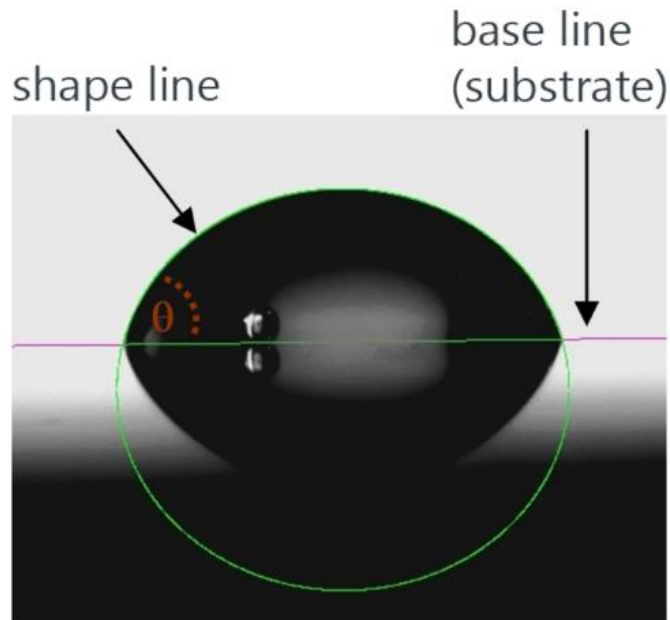
Fig. 5. Sessile drop with fitted contour (shown in green)

Source [9].

In the presented work the configuration of the experiment was the following:

- testing liquid: water,
- substrate/probe: woven fabric,
- gas phase: air.

During the test the software records successive steps each 0.1 s.

3. Results

Results from the Drop Shape Analyzer are presented in Tab. 2a – b which present mean values from measurements and the standard deviation of the results (in brackets).

Tab. 2a. Results from Drop Shape Analyzer.

Sample	Weave	CA(m), [°]	CA(l), [°]	CA(r), [°]	Diameter, [mm]
1	plain	112.13 (2.17)	112.26 (2.34)	112.00 (2.08)	9.41 (0.15)
2	twill 3/1 S	70.91 (16.05)	70.91 (16.05)	70.91 (16.05)	12.11 (0.63)
3	twill 2/2 S	-	-	-	-
4	rep 2/2 (2)	43.39 (24.88)	42.4 (23.61)	44.38 (26.18)	9.97 (1.32)
5	rep 1/1 (0,1,0)	52.44 (30.82)	51.00 (30.98)	53.88 30.98	12.76 (0.92)
6	hopsack 2/2 (0,2,0)	52.68 (20.98)	56.64 (24.43)	48.72 (19.88)	12.1 (0.36)

Tab. 2b. Results from Drop Shape Analyzer

Sample	Weave	Volume, [µL]	Three-phase point (l), [mm]	Three-phase point (r), [mm]
1	plain	414.956 (6.317)	24.8 (0.1)	34.2 (0.1)
2	twill 3/1 S	299.385 (74.192)	20.7 (0.6)	32.8 (0.1)
3	twill 2/2 S	-	-	-
4	rep 2/2 (2)	95.579 (74.129)	22.8 (0.9)	32.7 (0.5)
5	rep 1/1 (0,1,0)	220.352 (133.719)	20.1 (0.8)	32.9 (0.5)
6	hopsack 2/2 (0,2,0)	160.03 (64.277)	20.4 (0.3)	32.5 (0.3)

Legend:

CA – contact angle,

CA (m) – mean (mean from right and left side of drop),

CA (l) – contact angle of left side of drop,

CA (r) – contact angle of right side of drop,

three-phase point – is a common point for the boundary lines of three phases.

For a sessile drop on a solid surface in air, when measuring the contact angle, this is the transition point between the liquid/solid, liquid/gas and solid/gas boundary lines (Fig. 6).

Fig. 6. Schematic diagram of a three-phase system

Source: [10].

The graph below (Fig. 7) shows the dependence of CA (m) on the step number for sample 1. Elapsed time between every single step was 0.1 s.
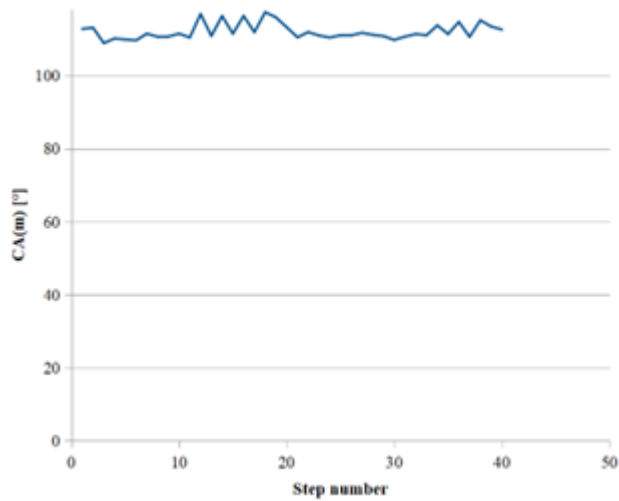
Fig. 7. Diagram CA (m) vs step number of plain weave woven fabric.

Legend: blue line: water (Air)–Y1

In the case of plain weave fabric, a drop of moisture was on the fabric surface of all the time, and no wetting occurred. This situation is presented in Fig. 8, where the image of a sitting drop during the measurement is presented. This situation was observed throughout the measurement. The program recorded 40 steps, the total measurement time was 1.9 s.
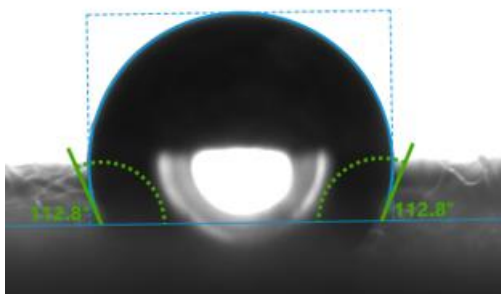
Fig. 8. View of sessile drop from measure of plain weave woven fabric.

Based on the results, it can be concluded that the plain weave woven fabric is waterproof. However, cotton is a hydrophilic fiber. Perhaps the type of weave and the large number of interlacing points between the weft and warp yarns caused that the drop could not penetrate the fabric.

In the case of the 2/2 S twill weave fabric, the drop was absorbed into the woven fabric right away. The program didn't manage to record any results.

Fig. 9. View of sessile drop from measurement for twill 2/2 weave woven fabric.

To compare the results, Fig. 10 and 11 show a graphical interpretation of the results for a fabric with a rep 2/2 (2) weave. The absorption of drop lasted 0.5 second. The program recorded the test in 6 steps. The CA (m) was 43.39°, indicating that the fabric is hydrophilic.

step 1 = 0.0 s   step 4 = 0.3 s   step 6 = 0.5 s
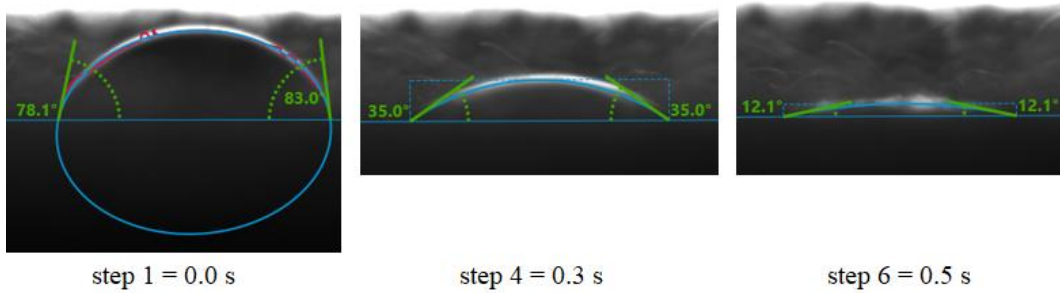
Fig. 10. View of sessile drop from measurement of rep 2/2 (2) weave woven fabric for 3 single steps.
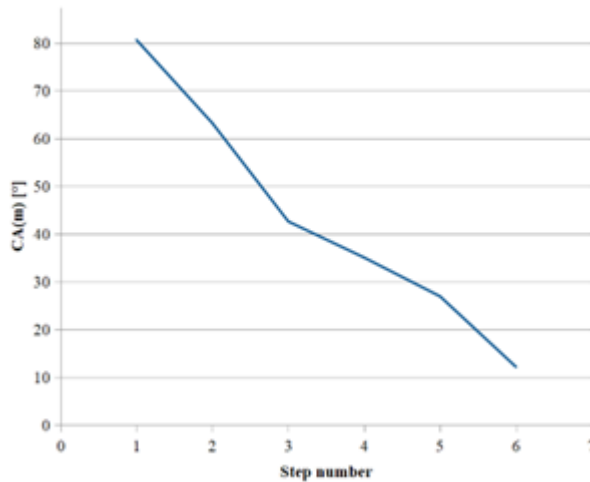
Fig. 11. Diagram CA (m) vs step number of rep 2/2 (2) weave woven fabric

Legend: blue line: water (Air)–Y1

Other fabrics achieved similar results. They have been rated as hydrophilic. In the case of fabrics, the effect on moisture absorption also depends on the surface roughness, which is the most often caused by the structure of the weave.

4. Conclusions

Based on the obtained results, it can be concluded that the plain weave woven fabric being investigated is classified as waterproof. The rest of the woven fabrics being the objects of the investigation were classified as hydrophilic. The woven fabric of 2/2 S twill weave was assessed as non-classified to whatever group of fabrics because it was impossible to record the shape of the drop.

Presented investigations are preliminary. We would like to show the new method and analyze the results provided by it. To find out what is the real effect of weave on contact angle, a bigger number of different studies should be undertaken. First of all, it is necessary to perform the measurements in different places of fabric being measured. The work will continue in this direction.

Acknowledgment

References

[1]   Bahners T., Thomas H., Gutmann J. S.: *Wettability characterization in textiles - Useand abuse of measuring procedures*, [in:] *Textile Finishing–Recent Developments and Future Trends*, K.L. Mittal, T. Bahners (red.), Wiley–Scrivener, Beverly, MA 2017, pp. 207-234.

[2] Zhong W.: *Surface tension, wetting and wicking*, [in:] *Chapter in textiles for protection*, Scott A. (red.), Woodhead Publishing Ltd, Cambridge England, 2005, pp. 136–155.

[3] Patnaik A., Rengasamy R. S., Kothari V. K.: Ghosh A., *Wetting and Wicking in Fibrous Materials*, Textile Progress Vol (**38:1**), 2006, pp. 1–105.

[4] Duprat C.: *Moisture in Textiles*, Annual Review of Fluid Mechanics, Vol (**54**), 2022, pp. 443-467.

[5] Parada M., Derome D., Rossi R., Carmeliet J.: *A review on advanced imaging technologies for the quantification of wicking in textiles*, Textile Research Journal, Vol (**87:1**), 2017, pp. 110-132.

[6] ASTM D7334–08(2013), Standard Practice for Surface Wettability of Coatings, Substrates and Pigments by Advancing Contact Angle Measurement, ASTM International, West Conshohocken, PA.

[7] Seongpil J., Hye–Won K.: *Chapter 3 - In situ real–time monitoring technologies for fouling detection in membrane processes*, Xuan-Thanh B., Wenshan G., Chart C., Ashok P. (red.), Current Developments in Biotechnology and Bioengineering, Elsevier, 2023, pp. 43-64.

[8] https://www.kruss-scientific.com/en/know-how/glossary/contact-angle.

[9] https://chem.libretexts.org/Bookshelves/Physical_and_Theoretical_Chemistry_Textbook_Maps/Supplemental_Modules_(Physical_and_Theoretical_Chemistry)/Physical_Properties_of_Matter/States_of_Matter/Properties_of_Liquids/Contact_Angles.

[10] https://www.kruss-scientific.com/en/know-how/glossary/three-phase-point.

Evaluation of electrically conducting fabrics for use as layers protecting against mechanical damages

Ocena tkanin elektroprzewodzących pod kątem zastosowania jako warstw chroniących przed uszkodzeniami mechanicznymi

Magdalena Tokarska[1]*, Natalia Czyżnik[1]

[1] Lodz University of Technology, Faculty of Material Technologies and Textile Design, Institute of Architecture of Textiles, Lodz, Poland

Abstract

The unique characteristic of the electroconductive fabric-based sensor is its ability to generate an electric signal directly in response to external stimuli. A fabric-based layer can protect objects and simultaneously monitor changes in resistance. It was found that the electrical resistance of fabric increases with increased mechanical damage to its surface. As the resistance increases, the fabric loses its protective properties, which may damage the object. The analysis of static characteristics enabled the selection of fabrics characterised by the widest range of electrical resistance, which results in a desirable higher sensitivity factor of the fabric-based sensor.

Abstrakt

Unikalną cechą sensora na bazie tkaniny elektroprzewodzącej jest jego zdolność do generowania sygnału elektrycznego bezpośrednio w odpowiedzi na bodźce zewnętrzne, np. uszkodzenia mechaniczne. Warstwa tkaniny może chronić obiekty i jednocześnie monitorować zmiany rezystancji. Stwierdzono, że rezystancja elektryczna tkaniny wzrasta wraz ze wzrostem uszkodzeń mechanicznych jej powierzchni. Wraz ze wzrostem oporu tkanina traci swoje właściwości ochronne, co może skutkować uszkodzeniem obiektu. Analiza charakterystyk statycznych umożliwiła wybór tkanin charakteryzujących się najszerszym zakresem rezystancji elektrycznej, co skutkuje większą czułością sensora.

Keywords: electroconductive fabrics, resistance, sensors, damages, protection

Słowa kluczowe: tkaniny elektroprzewodzące, rezystancja, sensory, uszkodzenia, ochrona

1. Introduction

Wearable devices have become an integral part of human life. However, the products have to meet ever-greater demands and expectations. Wearable technology is developing, and wearable electronics are evolving along with it [1,2]. Electroconductive fabrics combine the advantages of traditional woven fabrics with the ability to sense and transmit electrical signals. They are a significant part of wearable electronics [3-6]. The flat textile materials can be integrated into composite structures. The thin, flexible textile-based products called wearable textronics [1] can act as heating elements, electrodes, connectors, signal lines, and sensors [7-13]. From the point of view of a wide range of applications, textile-based sensors deserve attention. They are resistive, capacitive, piezo-electric, and electrochemical sensors [14-17]. The resistive sensor operation relies on the detection and response in the form of a change in electrical resistance to some input from the physical environment [15,18]. The electroconductive woven fabrics can be used as a resistive sensor for damage detection [16,19,20]. Development of advanced application techniques to obtain electrical conductivity of textile materials, emphasizing metal-containing coatings, is observed [21-24]. Obtaining a continuous and uniform coating layer on the non-conductive fabric is essential from an electroconductive properties point of view. Cracks in the conductive layer influence its electroconductive properties, resulting from changes in the distribution of the potential and current density around the defects [25,26]. The increase in textile material electrical resistance is observed that is caused by defects [26]. The electroconductive fabric can be embedded within the structure, and any damage or structural changes can alter its electrical properties, enabling the detection of defects, cracks, or structural failures. The electrical resistance change technique has advantages over other methods since it employs the electroconductive properties of fabric coating as a sensor to measure the changes in the resistance. Therefore, the detection of damage can be measured directly [19].

The four-point probe (FPP) method [27] was used to measure the electrical resistance of samples to observe changes in resistances before and after testing [19,28]. The carbon fiber composite laminates were taken into consideration to detect barely visible impact damage [19]. Changes in electrical resistances resulting from damage were noticed. Moreover, it was observed the magnitude of resistance changes is dependent on the carbon fiber volume fraction. The higher the fiber content in the composite, the lower the resistance. The detection of defects in woven, knitted, and embroidered electrodes as a result of mechanical and chemical impact was the subject of research [28]. The content of copper and silver on the electrode surface guaranteed the ability of the products to conduct electric current. It was found, that the tests of resistance to washing, abrasion, and pilling caused an increase in the electrical resistance of the electrodes. Tests showed that the copper-based electrodes suffered the most damage, resulting in the greatest increase in resistance. An electrical response to damage of carbon fiber-reinforced polymer composites was also tested based on the multi-probe resistance method [29]. The change of different electrical potentials was observed for samples. It was stated, that no external sensors are needed because the technique provides direct information from the original output signal pointing at the sample damage. Detection of cracks from boundary measurements, voltages, and current was performed [30,31]. The Electrical Impedance Tomography (EIT) method was used as a non-destructive tool for building a conductivity map of the entire structure to localise cracks.

Electroconductive woven fabrics exhibit an electrical in-plane anisotropy, meaning that their electrical properties vary depending on the direction of measurement within the fabric [32-35]. It is observed that when multiple conductive yarns intersect within the fabric, the electrical resistance tends to be higher compared to fabrics with fewer intersecting yarns [32,35]. This suggests that the presence of intersections creates additional barriers to the flow of an electric current. The metallization process applied to non-conductive textile material significantly impacts the electrical resistance of electroconductive fabrics [36-38]. The surface

percentage occupied by the coating is significant from the point of view of forming percolation channels with metal conductivity begins [39]. The coating of a non-conductive fabric with a conductive material such as nickel, copper, silver, tin, or titanium results in a smoother surface. This smoothness leads to a decrease in woven fabric resistance, as the conductive coating reduces potential barriers or irregularities on the fabric surface [32]. Considering that electroconductive fabrics are anisotropic materials, it is essential to use an appropriate measurement method to evaluate their properties. In this context, the van der Pauw (VDP) method [40] proves to be a reasonable choice. The VDP method utilizes a specific configuration of four electrodes for resistance measurement, which enables the determination of electrical in-plane anisotropy in the fabric [14,32,33]. This method offers advantages over other methods. The FPP method is commonly used for resistance measurements but does not provide information on anisotropic behavior [41]. The EIT method [30,31] is time-consuming, and the multi-probe resistance method requires multi-variant measurements. In the case under consideration, when the size of the damage is essential, not its localization, the VDP method is entirely sufficient for the resistance determination of the electroconductive woven fabric. A relationship between changes in the resistance of the fabric and the properties being monitored or controlled needs to be specified for the fabric-based sensor. Understanding how variations in the fabric's electrical characteristics correspond to changes in the monitored parameters can be leveraged while designing electroconductive fabrics for various applications.

The unique characteristic of the fabric-based sensor is its ability to generate an electric signal directly in response to external stimuli, which is the damage to the fabric structure. The main aim of the research was to evaluate the electroconductive woven fabrics as a material intended for the damage sensors. Static characteristics of the fabric-based resistive sensors were determined. An electrical anisotropy of fabrics was considered when assessing the suitability of the textile material as a

protecting layer adjacent to an object flat surface while simultaneously monitoring changes in electrical resistance.

2. Materials and methods

Electroconductive woven fabric can play a significant role in measuring systems intended for damage detection. Woven fabric is a thin, non-stretchable, and flexible textile material that can easily adhere to a protected surface. A general idea of a measuring system is shown in Fig. 1. The electroconductive woven fabric can act as a protective layer adjacent to a flat surface of a monitored object, aiming to safeguard against mechanical damage. In the case under consideration, the location of the damage is irrelevant, but its size.
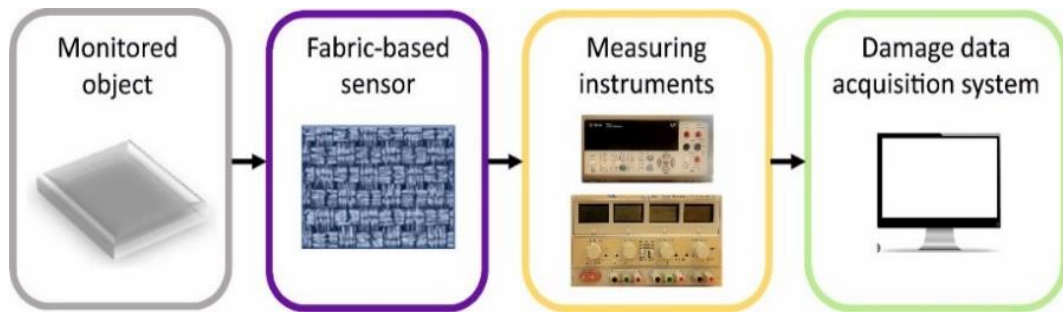
Fig. 1. Idea of measuring system for damage detection.

Due to the need for the fabric to adhere to the object, the frame can be used to clamp the fabric and object. The frame should enable leading the wires connecting four electrodes with the measuring instruments.

Four electroconductive woven fabrics were selected for testing. The parameters of fabrics are given in Tab. 1, where the variation coefficient is given in paratheses.

Tab. 1. Parameters of electroconductive woven fabrics.

Fabric	Raw material composition	Thickness, [mm]	Areal density, [g/m²]	Warp/Weft density, [yarns/cm]
S1	Silver-coated polyamide plain-weave fabric; declared surface resistance below 0.30 Ωsq^{-1}	0.106 (5%)	42 (0.1%)	45/44
S2	Nickel-coated polyester twill-weave fabric; declared surface resistance below 0.40 Ωsq^{-1}	0.270 (4%)	152 (0.2%)	46/35
S3	Copper and nickel-coated polyester plain-weave fabric; declared surface resistance below 0.05 Ωsq^{-1}	0.086 (6%)	77 (0.1%)	56/47
S4	Silver-coated polyamide plain-weave fabric; declared surface resistance below 0.03 Ωsq^{-1}	0.116 (8%)	72 (0.1%)	51/51

Square samples with a side of 5 cm were prepared in a variant without any damage and in variants with circular-shaped damages of different diameters □ located in the central part of the sample. As was confirmed, the maximum and minimum values of resistances of the textile material are connected directly with the weft/warp direction [32]. During the preparation of the samples, particular attention was paid to ensuring that the sides of the squares aligned parallel to either the warp or weft threads of the fabric. This alignment enabled controlling measurement results regarding the structural orientation of textile material. The variants considered in the investigation are presented in Fig. 2. In total, seven variants of samples from each electroconductive woven fabric were prepared to evaluate changes in resistance being an effect of sample structure damage.
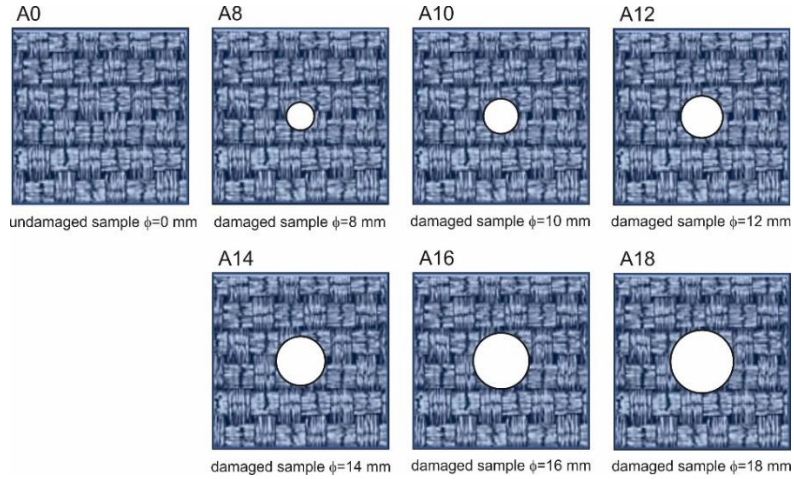
Fig. 2. Variants of woven fabric structure damage.

The van der Pauw method [40] was used for electrical resistance measurements of woven fabrics. Four cylindrical electrodes with a contact diameter with the substrate equal to 2 mm were placed in the corners of the sample (Fig. 3). Between two adjacent electrodes, the direct current *I* was fed. The remaining two electrodes were used to measure the voltage drop *V*. Based on Ohm's law; two resistances can be determined depending on how the electrodes are connected: a horizontal resistance R_h (Fig. 4a) and a vertical resistance R_v (Fig. 4b). In the electrode configuration, the electric current flows on the woven fabric surface, along the warp/weft threads.
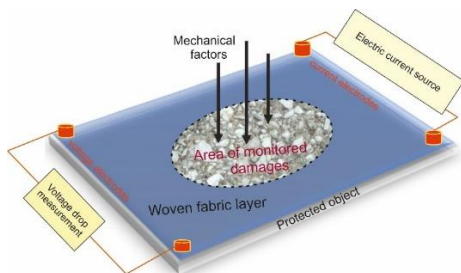
Fig. 3. Woven fabric as a layer protecting against mechanical damages.
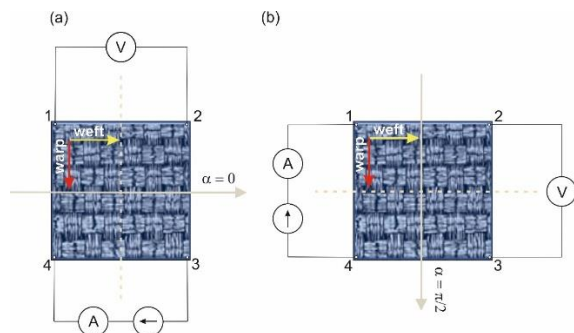
Fig. 4. Resistance measurement: a) horizontal, b) vertical.

Uncertainty analysis [42] of electrical resistance measurement was carried out. Assuming the 0.95 confidence level, the expanded uncertainty of output estimate (resistance) was obtained from the formula:

$$U = k_p u_c(R) \qquad (1)$$

wherein

$$u_C^2(R) = \left(\frac{\partial R}{\partial I}\right)^2 [u_A{}^2(I) + u_B{}^2(I)] + \left(\frac{\partial R}{\partial U}\right)^2 [u_A{}^2(V) + u_B{}^2(V)] \qquad (2)$$

where: k_p - the coverage factor (k_p=2), $u_C(R)$ - the combined standard uncertainty of R, $u_A(\cdot)$ - the Type A standard uncertainty, $u_B(\cdot)$ - the Type B standard uncertainty.

The constant value of electric current I=0.020 A was assumed. A DC power supply AX-3003D-3 Agilent E3644A with a resolution of r_1=0.001 A was used as an ammeter. Therefore $u_A(I)$=0 A, and $u_B(I) = \frac{r_1}{\sqrt{3}} = 5.8 \cdot 10^{-4}$ A. A multimeter Agilent 34410A with a resolution of r_2=0.001 mV was used as a voltmeter. Therefore $u_B(V) = \frac{r_2}{\sqrt{3}} = 5.8 \cdot 10^{-7}$ V. Measurements of the voltage drop V were repeated n=6 times, and the mean value $\bar{V}$ was calculated, and the Type A standard uncertainty was determined from the formula:

$$u_A(V) = \sqrt{\frac{\sum_{i=1}^{6}(V_i - \bar{V})^2}{n(n-1)}} \qquad (3)$$

The relative expanded uncertainty was calculated using the formula:

$$U_{rel} = \frac{U}{R} 100\% \qquad (4)$$

Static sensor characteristics were used for the assessment of electroconductive fabrics as sensory fabrics:

- input range is the maximum and minimum value of the physical variable that can be measured; damage diameter ϕ_{min} and ϕ_{max},

- operating range defines the minimum and maximum values of the measured quantity within which the sensor can provide accurate and reliable measurements; electrical resistance range $[R_{h\min},R_{h\max}]$ and $[R_{v\min},R_{v\max}]$,

- sensitivity is a measure of how well a sensor responds to changes in the measured quantity; it indicates the smallest detectable change in the input that the sensor can reliably measure; sensitivity factor $|dR_h/dA|$ and $|dR_v/dA|$, where A is fabric surface area.

3. Results and discussion

The voltage drop for the woven fabrics was measured according to the measuring scheme (Fig. 4). An uncertainty analysis was conducted for all undamaged and damaged samples. The expanded uncertainty *(1)* and relative expanded uncertainty *(4)* of the horizontal and vertical resistances were determined. Received results are juxtaposed in Tab. 2-5.

Tab. 2. Measurement uncertainty results for fabric S1.

Quantity	A0	A8	A10	A12	A14	A16	A18
R_h, [Ω]	0.1359	0.1284	0.1456	0.1636	0.1713	0.1673	0.2033
U, [Ω]	0.0083	0.0110	0.0086	0.0112	0.0102	0.0101	0.0136
$U_{rel,}$ [%]	6	9	6	7	6	6	7
R_v, [Ω]	0.0173	0.0181	0.0216	0.0236	0.0268	0.0322	0.0336
U, [Ω]	0.0019	0.0015	0.0021	0.0060	0.0027	0.0054	0.0044
$U_{rel,}$ [%]	11	8	10	25	10	17	13

Tab. 3. Measurement uncertainty results for fabric S2.

Quantity	A0	A8	A10	A12	A14	A16	A18
R_h ,[Ω]	0.0844	0.1015	0.0867	0.1031	0.1052	0.1167	0.1441
U, [Ω]	0.0097	0.0063	0.0091	0.0080	0.0072	0.0075	0.0089
$U_{rel,}$ [%]	11	6	10	8	7	6	6
R_v, [Ω]	0.0339	0.0361	0.0468	0.0454	0.0462	0.0604	0.0571
U, [Ω]	0.0046	0.0028	0.0040	0.0055	0.0032	0.0039	0.0040
$U_{rel,}$ [%]	14	8	9	12	7	6	7

Tab. 4. Measurement uncertainty results for fabric S3.

Quantity	A0	A8	A10	A12	A14	A16	A18
$R_{h,}$ [Ω]	0.0153	0.0183	0.0180	0.0204	0.0214	0.0243	0.0228
U, [Ω]	0.0028	0.0020	0.0031	0.0039	0.0022	0.0040	0.0041
$U_{rel,}$ [%]	18	11	17	19	10	16	18
$R_{v,}$ [Ω]	0.0095	0.0119	0.0126	0.0129	0.0132	0.0147	0.0154
U, [Ω]	0.0010	0.0020	0.0020	0.0014	0.0020	0.0023	0.0020
$U_{rel,}$ [%]	11	17	16	11	15	16	13

Tab. 5. Measurement uncertainty results for fabric S4.

Quantity	A0	A8	A10	A12	A14	A16	A18
$R_{h,}$ [Ω]	0.0083	0.0104	0.0099	0.0118	0.0126	0.0127	0.0139
U, [Ω]	0.0018	0.0016	0.0014	0.0016	0.0010	0.0020	0.0015
$U_{rel,}$ [%]	22	15	14	14	8	16	11
$R_{v,}$ [Ω]	0.0033	0.0043	0.0040	0.0043	0.0053	0.0055	0.0058
U, [Ω]	0.0006	0.0005	0.0006	0.0004	0.0005	0.0014	0.0007
$U_{rel,}$ [%]	18	12	15	9	9	25	12

Planar anisotropy of electroconductive woven fabrics is observed when the value of electrical resistance depends on the sample's orientation on a plane. Differences between mean values of vertical and horizontal resistances measured for seven variants (Tab. 2-5) of each fabric were assessed. The Mann-Whitney U-Test was used [43]. The test was performed using Statistica®, and the p-value (p) was calculated. The p-value is compared with the critical value α for rejecting the null hypothesis. If $α<p$, the null hypothesis must not be rejected. The critical value of $α=0.05$, being a significance level, was assumed. Results of the Mann-Whitney U-Test obtained for fabrics S1, S2, S3, and S4 are given in Fig. 5.

Based on the statistical analysis, it was found a significant difference between horizontal and vertical resistances at 0.05 significance level for all tested samples ($α>p$). Moreover, it can be concluded that electroconductive fabrics are characterized by planar electrical anisotropy.

(a)

S1

(b)

S2

(c)

S3

(d)

S4
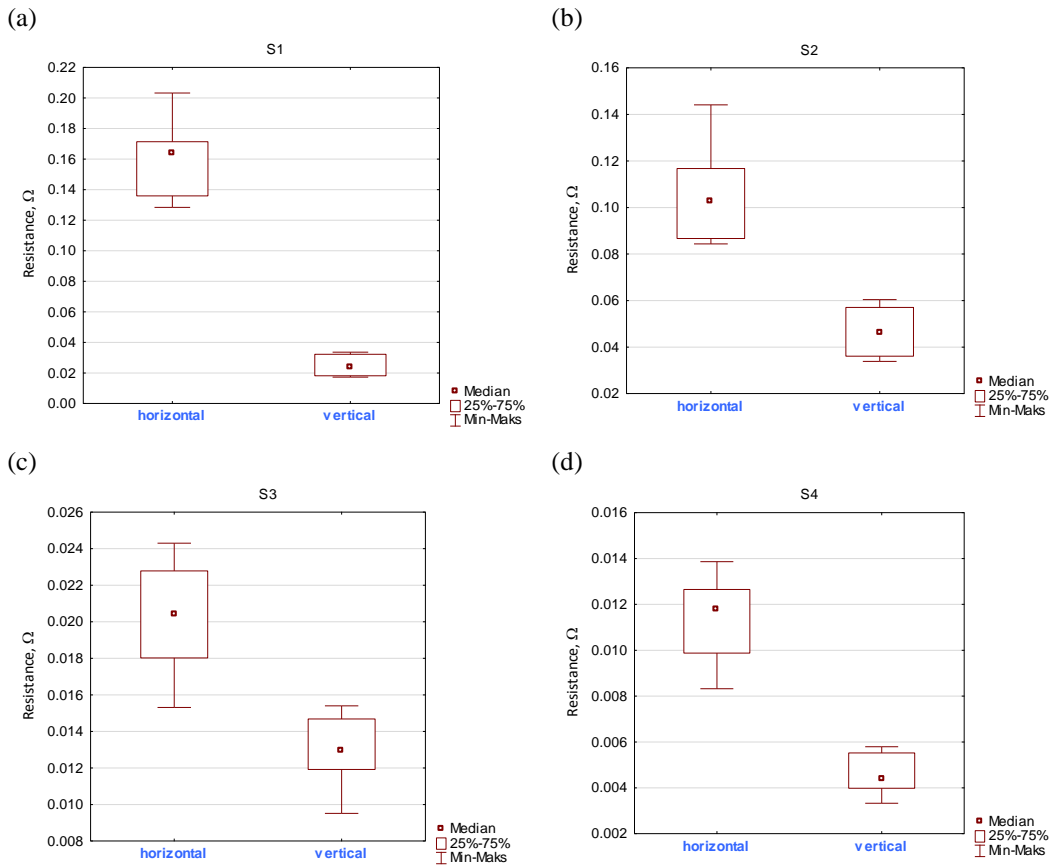
Fig. 5. Mann-Whitney U-Test: a) $p=0.003$, b) $p=0.002$, c) $p=0.002$, d) $p=0.002$.

The impact of fabric damage on electrical resistance was investigated. The initial fabric surface area was equal to 25 cm^2. Every damage caused a decrease in the area of a sample as presented in Tab. 6.

Tab. 6. The surface area of undamaged and damaged samples.

Variant	A0	A8	A10	A12	A14	A16	A18
Damage diameter ϕ, [mm]	0	8	10	12	14	16	18
Surface area A, [cm^2]	25.0	24.5	24.2	23.9	23.5	23.0	22.5

The dependence of the sample resistance on its surface, and thus the degree of fabric damage, is shown in Fig. 6 for fabrics S1, S2, S3, and S4.
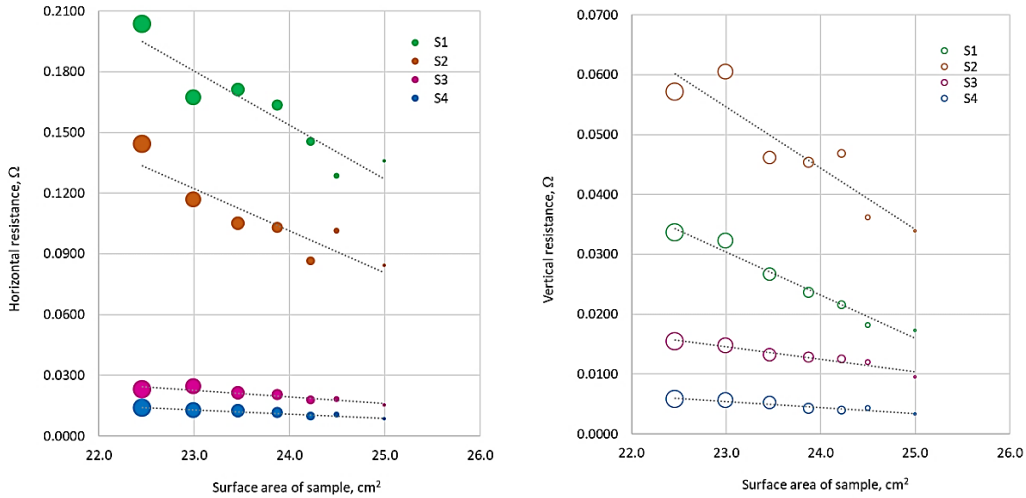
Fig. 6. Surface area of sample vs. electrical resistance (horizontal and vertical).

As the area of damage in the fabric increased, the increase in the electrical resistance exhibited by the sample was observed. This indicates a direct relationship between the size of the damage and the electrical properties of the fabric. Based on the results presented in Fig. 6, it was assumed that the dependence of the electrical resistance R (horizontal or vertical) on the surface area A can be described by a linear model $R(A)=aA+b$, where a, b are the model parameters. Statistical tests were used to assess the significance of the model parameters (Student's t-Test) and the model adequacy (Fisher F-Test). A significance level of α=0.05 was assumed. Results of statistical analysis for models $R_h=f(A)$ and $R_v=f(A)$ are presented in Tab. 7 and 8, respectively. A coefficient of determination (R^2) is given additionally.

Tab. 7. Statistical analysis of model $R_h=f(A)$.

Fabric	Significance of model parameters,				Adequacy of model,	
	a [Ω/cm^2]	p-value	b [Ω]	p-value	R^2	p-value
S1	-0.026741	0.002417	0.795437	0.000883	0.8645	0.000000
S2	-0.020779	0.004626	0.600213	0.001990	0.8254	0.000002
S3	-0.003273	0.002039	0.097955	0.000719	0.8732	0.000000
S4	-0.002082	0.000564	0.060881	0.000213	0.9235	0.000000

Tab. 8. Statistical analysis of model $R_v=f(A)$.

Fabric	Significance of model parameters,				Adequacy of model,	
	a [Ω/cm^2]	p-value	b [Ω]	p-value	R^2	p-value
S1	-0.007193	0.000060	0.195853	0.000031	0.9685	0.000000
S2	-0.010200	0.003375	0.289189	0.001556	0.8456	0.000002
S3	-0.002093	0.000503	0.062666	0.000169	0.9269	0.000000
S4	-0.000981	0.000541	0.027971	0.000230	0.9248	0.000000

It was found that the model parameters are significant, and the models are adequate at the significance level of $\alpha=0.05$. Fabric-based sensors are linear sensors. They produce an output proportional to the input quantity. The input range being the range of damaged surface area [0.5,2.5] cm^2 is assumed for all sensory fabrics. It means that the minimum damage diameter equals $\phi_{min}=8$ mm. Chosen sensor parameters were determined based on obtained linear characteristics (Tab. 9).

Tab. 9. Fabrics-based sensor static characteristics.

Fabric	Operating range [Ω]		Sensitivity factor [Ω/cm^2]	
	[$R_{h min}$,$R_{h max}$]	[$R_{v min}$,$R_{v max}$]	|dR_h/dA|	|dR_v/dA|
S1	[0.127,0.195]	[0.016,0.034]	0.027	0.007
S2	[0.081,0.134]	[0.034,0.060]	0.021	0.010
S3	[0.016,0.024]	[0.010,0.016]	0.003	0.002
S4	[0.009,0.014]	[0.003,0.006]	0.002	0.001

Statistical analysis allows us to conclude that there are significant differences between horizontal and vertical resistances for all electroconductive woven fabrics. The horizontal resistance is higher than the vertical one, so that is why the horizontal resistance should be measured in the system for damage detection. The sensitivity factors are also higher in this case. From the point of view of the sensory, fabrics S1 and S2 have an advantage over others (S3, and S4). The highest values of sensitivity factors are observed for S1 and S2 fabrics. The operating range is also the widest.

4. Conclusions

Fabric-based sensors can be used as a protective layer of objects and, due to their ability to generate an electric signal, can directly monitor changes in electrical resistance. It was found that the electrical resistance increases with increased mechanical damage to the fabric surface; the dependence is linear for all fabrics. As the resistance increases, the fabric loses its protective properties, which may damage the object. The minimum area of damage that can be detected using the fabric-based sensors is 0.5 cm^2, while the maximum is 2.5 cm^2. The permissible area of fabric damage should be determined individually depending on the protecting object. The attention was drawn to the fact that fabrics exhibit an electrical in-plane anisotropy. Significant differences exist between horizontal and vertical resistances for all electroconductive woven fabrics. From the sensory point of view, fabrics S1 and S2 are the best due to their highest values of sensitivity factors and widest operating ranges.

References

[1] Choudhry N.A., Arnold L., Rasheed A., Khan I.A., Wang L.: *Textronics - A review of textile-based wearable electronics*, Advanced Engineering Materials, 23(12), 2023, pp. 1-19.

[2] Simegnaw A.A., Malengier B., Rotich G., Tadesse M.G., Van Langenhove L.: *Review on the integration of microelectronics for E-Textile*, Materials, 14(17), 2021, pp. 1-27.

[3] Biermaier C., Bechtold T., Pham T.: *Towards the functional ageing of electrically conductive and sensing textiles: A review*, Sensors, 21(17), 2021, pp. 1-32.

[4] Chatterjee K., Tabor J., Ghosh T.K.: *Electrically conductive coatings for fiber-based e-textiles*, Fibers, 7(6), 2019, pp. 1-46.

[5] Gaubert V., Boddaert X., Djenizian T., Delattre R.: *Textile electronic circuits from laser-patterned conductive fabric*, Advanced Engineering Materials 25(9), 2023, pp. 1-9.

[6] Du K., Lin R., Yin L., Ho J.S., Wang J., Lim C.T: *Electronic textiles for energy, sensing, and communication*, iScience, 25(5), 2022, pp. 1-24.

[7] Horrocks A.R., Anand S.C. (red.) *Handbook of technical textiles, 2nd edition, Vol. 2: Technical textile applications*, Elsevier 2016.

[8] Leśnikowski J.: *Research into the textile-based signal lines made using ultrasonic welding technology*, Autex Research Journal, 22(1), 2022, pp.11-17.

[9] Krzemińska S., Greszta A., Bartkowiak G., Dąbrowska A., Kotas R., Pękosławski B., Małachowski B., Miśkiewicz P.: *Evaluation of heating inserts in active protective clothing for mountain rescuers - preliminary tests*, Applied Sciences, 13(8), 2023, pp. 1-19.

[10] Kubiak P., Leśnikowski J., Gniotek K.: *Textile sweat sensor for underwear convenience measurement*, Fibres and Textiles in Eastern Europe, 24(6), 2016, pp. 151-155.

[10] Lam E., Alizadeh-Meghrazi M., Schlums A., Eskandarian L., Mahnam A., Moineau B., Popovic M.R.: *Exploring textile-based electrode materials for electromyography smart garments*, Journal of Rehabilitation and Assistive Technologies, 9, 2022, pp. 1-18.

[11] Leśnikowski J.: *Research on poppers used as electrical connectors in high speed textile transmission lines*, Autex Research Journal, 16(4), 2016, pp. 228-235.

[12] Husain M.D., Kennon R., Dias T.: *Design and fabrication of Temperature Sensing Fabric*, Journal of Industrial Textiles, 44(3), 2014, pp. 398-417.

[13] Shabani A., Hylli M., Kazani I.: *Investigating properties of electrically conductive textiles: A review*, Tekstilec, 65(3), 2022, pp. 194-217.

[14] Pizarro F., Villavicencio P., Yunge D., Rodríguez M., Hermosilla G., Leiva A.: *Easy-to-build textile pressure sensor*, Sensors, 18(4), 2018, pp.1-13.

[15] Cho S., Chang T., Yu T., Lee C.H.: *Smart electronic textiles for wearable sensing and display*, Biosensors, 12(4), 2022, pp. 1-30.

[16] Zhou Z., Chen N., Zhong H., Zhang W., Zhang Y., Yin X., He B.: *Textile-based mechanical sensors: A review*, Materials, 14(20), 2021, pp. 1-22.

[17] Capineri L.: *Resistive sensors with smart textiles for wearable technology: from fabrication processes to integration with electronics*, Procedia Engineering, 87, 2014, pp. 724-727.

[18] Alsaadi A., Meredith J., Swait T., Curiel-Sosa J.L., Hayes S.: *Damage detection and location in woven fabric CFRP laminate panels*, Composite Structures, 220, 2019, pp. 168-178.

[19] Hou L., Hayes S.A.: *A resistance-based damage location sensor for carbon-fibre composites*, Smart Materials and Structures, 11(6), 2002, pp. 966-969.

[20] Ojstršek A., Plohl O., Gorgieva S., Kurecic M., Jancic U., Hribernik S., Fakin D.: *Metallisation of textiles and protection of conductive layers: An overview of application techniques*, Sensors, 21(10), 2021, pp. 1-28.

[21] Castano L.M., Flatau A.B.: *Smart fabric sensors and e-textile technologies: a review*, Smart Materials and Structures, 23(5), 2014, pp. 1-27.

[22] Zeng W., Shu L., Li Q., Chen S., Wang F., Tao X.-M.: *Fiber-based wearable electronics: A review of materials, fabrication, devices, and applications*, Advanced Materials, 26(31), 2014, pp. 5310-5336.

[23] Guo R.H., Jiang S.X., Yuen C.W.M., Ng M.C.F., Lan J.W.: *Metallized textile design through electroless plating and tie-dyeing technique*, Journal of The Textile Institute, 104(10), 2013, pp. 1049-1055.

[24] Bierwagen O., Ive T., Van de Walle Ch.G., Speck J.S.: *Causes of incorrect carrier-type identification in van der Pauw-Hall measurements*, Applied Physics Letters, 93, 2008, pp. 1-4.

[25] Pawłowski S., Plewako J., Korzeniewska E.: *Influence of structural defects on the resistivity and current flow field in conductive thin layers*, Electronics, 9(12), 2020, pp. 1-12.

[26] Smits F.M., *Measurement of sheet resistivity with the four-point probe*, The Bell System Technical Journal, 37(3), 1958, pp. 711-718.

[27] uz Zaman S., Tao X., Cochrane C., Koncar V.: *Understanding the washing damage to textile ECG dry skin electrodes, embroidered and fabric-based; set up of equivalent laboratory tests*, Sensors, 20(5), 2020, pp. 1-16.

[28] Chen H.H.: *Damage detection of carbon fiber reinforced polymer using electrical measurement and analysis of acoustic emission signals*, Doctoral dissertation, University of Akron 2013.

[29] Liepa V., Santosa F., Vogelius M.: *Crack determination from boundary measurements reconstruction using experimental data*, Journal of Nondestructive Evaluation, 12(3), 1993, pp. 163-174.

[30] Schueler R., Joshi S.P., Schulte K.: *Damage detection in CFRP by electrical conductivity mapping*, Composites Science and Technology, 61(6), 2021, pp. 921-930.

[31] Tokarska M., Miśkiewicz P., Pawlak W.: *Research on the planar electrical anisotropy of conductive woven fabrics*, Advanced Engineering Materials, 25(13), 2023, pp. 1-10.

[32] Kazani I., De Mey G., Hertleer C., Banaszczyk J., Schwarz A., Guxho G., Van Langenhove L.: *Van der Pauw method for measuring resistivities of anisotropic layers printed on textile substrates*, Textile Research Journal, 81(20), 2011, pp. 2117-2124.

[33] Tyurin I.N., Getmantseva V.V., Andreeva E.G.: *Van der Pauw method for measuring the electrical conductivity of smart textiles*, Fibre Chemistry, 51(2), 2019, 139-146.

[34] Tokarska M., Gniotek K.: *Anisotropy of the electrical properties of flat textiles*, The Journal of The Textile Institute, 106(1), 2015, pp. 9-18.

[35] Kazakov F., Sattarova N., Aripova O.: *Metallized fabrics for environmentally safe applications in textile industry and filter production*, IOP Conf. Series: Earth and Environmental Science, 1112, 2022, pp. 1-7.

[36] Ojstršek A., Jug L., Plohl O.: A review of electro conductive textiles utilizing the dip-coating technique: their functionality, durability and sustainability, Polymers, 14(21), 2022, pp. 1-26.

[37] Lu X., Shang W., Chen G., Wang H., Tan P., Deng X., Song H., Xu Z., Huang J., Zhou X.: *Environmentally stable, highly conductive, and mechanically robust metallized textiles*, ACS Applied Electronic Materials, 3(3), 2021, pp. 1477-1488.

[38] Tomilina O.A., Berzhansky V.N., Tomilin S.V.: *The influence of the percolation transition on the electric conductive and optical properties of ultrathin metallic films*, Physics of the Solid State, 62, 2020, pp. 700-707.

[39] Van der Pauw L.J.: *A method of measuring specific resistivity and Hall effect of discs of arbitrary shape*, Philips Research Reports, 13(1), 1958, pp. 1-9.

[40] Kazani I., De Mey G., Hertleer C., Banaszczyk J., Schwarz A., Guxho G., Van Langenhove L.: *About the collinear four-probe techniques inability to measure the resistivity of anisotropic electroconductive fabrics*, Textile Research Journal, 83(15), 2013, pp. 1587-1593.

[41] ISO/IEC Guide 98-3:2008(En). Uncertainty of Measurement-Part 3: Guide to the Expression of Uncertainty in Measurement.

[42] Corder G.W., Foreman D.I.: *Nonparametric statistics for non-statisticians: A step-by-step approach*, Wiley, Hoboken 2009.

Study on the friction coefficient between eggshells and powders with various chosen surfaces

Badania współczynnika tarcia między skorupkami i proszkami jaj a różnymi wybranymi powierzchniami

Marek Wozniak[1], Maciej Kuchar[1], Sergiusz Zakrzewski[1], Krzysztof Siczek[1*],

Andrzej Obraniak[2], Adam Rylski[3], Przemyslaw Kubiak[4]

[1] Department of Vehicles and Fundamentals of Machine Design, Lodz University of Technology, Stefanowskiego Str. 1/15, 90-537 Lodz, Poland; [2] Faculty of Process and Environmental Engineering, Lodz University of Technology, Wolczanska Str. 213, 90-924 Lodz, Poland; [3] Institute of Materials Science and Engineering, Lodz University of Technology, Stefanowskiego Str. 1/15, 90-537 Lodz, Poland; [4] Division of Ecotechnics, Lodz University of Technology, Wolczanska Str. 221, 93-005 Lodz, Poland.

Abstract
Transport of fresh or powdered chicken eggs uses conveyors with elements made of steel or plastics, and surfaces often coated by Teflon. Various forms of eggs contact with said surfaces and are subject to friction processes between them. The frictional resistances cause a load on the devices driving the conveyors and a local and temporary increase in temperature in the contact zones and allow the abrasive wear of both the surfaces of the conveyors, packages and the eggshells themselves. This study aimed to determine such the coefficient of friction and wear intensity at various contacts. The friction and wear tests were conducted on two tribotesters and the results are shown in the article.

Abstrakt
Transport świeżych lub sproszkowanych jaj kurzych wykorzystuje przenośniki z elementami wykonanymi ze stali lub tworzyw sztucznych, a powierzchnie często pokryte teflonem. Różne formy jaj stykają się ze wspomnianymi powierzchniami i podlegają procesom tarcia między nimi. Opory tarcia powodują obciążenie urządzeń napędzających przenośniki oraz lokalny i tymczasowy wzrost temperatury w strefach styku i pozwala na zużycie ścierne powierzchni przenośników, pakietów i samych skorupek jaj. Badanie to miało na celu określenie takiego współczynnika tarcia i intensywności zużycia w różnych stykach. Testy tarcia i zużycia przeprowadzono na dwóch tribotesterach, a wyniki pokazano w artykule.

---

*corresponding author e – mail: ks670907@p.lodz.pl

1. Introduction

Fresh or powdered eggs, mainly of chicken, are used and processed in the production processes of the food industry. They are transported either by gravity on inclined chute surfaces of fixed structures used during a specific production process, or by means of various conveyors, the elements of which are made of various materials, such as stainless steel or some plastics. The surfaces of these elements can be covered with protective coatings, such as Teflon. During transport between different devices of the production process, the different forms of eggs come into contact with said surfaces and are subject to friction processes between them. Such friction occurs with relatively small loads and displacements of various nature and size. These can be both small vibration movements, such as when transporting fresh eggs in packages, and large movements, when transporting powdered egg or shells on conveyors. The existing frictional resistance causes the load on the devices driving the conveyors and the local and transient increase in temperature in the contact zones, and allows the surface of the conveyors, packaging and the eggshells to be worn. The proper flow of egg production, processing and packaging is strongly affected by physical features of eggs and their resistance to damage via a mechanical shock. The size of an egg depends on age, breed and weight of the chicken. Eggs can belong to various strict size categories according to weight (more specifically to minimum net weight expressed in oz per dozen), including peewee (35–42 g), small (42–49 g), medium (49–56 g), large (56–65 g), extra large (65–70 g) and jumbo (70 g). The most commonly available are medium, large and extra large ones [1, 2]. Egg size and the eggshell thickness are highly correlated. The size of an egg mainly depends on the age, breed and weight of the hen. As the hen ages, her eggs increase in size. Pullets with significant underweight at sexual maturity produce small eggs. The egg weight is weakened by heat, stress, overcrowding and poor nutrition. Chicken eggs are commonly treated as packaged food. During transportation, a crucial role of the packaged egg

material plays the mechanical strength of the eggshell. Eggshell quality is affected by egg size and weight. Egg shape index and eggshell thickness decide to the number of damaged eggs over handling and transport [3].

Cahya and Marfuah [4] found that eggshells of domestic chicken, chicken broiler, duck and quail had almost the same initial structure with $CaCO_3$ rhombohedra crystals. According to Athanasiadou et al. [5] eggshells create a hard, protective biomineralized chamber for embryonic growth. In the calcitic chicken eggshell, the mineral and organic phases organize hierarchically across various length scales. Variation in nanostructure across the shell thickness influences its hardness, elastic modulus, and dissolution features. The nanostructure varies during egg incubation, weakening the shell for chick hatching. The above mentioned powdered eggs are often used in the production of food products such as cakes or ice cream in order to reduce the penetration of Salmonella bacteria, sometimes present in raw eggs, into the processed raw material. Belyavin [6] stated that, there are four major headings of dried egg products available: dried egg white, dried plain whole egg and yolk, dried blends of whole egg and yolk with carbohydrates, and special types of dried egg products. A weakening of the moisture content in egg powder from around 74% to 2–4% by weight decreases weight and volume and a concentration of food value. The physical properties important for dried egg products are bulk density, dispersibility, solubility, and reconstituted viscosity

In Ref. [7] was explained that the microwave generated by the microwave drying machine of egg powder and yolk powder can penetrate the inside and outside of the object and heat it simultaneously. The friction between molecules generates heat itself to achieve the effect of rapid drying. According to [8] values of temperature above 43 °C are not recommended for the storage of egg powder.

The study aimed to determine the coefficient of friction at various contacts of eggshells and egg powder with samples made of stainless steel with and without Teflon coating, often used in various production processes. Additionally, the wear intensity in contacts between eggshells was determined.

2. Properties of egg, eggshells, egg powders and products containing eggshells

The physic-chemical properties of fresh and processed eggs and egg-related products are very important, particularly as they affect the safe conditions of storage and transport of such products and therefore have been extensively studied at various centres.

2.1. The physic-chemical properties of fresh and processed eggs and egg products

The eggshell strength is the important parameter of the egg quality [9-17]. Eggshell strength is affected by the thickness of eggshell, shell stiffness and rupture force and energy [18-20]. The highest correlation existed between the physical and the mechanical features of chicken eggs [21, 22]. Several studies were carried out on the properties of chicken and Japanese quail eggs under various compression loads [18, 22-24]. The eggshell strength was strongly affected by the compression speed [18, 19]. There were significant correlations between egg palisade length and breaking strength, shell thickness and stiffness [25]. Kumbar et al. [26] determined weight, weight loss, shape index, yolk height, albumen height, yolk index, albumen index, and Haugh units of the geese eggs. They also studied the rheological behavior of liquid egg products (egg yolk, albumen, and whole liquid egg) using a concentric cylinder viscometer. Flow curves of all liquid egg products exhibited non-Newtonian shear thinning behavior well described by the Herschel-Bulkley model or the Ostwald-de Waele model. The storage duration affected the rheological behavior of various liquid egg products in a different manner. Except the very low shear rates, the viscosity of the egg yolk as well as of the whole liquid egg weakened with storage time. At lower shear rates the albumen viscosity enhanced with storage duration. The ultimate tensile strength, fracture strain, and fracture toughness of the eggshell membrane enhanced with the loading rate but decreased during the egg storage.

Mahmoodi et al. [27] found that the exposition of egg samples to the magnetic field enhanced the shell's resistance to failure. Additionally, samples immersed in sunflower oil had a lower failure force than those not immersed in such an oil. Eggshells are more and more utilized in the form of nano powders, particularly in medicine [28] and biomedicine [29-33]. There are various experimental techniques used for the eggshell strength measurement [34-48], both destructive and non-destructive. The shell strength of a chicken egg is usually determined by the quasi-static, non-destructive compression of an egg betwixt two parallel steel plates [21].

Interestingly, Severa et al. [44] discussed the suitability and applicability of a Berkovich indentation for determination of mechanical properties of hen's eggshell tested in the area surrounding equator line. Nanoindentation was found as a suitable tool for determining local variations of mechanical properties of eggshells. The very important problem for the food industry is the occurrence of various contaminations in eggs and their shells [45-48] such as Salmonella, antibiotics, dioxins and others.

The presented literature reports show that the physical and the mechanical properties of eggs, particularly of chicken ones are strongly corelated. A number of parameters characterizing the properties of eggs have been distinguished, such as i.e., weight of eggs and shells, protein content, crude fat, crude fiber, ash content, total and essential amino acids. The eggshell strength and its possible brittle cracking strongly affect the wear of a whole egg. Various methods allowing measuring eggshell strength can be useful for determining the model parameters of the egg mechanical wear, however, no model even partially described wear of the whole egg has been found in the literature so far. Additionally, no model describing the effect of contamination in egg and in eggshell on the wear of the whole egg or on the friction between eggshell and other eggshell or other surfaces has been found in the literature so far.

2.2. The properties of egg powders

According to [49], the powdered eggs have an advantage over the fresh ones that their contamination from the breakage of shells is impossible. Daramola [50] reported that whole egg powders produced by spray, freeze or dehydrator methods are generally accepted and serve as good alternatives to fresh eggs in addition to their use in the confectionery industry not compromising the final product quality. Huda et al. [51] compared the physicochemical characteristics of egg white powder from eggs of various types of bird (local kampung chicken, local fighting chicken, local serama chicken, leghorn chicken, turkey, and guineafowl). The mentioned characteristics of egg white powder varied noticeably among eggs from various types of bird. Koç et al. [52] studied the effect of moisture on the glass transition temperature (Tg), flow properties, color, and morphology of spray-dried powdered egg. They found that the glass transition temperature of powdered egg weakened with an enhancement of water activity. At low water activity values, the powder exhibited poor flowability and high cohesiveness. Koç et al. [53] studied physical properties and oxidative stability of egg powder microencapsulated by spray drying. They reported that the use gelatin as wall material highly enhanced the moisture content and water activity of egg powder over storage and it increases flowability. Egg powders comprising pullulan as wall material had a fibrous structure and the lowest bulk density. Insertion of lactose as wall material improved the oxidative stability. Lai [54] studied water sorption and flow characteristics of whole egg powder with and without flow conditioners. Flow conditioner silica and sodium silico-aluminate enhanced the egg powder's flowability due to particle surface modification. Insertion of the conditioners eliminated the hysteresis loop and increased the moisture uptake by powders. Ndife et al. [55] reported that egg yolk powder exhibited higher emulsification capacity and stability in comparison to whole egg and egg white powder. The egg white powder exhibited higher foam stability and capacity compared to whole egg and egg yolk powders. The highest

coagulation temperature was for egg yolk, followed by whole egg and egg white. The highest solubility occurred in egg white, followed by whole egg and egg yolk powders, while the inverted tendency occurred for the water and oil absorption properties. The total solids were high in all powders studied. Kudre et al. [56] studied physicochemical and functional features of freeze-dried egg powders from Japanese quail and white Leghorn chicken. The β-sheet showed to be the major secondary structure of all egg powders. The quail egg powders exhibited higher protein solubility than corresponding chicken egg powders at all pH tested. Quail egg powders exhibited higher emulsion activity index and emulsion stability index with higher foam expansion and stability than the corresponding chicken egg powders. Asghar and Abbas [57] studied the effect of utilization of whole egg powder with the replacement of fresh eggs in the bakery products. Chemical analysis of whole egg powdered cake at different doses showed the mean values of 29% moisture content, 1.5% ash, 8% fat, 5.8% protein, 2% fiber and 1.4% water activity. The sensory evaluation of cakes having 100% substitution showed the high results' significance.

Using the conductivity technique [58] studied emulsifying properties of oil in water emulsions using quail egg white protein as an emulsifying agent. They investigated the effect of various salt concentrations (NaCl) when mixed with carious egg white concentrations for corn and soybean vegetable oils. They found that emulsifying activity and emulsion stability enhanced with the increase of salt concentration. The increase of the egg white concentration weakly influenced emulsifying activity, increasing only the emulsion stability. It is clearly visible that the egg powder is a moisture of different egg components and varying amount of water, which can strongly affect the friction inside such a moisture or between the moisture and various surfaces. No model describing the effect of composition of egg powder and particularly a water amount therein on the friction inside egg powder or between egg powder and the other surfaces has been found in the literature so far.

2.3. Friction behavior of egg and egg-related product

Some authors investigated friction between egg and different surfaces. Altuntas and Sekeroglu [24] studied the effect of chicken egg weight on static coefficient of friction on various surfaces. The static coefficients of friction on glass, plywood, galvanized metal, rubber and chipboard, enhanced proportionally to an increase of egg weight tested. The rubber surface exhibited the maximum friction followed by plywood, chipboard, galvanized metal and glass. Polat et al. [23] reported that for Japanese quail eggs the values of the friction coefficient for quail eggs on the surfaces of plywood, glass, galvanized steel and fibreglass were equal to 0.301, 0.282, 0.274 and 0.266, respectively. Salawu et al. [59] studied the effect of pulverized organic carbon (Palm kernel shell and eggshell) on the mechanical properties of grey cast iron material with a chemical composition (wt.%) of 2.68C, 1.42 Si, 0.63 Mn, 0.13 S, 0.28 P. A mixture of 70 (wt.%) of pulverized palm kernel shell and 30 (wt.%) of pulverized egg shell was used for carburization of grey cast iron samples conducted at 900 □C for 60 minutes. There occurred the variation of force with time during sliding wear test carried out. The frictional force exhibited values of 0.0000796, 0.0000438 and later increased to a 0.086 and 0.10. The low friction observed at the initial stage of sliding was due to presence of oxide films and moisture at the interface of the material tested. The low friction was traceable to the high hardness value obtained from the mixture used during carburization. No information has been found about values of friction inside egg powder or eggshell powder and between eggshell and the other eggshell and also between egg powder or eggshell powder and other surfaces so far.

2.4. Wear of eggs end egg-related products

Some authors investigated wear properties of various egg-related products. Oladele et al. [60] studied the effects of calcined and uncalcined eggshell particles (ESP) and sisal fiber (SF) on the mechanical and wear characteristics of eggshell

particles/sisal fiber reinforced epoxy composites. They found that calcination decreased the content of Ca and enhanced that of O in eggshells. The strong $CaCO_3$ occurred in uncalcined eggshell while Fe and $Ca_2Fe_7O_{11}$ in calcined one. Flexural features, tensile modulus and hardness increased for uncalcined eggshell particle-based composites while impact and wear resistance enhanced for the calcined eggshell particles based one. Using a pin-on-disk operating under nominally non-abrasive conditions of samples investigated, Venkatesh et al. [61] studied the wear and friction of implants coated by naturally derived powders like Seashell powder, Eggshell powder and Aluminium Oxide (Al_2O_3). Such coating materials were used to protect the surface of the implant material and interface with biological system. The polymers namely Nylon and Teflon were used as substrate and coated with above powder by using thermal spray method. Wear test was carried out to determine the wear resistance of the coated specimen, to assure the wear properties which is essential requirements of implants. They found that plasma spray deposition provided proper coating thickness and phase purity of powder samples after deposition. The powders derived from natural sources like Aluminium oxide, eggshells and sea shell were naturally bio-active and biocompatible. Eggshell coated Teflon and Al_2O_3 coated Nylon exhibited the better wear properties compared to other specimens. Dwiwedi et al. [62] carried out wear test on Al6061/eggshell composites under controlled load, reinforcement and sliding distance. They found that reinforcement of eggshell particles increased the wear resistance of matrix noticeably. Parivendan and Ramesh [63] studied the mechanical, tribological and thermal characteristics of hemp fibre reinforced eggshell epoxy polymer composites. Particularly, they investigated the effect of fiber and filler amounts on the mentioned characteristics of epoxy-based polymer composites. They conducted mechanical test on hardness, tensile, impact and flexural strength. They also studied abrasive wear of the specimen using pin-on-disc machine. The thermal stability was evaluated using a thermo gravimetric analyzer. The effect of hemp fibre and filler were studied under various mechanical

and thermal conditions. They found that the insertion of fibre enhanced the load bearing ability of epoxy resin. Whereas insertion of eggshell filler enhanced thermal stability of composite. No information about values of wear of whole egg or eggshell and egg powder and no methods for their determination have been found in literature so far.

3. Properties of egg, eggshells, egg powders and products containing eggshells

3.1. The physic-chemical properties of fresh and processed eggs and egg products

3.1.1. The bulk density of the egg powder.

During the research, the bulk density was determined by weighing the samples on a digital balance and measuring their bulk volumes using a 250 cm3 glass measuring cylinder.

Bulk density values were calculated from equation *(1)*:

$$\rho_{egg-powder} = \frac{m_{ep+c} - m_c}{V_c} \qquad (1)$$

where:

m_{ep+c} - mass of the sample together with the measuring cylinder,

m_c - mass of the measuring cylinder,

V_c - volume of granules in the measuring cylinder.

It is necessary to differ between the loose volume and the compacted one of granulate.

The loose volume of granulate is obtained by gravity filling the measuring cylinder with the granulate to the nominal value of its volume.

The compacted volume of granulate is obtained by placing the cylinder with the granulate on a laboratory shaker, subjecting it to vibrations and adding granules by

gravity until the maximum organoleptically observed compacting of the granulate mass in the cylinder at the nominal value of its volume.

3.1.2. Natural repose angle

The angle β of natural repose is calculated from equation *(2)*:

$$\beta = \cot^{-1}\left(\frac{2h}{D}\right) \qquad\qquad (2)$$

where:

h - height of a cone of a granulate heaped on shedding plate,

D - diameter of the shedding plate.

The device for measuring the natural angle of repose of loose granulate is shown in Figure 1. It comprises a container (1), from which the granulate is poured, a shedding plate (2), on which a material cone forms, and a measuring plate (3), which is used to measure the height of the heap, and before emptying the container, it closes the discharge opening. These elements are attached to the frame (4) ensuring their proper position. The container is ended with a flange for mounting with the screws (6) of the discharge funnel (5). Due to the mounting on the support (7), the sheathed plate is tilting. The support leg is attached to the frame with wing bolts (8). The measuring plate with the slider (9) is lifted by the screw (10) fixed in the slide bearings (11) cooperating with it. The rotation of the screw is carried out by the knob (12). The entire device is leveled by means of four height-adjustable feet (13). There is a drawer (14) under the shedding plate, in which loose granulate is collected that is not stuck on the plate. The height of the poured cone is read on the scale (15).
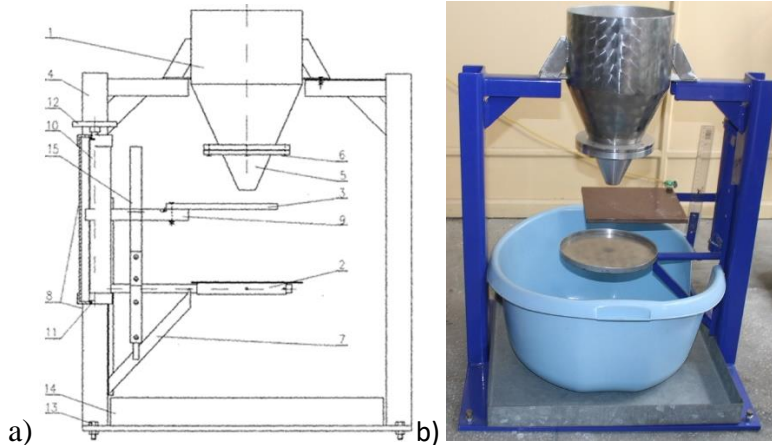
Fig. 1. A device for measuring the angle of repose (description in the text) designed in the Department of Process Apparatus of the Lodz University of Technology; a) scheme of the tester, b) view of the tester.

3.1.3. The coefficient of friction between the egg powder and the metal surface

To measure the friction angle between the egg powder and the surface of the apparatus plate, a test stand was used (Fig. 2). It comprised the measuring tabletop (1), measuring plate (2) made of the same material as the granulator disc and mounted on a hinge to the tabletop, on which the layer of the tested granulate (3) was placed, screw jack (4), which enables smooth lifting or lowering of the measuring plate, protractor (5) which measures the friction angle. The sample of the granulate was poured on the measuring plate in a designated place. Then, using a screw jack, the plate was lifted, and the behavior of the tested material was observed. The lifted plate was stopped as the material moved over the plate. In this state, the angle of the plate inclination relative to the horizontal was measured. Three measurements were made for each sample, and their average value was registered as the value of the angle γ of friction between the granulate and the plate surface. The value of the coefficient of friction μ was equal to tangent of the friction angle γ.
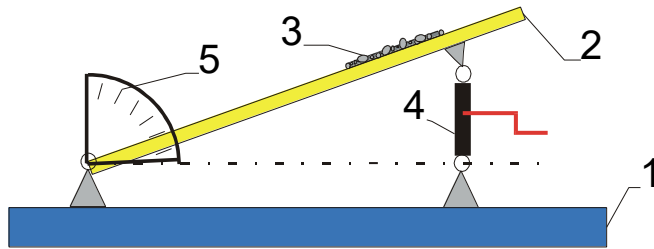
Fig. 2. The tester for measuring the friction angle between the granulate and the granulator disc built for this purpose at the Department of Process Apparatus of the Lodz University of Technology.

3.2. Measurement of eggshell roughness

Using the VHX Keyence digital microscope, the roughness parameters in 4 points chosen on the eggshell was measured before and after boiling of egg tested presented in Fig. 3.
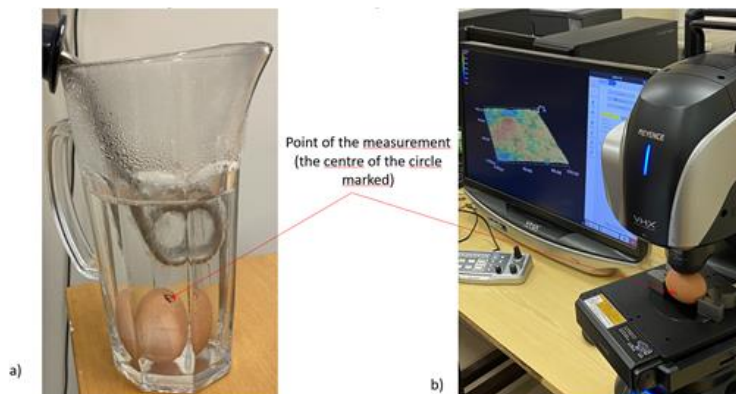
Fig. 3. Measurement of roughness in the 4 points chosen on the surface of eggshell before and after boiling. a) boiling of the egg studied, b) measurement of roughness via the digital microscope VHX KEYENCE.

3.3. Measurement of the friction coefficient between eggshell and surfaces of various base materials.

3.3.1. Preparation of the shell layer for the measurement of the friction coefficient in the shell contacts - metal surface and shells - Teflon coated surface.

The shredded eggshells of a defined medium size distribution were glued to the bottom surface of the paper box by means of starch. The average size of the shells was checked with a fine screen first and then a thin screen to fall within the range of 3mm to 6mm. The gluing process was as follows: a measured dose of crushed shells, sufficient to cover the area of 20 cm^2, was initially sprinkled on the metal surface of the auxiliary plate. The shredded shells had their outer side facing that surface of the plate. It was checked whether all the scattered shell particles met this condition, possibly using tweezers to correct the position of individual shells. The bottom part of the paper box, 53 mm x 35 mm in size, was covered with a thin layer of starch about 0.5 mm thick and at a temperature of about 40 ° C, local irregularities in the layer were smoothed out with a plastic tooth comb with dense distribution. After 5 minutes, the box was placed on a layer of shells and loaded with a metal cuboid weighing 200 g in order to exert a normal force forcing the shells to settle well in the starch layer. After the load was removed, the box was rotated to a position ensuring that the lightened shell layer was placed on its top surface. The resulting combination of the box surface, the starch layer and the shell surface were left for 1 hour for the starch to set. Excess dried starch particles protruding above the height of the lightened shell layer and possibly overlapping the shell surfaces were carefully removed with a razor blade.

3.3.2. Tribotester for determining the friction coefficient between eggshell and surfaces of various base materials.

The simple tribotester used for determining the friction coefficient between

eggshell and surfaces of various base materials studied is presented in Figure 4. Such base material can be made of uncoated stainless steel or of the same steel coated by various protective layer such as the Teflon one. The tribotester comprises the fixed part 1 and the tilting part 2 of the tribotester inclined plane connected by two hinges 4. In the pocket of the tilting part 2, replaceable thin cuboidal insole 3 made of the tested material is placed. The angle of inclination α of the tilting part 2 with respect to the fixed part 1 is measured with a protractor 5. The fixed part and the tilting one 2 cooperate with the leader 6 during measurement. The fixed part 1 and the tilting one 2, with a hinge 4, a leader 6, a swivel yoke 7 and a slider 8 form together the kinematic mechanism of the tribotester. A leader 6 is rigidly connected to the swivel yoke 7, which is rotationally connected with the fixed part 1 via its pin loosely seated therein. During small rotations of the tilting part 2 around the axis of hinges 4, the slider 8 with an eyelet with enlarged hole moves along the leader 6. Such a slider 8 is fixed to the tilting part 2. The motion of the slider 8 can be blocked by the thumbscrew retainer 9 in the needed position relative to the leader 6.
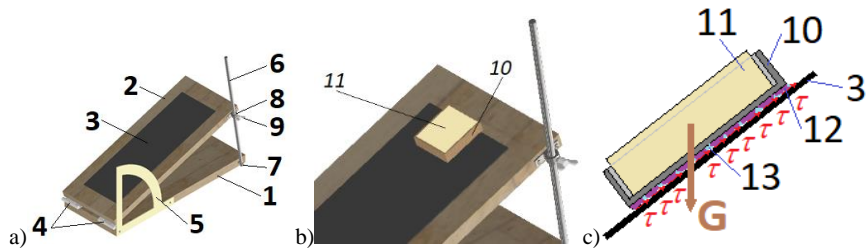
Fig. 4. Tribotester for determining the friction coefficient between eggshell and surfaces of various base materials. general view, b) initial position of paper box with eggshells glued to its bottom plane, c) the model of its contact with the replaceable insert loaded during tests on the tribotester. 1 – the fixed part of the tribotester inclined plane, 2 – the tilting part of the tribotester inclined plane, 3 - replaceable insole made of tested material, 4 – hinge, 5 – protractor, 6 – leader, 7 - swivel yoke, 8 - fixed slider with an eyelet with enlarged hole, 9 – thumbscrew retainer, 10 - paper box with eggshells glued to its bottom plane, 11 – loading metal box, 12- shredded eggshells, 13 – starch.

In the initial state the tilting part 2 with an insole 3 is situated parallel to the fixed part 1 of the tribotester. Then, the paper box 10 with the layer of shredded eggshells 12 glued via starch 13 to the bottom wall of the paper box 10 is placed on the top surface of the insole 3 near the movable end of the tilting part 2. Next, the paper box 10 is loaded by the weight of the metal cuboid 11 to create a contact pressure in the contact zone between shredded eggshells 12 and the surface of the insole 3. The weight of metal cuboid 11 can vary but is fixed during a single measurement. The movable end of the tilting part 4 is raised until the paper box 10 starts moving relative to the surfaces of an insole 3. Next, the thumbscrew retainer 9 is tightened in the threaded hole of the slider 8 until the contact pressure is generated on the retainer's front surface in the area of its contact with the leader 6 and, due to the frictional force resulted, the slider is immobilized against the guide. This allows reading a value of the measured angle α on the protractor 5 and estimating of the friction coefficient μ between eggshell and the surface of an insole 3 from equation *(3)*.

$$\mu(p_c) \approx \tan\alpha \qquad (3)$$

where:

p_c – average contact pressure between eggshell and the surface of an insole,

v – average sliding speed of paper box 10 relative to the surface of an insole 3.

The average contact pressure p_c is estimated from equation (4).

$$p_c \approx \frac{(m_{pb}+m_{mc})\cdot g\cdot\cos\alpha}{k\cdot a\cdot b} \qquad (4)$$

where:

m_{pb} – mass of paper box with a layer of mixture of shredded eggshells 12 and starch 13,

m_{mc} – mass of metal cuboid 11,

g= 9.81 m/s^2 – gravitational acceleration,

a= 53 mm, *b*= 35 mm – dimensions of rectangular bottom wall of the paper box 10, *k* - the factor of filling the surface of the bottom wall of the box by projections of the projecting surfaces of shells. It can be estimated using one of the methods described:

- moisten the surfaces of the eggshells with a colored liquid, e.g., ink, and imprint them on graph paper, and then count the number of colored unit areas (1 mm^2),

- place a transparent glass plate with a mesh scale applied to an inverted box with a group of shells glued to it and count the number of unit areas that overlap with the translucent areas of the shells - this method may, however, give much lower accuracy,

- take a photo of the surface of an inverted box with a group of eggshells glued on it, perpendicularly to this surface, scan the photo, apply a grid scale to the scanned photo and count the number of unit areas overlapping with the areas covered by the protruding eggshell surfaces,

- place the paper box 10 with the layer of shredded eggshells 12 glued, on the Surface Contact Pressure Sensitive Paper [64] placed on the top surface of the insole 3; than determine the area of contact between eggshell and insole surface from the measured values according to the standardized scale that exceeds the assumed minimum level of 5 Pa. It is the most exact method but also the most expensive.

During the present study the method utilizing moisten the surfaces of the eggshells with a colored liquid of the surface of an inverted box with a group of eggshells glued on it has been applied. However, this surface was photographed and placed on graph paper allowing the counting of colored unit areas (1 mm^2).

3.4. The friction torque between the rotating egg and the stationary eggs

3.4.1. Tribotester for determining the friction torque between the rotating egg and the stationary eggs

The friction torque between the rotating egg and the stationary eggs was estimated using the home-made 5-eggs tribotester presented in Figure 5. The measurement principle similar to that utilized in the popular four-ball tribotester was applied in the present tribotester. The four eggs 6 were placed in the recesses made in the plastic bottom holder 5 fixed to the basis 1 and axial-symmetrically arranged about the axis of the rotating screw joint 9. One egg was glued with carpentry glue to the recess in replaceable wooden holder 8 connected with the steel screw joint 9. The shaft integrated with the screw joint 9 is supported in radial plain bearing with the Teflon shell, placed in the bracket fixed to the middle holder 2. The upper end of that shaft was integrated with the rotating disc 10. The disc was also fixed with a vertical mandrel. On the upper surface of the disc 10 was placed the spring stop pin 12 mating with the one arm of the torsional spring 11. This spring was guided on the mentioned vertical mandrel. The second arm of the torsional spring 11 mated with the drive lever pin 13 fixed to the drive lever 14. Such lever was fixed to the rotating shaft integrated also with the pointed arrow 16 and the knob 17. The mentioned shaft with the knob 17 was supported in a radial plain bearing with the Teflon shell relative to the vertical mandrel and to the bracket fixed to the top holder 3. The pointed arrow 16 mates with the measuring scale 15 fixed to the top holder 3. The basis 1, the middle holder 2 and the top one 3 are connected to the vertical support 4. Rotation the knob 17 by hand allowed exerting a twisting torque in the torsional spring 11 able to overcome the sum of the resistance torque in the Teflon bearings and the frictional torque between the shells of the tested eggs 6 and 7. As the resistance torque in Teflon bearings was much lower than the friction torque between the shells of the tested eggs, it was neglected during the

measurement. The 5-eggs tester was calibrated with the screw joint 9 immobilized, applying a known torque to the knob 17 and reading the twist angle α of the spring 11 on the scale. The dependency $M(\alpha)$ of the torsional torque M as a function of the torsion angle α of the spring 11 were obtained. After attaching the rotated egg 7 to the holder 8, and this in turn to the screw joint 9 and releasing the screw joint 9, first the torque of the internal resistance M_{int} was measured, resulting, inter alia, from the bearing resistance of the screw joint 9. After reaching the contact between the rotating egg 7 and the stationary eggs 6, the total torque M_{tot} was measured which is the sum of the torque of internal resistance M_{int} and the friction torque M_T between the eggs. Subtracting from the torque M_{tot} the torque M_{int}, the estimated value of the torque M_T was obtained. The load between the eggs resulted practically only from the weight of the egg 7 rotated, due to the structurally introduced axial clearance between the tip of screw joint 9 with the glued egg 7 and the part connected to the rotating disc 10. Based on the value of the R reaction between the eggs obtained from the model and knowing the radius r from this model on which the friction force between the eggs acted the friction coefficient between them was determined from the formula *(5)*.

$$\mu_T = M_T/(R \cdot r) \qquad (5)$$
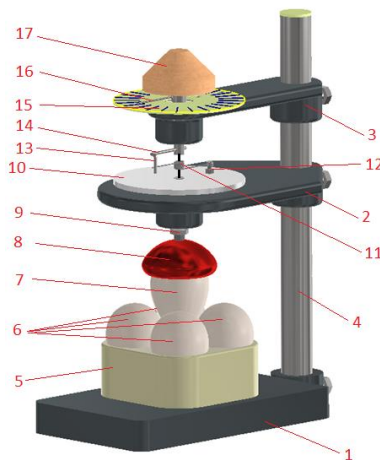
Fig. 5. The 5-eggs tribotester for determining of the friction torque between rotating egg and

the stationary eggs. 1 – basis, 2 – the middle holder, 3 – the top holder, 4 – support, 5 – fixed holder for stationary egg, 6 – stationary eggs, 7 – rotated egg, 8 – replaceable holder glued to the rotated egg, 9 supported via bearing the screw joint of the replaceable holder, 10 – rotating disc connected with the screw joint, 11 – torsion spring, 12 - spring stop pin, 13 - drive lever pin, 14 – drive lever, 15 - measuring scale, 16 - pointer arrow, 17 – knob

3.4.2. The model of 5-eggs tribotester

The normal force and contact pressure in contacts between eggs were obtained using the model of the 5-eggs tribotester elaborated using the Finite Element Method (FEM) and presented in Fig. 6. The material for 5 modelled eggs was assumed to be concrete. The bottom holder was assumed to be made of Polybutylene Terephthalate (PBT). During analysis the friction forces between eggshells were omitted as the relatively small ones. The grid of the tetrahedral finite elements was shown in Figure 7. Four options of average element size were utilized to conduct convergence evaluation in term of the effect of the average element size on the maximum values of calculated von-Mises stresses. The modelled eggs were connected each to other by contact elements with the option of 3D planar triangles and the option of their sliding/no separation while eggs with bottom holed were connected by the analogous contact element but with option of their bond behavior. The boundary conditions in the model were shown in Figure 8.
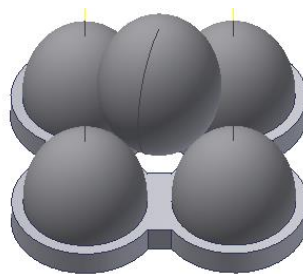
Fig. 6. The model of 5-eggs tribotester comprising a holder with 4 tested bottom eggs and 1 egg fixed to the loading head
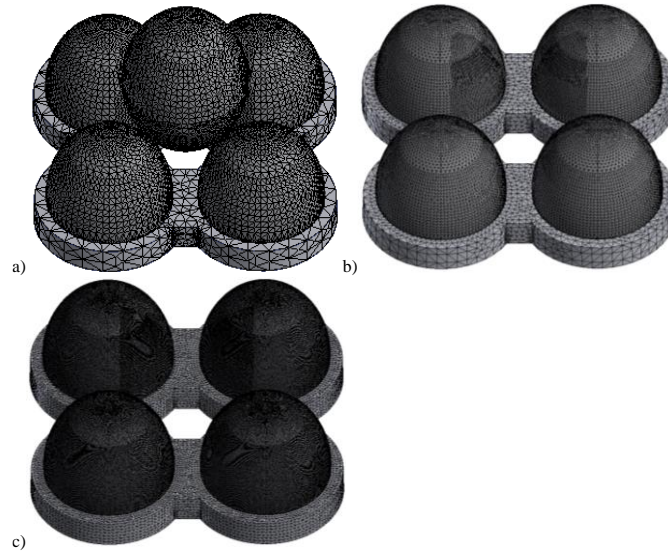
Fig. 7. The grid of tetrahedral finite elements for the model of 5-eggs tribotester. Average Element Size (as a fraction of bounding box length): (a) 0.1 – 61987 elements, 123043 nodes; (b) 0.05 – 218773 elements, 437969 nodes; (c) 0.02 – 1790257 elements, 3243643 nodes.
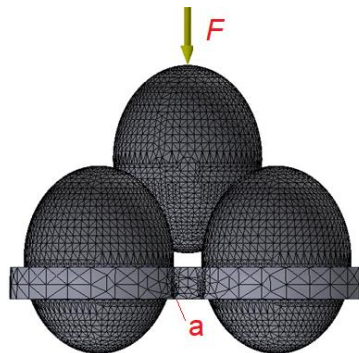
Fig. 8. The boundary conditions in the model of 5-eggs tribotester; F – loading force equal to the weight of the top egg, a – fixed bottom plain of holder with 4 tested bottom eggs.

3.5. Abrasive wear in the contact zones between the rotating egg and the stationary eggs

The abrasive wear in the contact zones between the rotating egg and the stationary eggs was determined using the other home-made 5-eggs tribotester

presented in Figure 9. The vertical force F (Fig. 9) loading rotating egg 1 was determined by initial measurement of force between screw joint 3 (without egg glued) connected to the head 6 and piezoelectric weight positioned on the bench drill table while the drill feed lever was loaded by successively increasing the predetermined values of the weight suspended from the arm with the fixed value and thus producing a known driving torque. It allowed introducing the driving torque relating to the vertical force F equal to 2 ± 0.5 N. The rotational speed n (Fig. 9) of the bench drill head 6 was equal to 500 rpm. The time t of the abrasive wear process was equal to 5 s.

The volumetric abrasive wear of rotating egg was determined from equation *(6)*:

$$V_{abrasion} = \pi \cdot d \cdot s \cdot h_{aver} \qquad (6)$$

where:

d= 33 mm – average diameter of the trace of abrasion, s= 1.5 mm – average width of the trace of abrasion,

h_{aver}= 0.02 mm – average depth of the trace of abrasion, obtained from measurements via the digital microscope VHX KEYENCE

To obtain values of the wear coefficient K the Archard model (7) [65] was utilized.

$$K = \frac{H \cdot V_{abrasion}}{S \cdot F_{egg-egg}} \qquad (7)$$

where:

H [MPa] – Hardness of eggshell. It was estimated that the average value a such a hardness was equal to the average value of Brinell hardness of various limestones presented in [66], which varied in range (13.9-36.2) MPa. Therefore, the average value of Brinner hardness of eggshell was equal to 25 MPa.

$F_{egg-egg}$ [N] – normal force in contact zone between eggs obtained from the model of the 5-eggs tribotester described in the subchapter 3.4.2. It was determined from equation *(8)*.

$$F_{egg-egg} = \sum_e p_{aver}(e) \cdot A_e(e) \approx p \cdot A = p \cdot \pi \cdot r_e^2$$

(8)

where:

r_e – radius of area A comprising loaded contact elements e,

p – average value of contact pressure in contact zone between eggs,

$p_{aver}(e)$ – average contact pressure for the finite element e,

$A_e(e)$ – area of 3D triangle contact element e ,

S [mm] - the distance of the abrasive wear process was obtained from equation (9).

$$S = \frac{\pi \cdot n}{30} \cdot \frac{d}{2} \cdot t$$

(9)
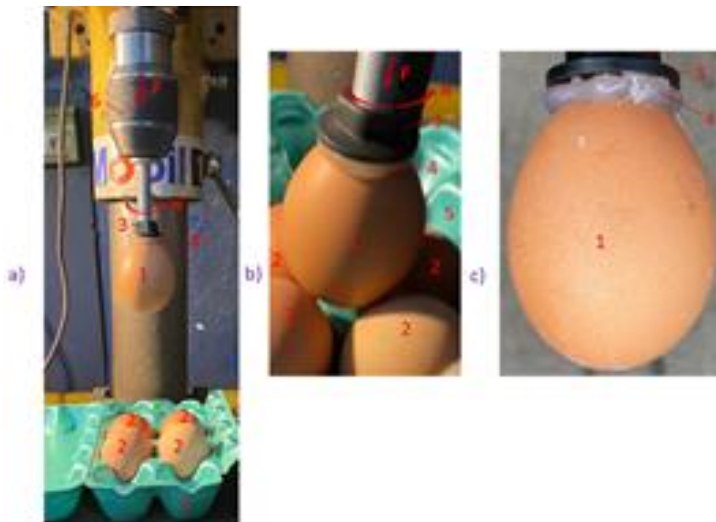
Fig. 9. The home-made device for studies of abrasion wear between rotating egg 1 driven by

the head 6 and contacted with four stationary eggs 2 fixed by glue to the support 5; a) general view of device, b) detailed view of rotating egg 1 mating with stationary eggs 2 fixed to the bottom support 5, c) detail view of rotating egg 1 connected to the screw joint 3 via a layer 4 of two-composite glue.

4.   Results and Discussion

4.1.   Physical properties of egg powder

The values of the density of egg powder in the loose and the compact state are presented in Table 1. Such density in the latter state is greater by 34 % than in the former one. The density of loose egg powder is higher by 42% compared to that reported in [67].

Tab. 1. Measured density of egg powder in the loose and the compact state.

State of egg powder	Density $\rho_{egg-powder}$, [g/dm³]
Loose	320
Compact	430

The measured angle β of natural repose (maximum) for egg powder is given by eq. *(10)*:

$$\beta = 56° \qquad (10)$$

It was higher by 24.4% compared to that for chalk (of the chemical composition close to eggshell powder) and for malt or wheat flour [68]. It was also higher by 27 % compared to that of spray-dried skim milk powder [69].

The values of parameters characterising the friction between egg powder and stainless-steel plate with and without Teflon coating are shown in Table 2. These values of static coefficient of friction were eight-fold higher than in case of contact

zone between UHMWPE polymer and stainless steel under egg albumen lubrication conditions and two order higher loading [70]. The wall friction angle for the whey protein powder on the stainless steel can vary in range 17°-22° [71]. As the coefficient of wall friction is the tangent of the wall friction angle [72] the wall friction coefficient in contact whey protein powder on the stainless-steel varies in range 0.3-04 which can be twice lower than static coefficient of friction in contact between egg-powder and stainless steel.

Tab. 2. The measured friction angle γ and calculated coefficient of friction in contact between egg powder and stainless-steel plate with and without Teflon coating

Contact type	Friction angle γ, [deg]	Static coefficient of friction μ, [-]
Egg powder - pure stainless steel	39° ± 7°	0.81 ± 0.12
Egg powder - stainless steel coated by Teflon	35° ± 6°	0.70 ± 0.11

4.2. Friction between eggshell and pure stainless steel and between eggshell and stainless steel covered by Teflon

The values of the static coefficient of friction between eggshell and pure stainless steel and between eggshell and stainless steel covered by Teflon under various loads were presented in Table 3. The calculated values of coefficient of friction was by an order higher than that obtained for contact between whole egg and galvanized metal surface [18]. The tendency to increase the friction coefficient with increase of loading the contact zone between eggshell and stainless-steel bot uncoated and coated by Teflon was in an agreement with the one to linear increase of the friction coefficient in contact between whole egg and galvanized metal surface with respect to egg weight [18].

Tab. 3. Static coefficient of friction μ between eggshell and stainless steel and between eggshell and stainless steel covered by Teflon under various loads determined using the tribotester based on the inclined plane.

Loading of contact zone	Loaded by box made of AZ63 (47 g)		Loaded by box made of Al alloy 2014 (69 g)	
Contact zone type	Measured tilt angle α, [deg]	Calculated coefficient of friction μ, [-]	Measured tilt angle α, [deg]	Calculated coefficient of friction μ, [-]
Eggshell-Stainless steel without coating	27°±11°	0.510±0.194	38°±7°	0.781±0.123
Eggshell-Stainless steel coated by Teflon	13°±9°	0.231±0.158	21°±11°	0.384±0.194

The example view of contact areas of eggshell glued to the bottom wall of paper box loaded by metal box with mass of 47 g was presented in Figure 10.
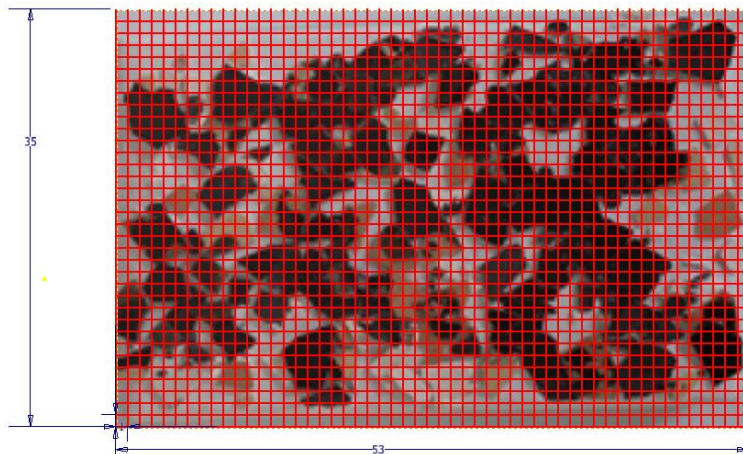
Fig. 10. The example view of contact areas of eggshell glued to the bottom wall of paper box loaded by metal box made of AZ63 with a mass of 47 g. The red lines – lines of measuring grid; black areas – eggshells covered with ink (being in contact with the core; beige areas – eggshell without coating by ink (not in contact with the core); grey areas – bottom wall of paper box covered by glue.

The values of parameter k in equation (4), calculated as the ratio of the number of black unit areas (1 mm^2) and the total number of the unit areas equal to 1855 (Fig. 11) for two mases loading the paper box with pieces of eggshells glued to its bottom wall were presented in Table 4. Also the calculated values of average contact pressure p between eggshells and the core were included. Such values were below 0.62 kPa for the case of the loading box made of AZ63 (47 g) and below 0.79 kPa for the case of the loading box made of Al alloy 2014 (69 g). The obtained values average contact pressure were by three orders lower than these caused formation of microcracks at the inner surface of the eggshell [73, 74].

Tab. 4. The values of parameter k being the ratio of the number of black unit areas (1 mm^2) and the total number of the unit areas equal to 1855 (Fig. 10) for two mases loading the paper box with pieces of eggshells glued to its bottom wall.

Loading of contact zone	K, [-]	Average contact pressure p_c, [kPa]
by box made of AZ63 (47 g)	0.52±0.11	0.51±0.11
by box made of Al alloy 2014 (69 g)	0.63±0.16	0.63±0.16

4.3. Roughness of eggshell before boiling of the egg tested

The measured roughness parameters in the 4 point chosen on the egg shell for the egg before boiling were shown in Figure 11 and in Figure 12 after boiling. In the latter case they are rather lower. The values of obtained roughness parameters Sa and Sq were by an order higher than these of roughness parameter Rq varying in range 0.1-0.5 μm [75].
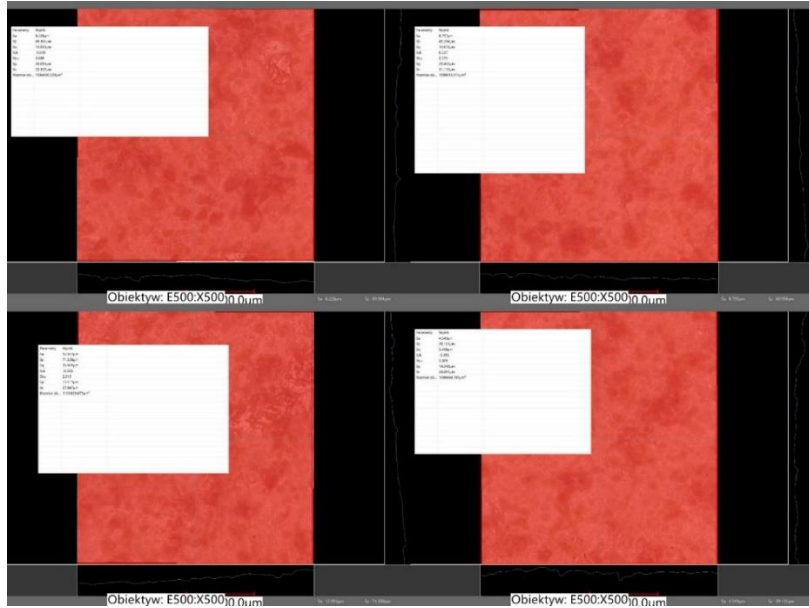
Fig. 11. The measured roughness parameter in the 4 point chosen on the eggshell before boiling.
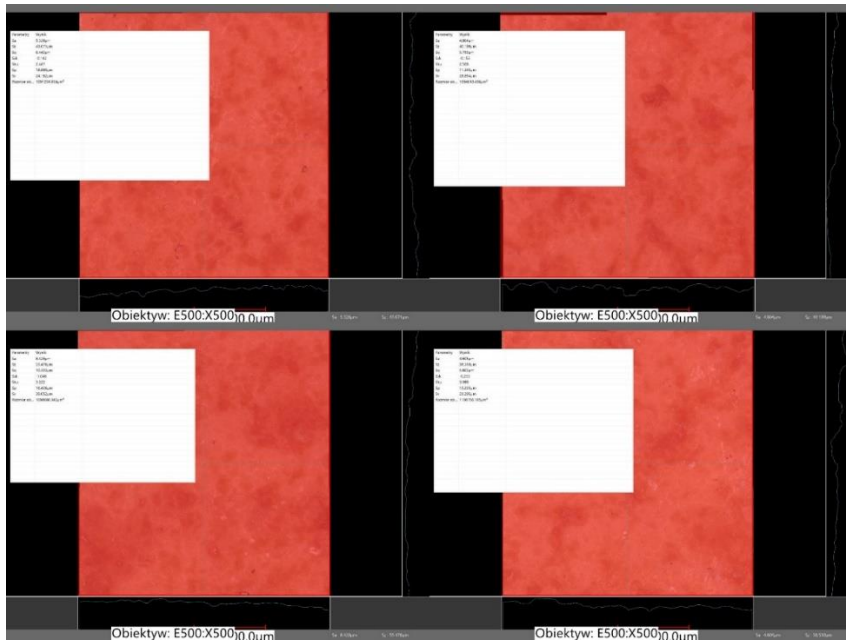
Fig. 12. The measured roughness parameter in the 4 point chosen on the eggshell after boiling.

4.4. Abrasive wear of eggshell

The shapes of abrasive wear of eggshells are shown in Figure 13.
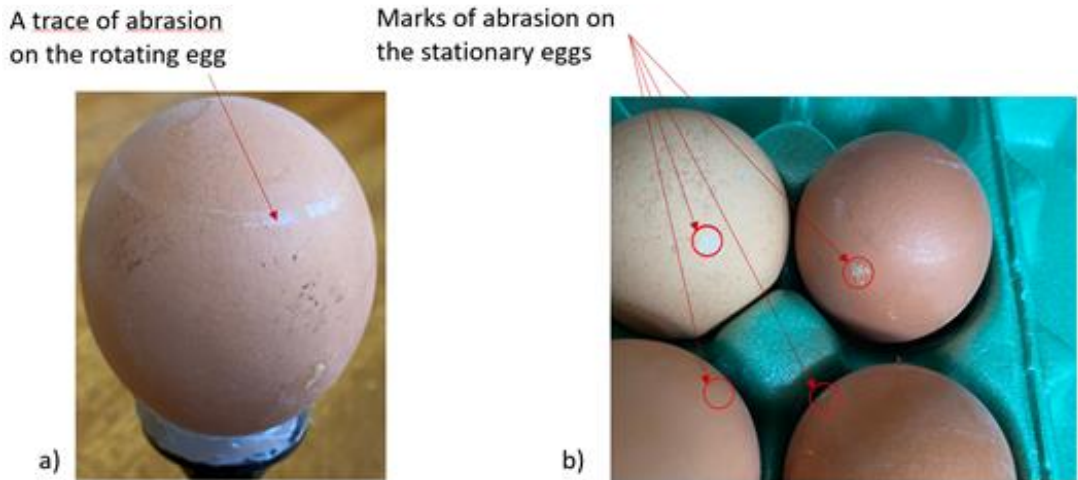
Fig. 13. Abrasive wear of eggshell obtained on the 5-eggs wear device; a) for rotating egg, b) for stationary eggs.

The average values of geometrical parameters characterizing the volumetric abrasive wear of the rotating egg was presented in Table 5. The average measured values of the diameter d, the width s and the depth h_{aver} of the trace of abrasion were equal to 33 mm, 1.5 mm and to 0.02 mm, respectively. Based of these values the calculated value of the volumetric abrasive wear $V_{abrasion}$ was equal to 3.1 mm^3.

Tab. 5. The average values of geometrical parameters characterizing the volumetric abrasive wear of the rotating egg.

Measured diameter of the trace of abrasion d, [mm]	Measured width of the trace of abrasion s, [mm]	Measured depth of the trace of abrasion h_{aver}, [mm]	The calculated volumetric abrasive wear $V_{abrasion}$, [mm^3]
33	1.5	0.02	3.1

The value of the distance S was equal to 4 318 mm. For the value of the force F equal to 2.5 N the estimated value of the force $F_{egg-egg}$ was equal to 1.4 N. The obtained value of the wear coefficient K between eggs was equal to 0.007. The wear studies conducted using rotary shear apparatus for the contact zone between Dover limestones was reported in [76]. During such studies for the slip velocity in range 0.1-0.15 m/s, normal stress 0.5 MPa, slip distance 1 m, the average wear rate was equal to 20 μm/m. Assuming that the hardness of Dover limestone was equal to 25 MPa, the estimated value of wear coefficient K utilized in the Archard model (7) was equal to 0.001, which was the seven-fold lower than that of the contact between eggs.

4.5.   Stresses and contact pressure in the model of the 5-eggs tribotester

The obtained values of the von-Mises stresses σ_{red} in the model of 5-eggs tribotester were shown in Figure 14. They were below 0.56 MPa. The values of the contact pressure were presented in Figure 15. They did not exceed 0.32 MPa. The obtained values of the average contact pressure were eight-fold lower than these caused formation of microcracks at the inner surface of the eggshell [73, 74].

The effect of the average element size on the maximum value of von Mises stresses σ_{red} was shown in Table 6.

Tab. 6. The effect of the average element size on the maximum value of von Mises stresses.

Average Element Size (as a fraction of bounding box length), [%]	von Mises stresses σ_{red} , [MPa]
10	0.51
5	0.55
2	0.56

It was assumed that the case with Average Element Size as a 2% fraction of

bounding box length was the optimal choose for the comparative analysis under the small costs of computation time and involvement of the computer RAM.
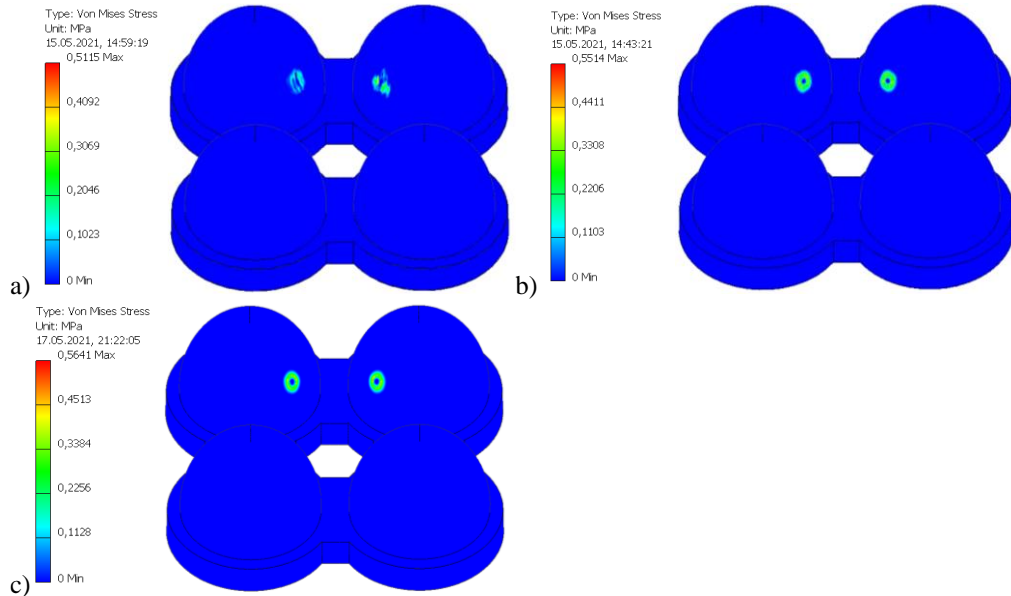
Fig. 14. The von-Mises stresses σ_{red} in the model of 5-eggs tribotester with the hidden egg fixed to the measuring head. Average Element Size (as a fraction of bounding box length): (a) 0.1; (b); (c) 0.02.
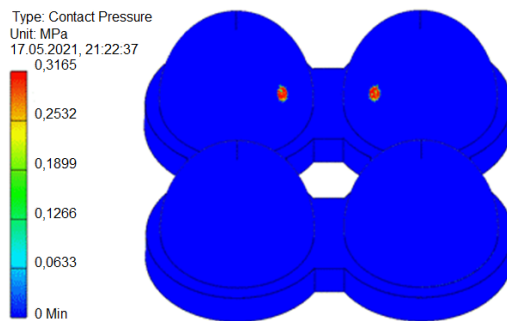
Fig. 15. The contact pressure p_c in the model of 5-eggs tribotester with the hidden egg fixed to the measuring head.

4.6.   Friction between eggshells

The values of the measured friction torque and the calculated coefficient of friction between eggshells under various loads were presented in Table 7. It was clearly visible that for heavier egg the friction coefficient was higher. The obtained values of coefficient of friction between eggshells were close to lower ones from the range 0.15-0.55 obtained in contact between limestones sliding at the average speed equal to 0.25 mm/s under loading of 0.75 MPa [77].

Tab. 7. The friction torque and the coefficient of friction between eggshells under various loads determined using the 5-egg tribotester.

Loading of contact zone	Loaded Medium egg 52.0 ± 1.5 g		Loaded by Jumbo egg 71.5 ± 2.5 g	
Contact zone type	Measured friction torque M_T [Nmm]	Calculated coefficient of friction μ [-]	Measured friction torque M_T [Nmm]	Calculated coefficient of friction μ [-]
Eggshell-Eggshell	2.01±0.08	0.1±0.004	2.67±0.08	0.12±0.003

5.   Conclusions

In this study the following quantities were determined: density and natural repose angle of egg powder, the coefficient of friction for the contact zones between egg powder and stainless steel with and without Teflon coating, between eggshell and stainless steel with and without Teflon coatings, and between eggshells. What is more, the wear coefficient utilized in the Archard model applied for the contact between eggs was also estimated. The measured density of egg powder in the compact state exceeds by 34 % that in the loose one. The coefficient of friction in contact between egg powder and stainless-steel plate with Teflon coating is lower by 16 % than in case of lack of such a coating. When transporting egg powder, the conveyor belts should be inclined at an angle of less than 32° for stainless steel belts and less than 29° for Teflon-coated stainless steel belts to avoid self-falling off of

the powder. When moving egg powder with chutes, they should be tilted more than 46° for stainless steel surfaces and more than 41° for Teflon-coated stainless steel surfaces to avoid unnecessary accumulation of powder deposits on the chutes.

The static coefficient of friction between eggshell and pure stainless steel is above twice higher, compared to that between eggshell and stainless steel covered by Teflon. In all cases studied, for about 30 % higher load the friction coefficient was also about 30% higher. When transporting eggshells, the conveyor belts should be inclined at an angle of less than 16° for stainless steel belts and less than 4° for Teflon-coated stainless steel belts to avoid self-falling off of the eggshells. When moving eggshells with chutes, they should be tilted more than 45° for stainless steel surfaces and more than 32° for Teflon-coated stainless steel surfaces to avoid unnecessary accumulation of eggshell deposits on the chutes. Boiling of an egg can result in a decrease in roughness parameters on the eggshell surface compared to these for the fresh egg. The home-made 5-eggs tester allowed determining value of the eggshell volumetric abrasive wear equal to 3.1 mm^3. The values of the von-Mises stresses in the model of the 5-eggs tribotester were below 0.56 MPa. The relating values of the contact pressure did not exceed 0.32 MPa and was eight-fold lower than these caused formation of microcracks at the inner surface of the eggshell. The obtained value of the abrasive wear coefficient K in contact zone between eggshells was equal to 0.007, being seven fold higher than one between limestones. The coefficient of friction between eggshells in the contact assembly applied in the 5-eggs tester for the case of the Jumbo eggs was higher by 20% than the one for the case of the Medium eggs. The further studies will be focused on the effect of temperature, humidity and slip velocity on the friction coefficient and wear coefficient in contact zones between eggshells and eggshell and various metallic surfaces with and without various coatings.

References

[1] United States, U. States, & Agricultural Marketing Service, A. Marketing Service. Egg-grading manual, Agriculture handbook (United States. Dept. of Agriculture), no. 75, 2000.

[2] Egg Marketing. A Guide for the Production and Sale of Eggs, Food and Agriculture Organization of the United Nations, Rome, Italy, 2003.

[3] Anderson, K.E., Tharrington, J.B., Curtis, P.A., Jones, F.T.: *Shell characteristics of eggs from historic strains of single comb white leghorn chickens and relationship of egg shape to shell strength*, Int. J. Poult. Sci., 3, 2004, 17–19.

[4] Cahya, M., Marfuah, N.: *Identification of Calcium Carbonate (CaCO₃) Characteristics from Different Kinds of Poultry Eggshells Using X-Ray Diffraction (XRD) and Fourier Transformation Infra-Red (FTIR)*, Proceedings of the 2014 International Conference on Physics and its Applications, 9, 2014, 138-142.

[5] Athanasiadou, D., Jiang, W., Goldbaum, D., Saleem, A., Basu, K., Pacella, M.S., Böhm, C.F., Chromik, R.R., Hincke, M.T., Rodríguez-Navarro, A.B., Vali, H., Wolf, S.E., Gray, J.J., Bui, K.H., McKee, M.D.: *Nanostructure, osteopontin, and mechanical properties of calcitic avian eggshell*, Science Advances, 4(3), 2018. eaar3219.

[6] Belyavin, C.G.: *Eggs: Use in the Food Industry*, Editor(s): Caballero, B., Finglas, P.M., Toldrá, F., *Encyclopedia of Food and Health*, Academic Press, 2016, 476-479.

[7] *Industrial microwave machine*, Microwave drying equipment for egg powder and yolk powder. https://industrialmicrowavemachine.com/microwave-drying-equipment-for-egg-powder-and-yolk-powder/ (accessed on 03 November 2023).

[8] Salinas Gonzalez, F.P.: *The Effect of Storage Temperature and Time on The Quality of Spray Dried Egg Powder*, LSU Master's Theses, 2017, 4583.

[9] Lin, J., Puri, V.M., Anantheswaran, R.C.: *Measurement of eggshell thermal - mechanical properties*, Transaction of the ASAE, 38, 1995, 1769–1776.

[10] Carnarius, K.M., Conrad, K.M., Mast, M.G., Mac Neill, J.H.: *Relationship of eggshell ultrastructure and Shell Strength to the Soudness of Shell Eggs*, Poultry

Science, 75, 1996, 656-663.

[11]   El-Boushy, A.R., Raterink, R.: *Egg shell strength: The cases of egg breakage in relation to nutrition, management and environment*. Poult. Advis., 26(11), 1993, 47-55.

[12]   Rezac, P., Poschel, M., Havlicek, Z.: *Relationship of plasma oestradiol - 17 beta and cholesterol levels to eggshell strength in laying hens*, Czech Journal of Animal Science, 45, 2000, 313–318.

[13]   Nirasawa, K., Takahashi, H., Takeda, H., Furukawa, T., Takeda, T., Nagamine, Y.: *Restricted maximum likelihood estimates of genetic parameters and genetic trends of chickens divergently selected for eggshell strength*, J. Anim. Breed. Genet., 115, 1998, 375-381.

[14]   Nirasawa, K., Takahashi, H., Takeda, H., Furukawa, T., Picman, J., Pripil, S.: *Is greater eggshell density an alternative mechanism by which parasitic cuckoos increase the strength of their eggs?* Journal for Ornitologie, 138, 1997, 531–541.

[15]   Hincke, M., Nys, Y., Gautron, J., Mann, K., Rodriguez-Navarro, A., McKee, M. *The eggshell: structure, composition and mineralization*, Frontiers in bioscience, 17, 2012, 1266-80.

[16]   Adeyeye, E.I.: *Comparative study on the characteristics of eggshells of some bird species*, Bull. Chem. Soc. Ethiop., 23(2), 2009, 159-166.

[17]   Tsai, W.T., Yang, J.M., Lai, C.W., Cheng, Y.H., Lin, C.C., Yeh, C.W.: *Characterization and adsorption properties of eggshells and eggshell membrane*, Bioresource Technology, 97(3), 2006, 488-493.

[18]   Altunas, E., Sekeroglu, A.: *Effect of shape index on mechanical properties of chicken eggs*, J. Food Eng. 85 (2008) 606-612.

[19]   Voisey, P.W., Hunt, J.R.: *Effect of compression speed on the behaviour of eggshells*, J. Agric. Eng. Res., 14, 1969, 40–46.

[20]   Abdallah, A.G., Harms, R.H., El-Husseiny, O.: *Various methods of measuring shell quality in relation to percentage of cracked eggs*, Poult. Sci., 72, 1993, 2038-2043.

[21]   de Ketelaere, B., Govaerts, T., Couke, P., Dewil, E., Visseher, T., Decuypere, L., de Baerdemaeker, J.: *Measuring the eggshell strength of 6 different strains of*

laying hens: techniques and comparison, Br. Poult. Sci., 43, 2002, 238-244.

[22]   Narushin, V.G., van Kepmen, T.A., Wineland, M.T., Christensen, V.L.: *Comparing infrared spectroscopy and egg size measurements for predicting eggshell quality*, Biosyst. Eng., 87, 2004, 367-373.

[23]   Polat, R., Tarhan, S., Çetin, M., Atay, U.: *Mechanical behaviour under compression loading and some physical parameters of Japanese quail (Coturnix coturnix japonica) eggs*, Czech. J. Anim. Sci., 52, 2007, 50-56.

[24]   Altuntas, E., Sekeroglu, A.: *Mechanical behavior and physical properties of chicken egg as affected by different egg weights*, Journal of Food Process Engineering, 33, 2010, 115-127.

[25]   Radwan, L.M.: *Eggshell quality: a comparison between Fayoumi, Gimieizah and Brown Hy-Line strains for mechanical properties and ultrastructure of their eggshells*, Animal Production Science, 56, 2015, 908-912.

[26]   Kumbar, V., Nedomova, S., Trnka, J., Buchar, J., Pytel, R.: *Effect of storage duration on the rheological properties of goose liquid egg products and eggshell membranes*, Poultry Science, 95(7), 2016, 1693-1701.

[27]   Mahmoodi, M.J., Azadbakht, M., Asghari, A., Dastar, B.: *Investigating the Amount of Resistance to Break the Eggshell Under the Influence of a Strong Magnetic Field (MRI)*, Poultry Science Journal, 7(2), 2019, 101-108.

[28]   Apalangya, V.A., Rangari, V.K., Tiimob, B.J., Jeelani, S., Temesgen, S.: *Eggshell Based Nano-Engineered Hydroxyapatite and Poly(lactic) Acid Electrospun Fibers as Potential Tissue Scaffold*, International Journal of Biomaterials, 2019, 6762575.

[29]   Mijan, M.A., Kim, D.-H., Kwak, H.-S.: *Physicochemical properties of nanopowdered eggshell*, International Journal of Food Science and Technology, 49, 2014, 1751-1757.

[30]   El-Shibiny, S., Abd El-Gawad, M.A.M., Assem, F., El-Sayed, S.: *The use of nano-sized eggshell powder for calcium fortification of cow's and buffalo's milk yogurts*, Acta scientiarum polonorum. Technologia alimentaria, 17, 2018, 37-49.

[31]   Azis, Y., Adrian, M., Alfarisi, C.D., Khairatand, Sri, R.M. Synthesis of hydroxyapatite nanoparticles from eggshells by sol-gel method. IOP Conf. Series: Materials Science and Engineering 345 (2018) 012040. doi: 10.1088/1757-

899X/345/1/012040.

[32]   Puspitasari, P., Yuwanda, V., Sukarni, Dika, J.W.: *The Properties of Eggshell Powders with the Variation of Sintering Duration*, IOP Conf. Series: Materials Science and Engineering, 515, 2019, 012104.

[33]   Krittirash Yorseng, Suchart Siengchin, Basa Ashok, Anumakonda Varada Rajulu, *Nanocomposite eggshell powder with in situ generated silver nanoparticles using inherent collagen as reducing agent*, Journal of Bioresources and Bioproducts, 5(2), 2020, 101-107.

[34]   Bain, M.: *A reinterpretation of eggshell strength*. In: Solomon S.E. (ed.): *Egg and Eggshell Quality*. Manson Publishing Ltd., London, UK, 1997, 131–141.

[35]   Bain, M.: *Recent advances in the assessment of eggshell quality and their future application*, World's Poultry Science Journal, 61(2), 2005, 268-277.

[36]   Voisey, P.W., Hunt, J.R.: *Measurement of eggshell strength*, Journal of Texture Studies, 5, 2007, 135-182.

[37]   Snapir, N., Perek, M.: *Evaluation of Various Methods of Measuring Eggshell Quality*, Annales de zootechnie, INRA/EDP Sciences, 18(4), 1969, 399-405.

[38]   Hamilton, R.M.G.: *Methods and Factors that affect the Measurement of Egg Shell Quality*, Poultry Science, 61, 1982, 2022-2039.

[39]   Mehdizadeh, S.A., Nadi, F.: *Experimental and Numerical Analysis for Prediction of Mechanical Properties of Eggshell*, nt. J. Food Eng. 12(3), 2016, 287–293.

[40]   Voisey, P.W., Hunt, J.R.: *Physical properties of eggshells*, British Poultry Science, 8(4), 1967, 263-271.

[41]   Hunt, J.R., Voisey, P.W., Thompson, B.K.: *Physical Properties of Eggshels: a Comparison of the Puncture and Compression Tests for Estimating Shell Strength*, Canadian Journal of Animal Science, 57(2), 1977.

[42]   Ketta, M., Tůmová, E.: *Eggshell structure, measurements, and quality-affecting factors in laying hens: a review*, Czech J. Anim. Sci., 61(7), 2016, 299-309.

[43]   Montenegro, A.T., Garcia, E.A., Molino, A.B., Cruvinel, J.M., Ouros, C.C., Alves, K.S.: *Methods to Evaluate the Eggshell Quality of Table Eggs*, Brazilian Journal of Poultry Science, 21(3), 2019, eRBCA-2019-1046.

[44]   Severa, L., Buchar, J., Votava, J.: *New approach of eggshell mechanical properties*

determination, Acta Universitatis Agriculturae et Silviculturae Mendelianae Brunensis, 58, 2010, 161-166.

[45]   Kan, C.A. (Kees): *Contaminants in eggs: effects of feed and environment*, Proceedings of XII European Symposium on the Quality of Eggs and Egg Products At: Prague, 2007.

[46]   Spitzer, H.: *An Analysis of Bacterial Contamination of Chicken Eggs and Antimicrobial Resistance*, All College Thesis Program 2016-2019, 2016, 27.

[47]   de Freitas Neto, O.C., Penha Filho, R.A.C., Barrow, P., Berchieri Jr., A.: *Sources of human non-typhoid salmonellosis: a review*, Brazilian Journal of Poultry Science, 12(1), 2010, 01-11.

[48]   Whiley, H., Ross, K.: *Salmonella and eggs: from production to plate*, International journal of environmental research and public health, 12(3), 2015, 2543-2556.

[49]   Hosoglu, M.I., Guneser, O., Yuceer, Y.K.: Chapter 2 - *Different Bioengineering Approaches on Production of Bioflavor Compounds*, Editor(s): Grumezescu, A.M., Holban, A.M., In: *Role of Materials Science in Food Bioengineering, Handbook of Food Bioengineering*, Academic Press (2018) 37-71. https://doi.org/10.1016/B978-0-12-811448-3.00002-4.

[50]   Daramola, E.I.: *Comparative Evaluation of Differently Processed Whole Eggpowder*, Ahmadu Bello University, Zaria, Nigeria, 2018.

[51]   Huda, N., Tze, W., Dewi, M., Hashim, H.: *Physicochemical Properties of Egg White Powder from Eggs of Different Types of Bird*, International Journal on Advanced Science, Engineering and Information Technology, 8(2), 2018, 4087.

[52]   Koç, M., Koç, B., Güngör, Ö., Kaymak-Ertekin, F.: *The Effects of Moisture on Physical Properties of Spray-Dried Egg Powder*, Drying Technology, 30, 2012, 567-573.

[53]   Koç, M., Koç, B., Sakin-Yilmazer, M., Kaymak-Ertekin, F., Susyal, G., Bağdatlıoğlu, N.: *Physicochemical Characterization of Whole Egg Powder Microencapsulated by Spray Drying*, Drying Technology, 29, 2011, 780-788.

[54]   Lai, C.C., Gilbert, S.G., Mannheim, C.H.: *Effect of flow conditioners on water sorption and flow properties of egg powder*, Journal of Food Engineering, 5(4), 1986, 321-333.

[55]   Ndife, J., Udobi, C.E., Amaechi, N.C.: *Effect of oven drying on the functional and nutritional properties of whole egg and its components*, African Journal of Food Science, 4(5), 2010, 254- 257.

[56]   Kudre, T.G., Bejjanki, S.K., Kanwate, B.W., Sakhare, P.Z.: *Comparative study on physicochemical and functional properties of egg powders from Japanese quail and white Leghorn chicken*, International Journal of Food Properties, 21(1), 2018, 957-972.

[57]   Asghar, A., Abbas, M.: *Effect of spray dried whole egg powder on physicochemical and sensory properties of cake*, Am. J. Sci. Ind. Res., 6(5), 2015, 97-102.

[58]   Lafetá Jr., J.A.Q., de Oliveira, M.J., de Oliveira, D.R.B., Santos, I.J.B., Saldaña, M.D.A., dos Reis Coimbra, J.S.: *Emulsifying properties of quail egg white proteins in different vegetable oil emulsions*, Acta Scientiarum. Technology, 43, 2021, e50067.

[59]   Salawu, E.Y., Ajayi, O.O., Inegbenebor, A., Akinlabi, S., Akinlabi, E.: *Influence of pulverized palm kernel and eggshell additives on the hardness, coefficient of friction and microstructure of grey cast iron material for advance applications*, Results in Engineering, 3, 2019, 100025.

[60]   Oladele, I.O., Makinde-Isola, B.A., Adediran, A.A., Oladejo, M.O., Owa, A.F., Olayanju, T.M.A.: *Mechanical and wear behaviour of pulverised poultry eggshell/sisal fiber hybrid reinforced epoxy composites*, IOP Publishing Ltd. Materials Research Express, 7(4), 2020, 045304.

[61]   Venkatesh, N., Hanumanthraju, H.G., Aravinda, Rachappa: *A Wear Study on Bio-Active Coating of Al2o3, Egg and Sea Shell Powder on Teflon and Nylon, elucidated*, IAETSD Journal for Advanced Research in Applied Sciences, 5(4), 2018, 583-595.

[62]   Dwiwedi, S.K., Srivastava, A.K., Chopkar, M.K.: *Wear Study of Chicken Eggshell-Reinforced Al6061 Matrix Composites*, Trans Indian Inst Met, 72, 2019, 73–84.

[63]   Parivendan, J., Ramesh, S.: *Mechanical, wear & thermal behaviour of Hemp fibre/eggshell particles reinforced epoxy resin bio composite*, Transactions - Canadian Society for Mechanical Engineering, 42(3), 2018, 280-285.

[64]   *Surface Contact Pressure Sensitive Paper Reveals Distribution and Magnitude*.

Available on: https://www.sensorprod.com/campaign/pressure-sensitive-paper/index.php?mcode=gc-pressure (accessed on 03 November 2023).

[65] Karaca, Z., Günes Yilmaz, N., Goktan, R.M.: *Abrasion wear characterization of some selected stone flooring materials with respect to contact load*, Constr. Build. Mater., 36, 2012, 520–526.

[66] Anikoh, G.A., Adesida, P.A., Afolabi, O.C.: *Investigation of Physical and Mechanical Properties of Selected Rock Types in Kogi State Using Hardness Tests*, Journal of Mining World Express (MWE), 4, 2015, 37-51.

[67] Chapter 2: *Conveyor Chain Designer Guide*. In *Conveyor chain. Installation, maintenance & designer guide*. Renold Superior Chain Technology 21-61. Available on: https://www.renold.com/media/165388/conveyor-ins-main-ren16-eng-10-10.pdf (accessed on 03 November 2023).

[68] Al-Hashemi, H.M.B., Al-Amoudi, O.S.B.: *A review on the angle of repose of granular materials*, Powder Technology, 330, 2018, 397–417.

[69] Ilari, J.-L., Mekkaoui, L.: *Physical properties of constitutive size classes of spray-dried skimmilk powder and their mixtures*, Le Lait, INRA Editions, 85(4-5), 2005, 279-294.

[70] Kahyaoglu, O.K., Unal, H.: *Friction and wear behaviours of medical grade UHMWPE at dry and lubricated conditions*, International Journal of Physical Sciences, 7(16), 2012, 2478-2485.

[71] *Protein Powder Rheology*, Centre of Industrial Rheology. Available on: https://www.rheologylab.com/articles/food/protein-powder-rheology/ (accessed on 03 November 2023).

[72] Hancock, B.C.: *The Wall Friction Properties of Pharmaceutical Powders, Blends, and Granulations*, Journal of Pharmaceutical Sciences, 108, 2019, 457-463.

[73] Bain, M.M., MacLeod, N., Thomson, R., Hancock, J.W.: *Microcracks in Eggs*, Poultry Science, 85, 2006, 2001–2008.

[74] MacLeod, N., Bain, M.M., Hancock, J.W.: *The mechanics and mechanisms of failure of hens' eggs*, Int J Fract, 142, 2006, 29-41.

[75] Li, Q., Wang, K., Zheng, J., Sun, C., Ge, C., Yang, N., Xu, G.: *Nanostructural basis for the gloss of chicken eggshells*, Poultry Science, 98(11), 2019, 5446-5451.

[76] Boneh, Y., Sagy, A., Reches, Z.: *Frictional strength and wear-rate of carbonate faults duringhigh-velocity, steady-state sliding*, Earth and Planetary Science Letters, 381, 2013, 127–137.

[77] Drennon, C.B. III: *Stick-slip friction of lightly loaded rock*. Retrospective Theses and Dissertations 1972, 5903.

Development of a system for detecting filling with urine in reusable diapers

Opracowanie systemu wykrywającego zapełnienie moczem pieluchomajtek wielokrotnego użytku

Ewa Skrzetuska*, Paulina Szablewska

Lodz University of Technology, Faculty of Material Technologies and Textile Design, Institute of Material Science of Textiles and Polymer Composites, 116 Żeromskiego Street, 90-924, Lodz, Poland

Abstrakt

Praca badawcza swoim zakresie obejmuje opracowanie i wykonanie systemu tekstronicznego wykrywającego zapełnienie moczem pieluchomajtek wielokrotnego użytku. Celem jest zastąpienie dotychczasowych rozwiązań na wyrób gotowy wielokrotnego użytku wraz z mobilnym system defektującym wypełnienie moczem. Taka propozycja minimalizowałaby nadmierne zużycie pieluch jednokrotnego użytku oraz narażenie na wszelkiego rodzaju podrażnienia, zakażenia i głównie zapobiegałaby powstawaniu pieluszkowego zapalenia skóry. W celu przygotowania prototypu zbadano materiały wchodzące w skład wyrobu gotowego budujące różne jego warstwy w celu analizy ich właściwości użytkowych. Wykonano trzy wzory haftów nicią elektroprzewodzącą – jeden jednowarstwowy oraz dwa dwuwarstwowe. Przeprowadzono badania użytkowe materiałów oraz haftów, które obejmowały czynniki obecne w codziennym użytkowaniu wyrobu gotowego. Po analizie uzyskanych wyników wykonano prototyp pieluchomajtki oraz zbadano jego pracę podczas symulacji. Wyniki wykazały poprawną pracę stworzonego prototypu.

Abstract

The scope of the research work includes the development and implementation of a textronic system that detects the filling of reusable diapers with urine. The goal is to replace the existing solutions with a reusable ready-made product with a mobile urine filling defect system. Such a proposal would minimize the excessive use of disposable diapers and exposure to all kinds of irritation, infections and mainly prevent the formation of diaper dermatitis. To prepare the prototype, the materials included in the finished product, building its various layers, were examined to analyze their functional properties. Three designs of electroconductive thread embroidery were made - one single-layer and two double-layer. Usage tests of materials and embroidery were carried out, which included factors present in everyday use of the finished product. After analyzing the obtained results, a prototype of the diaper pant was made, and its operation was tested during the simulation. The results showed the correct operation of the created prototype.

Słowa kluczowe: Tekstronika, czujniki wilgoci, haft, arduino, badania użytkowe

Keywords: Textronics, moisture sensors, embroidery, arduino, application research

1.   Introduction

In recent years, monitoring vital signs and activity has become very fashionable and available at one's fingertips [1-3]. Technology is developing to make life easier and easier access to information about medical data or the number of steps taken during the day. In addition to available devices, combinations of textiles and electrical systems are appearing on the market. Textronics combines knowledge from several leading fields of knowledge - electronics, textiles, and computer science, using concepts and tools in the field of automation and metrology [4]. The development of textronic systems means that solutions can have many skills. In addition to the necessary functions of measuring life processes and analyzing external factors, they may have alarm or data transmission functions [5]. The first need for such solutions appeared in high-risk professions. The firefighter's profession, due to its specific nature, was the first to need such solutions the most. The design of the intelligent firefighter suit included not only monitoring the user's heartbeat or breathing, but also having many additional functions, such as a body temperature sensor, ambient temperature sensor, hazardous gas sensors and a locator [6].

Textronic solutions have begun to enter the market dealing with the production of diapers and nappy pants. The main purpose of this procedure was to help not the users themselves, but the people taking care of them. It has become a support for nurses and carers of the elderly and disabled, and for children in hospitals and nursing homes [7]. This allowed the personnel to be informed about an overfilled diaper in a timely manner and to replace it efficiently without exposing the patient to infection or irritation. This problem also applies to the smallest patients. Nursing care in the first hours of a child's life, or later care by a parent at home can be improved and become more controlled through textronic solutions in diapers and nappy pants. In children, and especially often in infants aged 6 to 12 months, diaper wearing is accompanied by frequent inflammatory reactions in response to external

or internal factors. These may be the presence of moisture, infections, mechanical friction, or insufficient hygiene. Risk factors for infection or irritation may include mainly humidity and skin contact with urine and feces, the increased enzymatic activity of which, because of the conversion of urea into ammonia, causes a change in the skin's pH. The cause of excessive skin moisture may be a large amount of urine. It is estimated that a baby up to six months can urinate up to 20 times a day. When conditions are favorable for the appearance of diaper rash, the skin becomes irritated, becomes red and inflamed, and loses its protective barrier function [8].

Panty diapers are a product that is very similar to a disposable diaper. They are supposed to provide comfort of use, be very absorbent and provide a feeling of dryness. The main difference between diaper pants and diapers is the way they are put on, because in the case of the former we will not find velcro to fasten them. The method of putting on is the same as in the case of the lower part of the underwear - just slip them on the buttocks. The lack of velcro has an additional advantage, namely children cannot take them off by themselves. When removing them, disposable diapers can be torn off at the sides, and reusable ones can be slipped off. The most important difference between the two products is the way they are maintained and disposed of. While at the very end they end up in the same place, the life of reusable diapers is much longer [9].

From an ecological point of view, already in 2016, the population living in the United States noticed the problem of the price paid by the environment in exchange for the convenience of using disposable diapers. At that time, approximately 20 billion pieces of this product were used each year, generating 3.5 million tons of waste. One diaper takes at least 500 years to decompose, and during this process it produces methane and other toxic gases. Their production uses volatile chemicals that also pollute the ecosystem. According to the report of the US Environmental Protection Agency, there are consequences of the penetration of pathogens into the environment [10]. Scientists agree that most of them end up in water, which results in contamination of drinking water. Another disadvantage is the annual

consumption of approximately 200,000 trees just to produce disposable diapers [11,12].

The subject of the research work is the development of a textronic system that detects the fullness of urine in reusable diapers. The motivation to undertake research on this subject is several very important aspects of present life on earth. The first is the increasingly popular topic of ecology [10]. Segregation and, more importantly, minimization of waste produced is a salvation for the planet we live on. Secondly, considering ecological considerations, it is necessary to consider the convenience of use for children, their parents and mainly medical staff who have more than one small patient under their care. Reusable diapers will be machine washable, and their main advantage will be the detection of the diaper's filling with urine.

Currently, there are several projects and products using the idea of smart diapers. American Patent US 20015 /0080819 A1 describes a solution using an RFID radio tag. The article aims to provide a diaper structure which includes a body part formed by a fabric layer, a leak-proof layer, and an absorbent material layer successively from the inside to the outside, a communication chip, a metal antenna attached to the outer surface of the leak-proof layer, which are connected to each other to create an RFID tag. When the absorbent material absorbs urine passing through the fabric layer and the inner surface of the anti-leakage layer contacts the urine on the surface of the absorbent material layer, a change in the relative permittivity of the leakage layer causes a change in the impedance value of the metal antenna and, consequently, a change in the electromagnetic wave signal transmitted by the RFID tag. This enables quick detection of a wet diaper [13].

Patent No. 5,557,263 discloses an apparatus mounted in a diaper for detecting the presence of electrically conductive fluids, including urine and other body fluids such as wound exudate. It contains spaced apart electrodes covered with an absorbent material along with a housing containing a signaling device that produces a perceptible vibration, sound, light, or radio signal when a fluid in the absorbent

material provides a conductive path between the electrodes. Spring contacts on the housing provide connections to the electrodes and serve to secure the signaling device housing to a structure supporting the absorbent material. The encoded signals from many of these sensors can be identified and recorded so that they can be reproduced by machine along with other patients' data and analyzed statistically by a computer. Body fluid detection devices are particularly in demand for preventing diaper rash, for potty training infants, and for treating children with enuresis. The above equipment is intended for repeated use [14].

To sum up the introductory part, which introduced two problems related to changing diapers too or too rarely, and the ecological problem of avoiding and trying to stop these processes, this work presents a product that solves the problems mentioned above. By introducing an information system into reusable diaper pants, the product will provide information when the diaper is full and thus indicate when it should be replaced. This will prevent the child from being exposed to long-term skin contact with feces and from excessive monitoring.

2.   Materials and methods

Method of developing the textronic system for detecting filling with urine consisted of three steps. In the first step the materials, type of metal thread, sizes of embroidery, arrangement method and densities of embroidery were selected.

2.1.   Materials

Diapers must meet many requirements regardless of whether they are used for children or adults. The materials from which they are made must provide a feeling of comfort through a complete sense of cleanliness, must not cause skin allergies or any type of irritation, must absorb and distribute moisture evenly as quickly as possible and eliminate the feeling of dampness, and must have elastic elements to ensure the highest degree of fit to the body. For this purpose, widely known and

used products are used, such as polyethylene and polypropylene, polyester, polyacrylate polymers, synthetic rubber, and cellulose. Diaper pants often contain balm, which usually contains fatty substances, e.g., vaseline and/or liquid paraffin, plant extracts, mainly aloe, or may contain fragrances. In addition to carefully sewing all the elements together, adhesives made of thermoplastic polymers are used to keep individual layers of material in the right place [15].

Commonly used textiles to produce multi-layer systems such as diapers and diaper pants were selected. These materials have different raw material compositions and thus also different properties depending on the layer they are to be in the system. Absorbent, moisture-retaining and decorative properties can be mentioned, as in the case of the outer layer. Materials used in both single- and reusable products were tested to check their functional properties and possible predispositions for use in reusable products. The materials selected for the tests was: cellulose pad - skin layer, bamboo non-woven fabric - skin layer, viscose nonwoven - inner layer with embroidery, cellulose non-woven fabric with wood pulp - skin layer, microfiber - inner absorbent layer, laminate - internal layer that retains moisture, cotton knit - outer layer. Moisture-sensitive sensors was made of polyamide yarn, which includes silver. Noble yarn with the trade name X-STATIC was used. It is a yarn that has properties such as anti-static and thermoregulation. It also has high mechanical properties that ensure resistance to tearing. In addition, the product is characterized by the ability to absorb static and electrical discharges. The yarn is made of polyamide silk (85%) coated with a layer of pure silver in the amount of 15%. Sensors made of polyamide thread with the addition of silver were made in three different patterns on a viscose non-woven fabric. One of them includes only one piece of fabric with embroidery, the other two consist of two separate parts with a different element of the embroidery pattern. The purpose of such a procedure is to test which of the mentioned options for embroideries placement would have the best detection parameters. They consist of sensitivity to moisture and the right moment to inform about the need to replace the entire multi-

layer system with a new one. Two-element sensor systems will be separated by layers of absorbent materials, and thus they will inform about the filling when the electrical conductivity between the upper and lower part appears. The designs were created based on European and American patents. Figure 1 shows the embroidered sensors.
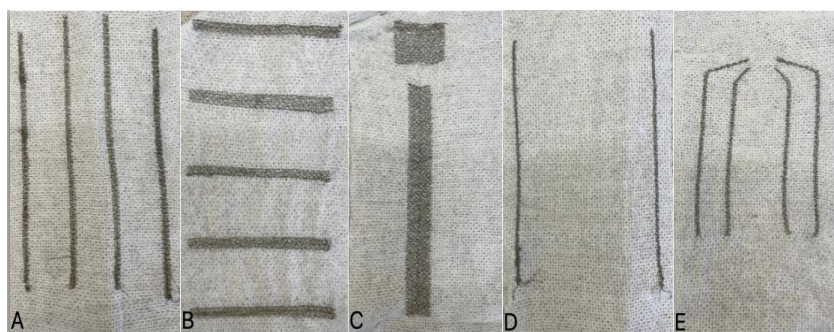
Fig. 1. A) First two-layer system - upper layer, B) First two-layer system - lower layer, C) Second two-layer system - upper layer, D) Second two-layer system - lower layer, E) Single-layer system.

2.2. Methods

The second stage was to perform functional tests of previously selected fabrics and embroidered sensors. The measurements were carried out on samples acclimatized for 24 hours in standard climatic conditions specified in the PN-EN ISO 139 standard, which currently specifies that the humidity should be $65\pm4\%$ and the temperature $20\pm2℃$.

- The test of determining the surface mass is carried out according to the PN-EN 12127: 2000 standard "Textiles - fabrics - determination of mass per unit area using small samples" [16].

- An attempt to determine the thickness of the tested samples was made in accordance with the PN-EN ISO 5084:1999 standard "Textiles - Determination of the thickness of textile products" [17].

- The air permeability test was carried out in accordance with the PN-EN ISO 9237 standard "Textiles - determination of air permeability of fabrics" [18].

- The grating resistance was determined in accordance with the PN-EN ISO 12945-2:2021-04 standard " Textiles - Determination of the surface tendency of a flat article to peel, pill and curl - Part 2: Modified Martindale method" [19].

- Determination of water vapor transmission through the products was carried out in accordance with EN 13726 - 2 "Test methods for direct wound dressings - Part 2: Transmission of moisture vapor through dressings with semi-permeable foil" [20].

- Determination of resistance to urine is a test of the resistance of the tested material to any staining. This test was carried out based on the PN ISO 105-C06: 1996 standard "Textiles - colour fastness test - colour fastness to household washing and communal." The urine produced in the laboratory includes urea weighing 3.75 g, salt weighing 4 g, a drop of tea [21].

- The study of changes in surface resistance was carried out based on the guidelines of the PN-EN 1149-1 standard "Protective clothing - Electrostatic properties" [22].

2.3. Arduino Uno

Arduino is an open-source hardware and software company [23]. It is a type of software in which the copyright holder grants users the rights to research, change, and distribute the software under a free software license [24]. Arduino is a design and user community that designs and produces single-board microcontrollers and microcontroller kits for building digital devices. Arduino boards are available commercially on the official website or from authorized distributors. Board designs use a variety of microprocessors and controllers. Arduino boards come with sets of digital and analog input and output pins that can be connected to various expansion boards or breadboards and other circuits. Microcontrollers can be programmed using C and C++ using an API, also known as the Arduino language, inspired by the Processing language with a modified version of the Processing IDE [23].

3. Results

Materials and embroidered sensors were subjected to functional tests to confirm the materials and learn about their parameters in the manufactured sensors. All the results among the materials confirmed their intended use in the finished product. The rest of this subchapter will present the results of the embroidery use tests and explain how the prototype was created.

3.1. Determination of surface mass

Table 1 shows the results for embroidery. The lowest values are for the embroideries with the smallest surface areas. These are the embroideries of a single layer system and the bottom layer of the second double layer system. For them, 55.720 g/m^2 and 56.120 g/m^2 were achieved. The remaining embroideries had very similar surface areas, therefore the results of determining the surface weight for them are also very similar. For the upper layer of the first two-layer system, the value of the tested parameter is 59.780 g/m^2, for the lower layer of this system 60.200 g/m^2 and for the upper layer of the second two-layer system 60.060 g/m^2.

Tab. 1. Test results determination of surface weight for all tested embroideries.

Viscose nonwoven fabric with embroidery	Surface mass [g/m^2]	Standard Deviation [g/m^2]
Single-layer system	55.720	0.577
The first two-layer system – the upper layer	59.780	0.583
The first two-layer system – the lower layer	60.200	0.863
The second two-layer system - the upper layer	60.060	1.001
The second two-layer system – the bottom layer	56.120	0.876

3.2. Determining thickness

The thickest embroidery turned out to be the upper layer of the first two-layer system, and the thinnest was the lower layer of the same system. All the results obtained for embroidery are very similar. The smallest value of this parameter for

the first two-layer system - the lower layer is only 0.4 mm away from the highest value for the same system but the upper layer. Please remember that the value for a single-layer system remains unchanged when incorporated into the finished product, but for two-layer systems, the results of both layers should be added up. According to the calculations, the first layer system together has a value for a thickness of 2.82 mm and the second two-layer system has a value of 3 mm. Figure 2 below shows very similar values for the thickness determination test for individual embroideries. Ten measurements were taken on the entire embroidery surface.
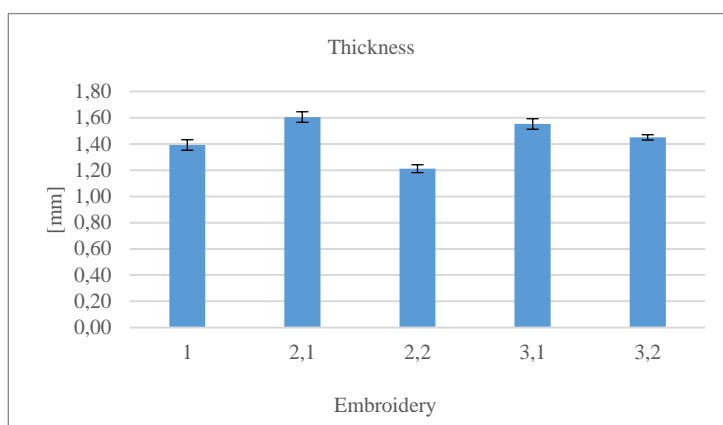
Fig. 2. Graphical presentation of the results of determining changes in thickness. Where: 1) single-layer system, 2.1) upper layer of the first two-layer system, 2.2) lower layer of the first two-layer system, 3.1) upper layer of the second two-layer system, 3.2) lower layer of the second two-layer system.

3.3. Determination of air permeability

Table 2 presents the results of the test for determining the air permeability of embroidery. As mentioned in Chapter 4, the embroidery was made on viscose non-woven fabric. The air permeability value for pure nonwoven fabric was 3232 mm/s. The results obtained for this embroidery study are very promising as the values are very close to the unembroidered fabric. The largest decreases are observed for the two top layers of the two-ply systems. Their results are 2868 mm/s and 2589 mm/s. It should be emphasized that these values are higher than all other results for

unembroidered samples. The result closest to the pure nonwoven fabric is the bottom layer of the first two-layer system and is 3167 mm/s. The remaining results for the single-layer system and the lower layer of the second two-layer system also remain at a very high level, they are very similar to each other, within a small range of 24 mm/s and amount to 3157 mm/s and 3133 mm/s, respectively. Ten measurements were taken on the entire embroidery surface.

Tab. 2. Test results determining air permeability for all tested embroideries.

Viscose nonwoven fabric with embroidery	Air Permeability [mm/s]	Standard Deviation [mm/s]
Single-layer system	3157	71
The first two-layer system – the upper layer	2868	137
The first two-layer system – the lower layer	3167	59
The second two-layer system - the upper layer	2589	38
The second two-layer system – the bottom layer	3133	112

3.4.   Determination of friction resistance

On a comparative scale from 1 to 5, the lowest number means the greatest noticeable changes in the structure of the tested material, the so-called pilling, while the highest one would indicate no changes in the structure. All tested embroideries obtained the same result for determining friction resistance, which was 1.5. It is worth emphasizing that they were made of viscose fibre, which obtained a value of 2 in the same test.

3.5.   Determination of urine resistance

The study was conducted in the context of the occurrence of discoloration, and the embroidery items subjected to the study were compared with those that were not. For all embroideries on a scale from 1 to 5, the result was 5. Two tests were performed for each material and one for embroidery.

3.6. Determination of surface resistance

Below are the results of the tests for the embroidered sensors that determine which design was used in the diaper pant. The initial resistance test was carried out, followed by the test of determining the resistance to friction and the test of determining the resistance to urine. Figure 3 shows graphical representation of the obtained results. Resistance data was collected for 60 seconds.
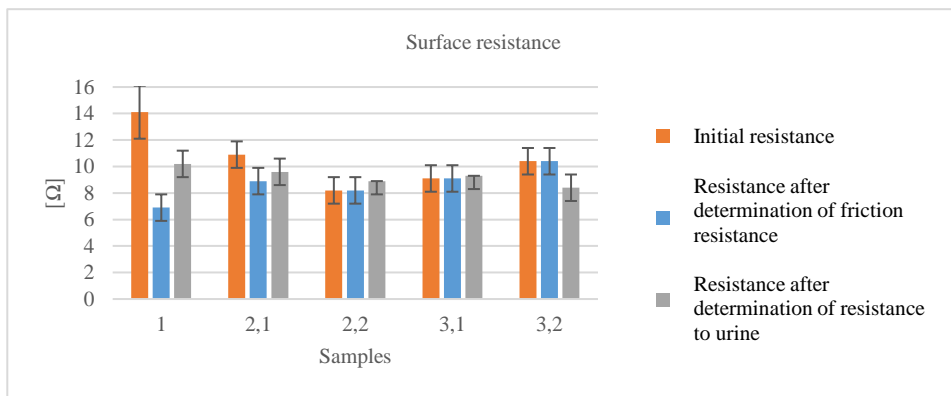
Fig. 3. Graphical presentation of the results of determining changes in surface resistance after utility tests for all tested embroideries. Where: 1) single-layer system, 2.1) upper layer of the first two-layer system, 2.2) lower layer of the first two-layer system, 3.1) upper layer of the second two-layer system, 3.2) lower layer of the second two-layer system.

The greatest changes in the resistance value were observed for a single-layer system. The results for this embroidery pattern range from 7 to 14 Ω. Other systems behaved more stable and changes in resistance values did not exceed 2 Ω. The lower layer of the first two-layer system and the upper layer of the second two-layer system deserve special mention. In these two cases the change was the least noticeable - within 1 Ω. Summing up the observations, the obtained results of the surface resistance are very even and remain at a similar level before and after the utility tests. Simulations of the sensitivity of the embroidery to the presence of moisture were made using an Arduino board with a previously prepared ohmmeter program. Simulations were performed for about 50 seconds, starting with a dry

material, and then imitating the process of urination by the user, water was sprinkled. The results were collected until the system stabilized after the two embroidery paths related to moisture.
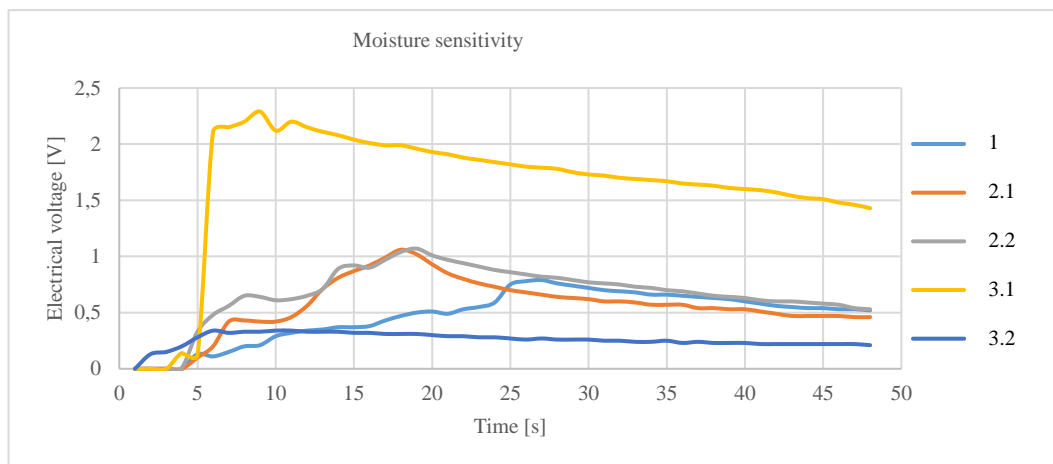
Fig. 4. Moisture detection simulation for tested embroideries. Where: 1) single-layer system, 2.1) upper layer of the first two-layer system, 2.2) lower layer of the first two-layer system, 3.1) upper layer of the second two-layer system, 3.2) lower layer of the second two-layer system.

The Figure 4 shows the difference during the simulation for embroidered detectors. For single-layer system after connecting the two paths of electrically conductive yarn with water, the electric voltage increased rapidly from 0 to 2.27 V and slowly decreased during the process. The electric voltage values collected for this system are twice as high as for the other tested embroideries. The first two-layer system achieves the value of the examined parameter slightly above 1 V. It is worth noting that the course of the simulation is very similar for both layers. The lowest values can be seen for the second two-layer system. The first layer recorded its highest value of electric voltage at the level of 0.7 V, while the second layer did not exceed 0.5 V. During the analysis of the obtained results, a dependence was noticed that the further apart the conductive embroidery paths are from each other, the lower the electric voltage arises between them when tested with the same volume of water.

The prototype of the diaper pant was made based on the products of diaper pants and disposable diapers already available on the market. A proven method of sewing a multi-layer product together was used. The materials tested in the previous chapters of the work were used - bamboo non-woven fabric and cellulose non-woven fabric with wood pulp as skin materials, viscose non-woven fabric on which embroidery was made, microfiber as an internal absorbent insert, laminate as a moisture-repellent membrane and cotton knitted fabric as an external material that holds the whole and decorative product, on which various types of patterns can be applied. The materials tested in the previous chapters of the work were used - bamboo non-woven fabric and cellulose non-woven fabric with wood pulp as skin materials, viscose non-woven fabric on which embroidery was made (two two-layers systems), microfiber as an internal absorbent insert, laminate as a moisture-repellent membrane and cotton knitted fabric as an external material that holds the whole and decorative product, on which various types of patterns can be applied. In addition, on the outer layer, the product has press studs, thanks to which it is possible to easily install the detachable electronic system. The electronic system itself based on the Arduino board is hidden and at the same time protected in the case. 3D printing technology was used to produce the case. Figure 5 shows the prototype made.

Fig. 5. A prototype of a reusable diaper pant with a pattern for boys.

To read the data coming from the inside of the diaper-pants, it was necessary to build an electronic system and write a program that supports it. The system includes

the Arduino UNO Rev3 board, two LEDs in red and yellow, four resistors (two 220 Ω and two 270 Ω), a set of connecting cables, breadboard, battery adapter and 9V alkaline battery. To check the correct operation of the prototype and the correlation of the finished product with the electronic system, simulations were carried out. The measuring station consisted of two computers recording changes in electric voltage and changes in heat, a thermal imaging camera, a syringe and hot water, and was presented in Figure 6. The electronic system based on the Arduino board was placed in a housing made by 3D printing from polyacrylonitrile.

Fig. 6. Measuring station to simulate prototypes.

The electronic system has two detection elements that allow to check the current flow at two points. For the first two-layer system, the wires were connected to the two extreme paths on each layer, for the second two-layer system, the wires were connected to the paths responsible for belly-back and side-side detection. It is worth noting that the paths do not connect with each other and there is no current flow between them. If an electric voltage greater than 0.1 V was detected between the tested embroidery paths, one of the diodes lit up, informing about the presence of conductivity at the expected point. Three floods of warm water with a volume of 20 ml per center of the panty diaper were made. The results of the simulation from the point of view of the thermal imaging camera are presented in Figure 7 below. The photos were taken dry and each time after pouring 20 ml of warm water.
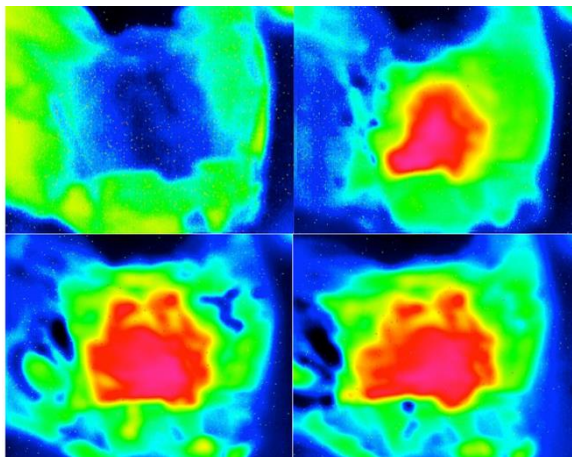
Fig. 7. Pictures taken with a thermal imaging camera in the following order: upper left corner - before the first flooding, upper right corner - after the first flooding, lower left corner - after the second flooding, lower right corner - after the third flooding.

4. Conclusions

The aim of this research was the development of a textronic system for urine leakage detection in reusable nappies. Tests allowed for the selection of the base material with the appropriate properties and size of the embroidery. The constructed prototype proved its correct operation during simulation of its operation. The key findings of this research are that the size, shape, and number of layers of the embroidered sensors has a significant impact on the functional properties of final products and affects its conductive properties, tests of the conductive properties of embroidered materials confirm the possibility of making textronic sensors that respond to the moisture. Additionally we confirmed that the functional properties of each material have a significant impact on the role it can play in clothing, the distribution of paths in one- or two-layer embroidery has a significant impact on the detection of the diaper's fullness with urine, the embroideries made after utility tests show signs of wear through changes in the values of the tested parameters in a minimal way, chemical solutions imitating urine do not affect the appearance of the tested materials, conducted tests of the conductive properties of embroidered

materials confirm the possibility of making textronic sensors reacting to moisture and the materials selected for the tests meet the requirements of materials used in the production of diapers and diapers.

Further development of the finished product can certainly take place in the modernization of the electronic system. Now, it is also small, but as the technology develops, electric cells will be created that will minimize the dimensions of the electronic system.

Acknowledgments/source of funding

References

[1] Choudhry N. A., Arnold L., Rasheed A., Khan I. A., & Wang L.: *Textronics - a review of textile‑based wearable electronics*, Advanced Engineering Materials, 23(12), 2021, 2100469.

[2] Michalak M., Krucińska I., Surma B.: *Textronic Textile Product,* Fibres & Textiles in Eastern Europe, 5 (59), 2006, 54-59.

[3] Lewandowski M.: *A Review of the Commercially Available ECG Detection and Transmission Systems—The Fuzzy Logic Approach in the Prevention of Sudden Cardiac Arrest*, Micromachines, 12, 2021, 1489.

[4] Wilgocka K., Skrzetuska E., Krucińska I. & Sujka W.: *Textronic Solutions Used for Premature Babies: A Review,* AUTEX Research Journal, 23(1), 2023, 18-28.

[5] Wojciechowski J, Skrzetuska E.: C*reation and Analysis of a Respiratory Sensor Using the Screen-Printing Method and the Arduino Platform*. Sensors, 23(4), 2023, 2315.

[6] Walczak, S.: *Inteligentne tekstylia–międzynarodowe innowacje w tekstronice*. Acta Innovations, (3), 2012, 103-121.

[7] Zaman Su, Tao X, Cochrane C, Koncar V.: S*mart E-Textile Systems: A Review for Healthcare Applications.* Electronics, 11(1), 2022, 99.

[8] Erasala, G. N., Merlay, I., & Romain, C.: *Évolution des couches à usage unique et amélioration de l'état cutané des du siège enfants.* Archives de pédiatrie, 14(5), 2007, 495-500.

[9] Ntekpe, M. E., Mbong, E. O., Edem, E. N., & Hussain, S.: *Disposable Diapers: Impact of Disposal Methods on Public Health and the Environment.* Am J Med Public Health, 1 (2), 2020, 1009.

[10] Diaper Industry Workshop Report. Project Summary, 1991.

[11] Arquillos L, Davies P, Colbach H, Lennon C, Mezaiti H, Conrads-Wetland A, et al.: *EDANA sustainability report 2007-2008*, Absorbent hygiene products. 2007, 71.

[12] American Patent US 20015 /0080819 A1.

[13] Patent No. 5,557,263.

[14] Dey S., Kenneally D., Odio M., & Hatzopoulos I.: *Modern diaper performance: construction, materials, and safety review*. International journal of dermatology, 55, 2016, 18-20.

[15] Febo P., & Gagliardini A.: *Baby Diapers Past and Present: A Critical Review. Bionanotechnology to Save the Environment*, 2016, 227.

[16] PN-EN 12127:2000. „Tekstylia – Płaskie wyroby włókiennicze – Wyznaczanie masy na jednostkę powierzchni z zastosowanie małych próbek".

[17] PN-EN ISO 5084:1999. „Tekstylia – Wyznaczanie grubości wyrobów włókienniczych".

[18] PN-EN ISO 9237. „Tekstylia – Wyznaczanie przepuszczalności powietrza wyrobów włókienniczych".

[19] PN-EN ISO 12945-2:2021-04. „Tekstylia -- Wyznaczanie skłonności powierzchni płaskiego wyrobu do pillingu, mechacenia i skłębiania -- Część 2: Zmodyfikowana metoda Martindale'a".

[20] EN 13726 – 2. „Metody badania bezpośrednich opatrunków ran – Część 2: Transmisja pary wilgoci przez opatrunki z folią półprzepuszczalną".

[21] PN ISO 105-C06:1996. „Tekstylia – badanie odporności wybarwień – odporność wybarwień na pranie domowe i komunalne".

[22] PN-EN 1149-1. „Odzież ochronna – Właściwości elektrostatyczne".

[23] McRoberts. *Beginning Arduino*, 2013, (2nd ed. 2013.)

[24] Arduino, S. A. *Arduino*. Arduino LLC, 2015, 372.

Use of DEM to characterize damage of delicate fruit on feeders with reciprocating drive

Wykorzystanie DEM do opisu uszkodzeń owoców delikatnych na podajniku z napędem posuwisto-zwrotnym

Tomasz P. Olejnik[1]*, Elżbieta Sobiecka[1], Dariusz Kryszak[2]

[1] Lodz University of Technology, Faculty of Biotechnology and Food Sciences, 171/173 Wolczanska Str., 90-573 Lodz,

[2] Mysak Group, 18 Bukowska Str., 62-069 Dabrowa k.Poznania

Abstrakt

W artykule opisano modelowanie technologią DEM uszkodzeń borówki wysokiej, podczas transportu na podajniku z napędem posuwisto-zwrotnym. Określono modelowe wartości sił normalnych oraz stycznych w punktach kontaktu borówki. Przeprowadzono symulacje uwzględniające wpływ zmiany wydatku masowego transportowanych owoców na wartości sił normalnych i stycznych. Wykazano, że zmiana wydatku masowego borówki nie powoduje przekroczenia dopuszczalnych sił stycznych i normalnych, oddziałujących pomiędzy owocami.

Abstract

This article describes the modeling by DEM technology of damage to highbush blueberries, during transport on a reciprocating feeder. The modeled values of normal and tangential forces at the blueberry contact points were determined, and the effect of changing the mass output of the transported fruit on the values of normal and tangential forces was studied. It has been shown that the change in the mass output of blueberries does not exceed the permissible tangential and normal forces, interacting between the fruits.

Słowa kluczowe: borówka wysoka, podajnik, siły styczne/normalne, DEM

Keywords: blueberry, feeder, tangential/normal forces, DEM

1. Introduction

The main purpose of the article is to familiarize the the reader with a description of the computational method for the movement of fragile fruit on a trough conveyor with reciprocating drive, so as to minimize the the number of damages to the transported raw material.

Soft fruits damages during transport is one of the most important problems to be solved in the food industry. Damage mechanisms are complex and interrelated. A significant part of technological operations requires the transportation of raw material using vibrating conveyors. Dynamic interactions of transport equipment and the interaction of fruits with each other cause deterioration of the physical and chemical properties of the raw material. During the transportation of food raw materials (fruits), unfavorable phenomena occur that reduce the quality of the raw material, leading to the loss of weight of the raw material, which can be subjected to further technological processes. It is assumed that transporting food is a mobile variety of storage, therefore, the transformations occurring in transported products are affected by the same factors that interact during its storage. The rate of these transformations depends on temperature, ambient humidity and oxygen and carbon dioxide content [1].

Soft fruits tend to behave like viscoelastic materials when subjected to stresses and strains [2-5]. The resulting mechanical behavior of an assembly of viscoelastic particles (fruits), is a complex, integrated effect defined by the geometry of the particles, their shape and roughness of the surface bounding the structure, and the number and strength of the objects' interaction points (contact points). They are a consequence of the shape, size, roughness and strength of the fruit, as well as any other external forces. The movement of stressed particles causes shear stresses that lead to a break in the continuity of the fruit surface. Experimental studies of the effect of external forces occurring during fruit transport have not led to reliable results on the behavior of individual particles/fruit in the studied crop [6-7].

Promising results are provided by the use of the DEM modeling method. During numerous simulations, it has been shown to be a numerical method suitable for modeling the behavior of discontinuous media with different physical properties. Therefore, it should be considered that DEM is a suitable tool in modeling bulk systems of soft and deformable particles.

The dynamic behavior of granular materials such as rocks, powders and agglomerates has been studied using DEM. However, its application to agricultural and food particles has been more limited [8].

The most common geometric shapes that have been used to represent particles in DEM modeling are circular disks or spheres [9]. This is because most available point-of-contact theories assume this shape, leading to a reduction in the initial model parameters and making calculations very simple. Other non-circular and non-spherical primitive shapes, as well as irregularly shaped particles, have been used to approximate more like real particles, which are usually irregularly shaped [10]. In DE modeling, during loading, the deformation of the particles is usually treated as a "virtual" deformation, meaning that the particles can overlap rather than deform due to the contact force. The particles then separate under the assumption that the original shape of each particle has been preserved. The advantages of preserving the shape of the particles are related to the method of calculating contact forces and the subsequent translation and rotation of the particles. Virtual boundaries are left in the DEM modeling, hence a particle that has moved beyond the boundary of the computational area on one side is returned to the system to preserve the total number of particles in the system [11].

The deformation of particles and their potential damage are important to the quality of the final product. In addition, the behavior of most soft, deformable particles is far from purely elastic, which is the most common assumption about particle behavior in DE simulations. In contrast, most agricultural and food materials exhibit viscoelastic behavior. Therefore, the feature of standard DE models that assumes "hard" particles tends to underestimate bulk density when

applied to systems of "soft" particles (viscoelastic), which deform significantly and thus reduce pore volume before failure [12].

In most DEM simulations, the behavior of many thousands of particles is modeled. However, these are always 4 to 8 orders of magnitude smaller than the actual values. Computational simplicity often results in the selection of larger particles with visible grain boundaries compared to the real system, in order to maintain acceptable computational analysis execution time within the assumed system boundaries and facilitate subsequent image analysis. The scaling effect, in which the number of particles represents only a very small, perhaps even insignificant, portion of the total spatial domain, is another problem to be addressed in DEM simulation [13-17].

Therefore, the purpose of this article is to present an innovative computational-simulation method using Rocky DEM software to describe the behavior of particles during their movement on the feeder. The adoption in the model of the deformability and viscoelasticity of spherical particles, corresponding to the shapes of highbush blueberries (*Vaccinium corymbosum*), makes it possible to overcome the limitations that have previously existed when using DEM.

To understand the causes and mechanisms of fruit interactions and impact damage, it is necessary to study the practical aspects of these interactions [18,19]. Impact analysis should take into account the individual interactions between fruits and the interactions of fruits on the feeder walls. In addition, the strength characteristics of the feeder and the fruit being transported should be taken into account. The mathematical description should take into account the damping properties of the raw material leading to load relaxation, friction between the fruit and between the fruit and the feeder trough. Finally, the computational model must take into account the susceptibility of the fruit to damage, determined as a function of its maturity, the temperature at which transport occurs, etc. [20]

2. Materials and Methodology

2.1. Computational model

Simulation calculations, using RockyDEM software, were carried out defining the following research objectives, which included:

1) multi-criteria simulation of the movement on a conveyor of highbush blueberries (*Vaccinium corymbosum*), commonly known as American blueberries,

2) calculation of normal forces and tangential interactions between the blueberry fruit and the walls of the conveying device,

3) calculation of energy restitution coefficients taking into account the physical and chemical properties of blueberry fruit.

The mathematical model used to analyze the interaction of tender fruit during transport involved determining the forces acting on individual particles due to their mass, and calculating interactions with walls and other particles. The highbush blueberry model shown in Figure 1 was used for the simulations.
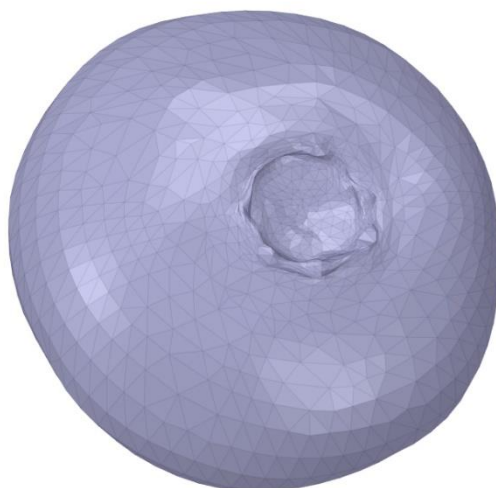
Fig. 1. Graphic model of the blueberry fruit

For the correctness of the simulation, the material constants (Table 1) of the transported raw material were assumed and the process conditions for which the

simulation was carried out were determined. A constant mass flow of blueberry fruit equal to 0.1 kg/s was assumed. The following diameter distribution was assumed for the analysis: 80% of blueberries with a characteristic diameter of 12 mm and 20% with a diameter of 15 mm.

Tab. 1. Summary of selected physical properties of blueberry fruits used in the model.

Variable	Value
Blueberry-wall static friction coefficient	0.6
Coefficient of dynamic friction blueberry-walls	0.6
Static friction coefficient between blueberries	0.7
Blueberry-blueberry dynamic friction coefficient	0.7
Bulk density of blueberry fruit, kg/m^3	640
Young's modulus, MPa	0.6092

A coefficient of restitution of 0.7 was assumed for initial calculations, while in further calculation steps a parametric analysis was carried out to study the effect of the coefficient on the values of forces acting on the fruit.

The analysis was conducted for a shaking conveyor, for which there is product movement in a plane parallel to the plane of the trough. In addition, the transported material slides in the trough under the influence of inertia forces. Figure 2. shows the CAD model of the conveyor.
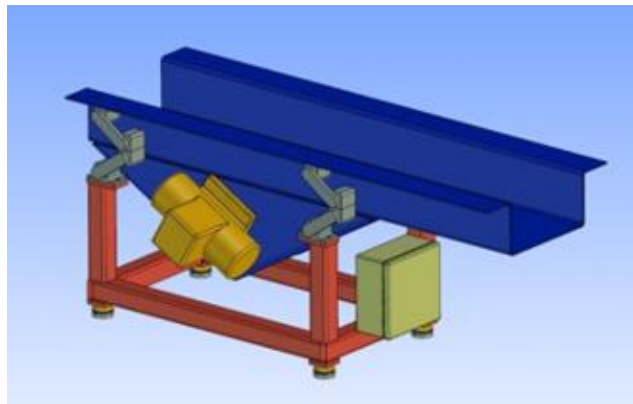
Fig. 2. CAD model of the conveyor

A linear spring hysteresis model was used to determine the normal forces [21]. This model describes elastic collision with energy dispersion due to the deformation of the particle. The model used is described by equation (1). Analyses were conducted in a non-stationary (time-varying) mode this equation was made time-dependent. The normal force at a given time step F_n^t is, according to the DEM Technical Manual [21]:

$$F_n^t = \begin{cases} min\left(K_{nl}s_n^t, F_n^{t-\Delta t} + K_{nu}\Delta s_n\right) \, if \, \Delta s_n \geq 0 \\ max\left(F_n^{t-\Delta t} + K_{nu}\Delta s_n, \lambda K_{nl}s_n^t\right) \, if \, \Delta s_n < 0 \end{cases} \tag{1}$$

where:

F_n^t and $F_n^{t-\Delta t}$ normal forces at design step t and t-Δt,

$\triangle s_n$ is the change in the distance of the particles in the normal direction (Fig.10), the value is positive when the particles approach and negative when the particles separate. K_{nl} and K_{nu} are the stiffness values of the particle in the normal direction with increasing and decreasing load.

The values of the particle stiffn K_{nl} i K_{nu} are dependent on the particle parameters, namely the particle's Young's modulus E, the coefficient of restitution ε and the particle size L. The material data associated with the particle are entered by the user. For contact between two particles or a particle and a wall, the stiffnesse K_{nl} i K_{nu} are described by equations (2) and (3):

$$\frac{1}{K_{nl}} = \begin{cases} \dfrac{1}{K_{nl,p1}} + \dfrac{1}{K_{nl,p2}} \\ \dfrac{1}{K_{nl,p}} + \dfrac{1}{K_{nl,b}} \end{cases} \tag{2}$$

$$K_{nu} = \frac{K_{nl}}{\varepsilon^2} \tag{3}$$

Where the subscr *p1* oraz *p2* efer to particle 1 and particle 2, respectively. The individual values of the stiffness of the particle $K_{nl,p}$ and the wall $K_{nl,b}$ are calculated according to the following formulas:

$$K_{nl,p} = E_p L \tag{4}$$

$$K_{nl,b} = E_b L \qquad (5)$$

where:
- E_p is the value of Young's modulus or elasticity of the particle material, which the user enters in the Rocky DEM editing panel,
- E_b is the Young's modulus or elasticity value of the wall material, which the user enters in the Rocky DEM editing panel,
- L is the size of the particle.

The tangential forces resulting from contact between the borings were determined using an elastic Coulomb model. In this case, the collision is treated completely elastically. In the ideal case (excluding frictional forces), it could be described by equation (6):

$$F_{\tau,e}^t = F_\tau^{t-\Delta t} - K_\tau \Delta s_\tau \qquad (6)$$

where:

$F_\tau^{t-\Delta t}$ is the value of the tangential force at time t-Δt,

Δs_τ S is the change in particle distance in the tangential direction,

K_τ is the value of the stiffness of the particle in the tangential direction defined as the fraction of the normal stiffness K_{nl} from equation (1).

Equation (6) describes the ideal case. However, in the simulation cases analyzed, it was necessary to additionally take into account the force limit as well, by determining the Coulomb limit:

$$F_\tau^t = min\left(\left|F_{\tau,e}^t\right|, \mu F_n^t\right) \frac{F_{\tau,e}^t}{\left|F_{\tau,e}^t\right|} \qquad (7)$$

Where μ is the coefficient of friction defined for a given contact pair. If the force determined from equation (5) exceeds the limit value described by the μF_n^t component, the force takes the value of this component and the sign determined for equation (5).

Simulation of blueberry transport was carried out on a trough conveyor, which

was designed in CAD. The digital model of the structure was then imported in STL format for simulation calculations. A reciprocating motion implemented along the feeder trough with deflections of 6 mm was assigned for the conveyor geometry. The return movement of the trough was faster than the forward movement and the time for each was 0.01 s and 0.03 s, respectively.

3. Results of simulation

3.1. Simulation of normal forces

Figure 3 provides a screen view of the Rocky DEM during the transport of blueberries on a smooth trough. The figure includes the distribution of normal forces acting on the blueberries in the conveyor trough.
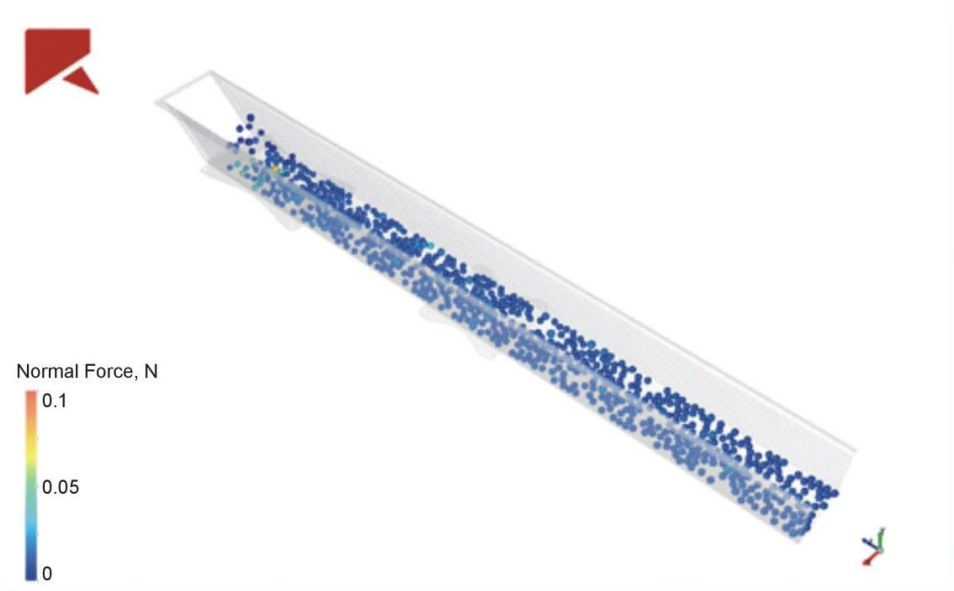
Fig. 3. Summary of normal forces acting on the blueberry
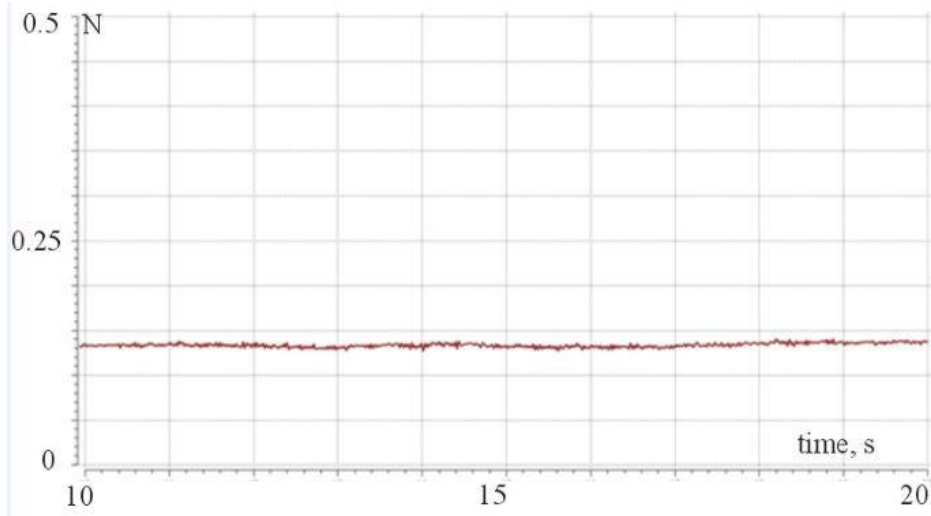
Fig. 4. Average forces in time acting on blueberry fruit in the normal direction

For a better interpretation of the results, Figure 4 shows the values of the average forces acting on the fruit in the direction normal to its surface. And Figure 5 shows the values of the standard deviation of the average force acting on the fruit in the direction normal to its contact surface.
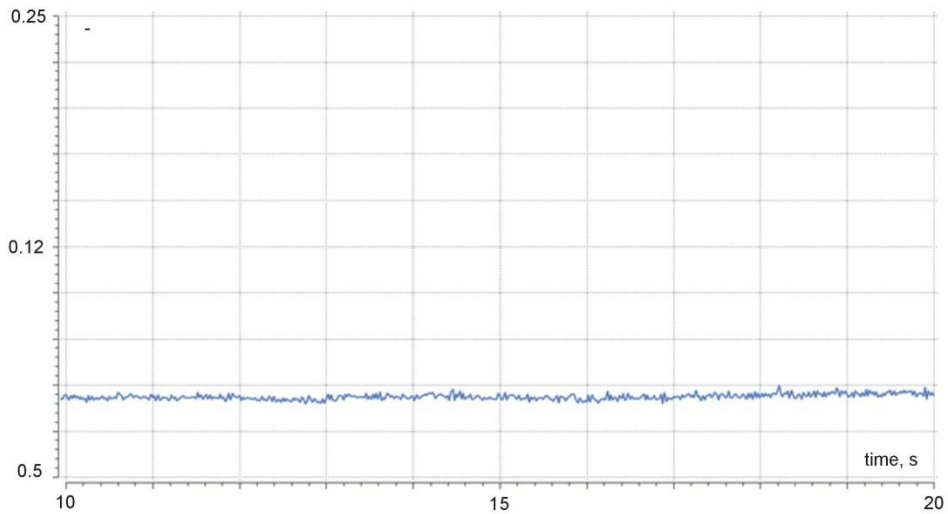
Fig. 5. Mean standard deviation (SD) of normal forces acting on blueberry fruit

3.2. Simulation of tangential forces

During the simulation, collision statistics of tangential forces acting on blueberries between fruits, as well as due to collisions with conveyor walls, were collected. Tangential forces, like normal forces, are an indicator of the quality of the transport as they are responsible for the damage caused on their surface, which indirectly affects the internal structure of the fruit. The results presented here are for the last 10 seconds of fruit movement on the feeder, while the simulation time was 20 seconds. This allowed the steady state operation of the feeders to be obtained and the simulation model to provide average values for a sufficiently long period of operation of the equipment. Figure 6 shows the results of the simulations obtained for tangential forces, while Figure 7 shows the changes in the standard deviation of the average force acting on the fruit in the tangential direction.
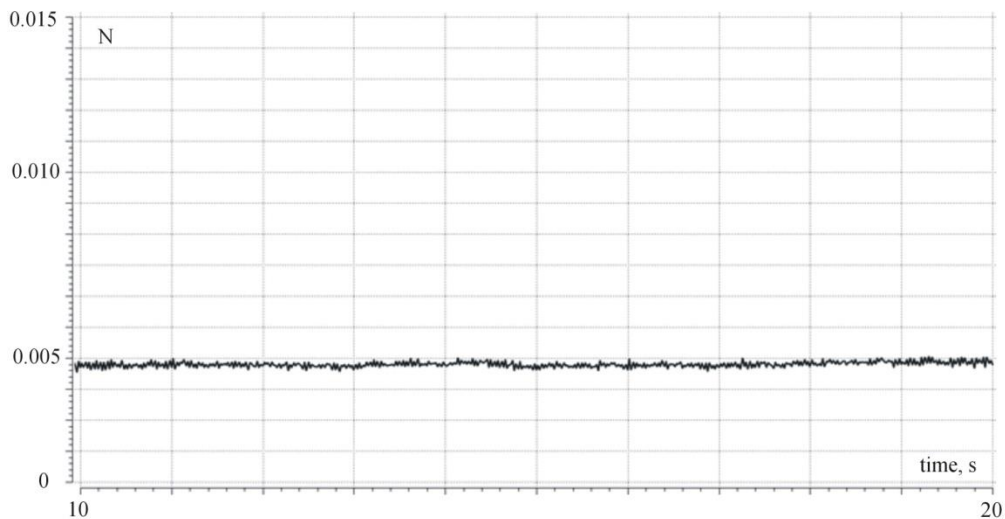
Fig. 6. Average forces acting in time on fruit in the tangential direction
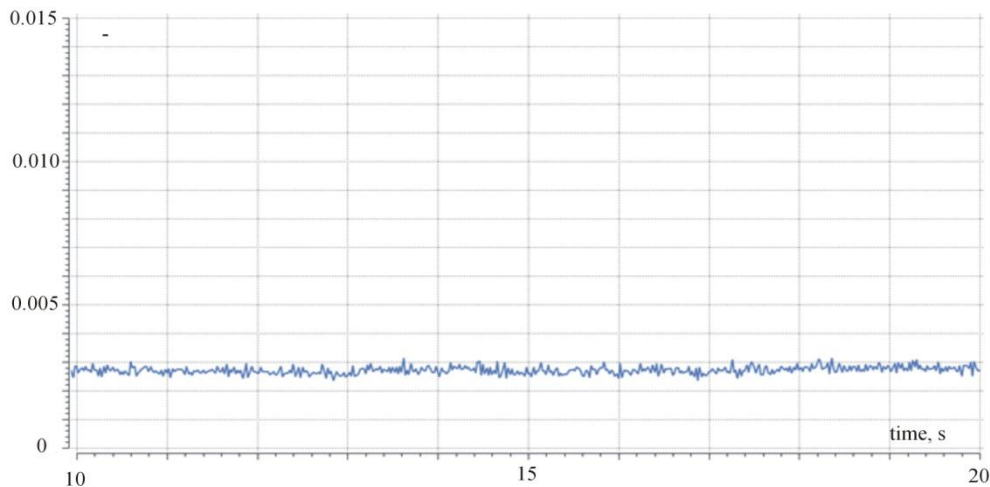
Fig. 7. Standard deviation (SD) of the mean force acting on the fruit in the tangential direction

3.3. Simulation of normal and tangential forces dependent on mass expenditure

In addition to simulating the normal and tangential forces acting on the blueberries, the interactions of the fruit and the transport chute were simulated, making the results dependent on the mass output of the transported fruit on the feeder.
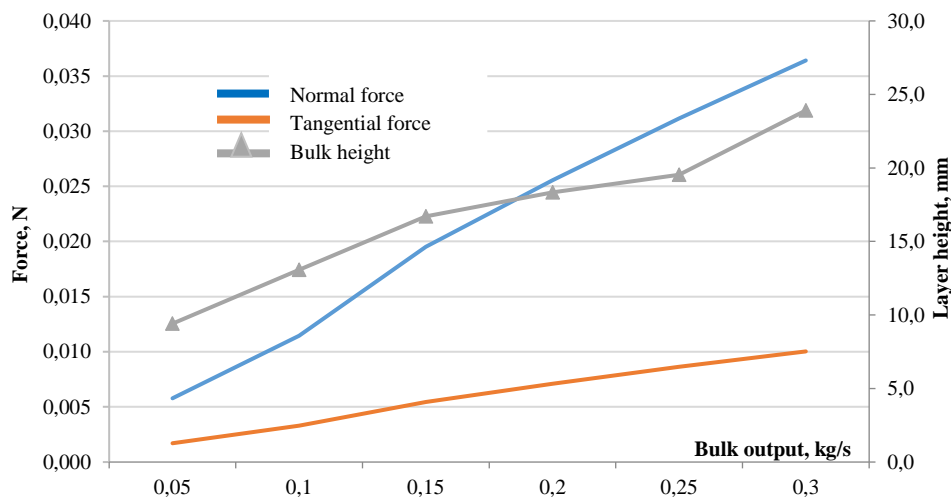
Fig. 8. Average normal and tangential forces acting on the fruit as a function of mass disbursement and layer height

In addition, complementary calculations of changes in the value of the energy restitution coefficient on the values of normal and tangential forces acting on the fruit were carried out. Figure 9 shows the calculated values of normal and tangential forces resulting from the change in the energy restitution coefficient.
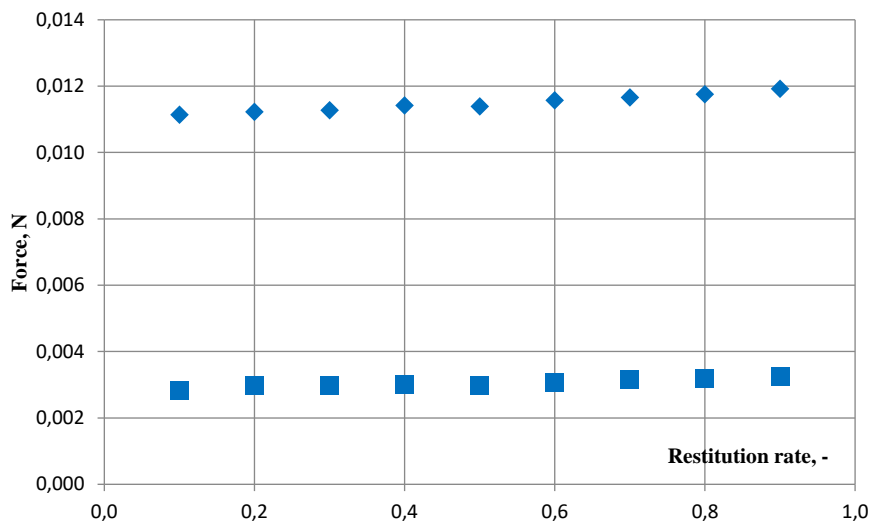
Fig. 9. Average values of forces acting on fruit in the normal and tangential directions depending on the value of the restitution factor; ◆ - normal forces, ◼- tangential forces

4. Discussion and conclusions

Based on the simulation results in Figures 3 to 7, it is noticeable that the normal and tangential forces acting on the blueberry fruit are almost unchanged. The normal forces for the tested fruits are about 0.013 N with an SD value of $\cong 0.0028$. Also, the calculated value of tangential forces during the movement of blueberries along the gutter does not show much change and was ~0.0038 N with SD $\cong 0.0028$. Such small values of forces occurring at the fruit contact points ensure the absence of mechanical damage during the movement of fruits on the conveyor transport gutter.

At the same time, a positive correlation was observed between normal and tangential forces during the variation of the mass output of blueberries transported on the conveyor trough. For the smallest simulated mass disbursement of 0.05 kg/s, the normal and tangential forces acting on the blueberry fruit were 0.0218 N and 0.09 N, respectively, with a stabilized blueberry layer height of 11 mm (Fig. 8.). For the highest mass output of 0.3

kg/s, the values of normal and tangential forces were 0.0365 N and 0.014 N, respectively, at a stabilized layer height of 30 mm. At the same time, there was no significant effect of the restitution factor on the value of tangential and normal forces (Fig. 9).

Conducting process simulations clearly indicated the advantages in using a conveyor with reciprocating motion for transporting blueberries and other soft fruits. The very limited number of fruits that can be damaged, during transport, applies to fresh (unfrozen) and frozen fruits. Conducting simulations using RockyDEM software made it possible to determine the forces acting on the transported material along the entire length of the trough conveyor. At the same time, the behavior of the deposit on the conveyor trough was described.

Reference

[1] Marks, W.: *Wpływ wilgotności na zużycie energii bezpośredniej w procesie rozdrabniania żyta i pszenżyta,* Inżynieria Rolnicza, 7, 2010, 125-130.

[2] Solnechnyi, E. M.: *The Dynamic Properties Investigation for a Distributed Thermomechanical Control Plant,* Eleventh International Conference *"Management of large-scale system development",* (MLSD Management of large-scale system development (MLSD)*, 2018 Eleventh International Conference*. 1-4 Oct, 2018.

[3] Jannatul A., Qinfu H., Albing Y.: *CFD-DEM simulation of drying of food grains with particle shrinkage*, Powd. Tech., 343, 2019, 792-802.

[4] Yiming Y., Liqiang Z., Xiaorong L., Keyu L., Tong J., Yanjun L.: *Influence of the grain sjape and packaging textures on thre primary porosity of sandstone: Insights from a numerical simulation*. Sedimentology, 70(6), 2023, 1856-1885.

[5] Tsuji, Y., Tanaka, T., Ishida, T.: *Langrangian numerical simulation of plug flow of cohesionless particle in a horizontal pipe*, Powder Technology, 71, 1992, 239–250.

[6] Burdilna E., Hrabko V., Mykhalchenko H.: *Transporter Control for Grain Handling in Granaries and Loading on Vehicles*, 2019 IEEE International Conference on Modern Electrical and Energy Systems (MEES)*, 182-185 Sep, 2019.

[7] Zhou F., Jin N., Zeng C., Wang Y.: *Investigatingthe stress-strain of wheat in silos using triaxial tests based on local deformation measurements,* Elsevier Ltd., Biosystems Engineering, 225, 2023, 69-82.

[8] Kleinert J., Simeon B., Dressler K.: *Nonsmooth Contact Dynamics for the large-scale Simulation of Granular Material,* Journal of Computational and Applied Mathematics*,* 316, 2017, 345-357.

[9] Lobo-Guerrero S., Vallejo L.E., Vesga L.F.: *Visualization of Crushing Evolution in Granular materials underCompression Using DEM*, Int. Jour. of Geomechanics, 6 (3), 2006, 195-200.

[10] Tanida, K., Honda, K., Kawano, N., Kawaguchi, T., Tanak, T., Tsuji, Y.: *Particle motion in screw feeder simulated by Discrete Element Method*. In: *International conference on digital printing technologies*, 1998, 429–431.

[11] Raji, A. O., Favier, J. F.: *Discrete element modelling of the impact parameters of a selected fruit: application*, Journal of Applied Science and Technology*,* 2 (1), 2002, 7–12.

[12] Desphande R., Mahiques E., Wirtz S., Scherer V.: *Resolving particle shape in DEM simulations from tabulated geometry ingormation,* Pow. Technology*,* 407, 2022, doi: 10.1016/j.powtec.2022.117700

[13] Descantes, Y.; Tricoire, F.; Richard, P.: *Classical contact detection algorithms for 3D DEM simulations: Drawback and solutions*, 114, 2019, DOI: 10.1016/j.compgeo.2019.103134

[14] Raji, A. O., Favier, J. F.: *Discrete element modelling of the impact parameters of a selected fruit: application*, Journal of Applied Science and Technology, 2 (1), 2002, 7–12.

[15] Knee, M., Miller, A. R.: *Fruit quality and its biological basis,* Sheffield Academic press, 2002, 157-179.

[16] Ahmadi, E.: *Dynamic modeling of peach fruit during normal impact*, J. Food Eng., 35, 2012, 483-504.

[17] Blahovec, J. and Paprštein, F.: *Susceptibility of pear varieties to bruising,* Postharvest Biol. Technol., 38, 2005, 231-238.

[18] Fu, H.: *Bruise Responses of Apple–to–Apple Impact*, In: *IFAC–Papers OnLine,* Vol. 49, 2016, 347-352.

[19] Shirvani, M., Ghanbarian, D., Ghasemi-Varnamkhasti, M.: *Measurement and evaluation of the apparent modulus of elasticity of apple based on Hooke's, Hertz's and Boussinesq's theories*, Measurement, 54, 2014, 133-139.

[20] Van Zeebroeck, M.: *Determining tangential contact force model parameters for viscoelastic materials (apples) using a rheometer*, Postharvest Biol. Technol.*, 33, 2004, 111-125.

[21] DEM Technical Manual, *rocky.esss.co.* 2019. Available at: https://rocky.esss.co/technical-library/

Effect of protein hydrolysate-based biostimulants on chlorophyll content in wheat leaves

Wpływ biostymulatorów białkowych na zawartość chlorofilu w liściach pszenicy

Dorota Gendaszewska[1*], Paulina Pipiak[1], Katarzyna Ławińska[1], Maria Stanca[2]

[1] Łukasiewicz Research Network – Lodz Institute of Technology, 19/27 Skłodowskiej-Curie Str., 90-570 Lodz, Poland,

[2] Leather Research Department, Research and Development National Institute for Textiles and Leather-Division Leather and Footwear Research Institute, 93, Ion Minulescu Street, 031215 Bucharest, Romania

Abstrakt

W artykule zbadano wpływ dolistnego nawożenia biostymulatorów białkowych na poziom chlorofilu i karotenoidów w pszenicy ozimej. Otrzymane wyniki wskazują na znaczący wzrost barwników fotosyntetycznych dla próbek II i III, które stanowiły rośliny traktowane biostymulatorami zawierającymi hydrolizat kolagenu i salicylan sodu oraz hydrolizat kolagenu i keratyny w połączeniu z askorbinianem tytanu (odpowiednio Bio-2 i Bio-3). W pracy potwierdzono również, że efektywność ekstrakcji chlorofilu i karotenoidów zależy od rodzaju rozpuszczalnika. Uzyskane wyniki pozwalają sformułować wniosek, iż najkorzystniejszym rozpuszczalnikiem do ekstrakcji barwników fotosyntetycznych z liści pszenicy jest etanol.

Abstract

This paper investigates the effect of foliar fertilisation with protein biostimulators on chlorophyll and carotenoid levels in winter wheat. The results obtained show a significant increase in photosynthetic pigments for samples II and III, which were plants treated with biostimulants containing collagen hydrolysate and sodium salicylate and collagen and keratin hydrolysate in combination with titanium ascorbate (Bio-2 and Bio-3, respectively). The study also confirmed that the extraction efficiency of chlorophyll and carotenoids depends on the type of solvent. The results obtained allow the conclusion to be drawn that the most favourable solvent for the extraction of photosynthetic pigments from wheat leaves is ethanol.

Słowa kluczowe: biostymulatory, pszenica ozima, chlorofile, karotenoidy, analiza spektrofotometryczna

Keywords: biostimulants, winter wheat, chlorophylls, carotenoids, spectrophotometric analysis

---

1. Introduction

In recent years, the growth and productivity of crop plants have been significantly affected by abiotic stresses. Regions with significant crop production, such as central Europe, south-central Asia, south-eastern South America and the south-eastern United States, are facing increasingly frequent occurrences of high temperatures and drought [1]. Biostimulants are essential for sustainable crop production in the face of climate change. Natural products such as seaweed extracts, humic substances, hydrolysate proteins and products containing amino acids or microorganisms contain bioactive substances that can improve nutrient efficiency, abiotic stress tolerance and/or crop quality traits, irrespective of their nutrient content [2,3]. Biostimulants also contribute to improved seed germination and induce plant biological activity [4]. One type of biostimulant is amino acids, which are produced by chemical synthesis or by hydrolysis of plant and animal proteins. Amino acids play a key role in construction, metabolism and transport. Tryptophan is known to be a precursor of the hormones responsible for stem and root elongation [5]. Glycine and glutamic acid are essential substrates for tissue formation and chlorophyll synthesis [5]. Proline, however, affects pollen fertility, thereby contributing to an increased yield [5]. Amino acids allow plants to make better use of their natural production potential, which is often suppressed by various stresses (e.g. drought, hail, frost). Supplying the plant with amino acids in the form of ready-to-use preparations during or before a biotic or abiotic stress factors ensures that the plant develops evenly and efficiently despite adverse conditions [6].

Chlorophylls are a widespread group of photosynthetic pigments found in higher plants, algae and cyanobacteria [7]. Chlorophyll molecules are esters of a dicarboxylic acid (chlorophyllins) and four five-membered pyrrole rings linked by methyl groups (-CH=) (protoporfirin ring) [8]. Chlorophyll is an essential pigment that plays a key role in the normal course of photosynthesis, in which the conversion of light energy into chemical bond energy is enabled by the absorption of light

quanta in redox reactions [7, 9]. Numerous genetic, morphological, physiological and abiotic factors affect its content in plant leaves [8]. Therefore, a change in chlorophyll content is one of the most obvious symptoms of plant stress [10]. The absorption properties of pigments allow their qualitative and quantitative analysis [8]. Both chlorophyll and carotenoids are lipid soluble compounds. Therefore, they can be extracted from living plant tissue containing water using organic solvents such as acetone, alcohols, ethers [11]. To accurately and precisely determine the content of chlorophylls and carotenoids, they must first be extracted from a fresh sample of plant tissue. The most common method for the determination of photosynthetic pigments in plant material is their extraction with solvents followed by spectrophotometric analysis. This method is reliable but time-consuming and requires high precision [8]. Many factors can affect the activity of a solvent, including the time needed for extraction, the amount of plant material or the percentage of moisture in the plant material form [12]. The efficiency of plant dye extraction depends on the type of solvent, which should selectively absorb the chemical compound of interest and not (or only slightly) absorb the other compounds present in the sample. The choice of solvent is therefore crucial [13]. The solvent extraction methods using polar aprotic solvents like acetone, dimethyl sulfoxide (DMSO), and N, N-dimethylformamide (DMF) and polar protic solvents like ethanol and methanol have been utilized widely [14].

The aim of the study was to investigate the effect of foliar application of protein biostimulants on the chlorophyll and carotenoids contents in winter wheat seedlings. In addition, the study tested several common organic solvents used for the determination of photosynthetic pigments in order to select the most effective one for wheat.

2. Materials and methods

2.1.   Plant material

The study material consisted of 30-days winter wheat seedlings (*Triticum aestivum* L.) grown under controlled conditions in a Royal Room growbox (200x200x100cm). The trial was carried out in the Łukasiewicz Research Network – Lodz Institute of Technology in Lodz, Poland. The winter wheat seed was obtained from Plant Breeding Strzelce (Poland). The wheat was grown in 58x40.5x7cm plastic trays (approximately 180 seeds per tray) in horticultural soil (pH: 5.5-6.5, EC<1.5 mS/m, organic matter: 2%). Plant growth conditions during the experiment included 6 hours of artificial lighting (Lumatek Attis 200W LED FULL SPECTRUM ATS200W), day/night temperature 21/19ºC respectively and relative humidity around 50%. At the 3-4 leaf emergence stage (about 14 days after sowing), foliar application of biostimulants prepared by the Łukasiewicz-Lodz Institute of Technology (Łukasiewicz-LIT) from Poland was carried out. The physical and chemical properties of three biostimulant formulations (Bio-1, Bio-2, Bio-3) are presented in Table 1. During the experimentation, solutions of biostimulants including protein hydrolysates obtained through scientific collaboration with the Leather and Footwear Research Institute Division (INCDTP, Romania), titanium ascorbate synthesized in the Łukasiewicz-LIT, and commercially available sodium salicylate obtained from Pol-Aura Sp. z o.o. (Poland) were used. The antifungal preparation Afrodyta was applied together with the biostimulant (in the dose recommended by the manufacturer). The nitrogen content of the samples was determined using the Kjeldahl method. The plants were collected 30 days after sowing and the chlorophyll and carotenoids of the shoots were determined spectrophotometrically. Samples: SI, SII and SIII are treated with Bio-1, Bio-2 and Bio-3 biostimulants, respectively. The control sample of the experiment were untreated plants (C).

Tab. 1. Composition of applied biostimulants

No.	Protein Hydrolysate	Active Substance	Total N	Code
1	Collagen (0.50%)	Sodium salicylate (0.03%)	1.35%	Bio-1
2	Collagen (0.50%)	Titanium ascorbate (0.01%)	1.00%	Bio-2
3	Keratin (0.50%), Collagen (0.50%)	Sodium salicylate (0.03%)	1.20%	Bio-3

2.2. Photosynthetic pigment contents determination

Photosynthetic pigment contents determinations were conducted by selecting fully developed wheat leaves at random from each wheat variety cultivated during the experiment. For the measurement of chlorophyll and carotenoids, 0.5 g of fresh leaves were used. The leaves were crushed in a mortar with 3 ml of solvent, and a small amount of sand and $CaCO_3$. The solution was quantitatively transferred to centrifuge tubes by rinsing the mortar and pestle with 2 ml of solvent. The homogenized sample mixture was centrifuged at 10 000 rpm for 10 minutes at room temperature. Then 0.5 ml of the supernatant was removed and 4.5 ml of solvent was added. Chlorophyll content was determined using UV-9200 by RayLeigh spectrophotometer at wavelengths appropriate to the solvent used. All chemicals and solvent were of analytical grade. The contents of chlorophyll a, chlorophyll b and carotenoids were calculated according to formulae available in the literature [15-17]. These formulae are shown in Table 2.

Tab. 2. Formulas for determining the contents of photosynthetic pigment

Type of solvents	Equation/Formula
Acetone	$Ch_a = 12.25A_{663} - 2.79A_{645}$ $Ch_b = 21.5A_{645} - 5.1A_{665}$ $C_{x+c} = (1000A_{470} - 1.82C_a - 85.02C_b)/198$
Ethanol	$Ch_a = 13.36A_{663} - 5.19A_{645}$ $Ch_b = 27.43A_{645} - 8.12A_{663}$ $C_{x+c} = (1000A_{470} - 2.13C_a - 97.63C_b)/209$
Diethyl-ether (DEE)	$Ch_a = 10.05A_{663} - 0.97A_{645}$ $Ch_b = 16.36A_{645} - 2.43A_{663}$ $C_{x+c} = (1000A_{470} - 1.43C_a - 35.87C_b)/205$

3. Results and discussion

The experiments investigated the effect of foliar application of biostimulants developed at Łukasiewicz-LIT (biostimulant composition in Table 1) on photosynthetic pigment contents in wheat leaves. The contents of chlorophyll a, chlorophyll b and carotenoids was determined in each of the samples tested (SI, SII, SIII and C) in the spectrophotometric analyses. In addition, in order to select the optimum solvent for the extraction of these pigments from wheat leaves, the study compared the effectiveness of three commonly used solvents, e.i. acetone, ethanol and diethyl ether (DEE). The results of the spectrophotometric analyses are summarized in Table 3. The concentration of photosynthetic pigments was determined from the absorbances measured, according to the formulae in Table 2.

Tab. 3. Spectrophotometric determination of absorbance for chlorophyll a, chlorophyll b, carotenoids with various extracting solvents.

Sample	Type of solvents								
	Acetone			Ethanol			Diethyl-ether		
	A663	A645	A470	A663	A645	A470	A663	A645	A470
SI	0.31±0.01	0.10±0.01	0.26±0.01	0.59±0.01	0.20±0.01	0.56±0.01	0.58±0.05	0.19±0.05	0.37±0.02
SII	0.57±0.02	0.19±0.01	0.47±0.01	0.82±0.02	0.28±0.01	0.75±0.03	1.46±0.20	0.51±0.02	0.99±0.05
SIII	0.59±0.02	0.20±0.01	0.50±0.02	0.68±0.02	0.23±0.01	0.66±0.02	1.51±0.25	0.53±0.05	0.99±0.04
C	0.27±0.01	0.10±0.01	0.24±0.01	0.42±0.01	0.15±0.01	0.41±0.01	0.32±0.01	0.12±0.01	0.23±0.02

Figure 1 compares the content of chlorophyll a in all the samples tested after application of the biostimulants, depending on the solvent used. The main conclusion from this experiment is that the highest contents of chlorophyll a values were obtained for SII and SIII. The obtained results most probably result from the biostimulating properties of the applied substances. SII were treated with a Bio-2 containing collagen and titanium ascorbate. Literature data indicate that collagen hydrolysate is primarily a source of nitrogen for plants. Furthermore, the composition comprises amino acids such as glycine, serine, and proline, which exhibit heightened accumulation in response to environmental stresses within plants [18]. Collagen is a fibrous protein with amphiphilic properties and the ability to

buffer pH fluctuations, chelate micronutrient ions, adhere to leaves, and act as a reservoir of organic nitrogen and amino acids. In addition, titanium ascorbate was used as an active ingredient in Bio-2. The literature acknowledges the positive impacts of titanium ascorbate on plants, leading to increased iron ion activity, enhanced pollen grain vigour and a higher nutrient uptake rate [19]. The effects of foliar-applied organic titanium salts on plants are documented extensively in review publication [20].
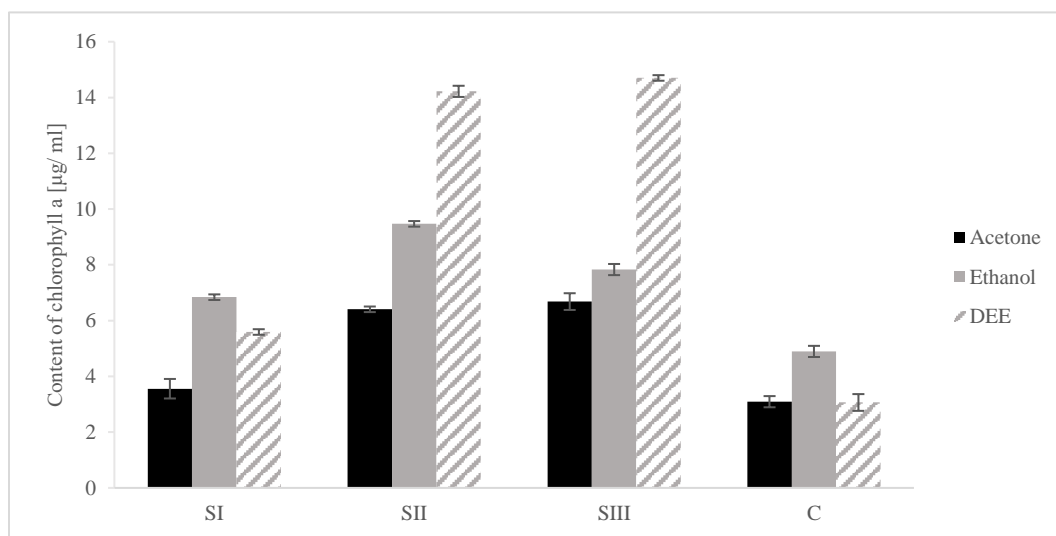
Fig. 1. Comparison of chlorophyll a content in the tested sample after application of biostimulants depending on the solvent used

On the other hand, SIII were treated with Bio-3, which contained collagen, keratin and sodium salicylate. The hydrolysate proteins used provide a rich source of nitrogen in the formula. Keratin is rich in cysteine (a sulphur-containing amino acid), which distinguishes it from other biopolymers. The cysteine and cystine content of the amino acid sequence is 7-12%. Keratin preparations exhibit a substantial concentration of amino acids, namely, glycine, alanine, serine, and valine. Meanwhile, their composition of methionine, lysine and tryptophan is relatively low [21]. An additional active ingredient utilized in the formulation Bio-3 is salicylic acid, an endogenous plant growth regulator with the capacity to

stimulate the systemic acquired resistance (SAR). This substance regulates processes including seed germination, growth of roots and leaves, synthesis of proteins and chlorophyll, flowering of plants, resistance to pathogens, as well as the transport of metabolites, particularly divalent metal cations [22]. Salicylic acid stabilizes cell membrane structure and permeability, facilitating increased nutrient uptake by increasing nitrate concentration in the plant. Research indicates that salicylic acid and its derivatives have a beneficial effect in reducing the impact of abiotic stressors on the growth, development and yield of plants [23]. Another important observation was that there are considerable differences in chlorophyll a concentration depending on the solvent used. Similar observations have been made in several reports [24,25,26]. In most cases, the highest extraction of selected pigments is observed with the DEE solvents, especially in SII and SIII. In other cases, the results obtained for DEE and ethanol are at a similar level and were 5.59 µg/ml (DEE) and 6.84 µg/ml (ethanol) for sample I and 3.06 µg/ml (DEE) and 4.89 µg/ml (ethanol) for the control sample. This observation is supported by the polar nature of the chlorophyll molecule, which allows greater solubility in DEE, which is characterized by a large dipole moment [25]. Similar observations were made for chlorophyll b for each sample.

In turn, Figure 2 showed the content of carotenoids in all the samples tested after application with the biostimulants, depending on the used solvent. The results collected in this graph show a similar relationship as in Figure 2. The highest values of photosynthetic pigment were obtained for SII and SIII, confirming the positive effect of the biostimulants. Much lower carotenoids contents were obtained in the C and SI samples.
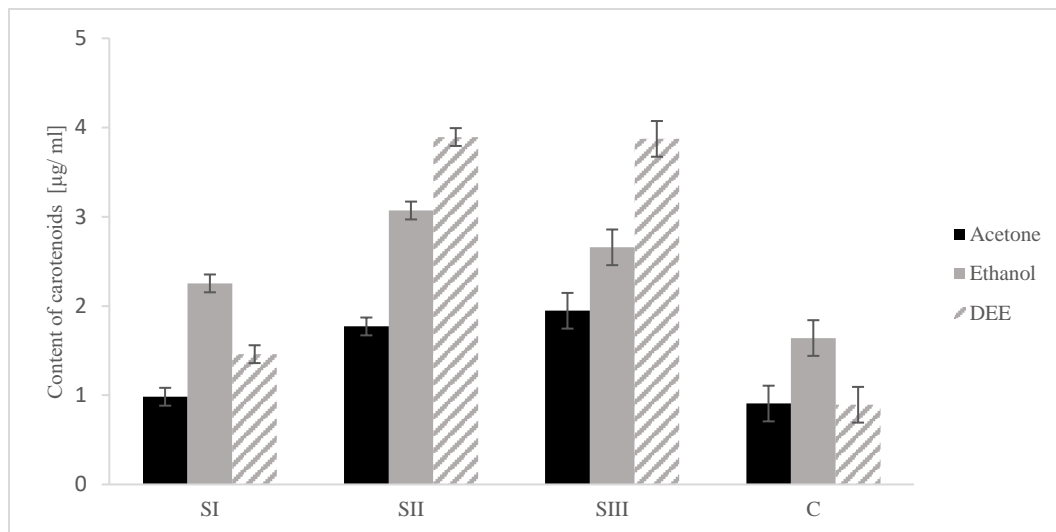
Fig. 2. Comparison of carotenoids content in the tested sample after application of biostimulants depending on the solvent used

The next part of the research was to compare commonly used organic solvents in order to select the most appropriate extractant for the determination of photosynthetic pigment contents in wheat leaves. Standardization of chlorophyll extraction is very difficult due to the variable chlorophyll content in leaves and between different plants. In addition, extraction efficiency is influenced by solvent polarity, solution pH, light, temperature. Studies Saito [27] showed the dependence of the absorption coefficients of pure chlorophyll a and chlorophyll b on the used solvent . In addition, trends in solvent usability vary according to the plant species studied. When choosing a solvent, a compromise must be made between selecting a solvent for efficient quantitative extraction of chlorophyll and using a solvent best suited for spectrophotometric assays. For example, acetone is an ideal solvent for chlorophyll determination as it gives very sharp chlorophyll absorption peaks [24, 28]. However, this compound is a poor extractant of chlorophyll for some plants. Furthermore, acetone is volatile and highly flammable. In addition, acetone reacts with polystyrene and polymethylacrylate making latex or plastic gloves and plastic cuvettes unsuitable [25]. Solvents such as methanol and ethanol are often more

effective extractants than acetone [10,24]. The toxicity of methanol unfortunately rules out this solvent in terms of safety for the test worker. A much safer solvent for chlorophyll determination is ethanol [25]. Although flammable, it is not highly toxic and is suitable for use in the laboratory [24]. A fourth common solvent used for green dye assays is diethyl ether (DEE) [25]. It is not the solvent of first choice for laboratory work because it is volatile, flammable, explosive and narcotic. Furthermore, it should be noted that plastic cuvettes and the majority of plastic laboratory equipment lack resistance to diethyl ether [25]. Other solvents used for the determination of chlorophylls in leaves can be found in the literature, such as chloroform, dimethyl sulphoxide (DMSO) and dimethyl formamide (DMF), but are not routinely used [29].

Acetone, ethanol and diethyl ether were used to extract photosynthetic dyes. In all samples tested, the contents of chlorophyll a were higher than those of other photosynthetic pigments (Fig. 3). For the control sample and for SI, the highest content of chlorophyll a during extraction with ethanol was observed, respectively 4.89 µg/ml and 6.84 µg/ml. However, for SII and SIII, the highest chlorophyll a content was determined using DEE. The most effective extractant chlorophyll b was found to be DEE. The contents of chlorophyll b varied from 1.13 µg/ml. for the control sample to 4.99 µg/ml for SIII. The effectiveness of the organic solvents used in this case presents itself in the following order: DEE>acetone>ethanol. In contrast, the highest carotenoid concentrations were determined during extraction of DEE (3.89 µg/ml SII and 3.87 µg/ml SIII). In contrast, for SI and the control sample, ethanol proved to be the most effective carotenoids extender. The solubility of photosynthetic dyes depends on the structure of the compound. Chlorophyll a and chlorophyll b molecules are non-polar. The long hydrocarbon (phytol) tail attached the porphyrin ring makes chlorophyll fat-soluble and insoluble in water. Chlorophyl b is more polar than Chlorophyll a due to the difference in their structure. The solubility also differs for both the pigments. Chlorophyll a is less soluble in polar solvents. According to the results (Fig. 3) obtained in the

experiment and taking into account the physico-chemical properties of the solvents, the most favourable pigment for the extraction of photosynthetic pigments is ethanol.
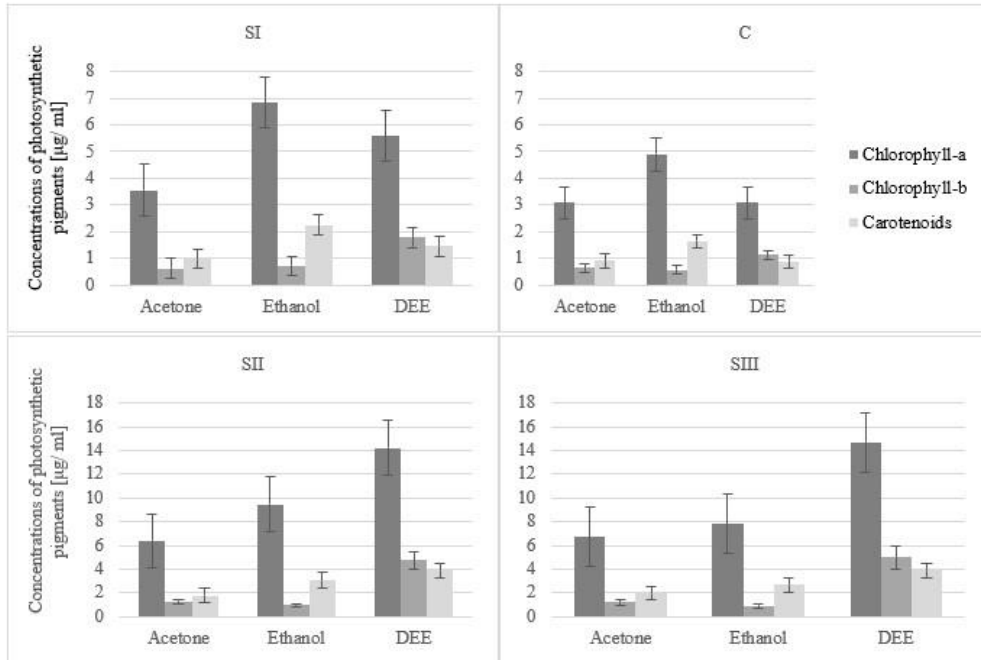
Fig. 3. The average concentrations (µg/ml) of chlorophyll a, b and carotenoids in winter wheat (Samples: C, SI, SII, SIII).

4. Conclusions

In sustainable crop production, biostimulants play an important role in improving plant growth and crop quality. Assimilation area and chlorophyll content are important parameters to assess plant growth. The chlorophyll content of leaves is a key factor in determining the rate of leaf photosynthesis. Since the nitrogen content of a leaf is made up of photosynthetic and non-photosynthetic nitrogen components, determining the chlorophyll content is a better characterisation of the photosynthetic capacity of the plant than testing the nitrogen content of the leaf. In this work, the effect of foliar application of protein biostimulants on the amount of photosynthetic pigments in wheat leaves was investigated. The highest levels of

chlorophyll and carotenoids were found in SII and SIII, plants treated with Bio-2 (containing collagen and titanium ascorbate) and Bio-3 (containing collagen, keratin and sodium salicylate). The results of the study thus confirmed the beneficial effect of protein biostimulants in increasing the efficiency of biochemical processes occurring in the leaves of the plant under study. The work also confirmed that the extraction efficiency of plant pigments depends on the type of solvent used. In most cases, the highest extraction of selected pigments is observed with DEE solvent, followed by ethanol and acetone. However, as the properties of ether (volatile, flammable, explosive) cause some inconveniences when working with this solvent, ethanol was chosen for the determination. Studies have shown that ethanol can be successfully used as a solvent for the determination of photosynthetic pigments.

References

[1]   Carrão H., Naumann G., Barbosa P.: *Mapping global patterns of drought risk: An empirical framework based on sub-national estimates of hazard, exposure and vulnerability*. Glob. Environ. Chang., **39**, 2016, pp. 108–124.

[2]   Wadas W, Dziugieł T.: *Changes in assimilation area and chlorophyll content of very early potato (Solanum tuberosum L.) cultivars as influenced by biostimulants.* Agronomy, **10(3),** 2020, p. 387.

[3]   Bulgar R., Franzoni G., Ferrante A.: *Biostimulants application in horticultural crops under abiotic stress conditions.* Agronomy, **9**, 2019, pp. 306.

[4]   Popko M, Michalak I, Wilk R, Gramza M, Chojnacka K, Górecki H.: *Effect of the new plant growth biostimulants based on amino acids on yield and grain quality of winter wheat,* Molecules, **23(2),** 2018, pp. 470.

[5]   Popko M., Wilk R., Górecki H.: *New amino acid biostimulators based on protein hydrolysate of keratin*. Przemysł chemiczny, **93(6),** 2014, pp.1015-1012. [in Polish]

[6]   https://modr.pl/technologie-ekologicznej-uprawy-rolniczej/strona/aminokwasowe [online access in 29.10.2023]

[7]   Baker N. R.: *Chlorophyll fluorescence: a probe of photosynthesis in viv,*. Annual Review of Plant Biology, **59(1),** 2008, pp. 89–113.

[8]   Pavlović D., Nikolić B., Đurović S., Waisi H., Anđelković A., Marisavljević D.: *Chlorophyll as a measure of plant health: Agroecological aspects.* Pestic. Phytomed. (Belgrade), **29(1),** 2014, pp. 21–34.

[9]   Croft H., Chen J.M., Luo X., Bartlett P., Chen B., Staebler R.M.: *Leaf chlorophyll content as a proxy for leaf photosynthetic capacity,* Global Change Biology, **23(9),** 2017, pp. 3513–3524.

[10] Lichtenthaler H. K., Babani, F: *Light adaptation and senescence of the photosynthetic apparatus. changes in pigment composition, chlorophyll fluorescence parameters and photosynthetic activity.* In: Papageorgiou, G.C., Govindjee (eds) Chlorophyll a Fluorescence. Advances in Photosynthesis and Respiration, vol **19**, 2004, Springer, Dordrecht.

[11] Ebrahimi P., Shokramraji Z., Tavakkoli S., Mihaylova D., Lante A.: *Chlorophylls as Natural Bioactive Compounds Existing in Food By-Products: A Critical Review.* Plants*,* **12(7),** 2023, pp. 1533.

[12] Jelić G., Bogdanović M., Nikolić B.: *Metode za određivanje fotosintetskih pigmenata.* Acta herbologica, **1(2),** 1992, pp. 235-242.

[13] Sitarek M., Dobrzyński J., Orliński P.: *Extraction of chlorophylls and carotenoids - a review of methods including accelerated solvent extraction. Zagadnienia aktualnie poruszane przez młodych naukowców*. Creativetime. Kraków 2016. [in Polish]

[14] Lichtenthaler H. K., Buschmann C.: *Extraction of Phtosynthetic Tissues:Chlorophylls and Carotenoids Current Protocols in Food Analytical Chemistry,* **1**, 2001, F4.2.1-F4.2.6

[15] Porra R. J., Thompson W. A., Kreidemann P. E.: *Determination of accurate extinction coefficients and simultaneous equations for assaying chlorophylls a and b extracted with four different solvents: verification of the concentration of*

chlorophyll standards by atomic absorption spectrometry, Biochim. Biophys. Acta, **975,** 1989, 384–394

[16] Lichtenthaler H. K.: *Chlorophylls and carotenoids: pigments of photosynthetic membranes*, Method Enzymol., **148**, 1987, pp. 350–382.

[17] Lichtenthaler H. K., Wellburn, A. R.: *Determinations of total caroteneoids and chlorophylls a and b of leaf extracts in different solvents*, Biochem. Soc. Trans., **11**, 1983, pp. 591–592.

[18] Ali Q., Athar H., Haider M, Z., Shahid S.: *Role of aminoacids in improving abiotic stress tolerance to plants*, Plant Tolerance to Environmental Stress, 2019, pp. 175-204.

[19] Borkowski J., Felczyńska A., Dyki B.: *Effect of calcium nitrate*, *Biochicol 020 PC and Tytanit on the healthiness of chinesecabbage, the yield, the content of fenolic coumpounds and calcium*, Polish Chitin Soc. Monograph, **12**, 2007, pp. 225–229.

[20] Lyu S., Wei X., Chen J., Wang C., Wang X., Pan D.: *Titanium as a Beneficial Element for Crop Production*, Frontiers in Plant Science, **8**, 2017, pp. 597.

[21] Staroń P., Banach M., Kowalski Z.: *Keratyna – źródła, właściwości, zastosowanie*, Chemik **65 (10**), 2011, pp. 1019-1026. [in Polish]

[22] Czerpak R., Bajguz A.: Akt*ywność fizjologiczna i metaboliczna kwasu salicylowego u roślin*, KOSMOS, **1**, 1998, pp. 83-93. [in Polish]

[23] Woznica Z., Idziak R., Sawinska Z., Sobiech Ł.*: Effect of salicylicacid on growth and grainyield of winterwheat*, Przemysł Chemiczny, **93 (4),** 2014, pp. 540-513. [in Polish]

[24] Ritchie R.J.: *Consistent sets of spectrophotometric chlorophyll equations for acetone, methanol and ethanol solvents*, Photosynth. Res., **89**, 2006, pp. 27-41.

[25] Sumanta N., Haque Ch.I., Nishika J, Suprakashumanta R.: *Spectrophotometric analysis of chlorophylls and carotenoids from commonly fern species by using various extracting solvents,*. Res. J. Chem. Sci., Vol. **4**, Issue (9), 2014, pp. 63-69.

[26] Vicaş S., Laslo V., Pantea S., Bandici G., *Chlorophyll and carotenoids pigments from Mistletoe (Viscum album) leaves using different solvents,* Fasc. Biol., **17**, 2010, pp. 213-218.

[27] Saito K, Suzuki T., Ishikita H.: *Absorption-energy calculations of chlorophyll a and b with an explicit solvent model Journal of Photochemistry and Photobiology A,* Chemistry, **358**, 2018, pp. 422–431

[28] Arnon D. I.: *Copper enzymes in isolated chloroplasts. polyphenoloxidase in beta vulgaris*, Plant Physiology, **24(1),** 1949, pp. 1-15.

[29] Ergun E., Demirata B., Gumus G., Apak R. P.: *Simultaneous determination of chlorophyll a and chlorophyll b by derivative spectrophotometry,* Anal Bioanal Chem., **379(5-6),** 2004, pp. 803-11.

Granulation of waste tannery shavings

Granulacja odpadowych stużyn garbarskich

Andrzej Rostocki[2,3*], Andrzej Obraniak[1], Paulina Bandrow[4,5], Malwina Wachulak[6], Tomasz Olejnik[7], Julia Bartyzel[1], Katarzyna Ławińska[2], Remigiusz Modrzewski[1], Szymon Szufa[1], Magda Orczykowska[1]

[1] Lodz University of Technology, Faculty of Process Engineering and Environmental Protection,

[2] Lukasiewicz Research Network – Lodz Institute of Technology,

[3] Lodz University of Technology, Interdisciplinary Doctoral School,

[4] Bader Polska Sp. z o.o.,

[5] Institute of Fluid-Flow Machinery Polish Academy of Sciences,

[6] Goudenkorrel S.A.,

[7] Lodz University of Technology, Faculty of Biotechnology and Food Sciences

Abstrakt

W pracy oceniono proces granulacji odpadów grabarskich (strużyn garbarskich) połączonych z cementem i sulfogipsem. Do zwilżania surowych materiałów w procesie granulacji wykorzystywano wodny roztwór szkła wodnego w stężeniu 20% i 40% oraz wodę. Zmiennymi parametrami zastosowanymi na wejściu były: rodzaj i masa cieczy oraz różny stosunek surowców sypkich. Ocenę jakościową uzyskanych granulek przeprowadzono w oparciu o skład granulometryczny, gęstość nasypową, kąt naturalny zsypu, współczynnik kształtu aglomeratów oraz ich wytrzymałości na ściskanie.

Abstract

In this paper, the process of disc granulation of tannery industry waste (tannery shavings), with the addition of cement and sulfogypsum, was studied. An aqueous solution of 20% and 40% water glass and water were used to moisten the raw materials. The variable parameters were the type and weight of the binding liquid and the proportions of the bulk materials added. Qualitative evaluation of granules was carried out based on the determined granulometric composition, bulk density, angle of natural repose, shape factor of agglomerates and their compressive strength.

Słowa kluczowe: strużyny, odpady, proces granulacji, granulacja talerzowa

Keywords: shavings, waste management, granulation, disc granulation

1. Introduction

Waste from the tanning industry and its disposal

Tanning is an industry whose impact is particularly hazardous to the environment.
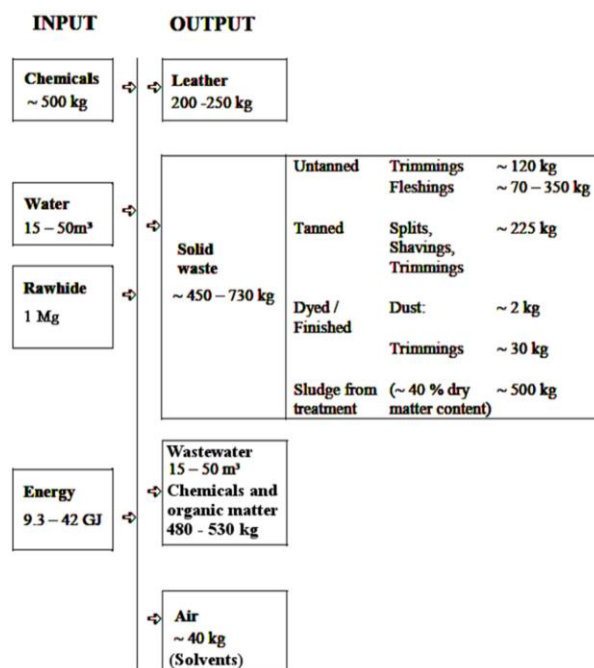
Fig. 1. Mass balance of the leather tanning process [1].

The process of leather tanning is extremely time-consuming and consists of many complex steps involving the use of a large number of chemicals, such as tannins, chromium (III) salts, aldehydes, and the generation of a huge amount of waste. It is estimated that only 20 – 25% of the weight of raw hides is converted into the final product [2]. The exact mass balance of the tanning process is shown in Figure 1. The remainder of the initial raw material is waste, which consists of biologically unstable waste (e.g., unneeded tissue that is separated from the dermis) and non-biodegradable waste (e.g., flashings, splits, shavings, cuttings). Waste from tanneries can be divided into by-products, hazardous waste and non-hazardous waste. A detailed list of wastes and their characteristics has been created by the European Commission, as shown in Table 1 and Table 2.

Tab. 1. List of tanning wastes according to Commission Decision of 3 May 2000 establishing a list of wastes [2000/532/EC].

Code number in the waste catalog	Types of waste
04 01	Wastes from the leather and fur industry
04 01 01	fleshings and lime split wastes
04 01 02	liming waste
04 01 03	degreasing wastes containing solvents without a liquid phase
04 01 04	tanning liquor containing chromium
04 01 05	tanning liquor free of chromium
04 01 06	sludges, in particular from on-site effluent treatment containing chromium
04 01 07	sludges, in particular from on-site effluent treatment free of chromium
04 01 08	waste tanned leather (blue sheetings, shavings, cuttings, buffing dust) containing chromium
04 01 09	wastes from dressing and finishing
04 01 99	wastes not otherwise specified

Tab. 2. Characteristics of tannery waste [3].

No.	Types of waste	Amount of waste kg/1 Mg of raw material	Total organic content	Moisture content	Ash content	Calorific value kJ/kg
1	shavings	150	87.5	53.6	7.8	6 663
2	sediment	approx. 100	65.5	54.7	24.3	716
3	buffing dust	0.1 – 0.2	87.4	14.3	6.2	16 953
4	cuttings (product)	9	87.7	10.2	4.7	19 772
5	cuttings (raw material)	260	86.9	59.9	4.7	7 753
6	fleshings	300	91.4	59.5	4.6	8 952

Some of the tannery waste, is processed into gelatin, fertilizer or feed ingredients. Tannery waste can also serve as a raw material for biofuels, such as biodiesel and biogas [4] and can also be subjected to dehydration, melting and composting. Several method proposals have also been developed to dispose of tannery waste through incineration. Pilot plants have been established using tunnel kilns. These

furnaces allow the wet waste to be dried first, which is then degassed and burned. However, this process needs to be more carefully optimized so that complete combustion occurs and the amount of gaseous pollutants is inert to the environment [5]. In practice, disposal mainly consists of landfilling, usually in on-site landfills.

Tanning shavings – waste management possibilities

One of the types of waste mentioned is tanning shavings, otherwise known as tanning shavings. They are created as a result of planning leather. This is a process that allows the thickness of the entire leather to become uniform.

Tanning shavings can be processed to produce secondary leather, which is used to make shoe soles, upholstery material, and bookbinding. Another option is to process shavings into protein hydrolysates, and fertilizers. They can also be composted, heat treated and stored. Unfortunately, tanning shavings are characterized by a number of unfavorable features from the point of view of reuse. They take the form of flocculent fragments that clump together into larger agglomerates (Fig. 2). They have a very low bulk density and are subject to dusting. The above-mentioned characteristics result in difficult transport, storage, as well as batching, or dumping of shavings [6].

In order to solve these problems, it is necessary to give the shavings a different, more usable form. This is possible by using a pressure-free granulation process. During granulation, the shavings are mixed with a suitable binding liquid and other additives (e.g., minerals), resulting in a free-flowing deposit in the form of granules that can be easily handled (transported, dosed, stored or used as an intermediate for other processes) [7].
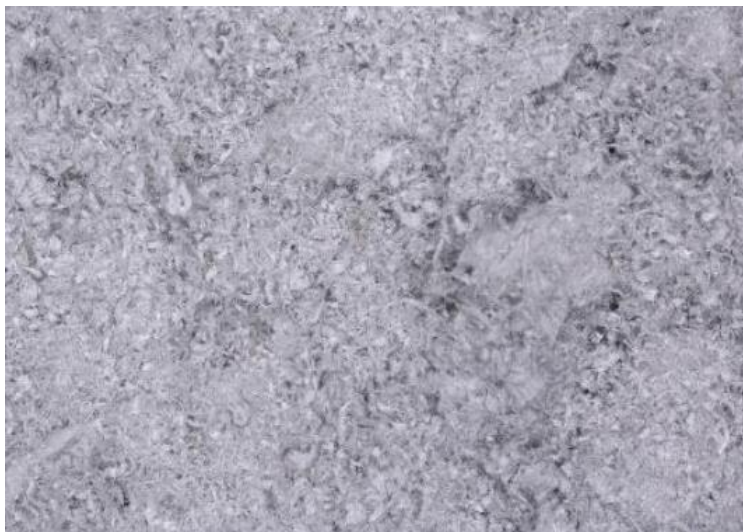
Fig. 2. Tannery structures under magnification [8].

Ławińska and co-authors [9] investigated the possibility of minimizing the environmental impact of shavings storage and transportation by granulating the waste with dolomite and sulfogypsum, which is a waste material generated in the flue gas desulfurization process. A 50% and 75% aqueous glass solution was used as a wetting liquid. Granulation was carried out in a disc granulator. Pre-granulation of the shavings themselves proved problematic. Very large granules were formed next to the non-granulated material. It was therefore necessary to add mineral material (dolomite and sulfogypsum). The result was granules with good mechanical strength, a bulk density five times greater than the starting shavings, and easy to transport and store. The product so produced could have applications in the manufacture of composite materials based on collagen fibers.

In 2020, Ławińska and co-authors [10] proposed a new method for granulating tanning shavings. Instead of the traditional method of disc granulation, where a wetting liquid is added to the dry bulk material while granulation is carried out, a wet pulp containing shavings and other minerals (dolomite and gypsum) was first prepared. The binding liquid was water glass. The wet bed prepared in this way was subjected to granulation on a disc granulator without additional wetting liquid. The

effect of shavings particle size on granule quality was also investigated. For this purpose, tests were carried out to granulate shavings with sizes smaller than 2 mm (selected by previous sieve analysis) and shavings that had not undergone previous selection. The quality of the obtained granules was examined. Their granulometric composition and mechanical strength were determined. The results showed that the prior wetting of the material has a beneficial effect on the granulation process, and also the pre-screening of the shavings contributed to the formation of granules of the best quality. The product proved to be durable and mechanically stable.

In 2021, Ławińska [11] presented methods of tannery waste management in the form of composite material production, encapsulation and granulate production. The composite was produced based on shavings, mineral filler (dolomite, kaolin, bentonite) and four types of adhesive agent: aqueous solution of polyvinyl acetate, gelatin glue, latex glue, epoxy resin. The mixtures were solidified by using a hydraulic press, dried, and then subjected to tensile tests. Some tests were examined for water absorption. Tensile strength results showed that the resulting composite could be classified in the same group as polymers and elastomers. On the other hand, the granulation of shavings was carried out in a disc granulator with the addition of dolomite or gypsum. The process was realized by two methods. The first was to moisten the dry shavings and mineral material in the plate granulator with an aqueous glass solution (concentration of 50% or 75%), and in the second method the shavings were first soaked in the glass solution and then granulated with the dry mineral material. This made it possible to obtain particles of good quality (appropriate size, shape, physical and chemical properties), which translates into easy transportation and storage. Waste collagen substances were used to envelope the seeds to increase their drought resistance. Disc granulation was also used in this process. Seeds were first coated with collagen hydrolysate or molasses, and then coated with a mineral additive in the granulation process. Closed, spherical and durable seed coatings were obtained.

2.　　　Materials and method

Purpose of the work

The purpose of the study was to develop a method for granulating tannery waste – tannery shavings using cement or sulfogypsum as a mineral component.

Test materials and parameters of the tests conducted

Since preliminary tests showed the impossibility of granulating the bulk material, which consisted only of tannery shavings, it was decided to subject a mixture of this waste and mineral material to the process The base waste material subjected to the granulation process was therefore a mixture containing contaminated tannery shavings sieved on a 3.15mm sieve (Fig. 3) and cement or sulfogypsum. In each sample, the weight of the shavings used was 200 g. The exact composition of the contaminated shavings is shown in Table 3. The bulk density of this waste was about 178 kg/m^3, and the angle of natural repose was about 53°. Tannery shavings were mixed with various weights of cement (from 200g to 1000g). An additional waste material used in the study was sulfogypsum, an end product formed in the flue gas desulfurization process. Water or an aqueous solution of sodium water glass of 20% and 40% concentration was used as a binding liquid. Soda water glass is a viscous liquid, with a density between 1260 kg/m^3 and 1710 kg/m^3.

Fig. 3. Tanning shavings used in granulation (source: own research data)

Tab. 3. Composition of contaminated shavings used for granulation (source: own research data).

Dry mixture composition			
Sludge	Shaving	Trim	Charcoal
30%	30%	30%	10%

Mixture moisture content			
Sludge	Shaving	Trim	Charcoal
70%	50%	10%	2%

Composition of the mineral fraction of the mixture				
Element	Sludge	Shaving	Trim	Charcoal
C	26.19	42.32	69.3	82.4
H	2.38	5.74	3.96	2.8
N	0.99	10.09	7.4	0.9

The parameters characterizing each sample are shown in Table 4 below.

Tab. 4. Weight of materials used and parameters in each sample (source: own research data).

No.	Material, [g]	Wetting liquid, [g]	Wetting time	Granulation time	Mass of wetting liquid, [g]
1	Shavings 200 + cement 300 + cement powdering 100	Water glass 40% 376	2 min 30 sec	6 min	376
2	Shavings 200 + cement 300 + cement powdering 100	Water glass 40% 482	3 min	6 min	482
3	Shavings 200 + cement 400 + cement powdering 100	Water glass 40% 448	2 min 30 sec	6 min	448
4	Shavings 200 + cement 400 + cement powdering 100	Water glass 40% 486	2 min	6 min	486
5	Shavings 200 + cement 400 + cement powdering 100	Water glass 40% 558	3 min	6 min	558
6	Shavings 200 + cement 500 + cement powdering 100	Water glass 40% 606	2 min 30 sec	6 min	606
7	Shavings 200 + cement 300 + cement powdering 100	Water glass 20% 290	2 min 30 sec	6 min	290
8	Shavings 200 + cement 400 + cement powdering 100	Water glass 20% 327	2 min 45 sec	6 min	327
9	Shavings 200 + cement 500 + cement powdering 100	Water glass 20% 401	3 min	6 min	401

10	Shavings 200 + cement 200 + cement powdering 100	Water 207	2 min 20 sec	6 min	207
11	Shavings 200 + cement 300 + cement powdering 100	Water 210	3 min	6 min	210
12	Shavings 200 + cement 400 + cement powdering 100	Water 243	3 min	6 min	243
13	Shavings 200 + cement 500 + cement powdering 100	Water 278	2 min 30 sec	6 min	278
14	Shavings 200 + cement 600 + cement powdering 100	Water 280	2 min 30 sec	6 min	280
15	Shavings 200 + cement 800 + cement powdering 100	Water 404	3 min	6 min	404
16	Shavings 200 + cement 1000 + cement powdering 100	Water 492	3 min	6 min	492
17	Shavings 200 + cement 500 + sulfogypsum 500 + sulfogypsum powdering 100	Water 371	3 min	6 min	371

Test apparatus and measurement methodology

Disc granulation

The granulation process was implemented in a disc granulator with a disc diameter of 500 mm. The schematic of the measuring station is shown in Fig. 4. The basic components are: geared motor (1), inverter (2), granulator disc (3), pressure sprayer (4), scraper (5), frame (6). A gearmotor drives the granulator disc. Thanks to the inverter, the speed of the granulator disc was controlled. The rotational speed was set at 24 rpm. The frame includes a movable support plate, which allows the angle of tilt of the disc to be adjusted. This angle for each sample was 45°. Each time, the granulation process was started by pouring the weighed amounts of shavings, cement and sulfogypsum onto the plate and mixing them. The granulator was then started and hydration was initiated using a pressure nozzle. At the end of the process, powdering was carried out for each sample using 100 g of the appropriate material. Powdering was performed to prevent the granules from sticking together. Efforts were made to maintain similar wetting time (which was 3 min) and granulation time (which was 6 min) for all samples. After granulation was completed, the resulting deposit was weighed and subjected to a drying process at

80°C for 48 h. After this time, the properties of the granules were determined for each sample.
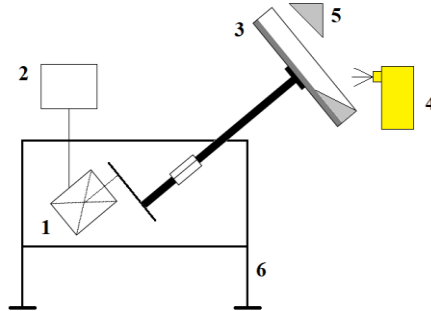
Fig. 4. Schematic of disc granulation station (source: own research data)

Components: geared motor (1), inverter (2), granulator disc (3), pressure sprayer (4), scraper (5), frame (6).

A set of sieves with mesh sizes was used to determine the granulometric composition: 12.5 mm, 10 mm, 8 mm, 6.3 mm, 5 mm, 4 mm, 3 mm, 2 mm and 1 mm. The test was performed by manually sifting the entire obtained material for each sample through successive sieves. Each fraction obtained was weighed on a digital scale. Bulk density and angle of natural repose were also tested for each obtained pellet.

Compressive strength test

Testing of the compressive strength of granules was carried out in an Instron 3345 Analyzer (Fig. 5). The basic components of the analyzer are a load frame (1), a stationary lower jaw (2), a movable upper jaw (3), and a base with a control panel (4) with which the position of the movable jaw can be adjusted. Carrying out the measurement began each time by placing a pellet on the stationary jaw and started the measurement. The upper jaw moves in the direction of the granule, at the moment of contact with the granule the jaw continues to move downward, which consequently leads to the destruction of the granule. The course of changes in the value of the compressive force during the measurement was recorded continuously

until the granule broke. For strength measurements, granules from the 4 – 5 mm, 5 – 6.3 mm and 6.3 – 8 mm fractions were randomly selected for each test. The speed of moving the moving jaw for all samples was 2 mm/min.
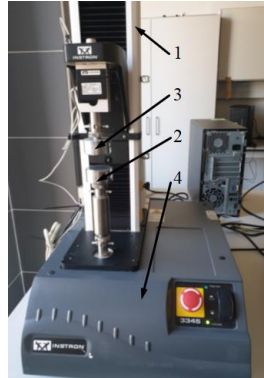
Fig. 5. Compressive strength test stand (source: own research data)

Components: load frame (1), stationary lower jaw (2), movable upper jaw (3), base with a control panel (4).

Determination of shape factor

The aspect ratio was determined using a Kamika Instruments AWK 3D analyzer. The measurement process is automatically controlled after entering the appropriate parameters on the computer. Tests were performed for 256 measurement classes and a maximum grain size of 31.5 mm. The measurement duration each time was 1000 s. The hopper was filled with the test material, after which the transfer of granules to the trough was stopped. During the duration of the measurement, the rate of granule spillage was controlled by adjusting the frequency of vibration of the trough so that as single a granule as possible flew through the measurement sensor.

3.   Research results

The granulation process was carried out successfully for each sample. Photos of the obtained granules after drying are shown in Figure 6.

Granulometric composition

Analysis of the granulometric compositions of the individual samples shows that the use of water glass with a concentration of 40% as a binding liquid results in granules with a uniform grain size. As shown in Figure 7, the mass proportions of the individual fractions are generally not very different. It can be seen that a higher mass of added cement reduces the amount of ungranulated material. For the addition of 300 g and 400 g of cement, the mass share of the 0-1 mm fraction was twice as high as for the addition of 500 g of cement. The higher mass of added cement also allows for a higher mass of granules with large sizes.

In sample 6 (addition of 500 g of cement), the highest mass shares were obtained for fractions larger than 8 mm.
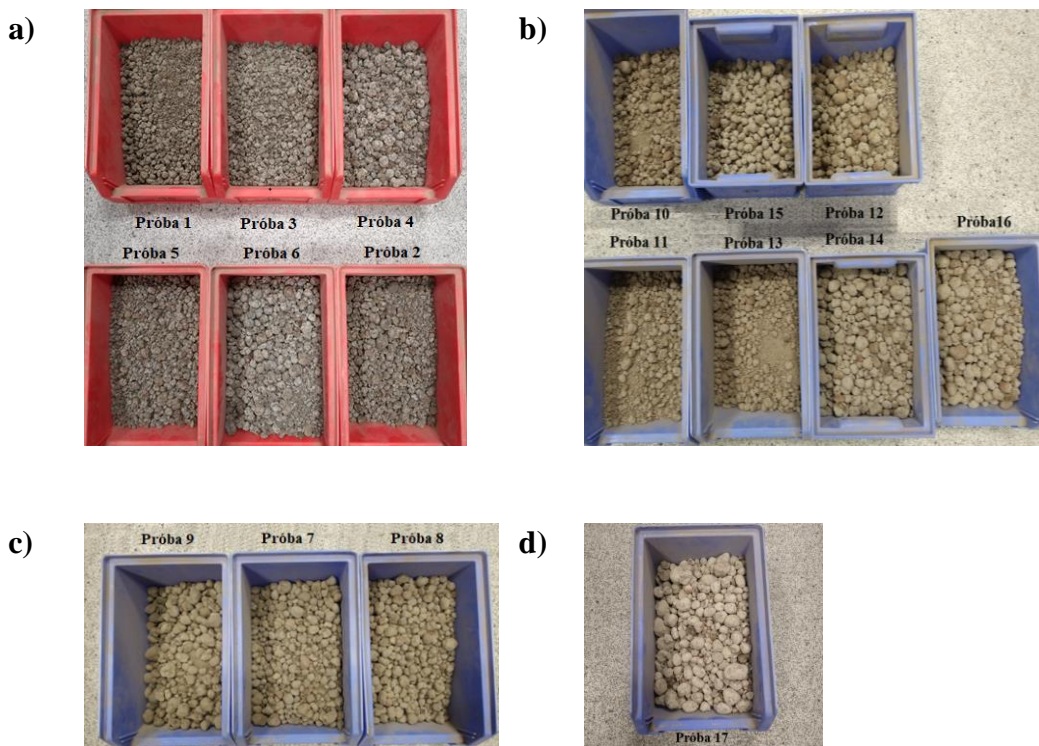
Fig. 6. Granules obtained using (a) shavings, cement, water glass with a concentration of 40%, (b) shavings, cement, water, (c) shavings, cement, water glass with a concentration of 20%, (d) shavings, cement, sulfogypsum, water.
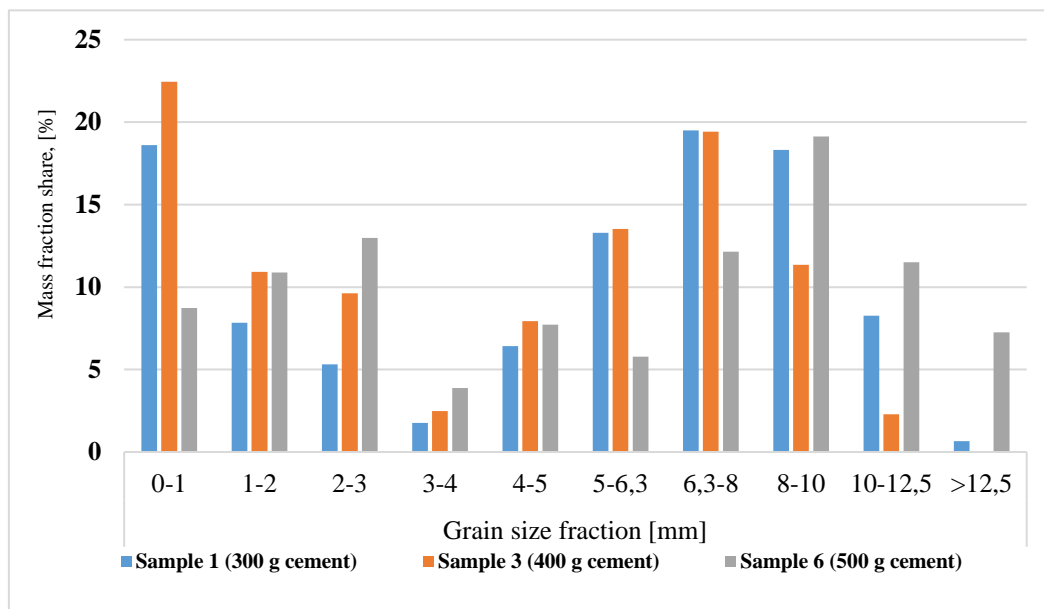
Fig. 7. Comparison of mass proportions of individual fractions using 40% water glass as a wetting liquid.

For granules with the addition of water glass, the effect of the weight of the applied binding liquid on the grain size of the resulting deposit was further analyzed. Fig. 8 shows that for the smallest mass of the applied water-glass solution with a concentration of 40%, the share of the non-granular fraction (0 - 1 mm) was 23%. The addition of a larger mass of liquid reduced the mass share of this fraction. In sample 5, the share of this fraction was three times lower than for sample 3. The mass of the binding agent used had little effect on the change in uniformity of grain size. However, it was noted that the result of more intensive wetting of the raw material during granulation was the production of a larger mass of granules with a size of more than10 mm.
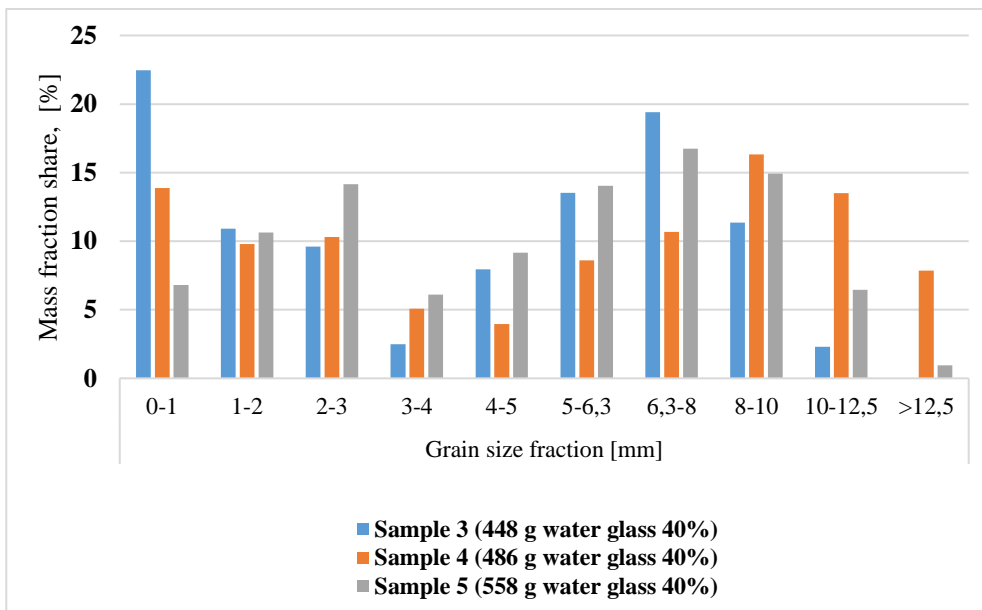
Fig. 8. Comparison of mass proportions of individual fractions using different amounts of water glass at 40% concentration.

Figure 9 illustrates how the weight of the cement used impacts the granulometric composition of samples with water added.
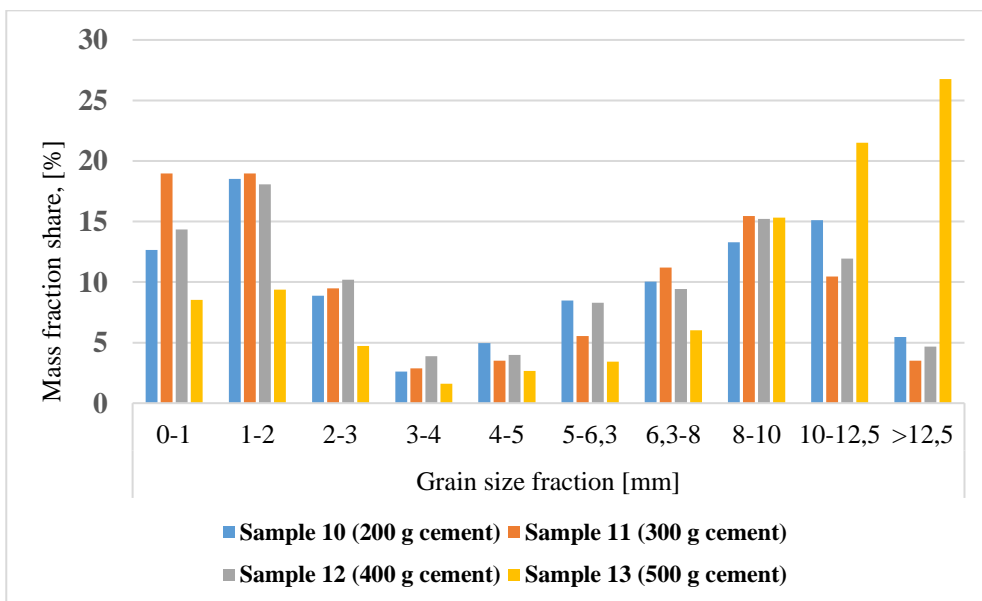
Fig. 9. Comparison of mass proportions of individual fractions when using water as a wetting liquid.

This graph shows that the lower mass of cement used during granulation results in a higher proportion of the ungranulated fraction (more than 10%). For these samples, there was also a small proportion of fractions with grain sizes larger than 10 mm. The samples where at least 500 g of cement was used had a significantly higher proportion of fractions with grain sizes larger than 10 mm, and at the same time the amount of material that was not granulated was reduced. This may also be the result of the greater mass of water added during granulation. For samples 15 and 16, 400 g to 500 g of water was used, increasing the mass proportion of the fraction larger than 12.5 mm to a value of at least 30%.
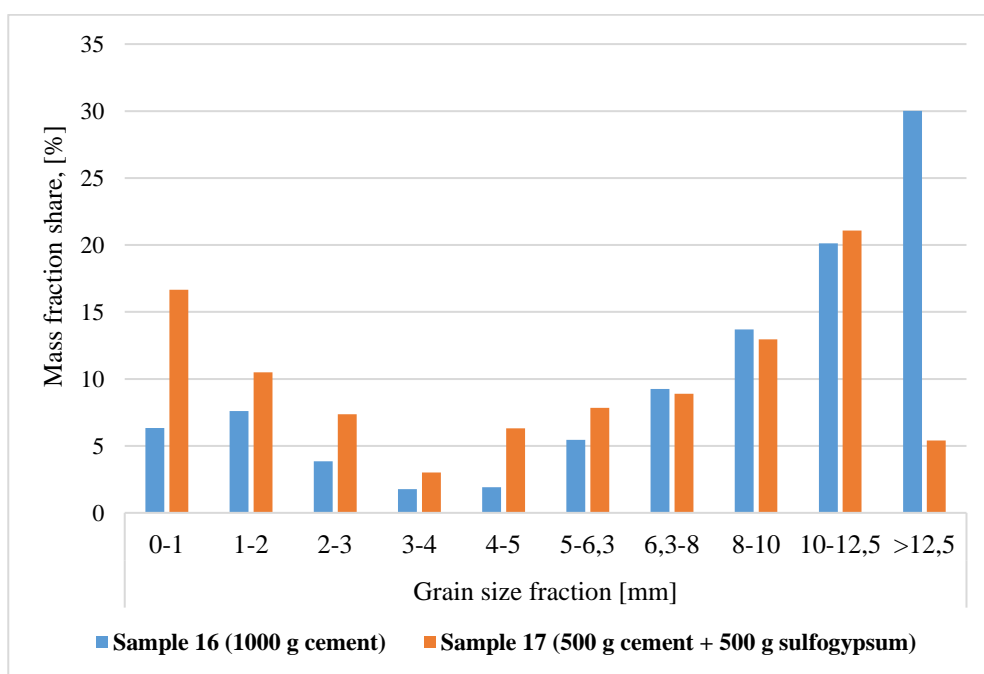
Fig. 10. Comparison of mass proportions of individual fractions using a mixture of cement with sulfogypsum and cement alone.

The study also analyzed the effect of the addition of waste sulfogypsum on the granulometric composition of the obtained product. It was found that a mixture of 500 g of cement and 500 g of sulfogypsum yielded a three times higher

proportion of the non-granular fraction than when 1000 g of cement alone was used (Fig. 10).
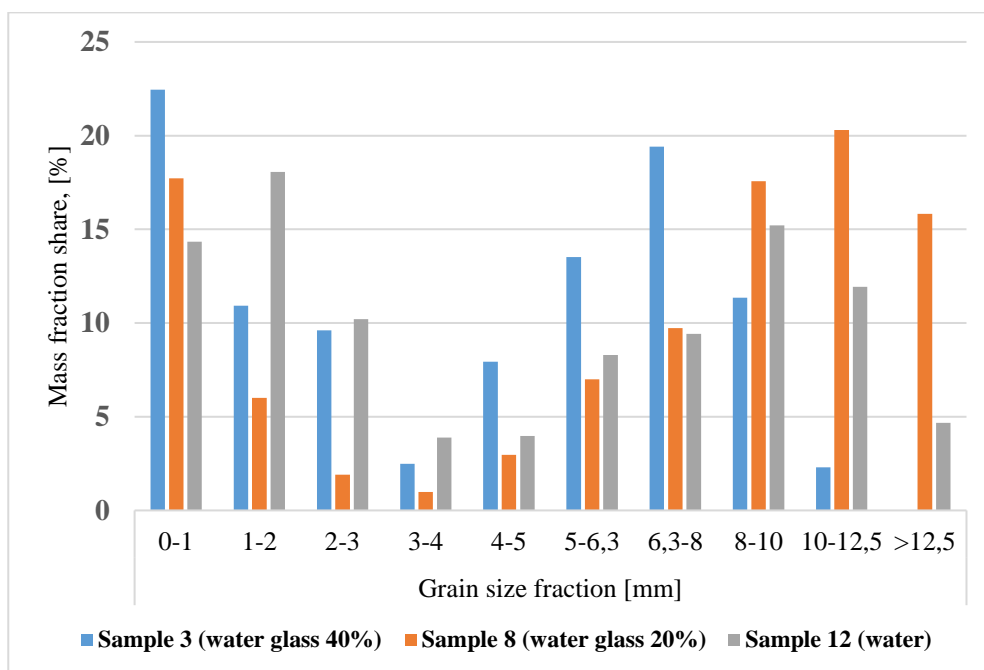
Fig. 11. Effect of the type of wetting liquid on the mass proportions of individual fractions for the addition of 400 g of cement.

It should be noted, however, that more than 100 g less water was added for sample 17 with the addition of sulfogypsum than for sample 16. Therefore, it is impossible to conclude unequivocally that the addition of sulfogypsum negatively affects the degree of granulation of the test material. It would be necessary to carry out an additional test, in which the addition of water would be similar to that for sample 16. The effect of the type of binding liquid used on the granulometric composition was also compared (Fig. 11). For the samples with the addition of 400 g of cement, it was noted that the lower content of water glass in the wetting liquid resulted in a lower proportion of the non-granular fraction. In addition, it was noted that the use of water glass at a concentration of 20% resulted in the smallest mass shares for fractions in the range of 1 - 6.3 mm.

Bulk density

Analyzing the determined values of bulk density (Table 5), it can be concluded that through the granulation process it was possible to increase them. The lowest value of 430 kg/m^3 was obtained for sample 10 (200g of shavings, 200 g of cement, 207 g of water, 100 g of powder cement), while the highest value of 654 kg/m^3 was obtained for sample 17 with the addition of sulfogypsum. In comparison, the bulk density of the shavings alone was 178 kg/m^3.

Considering the results obtained for the samples in which a 40% aqueous glass solution was used as a binding liquid (samples 1, 3, 6), it was noted that the value of bulk density increased with increasing mass of added cement. Samples 2, 4, and 5 were carried out to check the effect of the weight of the added wetting liquid on the bulk density. Comparing the obtained granular beds 1 and 2 (addition of 300 g of cement), a decrease in the value of bulk density was noted with a higher mass of added wetting liquid. Also for samples 3, 4, 5, it was observed that the highest bulk density occurred with the lowest mass of water glass solution (sample 3). Noteworthy is the fact that it was possible to obtain a similar bulk density for sample 1, using a smaller mass of cement and water glass, and for sample 5 (582 kg/m^3), to which 100 g more cement and nearly 200 g more water glass were added.

In the case of using a water glass solution with a concentration of 20% (samples 7, 8, 9), it can be seen that the use of the smallest mass of cement (300 g) proved to be the most advantageous. This made it possible to obtain a product with the highest bulk density among the three samples.

For the use of water as a binding liquid (samples 10 – 16), there was an initial increase in bulk density values with the increase in the added cement mass. The highest density value (604 kg/m^3) corresponded to the addition of 500 g of cement (sample 13). Larger masses of added cement resulted in a gradual decrease in bulk density.

However, the addition of 500 g of cement and 500 g of sulfogypsum appears to be the most optimal (sample 17). It was shown that in this case the highest bulk density was obtained, which is advantageous in terms of granular storage. It is also much less costly, since water can be used as a binding liquid. In addition, another waste material is also used, which is sulfogypsum.

The effect of the type of binder liquid used on the bulk density depends on the amount of cement used. Based on the analysis of samples 6, 9, 13 (addition of 500 g of cement) and samples 3, 8, 12 (addition of 400 g of cement), it can be concluded that the highest density values can be obtained by using water glass with a concentration of 40%. However, for samples 1, 2, 7, 11 (addition of 300 g of cement) it was found that the most favorable is the use of water glass with a concentration of 20%.

Angle of natural repose

The determined values of the angle of natural repose for all samples are shown in Table 5. The lowest angle (19°) was obtained for sample 12, while the highest value (42°) was obtained for sample 2. For non-granulated shavings, the angle was 53°. Granules formed from shavings, cement and water glass with a concentration of 40% (samples 1, 3, 6) were characterized by a decrease in the value of the angle of repose (greater flowability of the material) when increasing the mass of added cement. A similar relationship was observed for samples 7, 8, 9 formed from shavings, cement and water glass with a concentration of 20%.

Tab. 5. Determined bulk densities for the tests carried out.

Sample	Material	Amount of material, [g]	Type of liquid wetting	Angle of natural repose, [°]	Bulk density, [kg/m]^3
1	Shavings + cement	200 sh + 300 c + 100 cp	Water glass 40%	38	581
2	Shavings + cement	200 sh + 300 c + 100 cp	Water glass 40%	42	507

3	Shavings + cement	200 sh + 400 c + 100 cp	Water glass 40%	28	602
4	Shavings + cement	200 sh + 400 c + 100 cp	Water glass 40%	28	570
5	Shavings + cement	200 sh + 400 c + 100 cp	Water glass 40%	29	582
6	Shavings + cement	200 sh + 500 c + 100 cp	Water glass 40%	32	641
7	Shavings + cement	200 sh + 300 c + 100 cp	Water glass 20%	35	636
8	Shavings + cement	200 sh + 400 c + 100 cp	Water glass 20%	35	546
9	Shavings + cement	200 sh + 500 c + 100 cp	Water glass 20%	28	566
10	Shavings + cement	200 sh + 200 c + 100 cp	Water	30	430
11	Shavings + cement	200 sh + 300 c + 100 cp	Water	27	508
12	Shavings + cement	200 sh + 400 c + 100 cp	Water	19	526
13	Shavings + cement	200 sh + 500 c + 100 cp	Water	30	604
14	Shavings + cement	200 sh + 600 c + 100 cp	Water	31	597
15	Shavings + cement	200 sh + 800 c + 100 cp	Water	32	581
16	Shavings + cement	200 sh + 1000 c + 100 cp	Water	34	530
17	Shavings + cement+ sulfogypsum	200 sh + 500 c + 500 sg + 100 sgp	Water	34	654

Legends:

sh - shavings, c - cement, cp - cement used for powdering, sg - sulfogypsum, sgp - sulfogypsum used for powdering

Using water as a binding agent (samples 10 – 16), it was noted that initially increasing the amount of cement added resulted in a decrease in the value of the angle of natural repose, until the lowest value of 19° was obtained for the addition of 400 g of cement. Further increases in the amount of cement used resulted in an increase in the angle of repose. The effect of the weight of the added wetting liquid on the studied property was also analyzed. With the addition of 300 g of cement (samples 1, 2), an increase in the value of the angle of repose was noted with

increasing weight of the binding agent used. The same was true for the addition of 400 g of cement (samples 3, 4, 5), but the increase in the value of the parameter under study was less significant. Comparing the sample with the addition of 1000 g of cement (sample 16) and the sample with the addition of 500 g of cement and 500 g of sulfogypsum (sample 17), it was noted that the obtained granules had the same value of repose angle equal to 34°.

Taking into account that the granules obtained could potentially be subjected to further industrial operations (e.g., batching), the use of water as a binding agent and the use of an initial mass of 400 g of cement and 200 g of shavings prove to be the most advantageous (sample 12). Granules with the lowest angle of natural repose were obtained under these conditions. This significantly increases the flowability of the material.

Compressive strength testing of granules

Tests carried out on the Instron apparatus made it possible to determine the compressive force that destroyed the granules. An example graph of the change in the force acting on the granule as a function of the displacement of the measuring head is shown in Figure 12. The values of the destructive forces were identified as negative according to the agreement that tensile stresses are positive, while compressive stresses are negative. The extreme destructive force of the granule is, in the graph shown, the one followed by the relaxation of the test material (the characteristic peak) as a result of sample fracture.\

As was to be expected, the tested granules containing more cement were much harder to destroy. In the case of such granules, it was possible to observe on the graph of recorded destructive forces the characteristic rapid increase and immediate decrease in the destructive force after the granule broke.
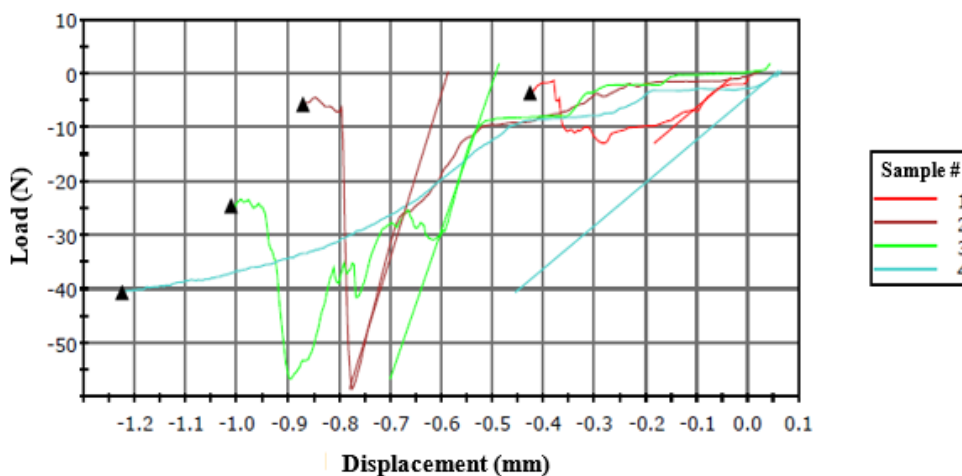
Fig. 12. The course of destructive forces for the 5 - 6.3 mm fraction for Sample 3.

From the results obtained, the averaged granule failure forces and compressive strength were determined – presented in Table 6 below.

Tab. 6. Determined granule failure forces and compressive strength for the tests performed.

Sample	Faction	Average granule destructive force, [N]	Average compressive strength, [MPa]
1	4 - 5 mm	3.5	0.22
	5 - 6.3 mm	3	0.12
	6.3 - 8 mm	25	0.62
2	4 - 5 mm	37.5	2.36
3	5 - 6.3 mm	55.5	2.21
	6.3 - 8 mm	42	1.05
4	4 - 5 mm	21	1.32
	5 - 6.3 mm	10	0.40
	6.3 - 8 mm	30	0.75
5	4 - 5 mm	40.5	2.55
	5 - 6.3 mm	65	2.59
	6.3 - 8 mm	40	1.00
6	4 - 5 mm	97.3	6.12
7	4 - 5 mm	5	0.31
8	4 - 5 mm	13.5	0.85
	5 - 6.3 mm	20.5	0.82
	6.3 - 8 mm	25	0.62

9	4 - 5 mm	15.3	0.96
10	5 - 6.3 mm	1	0.04
	6.3 - 8 mm	12	0.30
11	4 - 5 mm	94	5.91
12	4 - 5 mm	52.3	3.29
	5 - 6.3 mm	1	0.04
	6.3 - 8 mm	1.5	0.04
13	4 - 5 mm	81.7	5.14
14	4 - 5 mm	17	1.07
	5 - 6.3 mm	6.5	0.26
	6.3 - 8 mm	12.5	0.31
15	4 - 5 mm	25	1.57
	5 - 6.3 mm	33.5	1.34
	6.3 - 8 mm	19	0.47
16	4 - 5 mm	70	4.40
	5 - 6.3 mm	24	0.96
	6.3 - 8 mm	46.75	1.16
17	4 - 5 mm	7.5	0.47

For the granules formed with the addition of water glass at a concentration of 40% (samples 1 – 6), an increase in compressive strength can be observed with the increase in the amount of cement added. The highest strength was obtained in sample 6, where 500 g of cement was used. On the other hand, no significant effect of the amount of added binder liquid on the tested property was noticed (samples 3, 4, 5). In the case of samples with the addition of water glass with a concentration of 40%, it was difficult to select granules with a shape similar to a sphere. These granules were largely flattened in shape, which made it difficult to register the moment of their destruction. Under the pressure of the analyzer's moving jaw, there was no characteristic splitting of the granules, but further crushing. For these samples, the granulation process was very fast, so that the shavings were not thoroughly combined into larger agglomerates. It was also noted that some of the shavings and cement were granulated separately. The granules, which consisted mainly of shavings, despite the presence of water glass, were quite plastic, and were easily crushed by hand. For this type of specimen, there was no characteristic point on the recorded graph of the course of forces destroying the granule (no peak).

When considering the effect of the type of binder liquid used on compressive strength, no significant relationship was found. All the tested granules were characterized by average mechanical strength. This, in turn, would result in the destruction of the granules during transport or further processing.

Form factor

The Zingg classification generated by the software running the AWK 3D analyzer was used to evaluate grain shape.
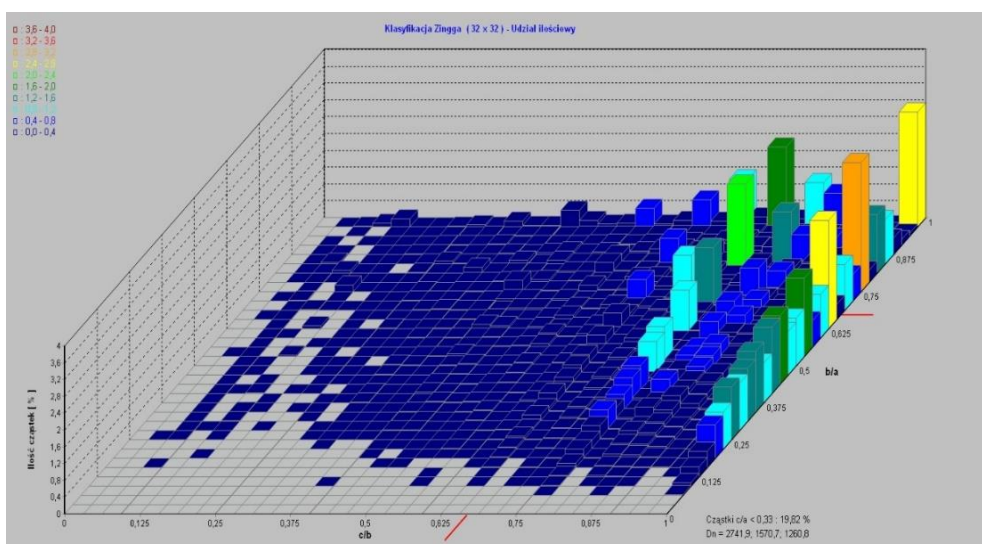
Fig. 13. Zingg classification as a quantitative share for sample 3.

The quantitative and volumetric (mass) proportion of each shape was determined. Analysis of the results obtained allows us to conclude that the type of binder liquid used and the mass of cement added affect the shape of the granules obtained. The use of water as a wetting liquid favors the formation of larger granules with a spherical shape. An example of the quantitative contribution in the form of a graphical Zingg classification is shown in Fig. 13, while the volume contribution is shown in Fig. 14. For the samples with the addition of water (samples 10 - 16), it was noted that the size of the spherical particles increases with the increase in the mass of added cement. This is evidenced by the increasing volume share of

spherical particles with the volume share remaining virtually constant for these samples. The largest spherical granules were obtained for sample 15 with 800 g of cement added. For this sample, the largest mass proportion of fractions with a size larger than 10 mm was observed on the determined granulometric composition.
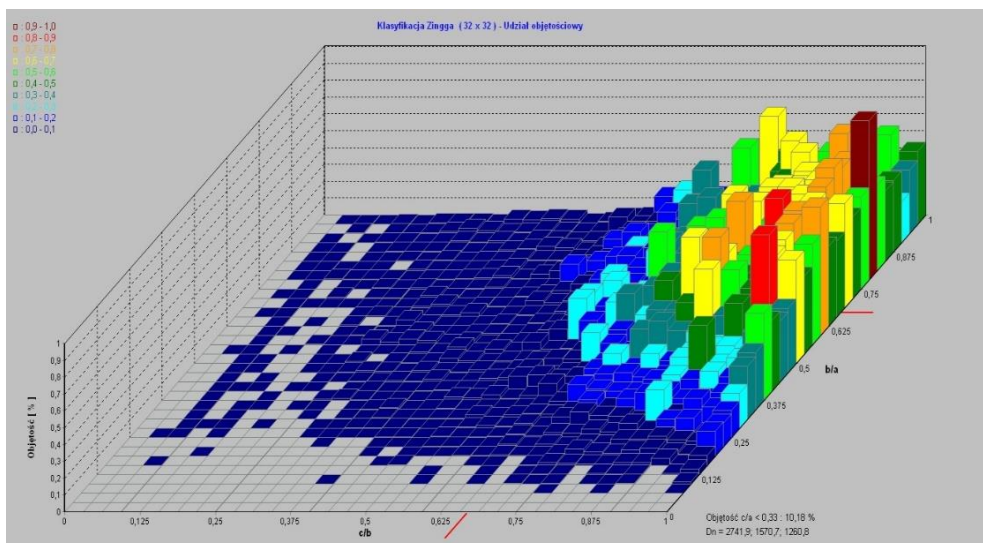
Fig. 14. Zingg classification as volume share for sample 3.

The results obtained are summarized in Table 7 below.

Tab. 7. Determined quantitative and volumetric shares of each shape

Sample	Sphere		Disc		Cylinder		Wedge	
	Quant. share, [%]	Vol. share, [%]	Quant. share, [%]	Vol. share, [%]	Quant. share, [%]	Vol. share, [%]	Quant. Share, [%]	Vol. share, [%]
1	32.48	55.3	8.95	6.84	51.09	34.48	7.48	3.39
2	40.62	54.45	12.67	7.57	40.43	35.05	6.29	2.92
3	36.78	45.42	9.63	7.3	47.43	42.43	6.15	4.85
4	38.14	59.96	9.54	5.69	46.99	31.7	5.33	2.66
5	40.6	55.13	10.32	6.41	43.23	35.47	5.85	2.99
6	37.95	52.07	9.64	5.8	46.95	38.92	5.46	3.21
7	34.23	68.86	9.61	5.09	50.01	23.8	6.14	2.25

8	37.53	61.21	10.45	3.95	45.57	32.67	6.54	2.17
9	37.38	65.06	10.87	4.04	44.81	29.44	6.94	1.46
10	31.98	50.94	10.44	6.93	49.43	37.94	8.15	4.19
11	37.34	47.04	11.23	6.6	44.62	41.92	6.8	4.44
12	35.99	53.23	11.16	6.93	45.59	35.33	7.26	4.51
13	37.1	65.35	22.95	3.8	43.02	28.65	7.93	2.2
14	34.97	63.68	9.26	3.89	49.25	30.35	6.53	2.07
15	35.5	71.49	9.43	2.07	48.16	25.29	6.9	1.15
16	37.8	69.67	12.9	3.67	41.3	24.69	8	1.97
17	29.29	69.32	9.18	4.96	52.81	23.41	8.72	2.3

4. Conclusions

1. Disc granulation of waste tannery shavings is a process that changes the properties of this material and allows it to form a loose bed of agglomerates that can be easily dosed stored and transported.

2. Granulation of tanning shavings with the addition of cement makes it possible to obtain a durable product with both water and aqueous glass solutions.

3. Disc granulation can be successfully used to increase the resulting product's bulk density, which positively affects transportability and storage.

4. Based on the analysis of the determined granulometric compositions, it can be concluded that adding larger masses of cement and wetting liquid increases the material's susceptibility to granulation, allowing to obtain larger granule sizes.

5. Obtaining positive results from the granulation of shavings using cement offers the possibility of using the agglomerates so obtained in the construction industry.

6. Using cement and water glass gives a high probability for "encapsulation" of the obtained granules and potential "encapsulation" of possible harmful substances present in the processed waste. Verification of this phenomenon requires additional research.

Bibliography

[1]   Bień J., Neczaj E., Worwąg M., Grosser A., Nowak D. Milczarek M., Janik M.: *Kierunki zagospodarowania osadów w Polsce po roku 2013*, Inżynieria i Ochrona Środowiska*,* 2013, pp. 375-384.

[2]   Bień J.: *Osady ściekowe teoria i praktyka,* Częstochowa: Wydawnictwo Politechniki Częstochowskiej, 2007.

[3]   Wieczorek-Ciurowa K., Famielec S., Fela K.: (2011). *Proces spalania odpadów przemysłu garbarskiego,* Chemik, 2011, pp. 917-922.

[4]   Lasek W.: *Zagospodarowanie stałych odpadów garbarskich, w tym odpadów chromowych*, Recykling, 2006, pp. 26-27.

[5]   Fela K., Wieczorek-Ciurowa K., Konopka M., Woźny Z.: *Comprehensive thermal treatment as a way of utilization of industrial leather waste,* Abstracts of 14th Conference on Environment and Mineral Processing, Part I, 2010*,* pp. 59-64.

[6]   Cabeza L.F., Taylor M.M., DiMaio G.L., Brown E., Marmer W.N., Carrió R., Celma P.J., Cot J.: *Processing of leather waste: Pilot scale studies on chrome shavings. Isolation of potentially valuable protein products and chromium.* Waste Management, 1998, pp. 211-218.

[7] Ławińska K., Kosińska K., Obraniak A., Modrzewski R.: *Sposób wytwarzania aglomeratu ze strużyn garbarskich* (Patent polski nr PL238881B1). 2018, Urząd Patentowy Rzeczypospolitej Polskiej.

[8] Wieczorek D., Lasoń-Rydel M., Gendaszewska D.: *Wpływ obecności strużyn garbarskich na wzrost drożdży z rodziny Dipodascaceae*, Technologia i Jakość Wyrobów, 2021, pp. 170-184.

[9] Ławinska K., Obraniak A., Modrzewski R.: *Granulation Process of Waste Tanning Shavings*, Fibres & Textiles In Eastern Europe, pp. 107-110, DOI: 10.5604/01.3001.0012.9994.

[10] Ławińska K, Modrzewski R, Obraniak A.: *Comparison of Granulation Methods for Tannery Shavings*, Fibres & Textiles In Eastern Europe, 2020, pp. 119-123. DOI: 10.5604/01.3001.0014.2396.

[11] Ławińska K.: *Production of Agglomerates, Composite Materials, and Seed Coatings from Tannery Waste as New Methods for Its Management. Materials*, 2021, DOI: 10.3390/ma14216695.

Notka o autorach:

mgr inż. Paulina Bandrów - absolwentka Wydziału Chemicznego na Politechnice Wrocławskiej. Doktorantka inżynierii mechanicznej w Instytucie Maszyn Przepływowych im. Roberta Szewalskiego Polskiej Akademii Nauk w Gdańsku. Badania do pracy doktorskiej wykonuje w ramach projektu pt. Modelowanie i weryfikacja eksperymentalna procesu ciemnej fermentacji odpadów garbarskich (umowa DWD/5/0397/2021) finansowanego przez Ministerstwo Edukacji i Nauki, w ramach V edycji programu pn. „Doktorat wdrożeniowy". Od 6 lat pracuje w branży Automotive w zakładzie, zajmującym się produkcją skórzanej tapicerki samochodowej, Bader Polska Sp. z o.o. na stanowisku Technologa. Obecnie pracuje na dziale Fabryki skóry, zajmującym się przetwarzaniem skór bydlęcych od skór Wet-Blue/Wet-White (surowiec) do gotowego wyrobu w postaci skóry wykończonej, gdzie zajmuje się wdrażaniem nowych projektów oraz optymalizacją procesu produkcyjnego. Ukończone szkolenia audytora wewnętrznego ISO 9001 i 14001, a także analizy FMEA procesów produkcyjnych wg AIAG&VDA. Udział w szkoleniach i prelekcjach dotyczących zagospodarowania odpadami.

mgr inż. Julia Bartyzel - ukończyła studia w roku 2022 na Wydziale Inżynierii Procesowej i Ochrony Środowiska Politechniki Łódzkiej. W ramach pracy dyplomowej pt. Badania procesu aglomeracji odpadów przemysłowych prowadziła badania dotyczące procesu granulacji odpadów drobnoziarnistych.

Ivana Čorak, mag. ing. techn. text - She has been employed at the University of Zagreb Faculty of Textile Technology as an assistant in the Young Researchers' Career Development Project Bio-innovated polyester material aimed for use in a hospital environment (HRZZ-DOK-2018-09-4254) since 2019. She worked as a quality specialist at Boxmark Leather d.o.o. for 3 years. She was a collaborator on the bilateral scientific research project Bio-innovated polyesters between Croatia and Serbia and is collaborator at the project HRZZ UIP-05-2019-8780 Hospital protective textiles. She received the Interim Deans Award for Excellence at the Postgraduate University Study of Textile Science and Technology in 2019/2020 and the Textile Science Research Center Award for the scientific research work in the field of textiles in category I: for young researchers at the TSRC Day 2021. She is working as an assistant from March 2023. Her scientific interest is related to methods of modifying polyester fabrics and the development of antimicrobial textiles and her teaching area is related to printing and dyeing. She co-authored 7 scientific and 1 professional paper in the journal, 16 full papers in proceedings and 8 abstracts.

inż. Natalia Czyżnik - w roku 2019 uzyskała tytuł zawodowy technika włókiennika. Absolwentka Wydziału Technologii Materiałowych i Wzornictwa Tekstyliów Politechniki Łódzkiej, kierunek: Włókiennictwo i Przemysł Mody. W 2023 roku obroniła pracę inżynierską pt.: „Identyfikacja uszkodzeń tkanin elektroprzewodzących w oparciu o czteropunktową metodę pomiaru rezystancji".

dr inż. Dorota Gendaszewska – jest absolwentką Wydziału Biotechnologii i Nauk o Żywności Politechniki Łódzkiej. W 2015 roku obroniła pracę doktorską pt.: „Biodegradowalność i usuwanie imidazoliowych cieczy jonowych ze ścieków". Obecnie pracuje na stanowisku Lidera Obszaru w Łukasiewicz – Łódzkim Instytucie Technologicznym.

ORCID 0000-0002-9909-0880

mgr inż. Dominika Kamińska ukończyła studia na Wydziale Technologii Materiałowych i Wzornictwa Tekstyliów Politechniki Łódzkiej na kierunku Włókiennictwo. Obecnie jest studentką studiów doktoranckich na kierunku Włókiennictwo na tym Wydziale. Jest laureatką V Edycji Konkursu im. Profesora Żurka na najlepszą pracę dyplomową o tematyce włókienniczej. Zajmuje się problematyką transportu wilgoci w materiałach włókienniczych. Obecnie pracuje w Instytucie Technologii Bezpieczeństwa "MORATEX".

dr inż. Gabriela Kosiuk - ukończyła studia doktoranckie na Wydziale Technologii Materiałowych i Wzornictwa Tekstyliów Politechniki Łódzkiej w dyscyplinie Inżynieria Materiałowa. Jest laureatką IV Edycji Konkursu im. Profesora Żurka na najlepszą pracę dyplomową o tematyce włókienniczej. Zajmuje się problematyką wiedzy w zakresie geometrycznej struktury powierzchni tkanin.

ORCID 0000-0003-3029-9982

dr inż. Dariusz Kryszak – jest absolwentem Politechniki Poznańskiej. W roku 2021 uzyskał tytuł doktora nauk rolniczych na Politechnice Łódzkiej. Pracuje w Mysak Group. Zajmuje się zagadnieniami analizy wykonalności instalacji przemysłowych.

dr hab. inż. Przemysław Kubiak prof. PŁ – profesor uczelni na Wydziale Organizacji i Zarządzania PŁ.

ORCID ID: 0000-0003-0225-9609

dr inż. Maciej Kuchar – adiunkt w Katedrze Pojazdów i Podstaw Budowy Maszyn Politechniki Łódzkiej.

dr hab. inż. Katarzyna Ławińska – Dyrektor Centrum w Łukasiewicz - Łódzkim Instytucie Technologicznym. Kierownik projektów badawczo-rozwojowych. Działalność: inżynieria i technologia - inżynieria chemiczna i materiałowa oraz inżynieria środowiska, górnictwo i energetyka.

ORCID 0000-0002-0064-3159

prof. dr hab. inż. Małgorzata Matusiak - jest profesorem zatrudnionym w Instytucie Architektury Tekstyliów, Wydziału Technologii Materiałowych i Wzornictwa Tekstyliów Politechniki Łódzkiej. Specjalistka w zakresie jakości i technologii bawełny, przędzalnictwa, włókienniczej inżynierii materiałowej, projektowania i technologii odzieży. Autorka licznych publikacji naukowych oraz wynalazków będących przedmiotem ochrony patentowej.

ORCID 0000-0002-9105-1166

dr hab. inż. Remigiusz Modrzewski w roku 1994 ukończył studia na Wydziale Inżynierii Procesowej i Ochrony Środowiska Politechnice Łódzkiej. W 2000 roku uzyskał stopień doktora, a w 2021 doktora habilitowanego. Jest zatrudniony na stanowisku adiunkta w Politechnice Łódzkiej w Katedrze Inżynierii Chemicznej. Jest współautorem ponad 80 publikacji naukowych. Jego zainteresowania badawcze obejmują modelowanie procesu przesiewania i granulacji materiałów ziarnistych oraz projektowanie i budowę przesiewaczy przemysłowych.

dr hab. inż. Andrzej Obraniak ukończył studia w roku 1989 na Wydziale Mechanicznym Politechniki Łódzkiej. W 2002 r. uzyskał stopień doktora zaś w 2020 roku stopień doktora habilitowanego na Wydziale Inżynierii Procesowej i Ochrony Środowiska Politechniki Łódzkiej. Jest profesorem uczelni w Katedrze Inżynierii Chemicznej na Wydziale Inżynierii Procesowej i Ochrony Środowiska Politechniki Łódzkiej. Dziedzina naukowa - inżynieria chemiczna. Prowadzi badania dotyczące procesu granulacji i otoczkowania.

prof. dr hab. inż. Tomasz P. Olejnik – jest pracownikiem naukowo-dydaktycznym na Wydziale Biotechnologii i Nauk o Żywności Politechniki Łódzkiej, zatrudnionym na stanowisku profesora uczelni. Posiada tytuł profesora w naukach technicznych w dyscyplinie ochrona środowiska, górnictwo i energetyka. Aktualnie prowadzi badania naukowe obejmujące biotechnologię, technologię żywności oraz

inżynierię procesową. Tematyka badawcza obejmuje między innymi: modelowanie procesów jednostkowych w przetwórstwie surowców mineralnych i spożywczych (rozdrabnianie, klasyfikację, granulowanie, mieszanie); transport masy i energii w tym modelowanie strumieni masy i energii (narzędzia CFD); optymalizację technologiczną przetwórstwa żywności wraz z optymalizacją konstrukcyjną maszyn i urządzeń. Jest autorem i współautorem przeszło 160 publikacji w czasopismach zagranicznych i krajowych, w tym 87 publikacji z listy JCR. Lista publikacji obejmuje monografie oraz książki. Ponadto jest autorem licznych ekspertyz i rozwiązań technologicznych zamawianych przez zewnętrzne otoczenie uczelni. Autor 59 patentów oraz 8 zgłoszeń patentowych.

ORCID 0000-0001-6941-4111

dr hab. inż. Magdalena Orczykowska - ukończyła studia na Wydziale Inżynierii Procesowej i Ochrony Środowiska Politechniki Łódzkiej, na którym pracuje do chwili obecnej. Kierunek prowadzonych przez nią badań obejmuje zagadnienia związane z właściwościami reologicznymi, a zwłaszcza lepkosprężystymi biomateriałów stosowanych w przemyśle spożywczym, farmaceutycznym i kosmetycznym.

ORCID: 0000-0002-0109-2563

dr Paulina Pipiak – ukończyła studia na Wydziale Chemii Uniwersytetu Łódzkiego. W 2018 roku obroniła pracę doktorską z chemii. Obecnie pracuje na stanowisku starszego specjalisty w Łukasiewicz – Łódzkim Instytucie Technologicznym.

ORCID: 0000-0002-3546-8258.

mgr Andrzej Rostocki w roku 2004 ukończył studia II stopnia na kierunku Gospodarka Przestrzenna na Wydziale Ekonomiczno-Socjologicznym Uniwersytetu Łódzkiego. Od 2019 r. pracuje w Sieci Badawczej Łukasiewicz – Łódzkim Instytucie Technologicznym jako specjalista ds. naukowo-badawczych. Doktorant na Wydziale Inżynierii Procesowej i Ochrony Środowiska Politechniki Łódzkiej, specjalność – inżynieria chemiczna. Badania do pracy doktorskiej wykonuje w ramach projektu pt. „Migracja składników z wytworzonych metodami bezciśnieniowymi granulatów uzyskanych z odpadów uciążliwych dla środowiska", który jest finansowany przez Ministerstwo Edukacji i Nauki w ramach V edycji programu pn. „Doktorat wdrożeniowy".

__mgr inż. Joanna Rutowicz__ ukończyła Wydział Chemiczny Politechniki Łódzkiej, specjalność technologia chemiczna. Zatrudniona w Łukasiewicz – Łódzki Instytut Technologiczny, Laboratorium Badań Produktów Spożywczych , Produktów Barwionych i Środowiska na stanowisku główny specjalista ds. badawczych. Specjalista w zakresie barwometrii.

__dr inż. Adam Rylski__ – adiunkt w Instytucie Inżynierii Materiałowej Politechniki Łódzkiej.

ORCID: 0000-0003-1445-5391

__dr hab. inż. Krzysztof Siczek__ – adiunkt w Katedrze Pojazdów i Podstaw Budowy Maszyn Politechniki Łódzkiej.

ORCID: 0000-0003-2216-3452

__dr hab. inż. Ewa Skrzetuska__ - profesor uczelni zatrudniona w Instytucie Materiałoznawstwa Tekstyliów i Kompozytów Polimerowych. Interesuje się wytwarzaniem innowacyjnych materiałów włókienniczych, haftem oraz drukiem funkcjonalnym przy użyciu polimerów elektroprzewodzących, przeznaczonych zarówno do zastosowań technicznych, jak również ochrony zdrowia i życia. Obecnie pracuje nad przede wszystkim otrzymywania nanokompozycji atramentowych oraz struktur haftowanych o właściwościach sensorycznych na bodźce chemiczne, termiczne i mechaniczne. Autorka licznych publikacji oraz nowoczesnych rozwiązań tekstronicznych.

ORCID 0000-0001-6565-1750

__dr hab. inż. Elżbieta Sobiecka__ ukończyła studia w roku 1996 na Wydziale Chemii Spożywczej i Biotechnologii (obecnie Wydział Biotechnologii i Nauk o Żywności), Politechniki Łódzkiej. W 1997 r. otrzymała tytuł zawodowy magistra na Wydziale Organizacji i Zarządzania. W 2001 r. uzyskała stopień doktora nauk technicznych zaś w 2015 r. stopień doktora habilitowanego. Obecnie pracuje w Instytucie Surowców Naturalnych i Kosmetyków PŁ na stanowisku profesora uczelni. Jest dyrektorem Instytutu Surowców Naturalnych i Kosmetyków PŁ. Specjalność – technologia chemiczna i chemia ekologiczna. Zainteresowania naukowe dotyczą zagadnień ochrony środowiska ze szczególnym uwzględnieniem procesów fitoremediacji.

ORCID 0000-0003-0016-5510

dr Maria Stanca – pracownik naukowy, INCDTP – Oddział: Instytut Badawczy Skóry i Obuwia w Rumunii. Działalność: inżynieria materiałowa i inżynieria chemiczna.

mgr inż. Otgonsuren Sukhbat ukończył studia w zakresie technologii odzieży w Mongolian University of Science and Technology w Ułan-Bator (Mongolia). Obecnie jest doktorantem w Instytucie Architektury Tekstyliów Politechniki Łódzkiej. Specjalizuje się w inżynierii projektowania tekstyliów, komforcie użytkowania odzieży oraz odzieży ochronnej.

mgr inż. Paulina Szablewska - ukończyła studia pierwszego i drugiego stopnia na Wydziale Elektrotechniki, Elektroniki, Informatyki i Automatyki Politechniki Łódzkiej na kierunku Inżynieria Biomedyczna. Obecnie jest studentką studiów trzeciego stopnia na Wydziale Technologii Materiałowych i Wzornictwa Tekstyliów Politechniki Łódzkiej w dziedzinie Inżynieria Materiałowa. Pracuje nad tekstylnymi czujnikami gazów.

dr inż. Szymon Szufa - specializes in distributed energy system using torrefied biomass, additives to bio-fertilizers. PhD thesis: Biomass torrefaction and co-firing - process modeling. Coordinator of Horizon Europe project BIOTRAINVALUE MSC SE: BIOmass Valorisation via Superheated Steam Torrefaction, Pyrolysis, Gasification Amplified by Multidisciplinary Researchers TRAINing for Multiple Energy and Products' Added Values: https://cordis.europa.eu/project/id/101086411. Participator: BECOOP, F-CUBED and CARBIOW Horizon projects.

dr inż. Lucjan Szuster - w roku 1970 ukończony Wydział Chemii, specjalizacja lekka synteza organiczna. W tym samym roku zatrudniony w OBR Przemysłu Barwników który przekształcono w Instytut Barwników i Produktów Organicznych. W Instytucie pełnił funkcje od asystenta naukowo badawczego do Zastępcy Dyrektora d/s Naukowych prowadząc wdrożenia nowych technologii w zakładach chemicznych „Boruta „ i „Zachem" Następnie zatrudniony w Instytucie Inżynierii Materiałów Polimerowych i Barwników na stanowisku p/o Dyrektora Oddziału Zamiejscowego. W latach 2012- 2018 zatrudniony na stanowisku pełnomocnika dyrektora ds. wdrożeń w Instytucie Przemysłu Skórzanego. Odbył stypendia naukowe Rządów francuskiego (Miluza) i włoskiego (Bergamo). Doktorat uzyskany na Uniwersytecie Łódzkim w obszarze kinetyki i syntezy

barwników. W latach 1992- 1994 zatrudniony na stanowisku „superviser„ w fabryce barwników Colorindo w Indonezji.

ASSOCIATE PROFESSOR, PhD Anita Tarbuk received her bachelor's degree in textile technology in 2001, her master's degree in 2005 and PhD in 2009 in technical science, textile engineering, all at the University of Zagreb Faculty of Textile Technology (UniZg TTF). In 2013, she completed pedagogic-psychological-didactic-methodical education for teachers at the University of Zagreb, Faculty of Education. Anita Tarbuk is the author and co-author of over 100 international publications

Her field of expertise are interface phenomena (electrokinetics, adsorption, surface free energy, hydrophilicity) and textile modification (cellulose mercerization and cationization, enzymatic pre-treatment, modification and finishing), and multifunctional finishing of textiles for protection and design. She teaches undergraduate, graduate, postgraduate and professional courses in Croatian and English.

dr hab. inż. Magdalena Tokarska – jest absolwentką Wydziału Fizyki Technicznej, Informatyki i Matematyki Stosowanej Politechniki Łódzkiej. Obecnie pracuje na stanowisku adiunkta w Instytucie Architektury Tekstyliów, Wydziału Technologii Materiałowych i Wzornictwa Tekstyliów Politechniki Łódzkiej. Zajmuje się badaniami eksperymentalnymi i modelowaniem właściwości elektroprzewodzących tekstyliów. W obszarze jej zainteresowań znajdują się również kompozyty tekstylne przeznaczone do ochrony przed czynnikami gorącymi.

ORCID 0000-0001-8102-1230

Malwina Wachulak - absolwentka Wydziału Biologii i Ochrony Środowiska Uniwersytetu Łódzkiego ze specjalizacją biologia stosowana i molekularna. Specjalistka w branży wymagającej nieszablonowego podejścia do procesu w Dziale Badań i Rozwoju GoudenKorrel S.A.

dr hab. inż. Krzysztof Wojciechowski - profesor PŁ. Ukończył Wydział Chemiczny Politechniki Łódzkiej w 1971r, specjalność: chemia i technologia barwników. Do 2003r. pracownik Instytutu Barwników PŁ, od 2003r. Instytutu Inżynierii Środowiska i Instalacji Budowlanych na Wydziale Budownictwa, Architektury i Inżynierii Środowiska PŁ. Od 2019 pracownik emerytowany.

dr inż. Marek Woźniak – adiunkt w Katedrze Pojazdów i Podstaw Budowy Maszyn Politechniki Łódzkiej.

ORCID: 0000-0001-9204-4024

dr inż. Sergiusz Zakrzewski - adiunkt w Katedrze Pojazdów i Podstaw Budowy Maszyn Politechniki Łódzkiej